UNIVERSITY OF
LIVERPOOL

Department of Engineering

PhD Thesis

Laser Forming of Fibre Metal Laminates

Thesis submitted in accordance with the requirements of The University of Liverpool for the degree of Doctor in Philosophy

By

Christian Carey

January 2009

Laser Group
Department of Engineering
The University of Liverpool
Brownlow Street
Liverpool
L69 3GH
UK

Declaration

I hereby declare that all of the work contained within this dissertation has not been submitted for any other qualification.

Signed:

Date: 10/6/09

Abstract

The work presented in this thesis is concerned with the process of shaping Fibre Metal Laminates (FMLs) using a laser source, in a process called laser forming or bending.

Laser Forming is a rapid, non-contact process developed in the late twentieth century for the shaping of metallic materials. It uses local thermal stress induced within the material to produce either out-of-plane or in-plane plastic deformations. The laser forming process is highly flexible, with accurate control of the process possible by a combination of delivery systems not possible with other techniques and computer control. Due to the flexibility of the process, laser forming can be used for numerous industrial applications, from both 2D and 3D forming of complete, serviceable parts, to distortion removal and rapid prototyping. While laser forming does compete with traditional forming and shaping methods in some areas, it is the shaping of FMLs where laser forming could offer a unique advantage over conventional methods.

The results in this thesis include investigations into the various aspects which affect the laser forming of FMLs, with particular concentration on the properties of fibre metal laminates.

The effects of laser power, the laser traverse velocity, wavelength and irradiation strategy on the resultant bend produced are also investigated and reported. The number, order and alignment of the layers present in the fibre metal laminate are investigated and the effect these have on the bend propagation and other factors important to the laser forming process are reported and discussed. Finally the effect that the laser forming process has on the materials is studied.

List of Publications to Date by Author

- Laser forming of fibre metal laminates,
  SEICO 09 Conference,
  C. Carey, W.J. Cantwell, G. Dearden, K.R. Edwards, S.P. Edwardson,
  K.G. Watkins

- Laser Forming: A viable forming method for fibre metal laminates,
  Thermal Forming and Welding Distortion,
  IWOTE '08 April 2008 pg 421-428,
  C. Carey, W.J. Cantwell, G. Dearden, K.R. Edwards, S.P. Edwardson,
  K.G. Watkins

- Effects of laser interaction with graphite coatings,
  Laser Assisted Net Shape Engineering 5, LANE 2007, pp673-686,
  C. Carey, W.J. Cantwell, G. Dearden, K.R. Edwards, S.P. Edwardson,
  J.D. Mullett, C.J. Williams, K.G. Watkins

- Low power laser forming of glass fibre based fibre metal laminates,
  Laser Assisted Net Shape Engineering 5, LANE 2007, pp645-655,
  C. Carey, W.J. Cantwell, G. Dearden, K.R. Edwards, S.P. Edwardson,
  K.G. Watkins

- Laser Forming for Ship Building Applications,
  Steel Tech Vol. 2 No. 4, July 2008,
  S.P. Edwardson, K.R. Edwards, C. Carey, G. Dearden, K.G. Watkins

- Laser peen forming for non-thermal forming of sensitive components,
  Thermal Forming and Welding Distortion,
  IWOTE '08 April 2008 pg 403-412,
  K.R. Edwards, S.P. Edwardson, C. Carey, G. Dearden, K.G. Watkins

- Effect of post forming heat treatments on laser formed components,
  Thermal Forming and Welding Distortion,
  IWOTE '08 April 2008 pg 315-322,
  E. Abed, S.P. Edwardson, K.R. Edwards C. Carey, G. Dearden,
  K.G. Watkins

- Laser peen forming for 2d shaping and micro adjustment,
  ICALEO® 2007 Congress Proceedings,
  Laser Microprocessing Conference Paper M605 pp156-165,
  K.R. Edwards, S.P. Edwardson, C. Carey, C.J. Williams, G. Dearden,
  K.G. Watkins

- Key factors influencing the bend per pass in laser forming,
  ICALEO® 2007 Congress Proceedings,
  Laser Materials Processing Conference, Paper P506, pp508-514,
  S.P. Edwardson, E. Abed, C. Carey, K.R. Edwards, K. Bartkowiak,
  G. Dearden, K.G. Watkins

- Laser peen forming for 2D shaping and adjustment of metallic components,
  Laser Assisted Net Shape Engineering 5, LANE 2007, pp569-580,
  K.R. Edwards, C. Carey, S.P. Edwardson G. Dearden, C.J. Williams,
  K.G. Watkins

- Factors influencing the bend per pass in multi-pass laser forming,
  Laser Assisted Net Shape Engineering 5, LANE 2007, pp557-568,
  S.P. Edwardson, E. Abed, C. Carey, K.R. Edwards, G. Dearden,
  K.G. Watkins

Acknowledgements

I would like to thank a number of individuals and groups for their help and encouragement during this study. My supervisors, Professor Wesley Cantwell and Dr Geoff Dearden, who offered support, guidance and encouragement throughout this research.

The members of the Laser Group at The University of Liverpool, particularly Professor Watkins and Dr Abed of the laser forming group, for their thoughts and ideas on this work. Dr Stuart Edwardson, for teaching me the various skills to undertake this research and providing invaluable assistance when required. My fellow students in the laser group, including Jack Mullett whose fault this is and Robert Dodd, Ken Edwards, Craig Williams, Jian Cheng, Joe Croft and Leigh Mellor as fellow members of 'The Laser Grazers' for giving me an outlet for my frustration. The various technicians who without them this work could not have occurred, including Andy Snaylam, John McCulloch and Dave Atkinson. And everyone at the Lairdside Laser Engineering Centre, including Dr P. French and Doug Eckford, for the use of the facilities and their experience.

The ESPRC for funding my work and BP Amoco for supplying material.

To my Mum, Dad and family for their generosity and patience throughout my time at university and my friends who convinced me that this was the right course of action, particularly Mark, Matthew and Chris. And to Howard and Rowan for their proof reading of this work.

And last, but by no means least to my beautiful wife Chloe for the support and help she has given me and for putting up with all this has caused.

Table of Contents

Declaration i
Abstract ii
List of Publications to Date by Author iii
Acknowledgements v
Table of Contents vi
List of Figures xi
List of Tables xix
List of Symbols xx
Chapter 1 Introduction 1
1.1 The Process 1
1.2 The Laser 2
1.3 The Material 3
1.4 Application 4
1.5 Motivation for Study 6
1.6 Objectives 7
Chapter 2 Literature Review 8
2.1 Laser Forming 8
2.1.1 The Laser 8
2.1.2 History of Thermal Shaping 11
2.1.3 Laser Forming Mechanisms 12
2.1.3.1 Temperature Gradient Mechanism (TGM) 13
2.1.3.2 The Buckling Mechanism (BM) 17
2.1.3.3 The Upsetting Mechanism (UM) 19
2.1.4 Mathematical Models 21
2.1.4.1 Analytical Models 21
2.1.4.1.1 Temperature Gradient Mechanism 21
2.1.4.1.2 The Buckling Mechanism 29
2.1.4.1.3 The Upsetting Mechanism 30
2.1.4.2 Numerical Modelling 31

2.1.4.2 1 Temperature Gradient Mechanism 32
2.1.4.2.2 The Buckling Mechanism 33
2.1.4.2.3 The Upsetting Mechanism 33
2.1.4.3 Current Research in Process Modelling 33
2.1.5 Fundamental Investigations in Laser Forming 34
2.1.6 Previous Experimental Work 38
2.1.6.1 Macro Scale 38
2.1.6.2 Micro Scale 43
2.1.6.3 Non Metallic materials 45
2.1.6.4 Micro Adjustment 46
2.1.6.5 Material and Metallurgical Studies 48
2.2 Fibre Metal Laminates 51
2.2.1 History of development 51
2.2.2 Manufacturing process 55
2.2.3 Constituents 56
2.2.3.1 Aluminium 56
2.2.3.1.1 Alloying Elements present in 2024 56
2.2.3.1.2 Heat Treating Process 58
2.2.3.2 Composites Layer 59
2.2.3.2.1 Glass Fibres 61
2.2.3.2.2 Epoxy Resin 63
2.2.3.2.3 Polypropylene 64
2.2.4 Shaping and forming 65
2.2.4.1 Splicing 65
2.2.4.2 Curved Panels 66
2.2.5 Mechanical properties 67
2.2.5.1 Tensile and Compression Strength 67
2.2.5.2 Residual Strength 68
2.2.5.3. Fatigue 69
2.2.5.4. Impact 71
2.2.6 Physical Aspects 72

2.2.6.1 Environmental Aspects 72
2.2.6.2 Lightening Strike 73
2.2.6.3 Flame Resistance 74
2.2.6.4 Maintenance, Inspection and Repair 75
2.3 Scope for further work 75
Chapter 3 Experimental Procedure 77
3.1. Hardware 78
3.1.1 Laser System 78
3.1.1.2 Beam Profile 81
3.1.1.3 Angle Measurement 82
3.1.2 Coating 84
3.1.2.1 Application Method 85
3.1.2.2 Effect of Coating Removal on Bend Rate 86
3.1.3 Dwell Time 87
3.1.4 Thermocouple Analysis 87
3.1.5 Strain Gauge Analysis 89
3.2 Material Manufacture 90
3.2.1 Process 90
3.2.1.1 PP FML Production 91
3.2.1.2 GF FML Production 92
3.2.2 Hardware 93
3.2.3 Quality Control 94
3.3 Microstructural Processing 95
3.3.1 Specimen Selection and Mounting 95
3.3.2 Optical Microscopy 97
3.3.3 Microhardness Tests 97
Chapter 4.Results and Discussion 98
4.1 Experimental Procedure 99
4.1.1 Forming Mechanism 99
4.1.2 Graphite Coating 101
4.1.2.1 Application of Graphite Coating 101

4.1.2.2 Coating burn off 103
4.1.2.3 Coating Reapplication 109
4.1.3 Dwell Time 109
4.1.4 Repeatability 111
4.1.5 Quality Control 112
4.2 Laser Parameters 113
4.2.1 Power 113
4.2.2 Velocity 117
4.2.3 Combined effect of Laser Power and Traverse Velocity 120
4.2.4 Scan Strategy 122
4.2.5 Spot Size 123
4.2.6 Wavelength 123
4.2.7 Thermal Effects 124
4.3 FML Parameters 126
4.3.1 Stacking Sequence 127
4.3.1.1 Cumulative Bend Angle 127
4.3.1.2 Bend Rate Per Pass 131
4.3.1.3 Bend Propagation 134
4.3.1.4 Thermocouple Data 149
4.3.1.5 Strain Gauge Analysis 155
4.3.2 Fibre Layer Parameters 166
4.3.2.1 Fibre Orientation 166
4.3.2.2 Composite layer 175
4.4. Effects of Laser Processing 182
4.4.1 Macro Effects 182
4.4.1.1 Structural Failures 182
4.4.1.2 Material Failures 187
4.4.2 Micro Effects 188
4.4.2.1 Microstructural Effects 188
4.4.2.2 Micro Cracking 190
4.4.2.3 Section Thickening 193

4.4.2.3 Micro Hardness 195

Chapter 5 Conclusions 198

5.1 Experimental Procedure 198

5.2 Laser Parameters 199

5.3 FML Parameters 200

5.3.1 Stacking Sequence 200

5.3.2 Fibre Layer Parameters 202

5.4 Effects of Laser Processing 203

5.4.1 Macro Effects 203

5.4.2 Micro Effects 203

5.5 Further Work 204

References 206

Appendix

A Thermocouple Data I

B Strain Gauge Data VII

List of Figures

Figure 1.1 T.H. Maiman's first laser 2
Figure 1.2 Typical Fibre Metal Laminate lay-up 3
Figure 2.1 Simplified cavity schematic 9
Figure 2.2 Molecular state at a) equilibrium and b) higher energy levels and generalized energy levels 10
Figure 2.3 Nd:YAG absorption spectrum compared to the emission spectra of a Kr flash-lamp [3] 11
Figure 2.4 Experimental variables for laser forming 12
Figure 2.5 Required Thermal conditions for TGM process and resultant strains 14
Figure 2.6 Schematic of Laser forming process 15
Figure 2.7 Principles of Temperature Gradient Mechanism 16
Figure 2.8 Stages of Buckling Mechanism 18
Figure 2.9 The Upsetting Mechanism 20
Figure 2.10 Two layer trivial model 22
Figure 2.11 Forces and moments acting in the two layer model 24
Figure 2.12 Layout for the residual stress model 27
Figure 2.13 Model geometry for buckling mechanism 30
Figure 2.14 Model for extrusion bending using upsetting mechanism 31
Figure 2.15 Decreasing bend rate with increasing scans over identical track 37
Figure 2.16 Ideal bend angle and exaggerated edge effect 40
Figure 2.17 Laser forming of 50μm thick wet-etch silicon samples 45
Figure 2.18 Image of audio head for Digital Compact Cassette head with special carrier for laser forming alignment 46
Figure 2.19 Actuator for CD lens adjustment by micro laser forming 47
Figure 2.20 Fokker F-27 Friendship 52
Figure 2.21 Classification of Composite Material Systems [96] 60
Figure 2.22 Chemical structure of polypropylene 64
Figure 2.23 FML splice concept [105] 66
Figure 2.24 Principles of roll forming and stretch forming [108] 66

Figure 2.25 The bridging effect of the intact fibre layers during crack propagation [130] 70
Figure 2.26 The crack growth behaviour of unidirectional GLARE 2; cross-plied GLARE 3, ARALL 2 and 2024-T3 for a fuselage loading [133] 71
Figure 2.27 Burn through test for post crash kerosene fuelled fires [150] 74
Figure 3.1 a) Image of system showing work-piece enclosure, galvanometer-head and laser head, b) schematic of laser head and c) Image of laser head internals 78
Figure 3.2 Image and schematic of clamping arrangement within work station enclosure 79
Figure 3.3 Lamp current supply against laser power output 80
Figure 3.4 3D and 2D beam profiles showing beam width and height and intensity at a) 20mm before the focal point, b) at the focal point and c) 30mm beyond the focal point 81
Figure 3.5 a) Sensor arrangement and b) measurement point plan 82
Figure 3.7 Agilent 34970A Data Acquisition unit. 83
Figure 3.8 Reflectivity of various metals as a function of wavelength [13] 84
Figure 3.9 Schematic of measurements taken of various graphite features 86
Figure 3.10 Plan of K-type thermocouple placement 89
Figure 3.11 Quarter bridge circuit 89
Figure 3.12 a) Picture frame type mould used for producing FMLs and b) plan view of lay-up 90
Figure 3.13 Mould Lay-up 92
Figure 3.14 Meyer Hot Press APV 2525/16 93
Figure 3.15 Instron 4204 tensile testing rig. 95
Figure 4.1 a) Delamination following Buckling Mechanism forming of FMLs after 2 passes b) after 10 passes (composite image) 100
Figure 4.2: Micrographs for a) thin, b) thick and c) saturated graphite application methods taken at x5 magnification 101
Figure 4.3: 2D VSI images of a) thin, b) thick and c) saturated application 400 x 500µm samples 102

Figure 4.4 Number of coatings against thickness of graphite 103
Figure 4.5 Number of laser passes verses trough depth CW processing of a thin (9.5μm) graphite layer 104
Figure 4.6 Number of laser passes verses width of trough for processing with thin (9.5μm) graphite layer 104
Figure 4.7 Number of laser passes verses trough depth for CW processing with thick (63μm) graphite layer 105
Figure 4.8 Number of passes verses width of trough for CW processing with thick (63μm) graphite layer 106
Figure 4.9 a) one pass, b) five passes and c) ten passes on thick (~50μm) graphite samples irradiated by Nd:YAG CW laser at 35W, 10mm/s and 0.2mm spot size 106
Figure 4.10 Trough features in Y direction after one, three and ten passes 107
Figure 4.11: 3D 50 μm AFM scans of the laser processed graphite layer, showing the graphite structure a) left side, b) centre and c) right side after 5 laser passes at nanometre resolution 108
Figure 4.12 Variation on CBA of various graphite recoating strategies 109
Figure 4.13 Recorded temperatures from lower surface of 0.3mm AL2024-T3 for various power levels and dwell times 111
Figure 4.14. Repeatability test using plain AL2024-T3 111
Figure 4.15 Load applied to the sample plotted against the crosshead displacement for a) GF and b) PP 112
Figure 4.16 CBA and BRPP against Number of Scans processed at 10mm/s and either 24W or 35W for Aluminium, GF and PP FMLs 114
Figure 4.17 Normalized BRPP values for a) Aluminium, b) 2:1 GF FML and c) 2:1 PP FML 115
Figure 4.18 MBRPP against laser power for a) 0.3mm Aluminium 2024-T3 b) 2:1 crowfoot weave GF based FM and c) 2:1 PP based FML 116
Figure 4.19 CBA and BRPP against Number of Scans processed at 35W and either 10mm/s or 40mm/s for Aluminium, GF and PP FMLs 118

Figure 4.20 Normalized BRPP values for a) Aluminium, b) 2:1 GF FML and c) 2:1 PP FML 119
Figure 4.21 Effect on MBRPP of varying processing velocity for various powers on a) AL 2024-T3 b) 2:1 Crowfoot weave GF FML and c) 2:1 PP FML. 119
Figure 4.22 Laser power against traverse velocity for laser forming of aluminium alloy and 2:1 FMLs of GF and PP 121
Figure 4.23 2:1 GF FML processed at 35W, 10mm/s, 30s dwell and graphite re-applied every 10 scans 122
Figure 4.24 AL2024-T3 processed on Nd:YAG and CO_2 laser systems at 25W 10mm/s, 30 second dwell and graphite reapplied every ten passes. 124
Figure 4.25 Peak recorded temperatures recorded at measurement point 110 125
Figure 4.26 Temperature data of single scan of 35W power and 10mm/s traverse velocity 126
Figure 4.27 CBA against number of passes for different lay-ups of both a) GF and b) PP based FMLs processed at 35W and 10mm/s 128
Figure 4.28 CBA against number of passes for a variety of lay-ups of both GF (a & c) and PP (b &c) based FMLs processed at 35W and 40mm/s (a & b) and 22W and 10mm/s (c & d) 129
Figure 4.29 CBA against percentage of formable thickness 130
Figure 4.30 Percentage of formable thickness against normalized CBA for PP and GF FMLs 131
Figure 4.31 BRPP against Number of Passes for a variety of lay-ups of both GF and PP FMLs processed at 35W 10mm/s, 35W 40mm/s and 22W 10mm/s 132
Figure 4.32 NBRPP against number of passes for a variety of lay-ups of GF FMLs and PP FMLs processed at 35W and 10mm/s 133
Figure 4.33 Bend angle against time for 2024-T3 134
Figure 4.34 Bend angle against time for pass one 135
Figure 4.35 schematic of the laser forming process showing the asymmetrical nature of the formation of the bend due to the point source 136
Figure 4.36 Variation of bend angle against time for a 1:1 GF FML 138
Figure 4.37 Variation of bend angle against time for a 1:1 PP FML 138

Figure 4.38 The variation of bend angle against time for 2:1 GF and PP FMLs 141
Figure 4.39 The variation of bend angle against time for 2:2 GF FML and 2:2 PP FML 142
Figure 4.40 The variation of bend angle against time for 3:2 GF FML and 3:2 PP FML Lay-up 144
Figure 4.41 Mean bend angle against time for various GF FML lay-ups 145
Figure 4.42 Normalized mean bend angle against time for a number of FML lay-up with glass fibre composite 146
Figure 4.43 Mean bend angle against time for various PP FML lay-ups 147
Figure 4.44 Normalized mean bend angle against time for a number of FML lay-up with PP composite 148
Figure 4.45 Bend propagation time against percentage of formable thickness 149
Figure 4.46 Thermocouple output on a 2:1 a) GF and b) PP FML 150
Figure 4.47 Thermocouple outputs for 2:1 PP FML a) parallel and b) perpendicular to line of irradiation 151
Figure 4.48 Change in bulk temperature for a) GF and b) PP FMLs 152
Figure 4.49 Change in peak thermocouple output for measurement point 102 153
Figure 4.50. Thermocouple output of measurement point 110 for a) GF and b) PP FMLs 154
Figure 4.51 Normalized thermocouple output for various laminate lay-ups with a) GF and b) PP composite 155
Figure 4.52 Propagation of the bend, transverse and longitudinal strains against time for aluminium 158
Figure 4.53 Sketch of tension/compression wave observed on sample surface due to asymmetrical formation of the bend 159
Figure 4.54 Propagation of the bend, transverse and longitudinal strains against time for 1:1 GF FML and 1:1 PP FML 159
Figure 4.55 Propagation of the bend, transverse and longitudinal strains against time for 2:1 GF FML and 2:1 PP FML 160
Figure 4.56 Propagation of the bend, transverse and longitudinal strains against time for 2:2 GF FML and PP FML 161

Figure 4.57 Propagation of the bend, transverse and longitudinal strains against time for 3:2 GF FML and PP FML 162
Figure 4.58 Normalized longitudinal strains against time on GF FMLs 162
Figure 4.59 Normalized transverse strains against time on GF FMLs 163
Figure 4.60 Normalized longitudinal strains against time on PP FMLs 164
Figure 4.61 Normalized transverse strains against time on PP FMLs 165
Figure 4.62 Cumulative bend angle verses fibre orientation angle verses fibre orientation angle for various FML lay-ups. Samples processed at 35w, 10mms^{-1} 167
Figure 4.63 CBA of 1:1 lay-up for various fibre angles normalized against 0° result 168
Figure 4.64 BRPP against number of passes for various fibre angles 169
Figure 4.65 Normalized BRPP for various fibre angles 170
Figure 4.66 Bend angle against number of passes for various fibre angles 170
Figure 4.67 Normalized bend angle against time for various fibre angles 172
Figure 4.68 Thermocouple output from measurement point 110 for a) 1:1 0° and b) 1:1 90° GF FMLs 173
Figure 4.69 Thermocouple output for measurement point 110 a) mean temperature change and b) normalized mean temperature change 174
Figure 4.70 Thermocouple output for measurement point 110 for three different sets of processing parameters 174
Figure 4.71 Number of scans verses cumulative bend angle for multiple composite layer FMLs and single composite layer FMLs, a) GF and b) PP 176
Figure 4.72 Propagation of the bend angle in time for 1:2 GF FML a) per pass and b) normalized mean 177
Figure 4.73 Variation in bend angle with respect to time for a) 1-2-1 PP FML and b) 2-2 PP FML 178
Figure 4.74 Normalized mean bend propagation for PP FMLs 178
Figure 4.75 Temperature change at point 110 a) data and b) normalized 179
Figure 4.76 Thermocouple output for measurement point 110 for PP FMLs a) variation in temperature and b) normalized against maximum temperature 179

Figure 4.77 Transverse strain recorded at pass seven 180
Figure 4.78 Longitudinal strain recorded at pass seven 181
Figure 4.79 Delamination due to over heating 182
Figure 4.80 Laser power against traverse velocity for laser forming of 2:1 GF FML 183
Figure 4.81 Delamination of lower layers of sample due to forced cooling. 184
Figure 4.82 Surface finish due to mechanical failure of the composite at x2 magnification 185
Figure 4.83 Cumulative delamination area verses velocity for various fibre orientations for the clamped and unclamped side of the sample processed at 35W 186
Fig. 4.84 Mean cumulative delamination area verses velocity for the clamped and unclamped side of the sample 186
Figure 4.85 Detail of burning of matrix at x5 magnification 187
Figure 4.86 Image of matrix failure in 1:1 0° GF FML at x40 magnification 188
Figure 4.87 Image of failure of fibres in 1:1 90° GF FML (fibres orientated vertically in image) at x10 magnification 188
Figure 4.88 Aluminium 2024-T3 as received x50 magnification 189
Figure 4.89 Laser processed aluminium 2024-T3 at X 50 magnification 190
Figure 4.90 Detail of dendritic structure at x100 magnification 190
Figure 4.91 Micrograph of irradiated zone of 3:2 GF FML after ten passes 191
Figure 4.92 Micrograph of irradiated zone of 3:2 GF FML after nine passes 191
Figure 4.93 Micrograph of irradiated zone of 3:2 GF FML after eight passes 192
Figure 4.94 Polished sample showing removal of solid solution 192
Figure 4.95 VSI images for 3:2 GF FMLs at x5 (a), x10 (b&c) and x20 magnification 193
Figure 4.96 Percentage increase in section thickness for both GF and PP FMLs 194
Figure 4.97 Localized Section Thickening in a) AL 2024-T3 and b) 3:2 PP FML 194
Figure 4.98 Radius of localized thickening for various GF FMLs 195

Figure 4.99 Schematic of micro-harness measurement set-up 196
Figure 4.100 Microhardness in Y-axis 196
Figure 4.101 Microhardness in Z-axis 197

List of Tables

Table 1.1 Degree of application potential of laser forming during the various stages of a product's life cycle 5
Table 2.1 Standard Glare grades 54
Table 2.2 Glass fibre composition 62
Table 2.3 Glass fibre properties 62
Table 3.1 Typical values of reflectivity of various surfaces to 10.64μm radiation at normal angle of incidence 86

List of Symbols

a	Measurement point off-set
A	Absorption
A_1	Area
b	Breadth of plastic zone
C_p	Specific heat capacity
d_1	Laser beam diameter
E	Elastic Modulus
F	Force
f	Volume fraction
h	Height
h_n	Height after n passes
h_0	Initial height
I	Moment of Inertia
K	Strain gauge factor
k_f	Temperature dependent yield stress
k, λ	Thermal conductivity
L, l	Length
l_1	Length of plastic zone
l_h	Length of heated zone
M	Bending moment
M^2	Beam Quality Factor
P, p_1	Laser power
s_0	Sheet thickness
s_1	Depth of plastic zone
T	Temperature
T_B	Temperature at boundary
T_c	Critical temperature for plastic flow
T_g	Glass transition temperature
t	Time

v_1	Traverse velocity
V_{in}	Voltage in
V_{out}	Voltage out
w	Width
x, y, z	Cartesian co-ordinates
Y	Yield Strength
α	Thermal diffusivity
α_b	Bend angle
α_{th}	Coefficient of thermal expansion
γ_{xy}	Shear strain in the xy plane
ε	Strain
ε_1	Strain in upper layer
ε_2	Strain in lower layer
ε_{pl}	Plastic strain
ε_{th}	Thermal strain
λ	Wavelength
ρ	Mass density
σ_A	Overall stress
$\overline{\sigma}_m$	Stress in matrix
$\overline{\sigma}_f$	Stress in fibres

Chapter 1

Introduction

1.1 The Process

The laser forming process is a non-contact method of producing alterations to a work-piece's parameters. It relies on inducing thermal stresses in the metallic work-piece to produce changes in either the membrane or through thickness strain, resulting in either a shortening of the workpiece or a bend. The method of strain production is dependent on the parameters of the incident beam and the properties and geometry of the work-piece. The process is highly flexible, as the

beam path is controllable by CAD/CAM, and accurate due to the highly controllable nature of the energy source. An advantage of laser forming is that the same laser source used for shaping the product can also be used for cutting, welding and drilling, with only a change to the processing parameters and optic path.

1.2 The Laser

The principles of how a laser works were set by Einstein in his work on the quantum mechanics of radiation, with the theory of stimulated emission [1]. The first working laser was a ruby based laser system produced by Maiman in 1960 at the Hughes Laboratory and is shown in figure 1.1 [2]. Since then a multitude of materials have found to lase but few have the level of efficiency required to be of practical use [3]. Those that do have the necessary efficiency include gases such as CO_2 [4] and solid state materials such as Nd:YAG [5].

Figure 1.1 T.H. Maiman's first laser

The laser itself consists of an optical resonator, an active medium and a method to excite the medium. The optical resonator usually consists of a mirror and leaky mirror (~95% reflectivity) facing each other and parallel. Between these mirrors is an active medium which when excited, by DC, RF or optical sources, produces a laser beam. The optical resonator allows light to oscillate between them causing a cascade effect improving the efficiency of the process.

The light produced is monochromatic and coherent in nature and owing to this has little divergence and a high radiance. The beam can be characterised by its wavelength, which is dependent on the active medium, and its spatial mode. The spatial mode is the intensity distribution of the beam and depends on the geometry of the cavity, homogeneity of the active medium and the pumping power.

1.3 The Material

Fibre Metal Laminates (FMLs) are hybrid composite sandwich structures comprising multiple layers of a thin aluminium alloy, less than 0.5mm in thickness, and alternating layers of composite material, as shown in figure 1.2. The first FML was Aramid Reinforced ALuminium Laminate (ARALL) developed at Delft University of Technology, and consists of layers of aluminium and epoxy/aramid fibres. FMLs combine the fatigue properties of aluminium alloys with vastly improved impact properties, lightness and directional strength of composites. Owing to their laminate structure they also exhibit crack bridging, which prevents catastrophic failure (of particular interest in the nuclear and aerospace industries), and flame resistance.

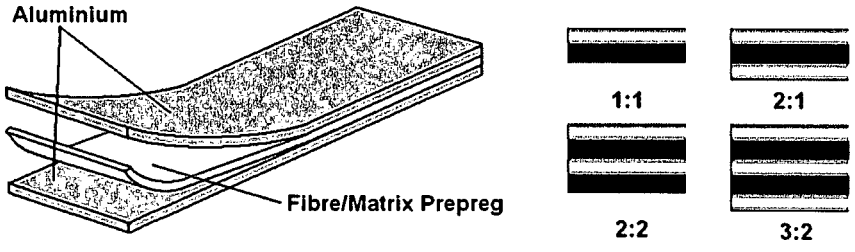

Figure 1.2 Typical Fibre Metal Laminate lay-up

A number of composite materials have been used to produce FML panels, from the initial aramid/epoxy composites, glass fibre/epoxy system commercially available as GLARE to various experimental combinations of Carbon fibre/PEEK or GF/PEI. Further work has been carried out on materials with more specialized

properties such as titanium metal layers and high-temperature composite systems for supersonic applications, and on using self-reinforced polypropylene to produce easily recyclable panels to meet manufacturers' 'end of life' commitments.

FMLs are described by a numeric code which shows the number and type of layers of both materials present: for example, a 2:1 lay-up consists of two sheets of aluminium and one composite layer. Commercial products have a slightly more complicated code, with the glare type followed by the number of layers and the thickness of the aluminium. For example

Glare 4B-4/3-0.4

is a Glare type 4B laminate with 4 layers of aluminium and 3 fibre layers and with each aluminium layer 0.4mm thick. In cases where varying thicknesses of aluminium are used the full list of individual layer thicknesses is given in the order of the lay-up, for example:

Glare 4B-4/3-0.4/0.3/0.3/0.4

Here the centre two panels are 0.3mm thick and the outer two are 0.4mm thick [6]. As stated, FMLs are a combination of aluminium alloy layers and a composite material. In this study the aluminium is 2024-T3, a common aerospace grade aluminium with good fatigue and strength properties, and two types of composite, a glass fibre epoxy resin system and a 100% polypropylene system.

1.4 Application

Any industry that requires the shaping of material has the scope for the application of laser forming. Laser forming has potential in a number of areas of a product's life cycle, as illustrated in table 1.1.

Degree of Application Potential	Stage of industrial application (Product Life Cycle)				
	Design & Development	Manufacture (processing)	Product Assembly	In-service Operation	Repair & Maintenance
High	Rapid Prototyping	Forming (Hybrid LF)	Precision Adjustment & Alignment		
Medium		Distortion & Shape Correction		On-board Automatic Correction	Damage & Distortion Control
Low		Forming (LF)			

Table 1.1 Degree of application potential of laser forming during the various stages of a product's life cycle [7]

Whilst current research includes looking at the effects of various parameters on the laser forming process, there is a marked move towards work on the control and prediction of the process and more specific application based research. The industries and applications involved can be split along two main lines, macro and micro scale. In the micro scale, and smaller, a number of specific applications are being investigated looking at in-service operation, repair and maintenance as part of a product's life cycle. At this scale large numbers of tiny adjustments are needed, varying from part to part, and the controllability of lasers therefore makes laser forming an ideal process. In the macro scale (which includes this study), where tolerances are not as fine, laser forming struggles to be cost effective against current mass manufacture techniques, such as stamping. This means that processes which require large production runs of identical parts, such as in the automotive industry, would not benefit from laser forming. However, in high-value industries with low production runs and large variability between individual products, laser forming has an advantage. The aircraft and shipbuilding industries have low volume production with great variability between parts and so the flexibility of the laser forming process has an advantage. This matches with the applications of FMLs whose light weight, superior impact properties and

relatively high cost are well suited to the aerospace industry. Whilst FML panels in this area tend to be shaped as they are cured in autoclaves, the possibility exists of using laser forming for the removal of distortion and the altering of these parts.

However the possibility for the use of FMLs in other industry sectors using the laser forming process as a method of production of complete parts also stands. Current methods for shaping flat panels of FMLs, such as stretch forming, have limitations in the geometries possible and the use of laser forming could overcome this. This would lead to greater demand for FML panels, reducing cost and opening up the scope for applications of the product.

1.5 Motivation for Study

Fibre Metal Laminates are attracting significant interest from various industrial sectors owing to their combination of impact resistance and fatigue properties at a low density. Currently processing and shaping of FMLs is limited to either shaping during the curing cycle or the processing of flat sheet by stretch forming. The shaping of panels during the cure cycle requires significant plant in the form of autoclaves and moulds to produce the desired geometry, and this has large financial implications. Also the use of moulds reduces the flexibility of the process and requires long lead times. Stretch forming is the other option for FML shaping, but the available geometries are limited; the cost of the shapers for forming the panel is also a consideration. There are two possibilities for laser forming. Entire production of FML parts has the advantage of flexibility in the final shape due to the computer controlled nature of laser processing. The ability to form complex shapes from flat panels would also allow mass production of FMLs leading to greater availability and cost reduction. The second option is for the removal of distortion from autoclave-produced panels. Given the unpredictable nature of large-scale composite structures, distortion away from the desired geometry can occur during the production cycle. Laser forming could be used to 'tweak' geometries of any misshapen panels.

1.6 Objectives

In order to investigate laser forming of fibre metal laminates a number of objectives were identified:

- To manufacture a number of FML panels using various composite materials in a consistent manner
- To identify the variables of the laser forming process and investigate the relevant areas
- To identify the variables of the fibre metal laminates relevant to the laser forming process and investigate their effects on resultant bend
- To investigate the effect of laser forming on fibre metal laminates

Chapter 2

Literature Review

2.1 Laser Forming

2.1.1 The Laser

A laser system basically consists of two mirrors, which are placed parallel to each other to form an optical oscillator, a lasing medium, which can be a number of materials although only a few have a positive efficiency, and an energy source, usually focused light in solid state lasers or DC or RF in gas lasers (figure 2.1).

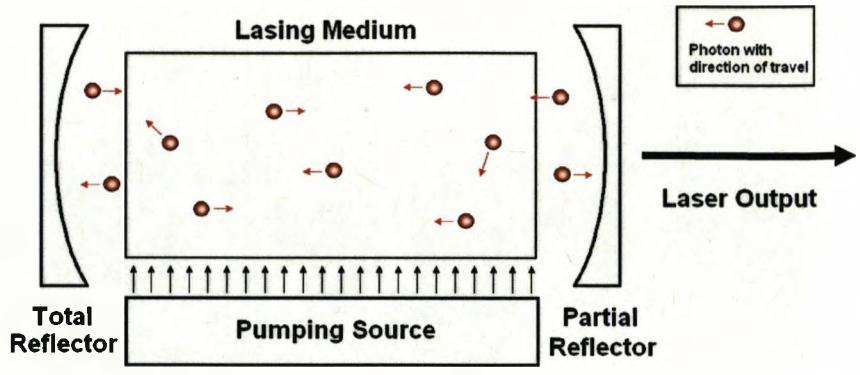

Figure 2.1 Simplified cavity schematic

When the lasing medium is pumped with energy from its respective source, molecules within the medium are excited to a higher energy state where the molecules vibrate either symmetrically, asymmetrically or off axis (figure 2.2a) depending on their energy level. In order to return to the ground state, the excited molecule emits a photon, lowering the energy level but not to the ground state. Any remaining energy is lost through radiation to the environment usually due to external cooling systems (figure 2.2b). This type of emission is described as spontaneous. These photons will travel in any direction but those which are travelling axially will oscillate between the mirrors forming the cavity. However these emitted photons may then interact with other excited molecules causing them to emit photons, which is stimulated emission. When stimulated emission occurs, photons produced in this manner are created in phase and with the same vector as the incident photon which produces a spectrally pure beam. In order for stimulated emission to occur, and therefore a laser to be positively efficient, population inversion is required. This is where a larger proportion of molecules in the medium are at an excited state than a lower energy state, increasing the likelihood of a collision and therefore stimulated emission occurring. This leads to gain or amplification of the laser power.

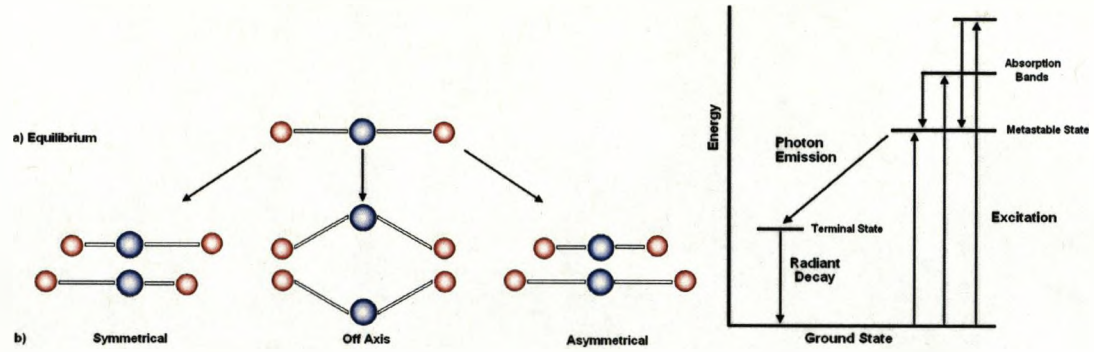

Figure 2.2 Molecular state at a) equilibrium and b) higher energy levels and generalized energy levels

As stated the lasing medium can be almost any material but only a few have a positive optical efficiency allowing a usable output. The system used in this investigation a solid state neodymium-yttrium aluminium garnet (Nd:YAG) lasing medium. Nd:YAG is a common solid state material for industrial laser systems which produces a 1064nm wavelength output. The colourless isotropic $Y_3Al_5O_{12}$ crystal, which has the cubic structure of garnet, has around 1% of its yttrium rare earth replaced with neodymium which produces within the lattice Nd^{3+} ions. When excited it is these ions which undergo the transition shown in figure 2.2 b). The Nd^{3+} ions absorb on specific absorption bands which then decay to a metastable state. It is from this metastable state that the lasing action occurs, producing the photon, when decaying to the terminal state. In order for the molecule to return to the ground state radiant decay is required. This is achieved in this laser system by a cooling system, using de-ionised water, which flows within the cavity containing the lamp and rod, cooling the lasing medium. The efficiency of the system is mainly down to the method used to pump the lasing medium. The most common technique is to use broad-band Kr flash lamps to illuminate the medium, however only a portion of the pumped energy can excite the neodymium ions as can be seen in figure 2.3 where the majority of the pumping source output wavelength corresponds to wavelengths with a low coefficient of absorption for the Nd:YAG lasing medium.

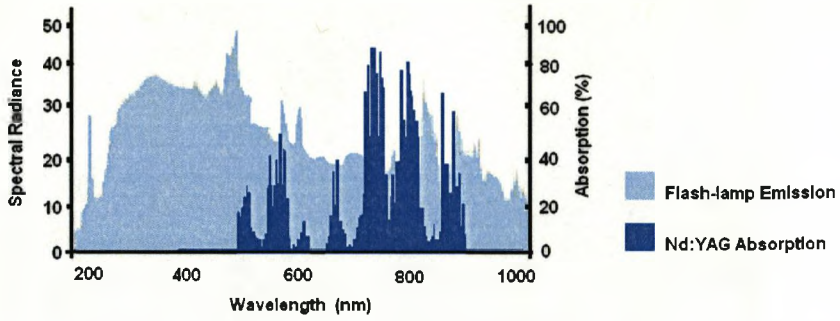

Figure 2.3 Nd:YAG absorption spectrum compared to the emission spectra of a Kr flash-lamp [3]

The light output from a lasing source has some unique properties that that are responsible for the effectiveness of the laser as an energy source. The light emitted by the laser is monochromatic, in that there is a small range of frequencies emitted by the source. This is especially useful in applications such as interferometry and holography. The light is also coherent in nature. Whilst as of yet it is not utilised in laser material processing, it is of use in measurement techniques. The light is also has limited diversion when compared to other light sources, which allows the transmission of the light of long distances with little loss and allows the focusing of the beam down to a high intensity spot. This ability to be highly focused is what is utilised in welding, cutting and drilling to give a very high energy intensity [3].

2.1.2 History of Thermal Shaping

The shaping (or forming) of metallic structures by the application of heat is a process long used in traditional heavy engineering [8]. It utilises a heat source, usually an oxy-acetylene torch, to induce asymmetrical thermal stresses in the material causing a bend to form [9]. This application has been used extensively in shipbuilding, for shaping the compound curvatures of the hull plates and the placement of fixtures and fittings such as piping, as well as large scale civil engineering projects [10-12]. Traditionally, an oxy-acetylene torch would be used by an operative of many years experience, to slowly bend the work-piece to the

desired shape. This method has a number of restrictions; firstly, due to the nature of the process it is difficult to predict the finished shape and requires many man hours of 'tweaking' by trial and error to get the desired result. The method of heat application limits the thermal gradient that can be achieved in the material and limits the level of control on the thermal input into the material. The time required for the operators to gain the necessary experience also limits the application of this method in wider industry [13].

2.1.3 Laser Forming Mechanisms

As with thermal bending, the laser forming process works by inducing thermal stresses through the thickness of the material. These thermal stresses induce plastic strains in the material that result in localized elastic-plastic deforming of the work-piece. The laser induces a constant heat flux through the surface of the material allowing the production of steep thermal gradients through the workpiece thickness. This makes thermal shaping of materials with high values of thermal conductivity, such as copper, or thin cross sections possible. The laser source is also very controllable, with the spot diameter controllable to tens of microns and the power level to the nearest milliwatt [13].

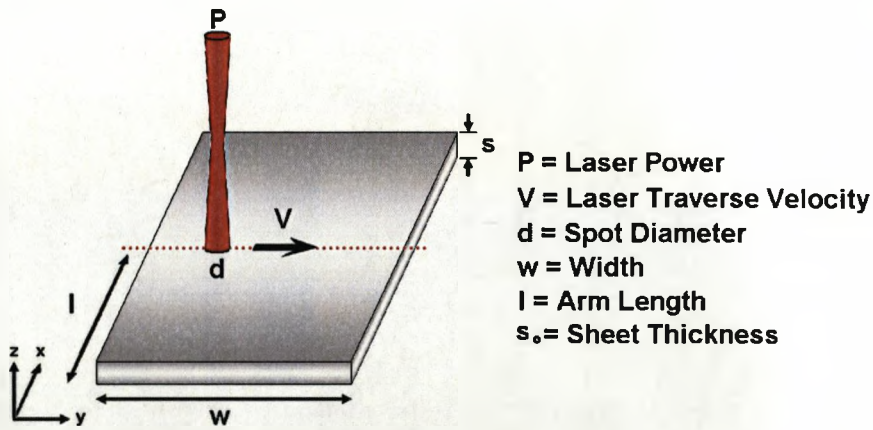

Figure 2.4 Experimental variables for laser forming

Namba [14] identified the variables indicated in figure 2.4 as well as the following parameters as affecting the final achievable bend when laser forming a material:

- Power density distribution of the laser beam
- Absorptivity of the material
- Number of laser passes
- Density of the material
- Specific heat capacity
- Thermal expansion coefficient
- Yield strength
- Young's modulus
- Poisson's ratio
- Fracture strength of the material
- Melting temperature of the material.

Depending on these parameters a number of different laser forming mechanisms can occur, as identified by Vollertsen [15]. This variation is caused by the temperature gradient produced in the material. The Temperature Gradient Mechanism (TGM) requires a steep thermal gradient though the thickness of the sample and always produces a bend towards the source. When an even increase in temperature is produced through the thickness of the material the Buckling Mechanism (BM) is active. This produces a bend either towards or away from the source, depending on the strains present in the work-piece. The upsetting or shortening mechanism occurs under similar thermal gradients as the buckling mechanism, but the part is constrained by its own geometry. This causes an overall shortening of the sample. The three main mechanisms are described below in more detail. There is a fourth mechanism, the Point Source Mechanism identified by Vollertsen, but it is not discussed here.

2.1.3.1 Temperature Gradient Mechanism (TGM)

The Temperature Gradient Mechanism (TGM) requires a high temperature gradient through the thickness of the material (figure 2.5). Typically, a beam

diameter of smaller or equal to the thickness of the sheet is required to activate TGM and produces a bend towards the laser source, as all plastic strains are produced on the side incident to the laser. The required laser parameters are dependent on the material properties. Materials with high thermal conductivity require high traverse velocities to induce the highest thermal gradient through the thickness that is possible. Slower velocities would allow deeper penetration of the thermal energy, leading to the buckling mechanism. The incident laser power is also constrained by the material properties, as too high an incident energy can lead to surface melting (which can relax the plastic strains), the activation of an undesired mechanism (due to little temperature difference between surfaces due to high values of thermal conductivity) and reduction in the forming efficiency (reducing the self-quenching effect due to excessive temperature increases). The irradiation path of the laser is incident with the bending edge.

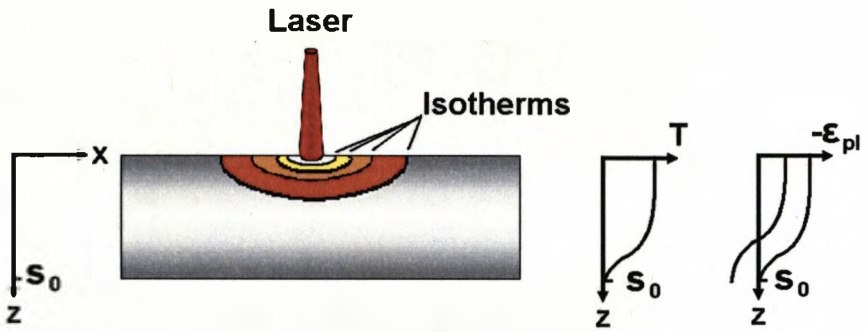

Figure 2.5 Required Thermal conditions for TGM process and resultant strains

When these parameters are met the TGM process produces a positive bend towards the source in the following steps illustrated in figure 2.6.

- Heating of the irradiated surface leading to thermal expansion which is constrained by the cold bulk of the material. (figure 2.6 a))
- Progression of thermal gradient through the thickness of the material. Thermal expansion leads to plastic compression of the surface. Counter bend may propagate at this moment if part geometry allows. (figure 2.6 c))

- Cooling of the heated zone, reduction of the elastic strains due to thermal expansion and thermal contraction. (figure 2.6 c))
- Development of the bend. (figure 2.6 d))

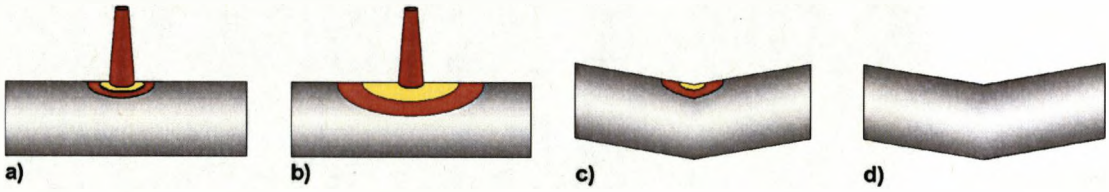

Figure 2.6 Schematic of Laser forming process

The initial step of the TGM is heating of the surface which leads to elastic strains. Were the process to be halted here the deformation would be fully recovered by the sample, with no permanent change in sample dimensions. The thermal expansion due to this heating can cause a counter bend to occur, as the surface incident to the laser has now increased in length. The amount of counter bending is dependent on the ratio of the spot size, which is relative to the heated area, to overall area of the sample. In most cases the heated area is of a small value when compared to the overall size of the work-piece and thus the forces generated are minimal when compared to the stiffness of the sample as a whole and therefore a measurable counterbend is rarely witnessed. The counter bend is detrimental to the overall bend produced as the stresses in the heated surface are relaxed. This leads to a lower fraction of the thermal strain being converted into the plastic strain which produced the permanent bend.

Further heating gives an increase in the thermal expansion and a reduction in the flow stress in the heated area. The increased thermal strains reach the yield stress of the material and any further increase in temperature results in plastic compressive strains. The yield stress is dependent on the material, the work-piece geometry and the work-piece temperature. As the temperature of the work-piece increases the yield point reduces, increasing the amount of plastic strain. When the laser source is removed the cooling cycle begins. Whereas the

thermal input was from a source outside the work-piece, the cooling occurs from within the system. The bulk of the material, unaffected but the laser, acts as a heat sink, self-quenching the heated area through conduction. Thermal losses to the environment by convection and radiation are minimal and can be disregarded. Where the heating phase was of the order of 0.5 seconds the cooling phase of the forming cycle is slower, taking 10-20s to cool the sample. As the thermal energy dissipates through the bulk of the material the elastic thermal strains that occurred during the heating phase recover, leaving the plastic strains due to compression of the surface. The final value of the bend angle depends on the coupled energy, the geometry of the part and the properties of the material. A single pass usually gives a bend rate of between 0.1° and 3°.

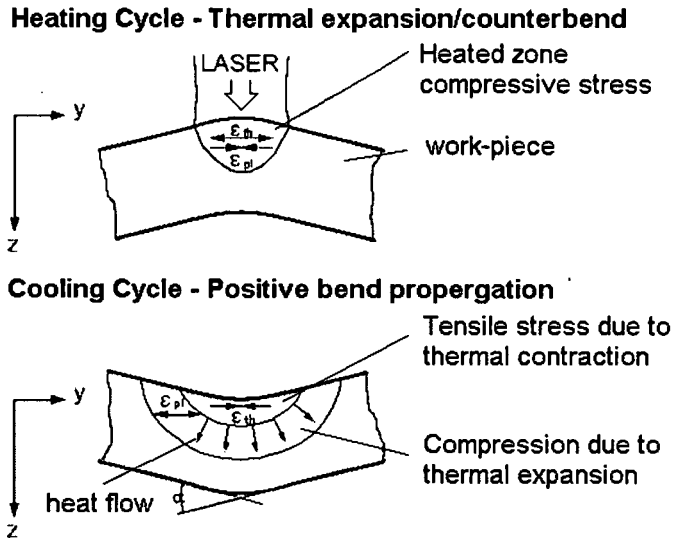

Figure 2.7 Principles of Temperature Gradient Mechanism

The reason why the thermal expansion leads to plastic compression and the thermal expansion does not lead to plastic tension of the material is due to the relatively slow cooling rate compared to the heating rate. During cooling of the irradiated area the temperature of the surrounding material sheet increases due to the transfer of heat away to the bulk of the material. The cooling occurs at a much faster rate than the material can remove the heat to its surroundings. As this whole area, including the irradiated area is now cooling simultaneously the

moments produced by the cooling only have to counter-balance the local stiffness of the part, which is much smaller than the global stiffness the counter bend has to overcome during heating. This gives nearly no cancellation of the plastic compression, created during heating, allowing large bending angles to develop. This asymmetry of the heating is essential for the development of a bending angle for this mechanism (figure 2.7).

So far this is an explanation for a two-dimensional representation of the sample cross section. In addition an explanation for the asymmetry and the effects due to that can be given from a three-dimensional observation of the sample. During heating only a small area with a cross-section equal to the square of the beam diameter is heated and exposed to thermal compressive stresses. These compressive stresses have to counterbalance the section modulus of the whole sheet and therefore the counter-bending is very small. In contrast, during cooling the whole edge of the sheet is cooling simultaneously. This is because the heating is very fast but cooling is much slower. Therefore, the moments produced by the cooling of a small section have to counter-balance the local stiffness of the part only, which is much smaller than the global stiffness during heating. So there is nearly no cancellation of the plastic compression and large bending angles can develop. This asymmetry of the heating and cooling phase is essential for the development of a bending angle for this mechanism [15].

2.1.3.2 The Buckling Mechanism (BM)

The buckling mechanism operates if the ratio of the laser beam diameter to the sheet thickness is large and the laser traverse velocity is low resulting in a small temperature gradient across the sheet thickness. It is also possible to produce the BM with other parameters, by slowly irradiating highly conductive thin foil materials with a relatively high power. The buckling mechanism proceeds by the following steps:

- Heating of a large area of the sheet metal and development of compressive stresses
- Onset of buckling
- Growth of the buckle
- Shifting the buckle through the whole sheet
- Relaxation of the elastic stresses.

The principle is shown in figure 2.8. Heating with the laser results in the thermal expansion of the material. This produces compressive stresses in the heated area due to the constraining effect of the bulk of the un-heated material. If the heated area is large enough, a small deviation from perfect flatness in the sheet creates instability. The direction of the buckling is determined by different factors, for example the pre-bending of the sheet and the relaxation of residual stresses.

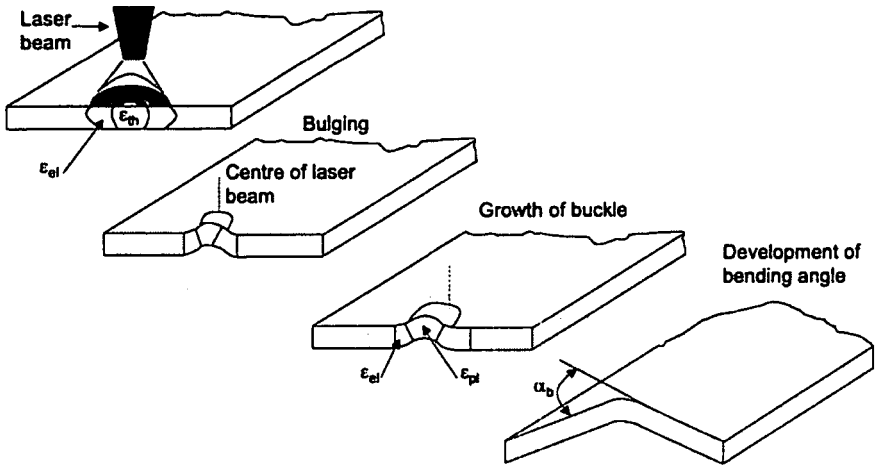

Figure 2.8 Stages of Buckling Mechanism [15]

In the centre of the buckle the temperature is very high so that the flow stress is low in this region. Therefore the bending in this region is nearly totally plastic. In contrast the root of the buckle which is far away from the centre of the beam is heated to a much lesser extent. So the temperature is low and the flow stress in

this region is high. Therefore the bending of the sheet in this region is fully elastic.

Due to further heating the thermal expansion of the material increases the magnitude of the buckle. As the laser beam traverses across the surface the buckle travels along the bending edge. Now the existing buckle predetermines the buckling direction of the remaining sheet. While the beam is traversed across the surface, the stiffness of the part is changed. At the beginning of the buckling process the bending arms were held in the original plane due to the stiffness of the surrounding material. As an increasing amount of the sheet is affected by the thermal input, the forces that hold the bending arms straight decrease. Therefore the elastic part of the buckle relaxes and only the plastic part remains in the sheet. This leads to the development of the bending angle which can be seen after irradiating the whole bending edge. After completion of the irradiation path the elastic strains are fully relaxed so that an angular section remains. The buckling mechanism results typically in bending angles between 1° and 15° degrees.

The significant increase in bend rate observed for the BM over TGM is due to the greater levels of energy that can be coupled into the work-piece in one step. Trying the same for the temperature gradient mechanism would result in either surface melting or buckling. Therefore the energy which can be coupled into the work-piece is restricted for the temperature gradient mechanism [15].

2.1.3.3 The Upsetting (Shortening) Mechanism (UM)

If the laser beam diameter is of the same order or greater than the sheet thickness, the path feed rate is low, the thermal conductivity of the material is relatively high and in addition the geometry of the part does not allow buckling of the material the Upsetting (Shortening) Mechanism operates. This is true for thick sheets (relative to length and width dimensions), extrusions and other stiff structures. The upsetting mechanism proceeds by the following steps:

- Heating of the cross section and thermal expansion.
- Further thermal expansion that exceeds the elastic limit, resulting in a plastic compression of the cross section.
- Cooling of the material without or with small tensile straining.

These steps are shown in figure 2.9. Using a low processing speed the sheet is heated nearly homogeneously through its thickness. Due to the temperature increase the flow stress decreases in the heated area and the thermal expansion approaches the elastic limit of the material. Further heating leads to plastic compression as the heated material is restricted in expansion by the surrounding material. Therefore a large amount of the thermal expansion is converted into a plastic compression. The plastic compression then remains during cooling causing the heated area to contract. Due to the low temperature gradient there is also a very small gradient in the plastic strain through the thickness.

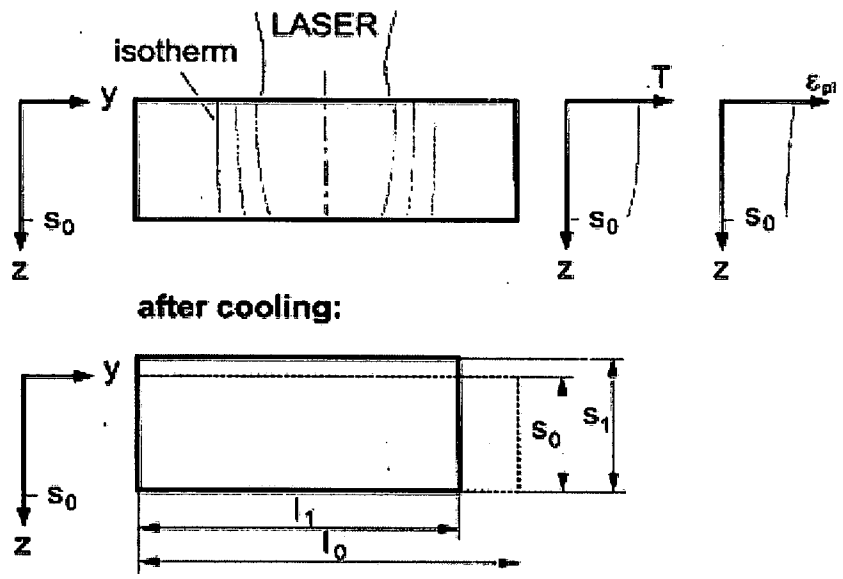

Figure 2.9 The Upsetting Mechanism [15]

The plastic compressive strain remains in the sheet for the same reason which hinders plastic tension occurring in the case of the temperature gradient mechanism. During heating the expansion is only local and is hindered strongly by the surrounding material. So the thermal expansion is converted into a plastic compression. During cooling, the cooling is active along the whole line which was heated and therefore the contraction is hindered less than the thermal expansion. This leaves nearly all the plastic compression remaining. This results in the shortening and thickening of the material. Whilst the upsetting mechanism has been described here as a separate mechanism, the similarities to both TGM (shortening due to compressive stresses) and BM (uniform temperature gradient through the material thickness) should be noted. When shaping with either mechanism it is possible, and some times necessary, to utilise UM to produce the desired shape, particularly when 3D forming using TGM.

2.1.4 Mathematical Models

Throughout the research carried out on the laser forming process a number of models, both analytical and numerical have been produced. A selection of the more important models are presented here.

2.1.4.1 Analytical Models

A number of analytical models have been developed to help the understanding of the various laser forming mechanisms and to predict the out come of laser forming. Some of the key results and concepts are outlined here.

2.1.4.1.1 Temperature Gradient Mechanism

Vollertsen and co-workers produced a number of analytical models for TGM. Vollertsen states that a complete model should take into account every possible variation from observations taken during experimentation. In the case of the temperature gradient mechanism there are four parts to consider [13].

These are:

1. The temperature field
2. The plastic strains
3. The curvature during cooling
4. The bend angle

The Trivial Model [13]

It would be difficult to produce an analytical model that takes all these variables into account. In an effort to simplify the model Vollertsen made a number of assumptions to produce a simple model of the process. These are:

- Temperature field is a step function
- The depth of the heated layer is half the work-piece thickness
- All thermal expansion in the heated layer is converted into plastic flow
- There is no straining of the compressed layer on cooling

A two dimensional representation of the process is used for calculations (figure 2.10).

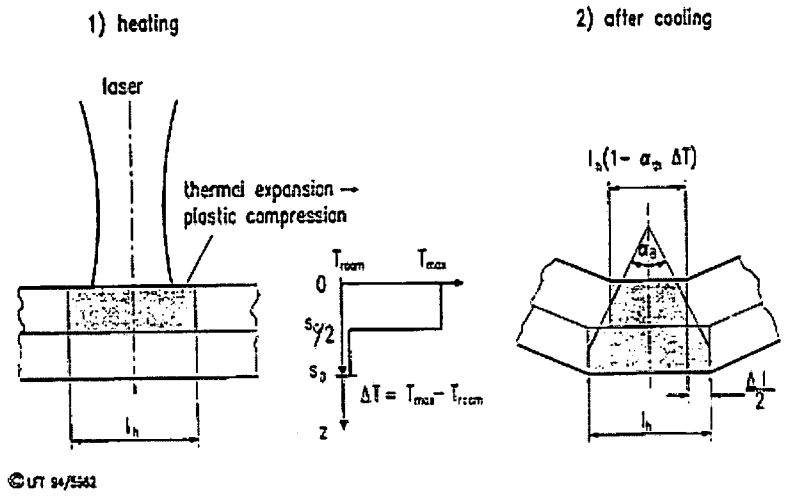

Figure 2.10 Two layer trivial model [13]

This results in the upper layer being shorter than the lower layer after processing and therefore producing a bend towards the laser. The bending angle can then

be calculated from the temperature increase and the linear coefficient of thermal expansion. The temperature increase of the upper layer is calculated from the energy approach. A similar energy approach is used for calculating the bend angle in flame bending. The resulting calculation for the temperature increase is given by the coupled power divided by the mass and the heat capacity of the material. This gives a formula for the bend angle:

$$\alpha_B = \frac{4Ap_1\alpha_{th}}{v_1 c_p \rho s_0^2} \qquad (1)$$

Two Layer models for TGM [16]

Vollertsen's two layer model continues from the trivial model, this model has been widely quoted and a number of comparative studies have been performed. The main difference between the two layer model and the trivial model is that in the trivial model the forces and moments while the sheet cools down are neglected. This is taken into account in the two layer model. The two layer model also has a variable thickness of the heated layer unlike the trivial model which assumes that the heated layer is half the thickness of the material. A two dimensional representation of the process is used for calculations. (figure 2.11) Some of the assumptions made are:

- The material properties are independent of temperature
- The heated layer is heated homogenously with no heating in the lower layer
- The thermal expansion is converted into plastic compression with no counter bending or elastic strains
- At the end of heating the two layers have the same lengths. This is because the thermal expansion is constrained by the bulk of the material.
- Forces and moments are produced during cooling

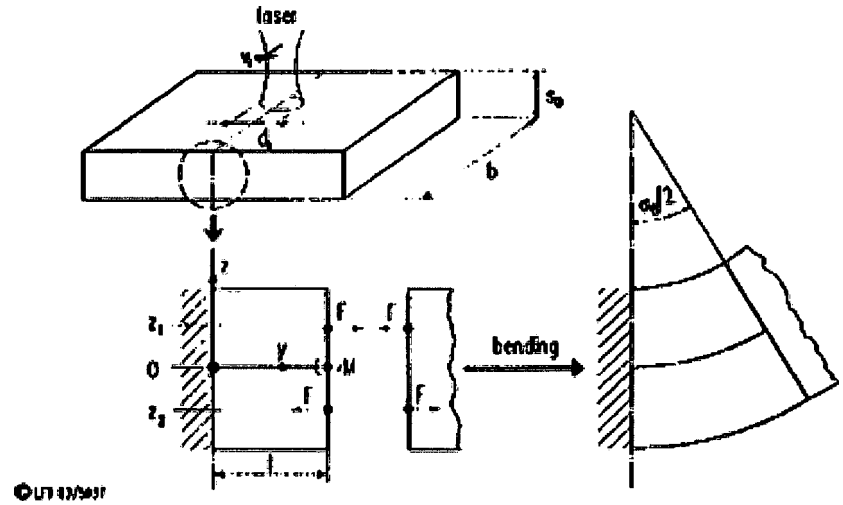

Figure 2.11 Forces and moments acting in the two layer model [17]

As with the trivial model the bending angle is calculated from geometrical considerations. The difference in strains in the upper layer, ε_1, and lower layer, ε_2, relates to the bend angle giving the following equation:

$$\frac{\alpha_B}{2} = \frac{l(\varepsilon_1 - \varepsilon_2)}{s_0/2} \qquad (2)$$

By using beam theory it is possible to calculate the strain in each layer and by considering the geometry given in figure 2.11 the strain in the upper layer is given by equation 3. This assumes that all the thermal expansion is converted into plastic compression.

$$\varepsilon_1 = \frac{F}{E_1 A_1} - \frac{M_1}{(EI)_1} z_1 - \alpha_{th} \Delta T' \qquad (3)$$

There are two differences when it comes to calculating the strain in the lower layer. The first is that z_2 is negative which makes the strain due to the moment positive. The second is that there is no thermal expansion as heating in the lower

layer is neglected in this model. This gives the following equation for the strain in the lower layer.

$$\varepsilon_2 = \frac{F}{E_2 A_2} - \frac{M_2}{(EI)_2} z_2 \qquad (4)$$

The expressions for ε_1 (equation 3), ε_2 (equation 4) and the expressions for the geometrical considerations are now combined to give:

$$\alpha_B = \frac{12\alpha_{th}\Delta T' l s_1 (s_0 - s_1)}{s_0^3} \qquad (5)$$

From this expression the temperature increase of the upper layer, the length of the heated layer and the thickness of the upper layer are unknown. It can be shown using the energy approach that:

$$\Delta T s_1 l (s_0 - s_1) = \frac{p_1 A s_0}{4 c_p v_1 \rho} \qquad (6)$$

Combining this with the previous equation (equation 5) gives an expression for bending angle which only has known parameters.

$$\alpha_B = 3\frac{\alpha_{th}}{\rho C_p}\frac{A p_1}{v_1}\frac{1}{s_0^2} \qquad (7)$$

In this work by Vollertsen [17] experimental data from other authors was presented and compared with the results from the analytical model. There was reasonable agreement between the analytical and experimental results. Although substantial improvement in the agreement between this model and experimental work was achieved (compared to previous analytical models for the flame forming process) some of the basic concepts were still omitted. The model

assumed that all of the energy was used for plastic deformation which ignored the energy used for the elastic straining.

In Yau's model [18] the two layer model approach was extended to include the counter-bending effect in order to account for some of the purely elastic straining. This modification resulted in two equations, one for the counter-bending angle and one for the bend angle at the end of the cooling cycle. The final equation for the bending angle (positive bend angle less counter-bend angle) including the temperature field equation in Yau's model is:

$$\alpha_b = 3\frac{\alpha_{th}}{\rho C_p}\frac{Ap_1}{v_1}\frac{1}{s_0^2}\left(\frac{7}{2}\right) - 36\frac{l}{s_0}\frac{Y}{E} \qquad (8)$$

Where, Y is the Yield Strength and E the Young's Modulus of the material to be formed. Comparing equation 7 with equation 8, Yau's solution includes some material and geometrical parameters which reduce the calculated bend angle compared to Vollertsen's solution. Both solutions were implemented and they differ only slightly for a single pass [19]. This is because under the conditions of the temperature gradient mechanism the counter-bending angle is very small and combined with the simplifying assumptions of the model the difference in the models is less than expected originally. Another factor in these models is that they predict a constant bend angle increase with increasing numbers of passes. It has been seen in a number of published studies that the bend angle rate falls off with increasing numbers of passes [19]. These equations do not take into account factors such as coating degradation (absorption dependent) and section thickening [19].

The Residual Stress Model for the TGM [20]

A critical assumption made by the trivial model and the two layer model is that the temperature field jumps from room temperature to a high temperature where the upper and lower layers meet. Vollertsen extended this work to include the

effects of a realistic temperature field [21].This model used the residual stress approach often used in welding analysis. Again this is based on a two dimensional representation (figure 2.12). Some of the assumptions made are:

- There is a boundary temperature; this is shown as the isotherm T_B
- There are two possible cases for the temperature field. The first is where the depth of T_B is the same or smaller than the sheet thickness and the second is where T_B is greater than the sheet thickness.
- Below the boundary temperature no plastic deformation takes place
- The thermal expansion is converted into plastic compression
- There are elastic strains. These are accounted for by subtracting them from the thermal expansion
- Thermal expansion that occurs above the recrystallization temperature does not produce added plastic strains
- The temperature field defines the plastic strain field
- This field is an elliptical shape
- Plastic strain is the source for the residual stresses which result in bending

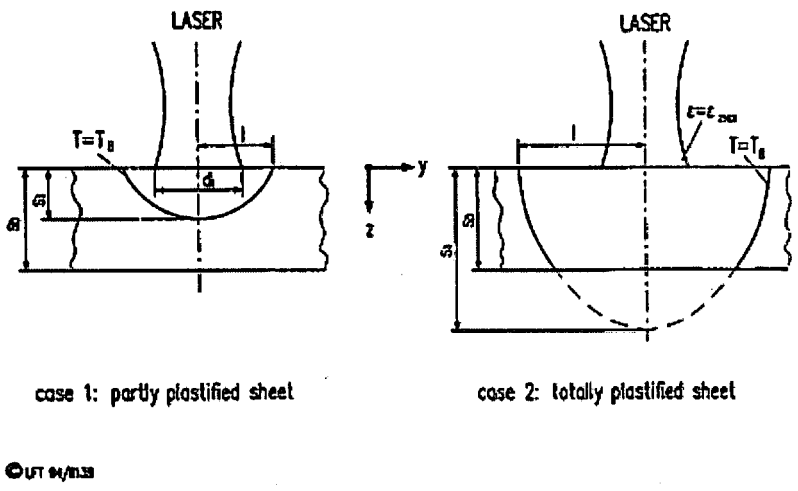

Figure 2.12 Layout for the residual stress model

As case 2, illustrated in figure 2.12, has a shallow temperature gradient, case 1, which best represents the TGM will therefore be considered here. The expression for the calculation of bend angle in case 1 is:

$$\alpha_b = \frac{\varepsilon\ l s_1}{s_0^3}(3\pi s_0 - 8s_1) \qquad (9)$$

Where ε is the plastic strain due to thermal expansion, minus the purely elastic strain during heating. If the change is temperature is greater than the recrystallization temperature, this value this is taken as the recrystallization temperature for the calculation. Plastic strain occurs if the strain due to the thermal expansion exceeds the purely elastic strain. The elastic strain is governed by temperature dependent properties, in that the flow or yield stress and Young's modulus fall as the temperature increases, thus making it easier to produce a plastic compression and hence bend a material. To calculate the bend angle the depth of the plastic zone, s_1 and the length of the plastic zone, l are required. An approximate solution in the range relevant to laser forming was used and details of this approximation can be found in the reference [22].

This model showed the importance of the thermal conductivity on the process. A slight change in the thermal conductivity changes the thermal expansion and the position of the elastic-plastic interface, as the average temperature in the irradiated zone is sensitive to slight changes in the thermal conductivity. Consequently it is possible that the bend angle itself is sensitive to small changes in the thermal conductivity. This is contrary to what was reported in the two layer model. In addition with this model the contribution of the thermal strain to the plastic bending was found by subtracting the fraction of the yield stress and the elastic modulus from the thermal expansion. As mentioned since both the yield stress and the elastic modulus are temperature dependent, this required the function which related those parameters to temperature to be known in order to calculate this contribution accurately.

Provided with accurate information about the temperature dependent mechanical properties the model can predict the bend angles with reasonable accuracy for an analytical route; this is shown by comparison with experimental data [11]. However this analytical route calculates the bend angle at the end of the process and does not describe the transient stages. Knowledge of the transient stages is useful for successful process control [19].

In analytical work by Magee [19] it was argued that the above models for the TGM, although they have advanced the understanding of the process on a rudimentary level, are incomplete in terms of practical laser forming due to gross simplifications. It was shown in this work that there are other forces and moments acting in laser forming apart from the transverse bending moments. This indicates that there should, in theory, be two bend angles in laser forming under certain conditions, the angle transverse to the direction of scanning and the angle parallel to the direction of scanning. The bending parallel to the direction of scanning has, more recently, been modelled analytically by Shuara *et al.* [23]. It is concluded that through investigation it can be found that under the TGM the plate bends about both the x and y axis. This work goes on to say that an analytical model to estimate the bend about the y axis (along the irradiation line) has also been created which approximately agrees with numerical simulation results.

2.1.4.1.2 The Buckling Mechanism [24]

In order to activate the Buckling Mechanism, a spot size of approximately an order of magnitude greater than the sheet thickness is required. The material's thermal conductivity must also be suitable to ensure a minimal temperature gradient through the thickness of the material. Using the large beam diameter results in a large amount of thermo-elastic strain which initiates the growth of an elastic-plastic buckle. The strain near the centre of the laser beam is plastic and the strain away from the centre of the beam is considered elastic in Vollertsen's model. The elastic strain is released when the laser beam traverses the exiting

edge of the sample and the plastic strain results in a curvature and a bend angle. The model is derived from the geometrical conditions (figure 2.13).

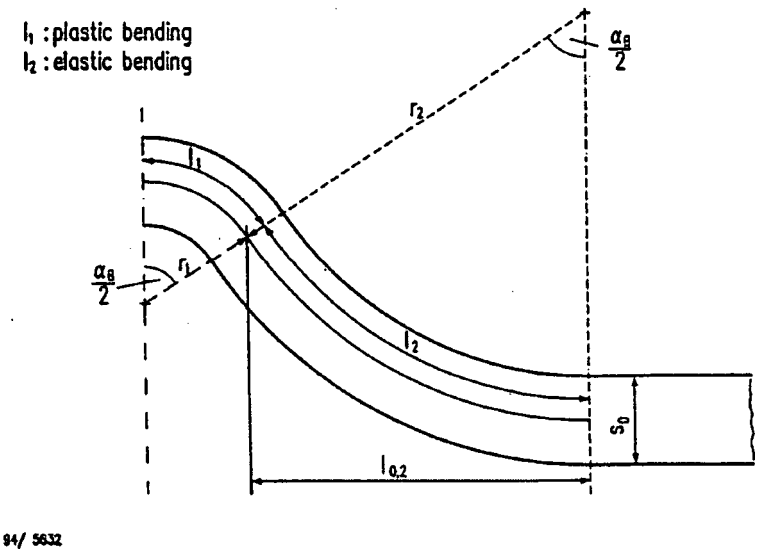

Figure 2.13 Model geometry for buckling mechanism [21]

In a similar approach to the TGM models a relationship between the geometry of the bend and the strain is drawn. The radius for the elastic region is attained from elastic bending theory and the plastic region radius as a result of the moment. The following equation was defined.

$$\alpha_b = \left[36 \frac{\alpha_{th} k_f(T_1)}{c_p \rho E} \frac{A p_1}{v_1} \frac{1}{s_0^2} \right]^{1/3} \qquad (10)$$

Of note here is the much lower dependency of the bend angle on the temperature gradient which is consistent with the buckling mechanism theory described earlier.

2.1.4.1.3 The Upsetting Mechanism

Kraus [22] has modelled box section laser bending. Using the upsetting mechanism box sections or extrusions can be made to bend out of plane by

careful selection of the sequence of irradiations. A similar approach has been used to Vollertsen's models where a geometry/strain relationship is drawn between the processing parameters and the bending angle. The final equation describing the bend angle in this case was found to be:

$$\alpha_b = \frac{1}{b}\left[\frac{2\alpha_{th} A p_1 b}{v_1 c_p \rho (2 d_1 s_0 - s_0^2)} - \frac{k_f(T_1) d_1}{E(T_1)}\right] \qquad (11)$$

The model assumed that three of the four sides of the box section were heated simultaneously to initiate the bending (figure 2.14). In reality the sides are usually irradiated sequentially. However for the purposes of an analytical model this effect would be very difficult to include. Numerical studies into the sequence of irradiations in extrusion bending have also been carried out by Kraus using finite element methods.

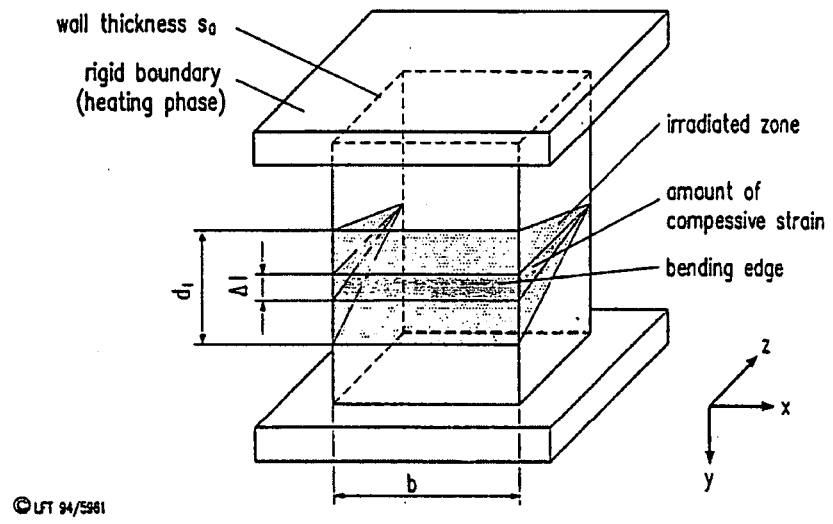

Figure 2.14 Model for extrusion bending using upsetting mechanism [15]

2.1.4.2 Numerical Modelling

In order to achieve the necessary accuracy of mathematical models the number of simplifying assumptions must be reduced. This however increases the

complexity of the models significantly which requires a numerical approach to solve them. A large number of models have been produced due to the accessibility of software such as ABAQUS and COMSOL and as no modelling is undertaken in this work a brief synopsis of the early work done in the field and some later results have been included for completeness. This is by no means an exhaustive list or summary of the multitude of approaches to the problem of modelling the laser forming process. Initial work was carried out on the modelling of the flame [9, 11, 23] and this was continued by those researching laser forming.

2.1.4.2 1 Temperature Gradient Mechanism

Vollertsen *et al.* [24] produced some of the earlier numerical modelling on TGM laser forming. A finite difference model for a two dimensional analysis of the process was developed. The model was simplified by linearly interpolating the temperature dependent variables and using the functions to relate the temperature to the material properties. The beam was simplified to a rectangle and the resultant two dimensional temperature field was used to calculate the thermal expansion, strains and stresses in the elements. Calculations were then made, taking into account the stiffness of the whole sheet, to work out the stress in each element. Where the stress exceeded the temperature dependent yield stress the elastic strains were converted to plastic strain. A loop was initiated which continued with this calculation until there was equilibrium of forces and moments. After the thermal field had finished being computed, the bending angle was calculated from the length of the upper and lower layers of an element in conjunction with the sheet thickness. This model provided a very fast means of calculating the effects of various process parameters, but the simple boundary conditions that limited this approach led to the modelling with the finite element analysis (FEA).

Another early exponent of numerical modelling was Alberti and co-workers [25, 26] who used a finite element method. A two stage approach was taken with a

temperature field produced first, which was then analyzed to produce the mechanical results. A constant decay law was assumed for the relationship between increasing temperature and decreasing yield stress. The work was also combined with laser assisted mechanical bending. Further FEA work was produced [27-29] emphasizing on the importance of different parameters have on the laser forming process. Novel approaches to the increasing complexity of these models has led to the use of re-meshing techniques [30] and dynamic explicit algorithms in place of traditional implicit models [31] in an effort to maintain accuracy but reduce computing times.

2.1.4.2.2 The Buckling Mechanism

In work by Holzer *et al. [32],* published in 1994, the buckling mechanism (BM) was modelled using the commercial finite element package ABAQUS. For this model it was assumed that the sheet was flat and free of residual stresses. The results of the model gave a convex bend away from the laser beam, as the resultant plastic strain in the non irradiated side of the sheet was greater.

2.1.4.2.3 The Upsetting Mechanism

In 1997 Kraus carried out a finite element analysis into extrusion forming [22]. Important information about the temporal development of the process resulted from this work, which could not be determined experimentally such as during the cooling phase a contraction in the irradiated zone takes place. This produces a tensile stress build up if the thermal contraction is hindered by the surrounding material and the work-piece stiffness. These stresses can reach the yield stress and a plastic restraining may occur. This effect is particularly noticeable in extrusion bending where the moment of inertia of the work-piece is high.

2.1.4.3 Current Research in Process Modelling

Current research in modelling of laser forming is concentrated in three main areas. The numerical modelling of specific processes with an eye to manufacturing, such as Zimmermann's work on micro-adjustment of optical fibre

systems [33] or laser forming of tubes [34]. Another area of interest is the improvement in the speed and accuracy of the modelling process, for example by moving mesh [35] and the final area a number of groups are working on is new analytical models which increase the speed of calculation without sacrificing accuracy [36].

2.1.5 Fundamental Investigations in Laser Forming

One of the earliest investigations into laser forming was published in 1985 by Namba [14, 37]. Experiments were carried out into the laser forming of titanium, aluminium, AISI 304 stainless steel and AISI 1045 carbon steel using a 1.5 kW CO_2 laser with a defocused beam at traverse speeds between 5 and 15m/min. It was proposed that a steep thermal gradient was produced resulting in thermal expansion, thermal stresses and plastic deformation. Namba described the following parameters as affecting the bend angle [14]:

1. Incident laser beam power
2. Laser beam diameter
3. Power density distribution of the laser beam
4. Absorptivity of laser beam on a material surface
5. Scanning speed of laser beam
6. Number of repetitions of laser beam scans
7. Density of the material, specific heat capacity of the material
8. Thermal expansion coefficient
9. Yield strength
10. Young's modulus
11. Poisson's ratio
12. Strain hardening coefficient

13. The dimensions of the work-piece
14. The melting temperature of the material and the fracture strength of the material

In 1987 Scully [38] determined that the positive bend angle can be calculated using a relationship taken from earlier work by Masubuchi *et al.* [39] on flame forming. This is given by equation 12

$$\alpha_b = \frac{p_1}{s_0\sqrt{v_1}} \qquad (12)$$

Later work by Vollertsen also shows that there is a strong linear dependence of the bend angle on the laser power and processing speed [15]. Vollertsen is credited with producing a considerable amount of the early fundamental research on laser forming. Some of the key results and conclusions drawn from this research are discussed here. In the experiments carried out relating to processing speed dependence, a power law was assumed between the bend angle and the processing speed. A linear dependence was obtained for 3.5mm mild steel sheet with scanning speeds in the range of 7-70 mm/s, the gradient was found to be -0.63. A negative slope was to be expected as an increase in laser traverse velocity will relate to a reduction in the coupled energy and therefore a reduction in the achievable bend angle. However at lower traverse velocities it was found that this is not the case and the bend angle continues to increase up to a point with increasing traverse speed. This behaviour may be caused by the reduction of the steep temperature gradient due to the decrease in laser traverse velocity. Ultimately an increase in speed results in a greater difference of the plastic strains between the upper and the lower layer of the sheet and therefore a larger bend angle per unit time can be achieved. If the laser traverse velocity is increased to a high value then the temperature rise that the work-piece undergoes will be relatively small, leading to minimal plastic

strains occurring. Vollertsen also introduced a concept of a threshold energy level for the laser forming process to occur as below a given energy input only elastic deformation occurs.

The importance of the thermal conductivity of the material is also discussed, its importance in the development of the temperature field produced and therefore the mechanism produced and the level of strain. Vollertsen identified that materials with high thermal conductivity would be difficult to produce the TGM in, as the temperature gradient through the thickness would be shallow. Another important variable identified by Vollertsen is the relationship between thickness of the work-piece and the development of the bend angle. The bend angle is related linearly to the inverse of the square of the sheet thickness for the temperature gradient mechanism [15].

Other geometrical effects have also been identified, both in laser forming research and earlier flame bending work. Suhara [23] states that the length of the bending edge is also of significance for the development of the bend angle. If the length of the bending edge is increased from 5 to 13 mm then the bend angle is increased by a factor of 3. This is due to the changing section modulus with changing length and the difference in the temperature field due to the change of length in the lateral direction.

Another factor influencing the bend angle is the length of the bending leg. If the bending leg is short then the cooling of the work-piece is restricted to one side and the temperature gradient decreases and hence the bending decreases. If the bending leg is long then the gravitational forces acting on the length will reduce the bend angle accordingly. The load on the work-piece due to the bending leg results in a tensile stress on the surface reducing the compressive stresses.

Secondary geometrical effects were reported by Scully *et al. [38]*. In this work less distortion occurs near the edges of the plates. This is because the heat flow

pattern is altered in comparison to the innermost part of the plate where the heat flow is to surrounding material. This results in less distortion near the edge of the work-piece. This was also attributed to the rigidity of the plate becoming non symmetric near the plate edge.

For multiple passes both Scully [38] and Masubuchi [39] reported a linear relationship between the number of passes over an identical track and the resultant bend angle. In later work this linear relationship of the bend angle on the number of passes was not found to be true for a range of materials. Sprenger [40] showed that there is a decreasing bend angle rate with increasing scans due to the strain hardening of the material (figure 2.15).

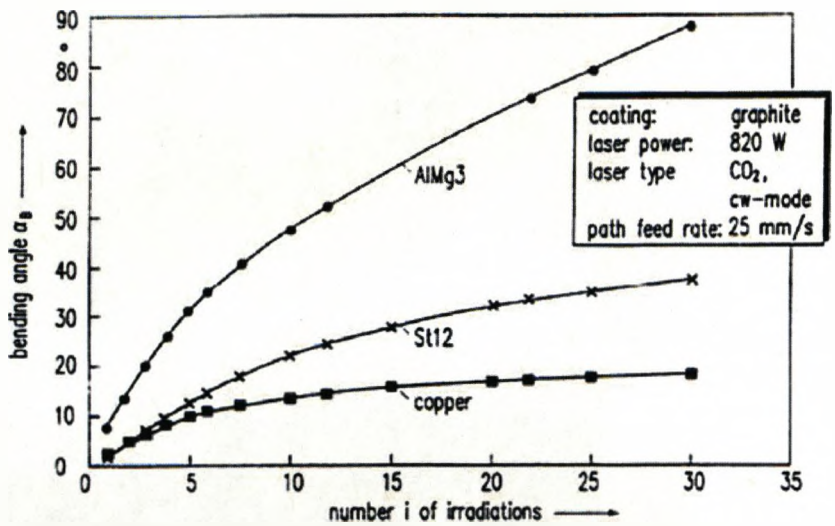

Figure 2.15 Decreasing bend rate with increasing scans over identical track [39]

Two main reasons for this were discussed as possibilities for this, the effect of the change in thickness along the bend edge and effect of strain hardening of the material. The effect of the change in thickness along the bend edge is due to the thermal expansion, which is converted into plastic deformation, and is not cancelled out during cooling. This results in a bend angle. Because the material has thickened due to the plastic compression altering the modulus of the section

and the same laser parameters are used for subsequent scans the angle achievable decreases each time. The other possibility is the effect of strain hardening of the material. In materials with a large strain hardening coefficient and which are relatively thick it has been shown that the cold working of the underside of the sheet contributes significantly to the decreasing bending rate [40].

2.1.6 Previous Experimental Work

2.1.6.1 Macro Scale

The majority of research in laser forming has occurred in the macro scale, with a large number of publications covering a variety of topics. Some of the more important are discussed here.

Mucha *et al.* [41, 42] showed that the distribution of the incident energy has an important effect on the laser forming process. By comparing circular and rectangular beams it was shown that for the same parameters a bend angle of 1.3 to 2.5 times that of a circular beam was produced when using a rectangular beam. An extensive analytical model was also presented and it was argued that the dimensionless form of the derived dependencies would be a useful method of selecting processing parameters for any material. Later work has concentrated on efficiency of the laser forming process with respect to a number of dimensionless parameters; surface temperature, Fourier number and the ratio of beam width to sheet thickness.

Large amounts of work in the field of laser forming are being produced in China. In particular the Harbin Institute of Technology has published a number of interesting studies. Liqun *et al.* [43, 44] have produced work looking at the effect of varying the method of cooling the work-piece and the effect that has on the laser forming process. A number of methods were investigated and it found that the use of an effective cooling method increased the possible temperature gradient achievable through the thickness of the material. However forced

cooling had a number of downsides with a reduction in peak temperature achieved and therefore a reduction in the plastic strains. An additional detrimental effect was to cause unwanted metallurgical effects such as increased hardness. Further work identified the factors influencing the bend angle fall off observed with multiple pass irradiation strategies. Whilst the results had been witnessed and reported in previous work [13, 45], the key results identified the thickening effect to be a cause of the bend rate drop. It was also identified that the tensile strength of the samples decreased as the number of passes increased, ruling changing tensile strength out as possible cause of the bend rate drop.

Macro scale research carried out at the Laser Group at the University of Liverpool has mainly consisted of works by Magee [19] Edwardson [46] and Abed [47]. Magee [19] carried out a selection of empirical studies concentrating on AL2024-T3 aluminium alloy and Ti6Al4V titanium alloy. Parametric studies were carried out into the single and multi-pass, large and small beam diameter 2D laser forming of these materials. Also developed was a laser forming demonstrator consisting of a 2D formed part cylinder and initial studies into the irradiation paths required for 3D forming. The studies found that for the titanium alloy both large and small beam diameters produced a TGM due to the low thermal conductivity of the material. An optimum traverse velocity was identified when the beam size was of the order of 12 times the thickness of the material. The aluminium study found that for low traverse velocities a BM was induced where as at higher velocities a TGM process was prevalent. A relationship between the reduction in bend rate on repeat passes was previously attributed to strain hardening of the material [48] and a change in the absorption of the laser energy as the number of scans increased. However this study concluded that the thickening effect observed was of greater significance [19].

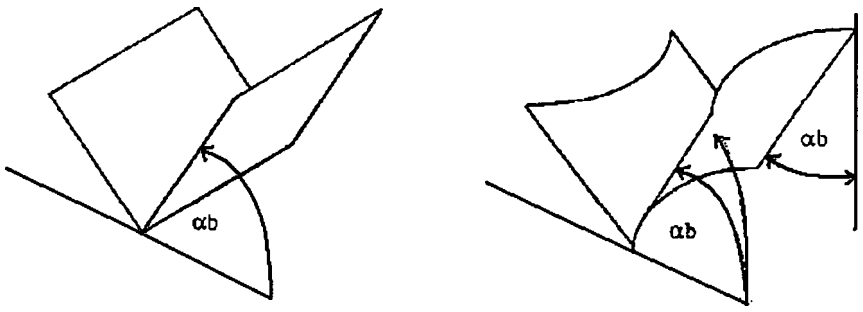

Figure 2.16 Ideal bend angle and exaggerated edge effect [48]

Also investigated was the edge effect, illustrated in figure 2.16. This effect is attributed to the changing mechanical restraint which restricts the thermal expansion of the heated zone. The effect is also attributed to thermally dependent material properties and contraction in the laser traverse direction. The effect could be minimized by reducing the energy input at the edges of the sample. Later work on the edge effect by Bao *et al.* [49] and Gopal *et al.* [50] furthered work on this phenomenon. Bao successfully numerically modelled the effect with some base assumptions and Gopal successfully controlled the effect by varying the laser parameters.

In an effort towards demonstrating the effectiveness of laser forming as an industrial process a part cylinder of 900mm radius was formed out of 2024-T3 aluminium using a CW CO_2 laser system, CNC tables and 3D CAM measurement system [19]. The system relied on user intervention to identify a number of variables such as next scan pattern, next starting point and direction of scan, clamping location and level of energy input. With this input it was possible to create a part of acceptable quality. A number of 3D scan patterns to produce a dish were identified and the following points drawn to achieve a smooth symmetrical shape.

- Geometrical symmetry should be reached as soon as possible after the initial irradiations

- A symmetrical temperature distribution over the plate surface should be realized
- Any pre-orientation bend should be avoided
- The laser beam parameters, particularly the irradiation angle of incidence and the irradiation spot diameter, should be held constant

Magee also carried out a metallurgical study into the effects of laser forming of the aluminium and titanium alloys and these findings are more fully discussed in the relevant section.

Edwardson [46] carried on the work started by Magee. A number of empirical studies were carried out on mild steel (CR4), titanium (TiAl4V) and aluminium (AL 1050 and AL6061 0/T4/T6) of various thicknesses from 0.9 to 1.6 mm. The process maps for each material were ascertained for various beam diameters, laser powers and laser traverse velocities. These revealed the unique forming characteristics of each material and concluded that the thermal conductivity, material strength and material thickness were the major factors that result in variation of the bend angle achieved. It was also found that TGM could be activated with a beam diameter larger than the thickness of the sheet being formed. The effect of the time between passes was investigated and it was found that to improve the efficiency of the laser forming process a balance was needed. Too long a pause between scans led to an increase in bulk temperature which reduced the ability to self quench and the thermal gradient and too short a pause did not reduce the flow stresses present. It was also found in the case of the aluminium samples studied that the heat treatments had an important effect on the formability of the aluminium. Thermal analysis was carried out and this showed the effect the various forming strategies had on the peak temperature achieved and the rise in bulk temperature. It was found that the process stabilised when the losses to the environment balanced with the heat input per

pass. A metallurgical study was also carried out and is discussed in the relevant section.

Edwardson also initially investigated the possibility of laser forming fibre metal laminates [51]. Tests were undertaken on a 1.2kW CO_2 system with a work-piece size of 40x80mm. A number of thicknesses of aluminium were used (0.3 to 0.9mm) and a number composites including self-reinforced polypropylene and a number of glass fibre reinforced thermosetting composites. Edwardson found that it was possible to activate TGM in the top layer of aluminium and then use this to mechanically form the lower layers. Using TGM through the thickness of the material led to buckling and failure of the composite layer. Edwardson also found that increasing the number of layers in the laminate lay-up and varying the direction of the fibres in the laminate reduces the achievable bend angle. Also identified were number of material failure modes. Aluminium failure due to excessive heating was encountered as were a number of failures of the composite material. These included delamination due to failure in the bonding layer to burning of the composite due to excessive heat input.

In other work a system was presented that could produce accurate bends using closed loop control for 2D laser forming of two materials, 1.5mm mild steel and 0.9mm AL1050 - H14. The factors considered essential for control of the process were:

- The current bend angle
- The difference between current and desired bend angle
- The current bend angle rate or bend angle increase per pass
- Selection of a bend angle rate per pass so as to avoid overshoot (when the bend angle difference between current and desired angle is small, i.e. bend angle rate should be less than or equal to the required deformation)

3D laser forming work carried out consisted of an empirical study and the development of a Matlab system for a geometry based model for automated 3D laser forming. A number of different techniques were applied, such as Bezier surface patch technique and contour lines of constant high, and found to give acceptable results for the production of 3D laser formed shapes [46].

Abed [47] carried on the development of 3D forming, looking at the effects of geometrical influences on the laser forming process. Of particular note was work on the effect of the clamp on multi-pass forming. It was concluded that the method of clamping had an effect on the final bend angle achieved and the bend rate per pass. Also that as the bend angle increases the area of the beam is distorted, reducing the energy density and therefore reducing the efficiency of the laser forming process. A 'V-clamp' was used to investigate this and it was found that after 25 passes no reduction in bend rate per pass was observed confirming the geometrical effect on the beam due to bend angle of the sample. Abed also identified that post heat treating of laser formed parts produced no significant change in geometry of the parts and the distortion that did occur was due to the relaxing of residual stresses. After the effects of annealing, which resulted in minimal distortion, no further effects of post forming heat treatments were observed that are linked to the laser forming process. A significant proportion of Abed's work concentrated on the development of a geometric model for the closed-loop production of laser formed parts.

2.1.6.2 Micro Scale

Chan and co-workers at The Hong Kong Polytechnic University investigated the possibility of laser forming AISI 304 stainless steel sheets in two dimensions [52]. Sample thickness of 0.25, 0.5, 0.75 and 1mm were processed using an Nd:YAG source with no surface preparation or coating to improve absorption. Investigations into the effects of varying power and velocity were undertaken and they concluded that bending angle was almost linearly related to the number of

irradiations. A minimum heat input value was identified and a simple model based previous flame bending work was also presented.

In work by Yoshioka *et al.*[53, 54] has investigated the forming of thin foils using low power diode lasers and have developed a method for reducing the unwanted distortion they observed. A sample was held in place using a glass plate over it, the sample was then irradiated through the glass and not allowed to deform asymmetrically. Once the glass plate was lifted after processing, the part sprung into the desired shape, thus eliminating any asymmetric or temporal effects. For more complex shapes a mask was used to hold the sample down during processing.

Dearden *et al.* [55, 56] processed mild and stainless steel materials from 0.075 to 0.2mm thick using a low power Nd:YAG source. It was found that at lower speeds the buckling mechanism was activated in both thicknesses of material whilst increase in velocity led to the temperature gradient mechanism. On the thicker material (0.2mm) the temperature gradient mechanism was easier to activate with a larger range of parameters than the foil material. Thermocouple investigations showed the progression of the thermal field to be similar to those found in macro scale forming. Strain gauge work was also undertaken and it was identified that a number of passes were required to 're-write' the residual strains before a repeatable strain cycle was observed. A tensile/compression wave was evident around the beam. Also identified were a number of scan strategies to produce various three dimensional shapes such as saddles and pyramids. However significant distortion was observed and this was accounted to the considerable residual stress present in the thin section foils from production.

Bartkowiak *et al.*[57] also furthered this work into non ferrous materials. Alclad 2024-T3 and Brass (CuZn30) were processed at a variety of laser parameters with laser paths which produce both two dimensional and three dimensional deformations. Overall the effects witnessed in the ferrous materials were present

here, with the bend rate dropping off as the number of passes increased and the type of mechanism activated depending on the level and method of energy input. A level of microsturctural effect was observed in the Alclad aluminium with a reduction in microhardness and some melting of the surface. The brass sample underwent little or no microsturctural changes, which was attributed to the high thermal conductivity of the material preventing the necessary temperature rise.

More recent work in the area of thin section forming has covered the modelling of the process. A number of sources are looking at Finite Element Analysis of the process [20, 58]. This will allow a greater understanding of the process and lead to the application of this process in an industrial area.

2.1.6.3 Non Metallic materials

A number of non metallic materials have been laser formed. Gartner *et al.* at Chemnitz and Mittweida Universities in Germany have laser formed wet etched silicon microstructures [59, 60]. The previous method to shape silicon requires the samples to be heated to >700°C and use a specially designed tool to alter the sample. By using a 5W Nd:YAG system it was possible to produce bends of up to 22° with multiple passes (figure 2.17).

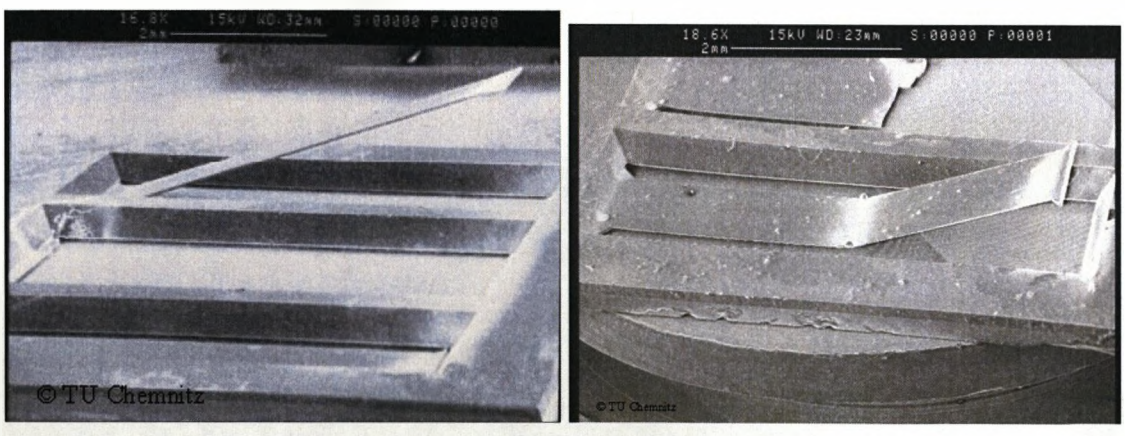

Figure 2.17 Laser forming of 50µm thick wet-etch silicon samples [59, 60]

The laser forming of plastic (HDPE) has been investigated by Okamoto and co-workers at West Japan Railway Co in Osaka. The method was to apply a black resin to the surfaces to be altered by laser forming which absorbed the laser wavelength. The thermal energy was transmitted through to the material and a bend produced using TGM. The very low power laser (0.5W) irradiates the surface for a relatively long time (5s) and produces bend per pass values similar to that of metallic structures. Current work is on the effect of the irradiation path and how this varies the result achieved [61-63].

2.1.6.4 Micro Adjustment

A great deal of microscale thermal forming has occurred in the area of precise adjustment of parts too small or fragile to adjust by traditional methods. Hoving [64] undertook pioneering work with Philips by using the Shortening or Upsetting Mechanism to align various electrical components.

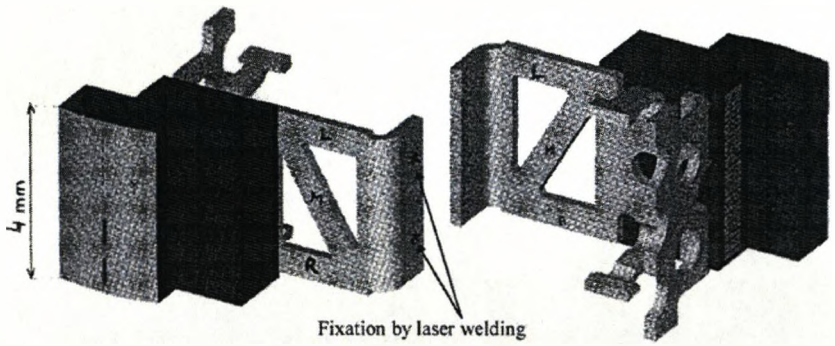

Figure 2.18 Image of audio head for Digital Compact Cassette head with special carrier for laser forming alignment [64]

An early reported use was the adjustment of Digital Compact Cassette audio head which used a special carrier (figure 2.18) to adjust the positioning. By activating the upsetting mechanism in the indicated places it was possible to align the head by a few micro or milli degrees at a time. The next application of laser forming for electrical micro-alignment was the adjustment of reed switches. Here a 30W CW Argon laser and TGM process was used to adjust the 50 micron

gap between two nickel iron reed heads to within customer demands, which led to much lower rejection rates. The third application took the special carrier for the DCC audio head and developed it for a greater level of control. A number of different designs of actuator to control the alignment of audio compact disc systems optical train were investigated. The 'Basket Ball Basket' (figure 2.19) was found to be the best for manipulation giving microns of either membrane or out-of plane adjustment [65].

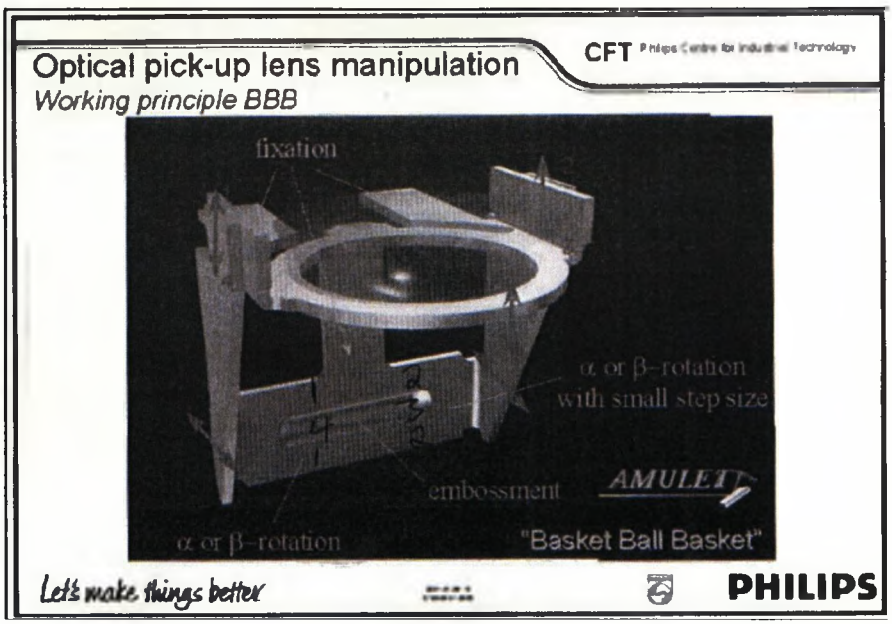

Figure 2.19 Actuator for CD lens adjustment by micro laser forming [65]

Tam *et al.* [66] at IBM Almaden developed and implemented a novel micro-bending technique in manufacture called Laser Curvature Adjust Technique (LCAT) for adjusting the curvature of magnetic head sliders in a hard disk. This development addressed a need for precise and highly controlled adjustment of the positive camber curvature of a slider, to improve its tribological properties and allow reduced flying heights (below 25nm) above the disk surface to provide increased disk storage density. The LCAT process induces surface stress changes in the alumina-based ceramic by the scribing of microscopic patterns on the reverse of the arm. A numerical investigation into the adjustment of hard disk

suspension was investigated by Zhang *et al.* [67]. A three dimensional model showed that an accuracy of 0.1° could be achieved over scan lengths of 50 to 200μm using a 20W laser source.

The use of microforming for adjustment is being developed in the alignment of optical fibres to micro-lenses by Zimmermann *et al.* [33]. Here a 10W Nd:YAG system uses 10ms pulses to align a number of fibres in large arrays to the nearest micron. Other groups are also researching fixtures for microalignment [68-70]. The advantage of this non-contact adjustment is the ability to carry out flexible and efficient adjustment of sensitive components in the final stages of production. A further possibility is on-board adjustment of components whilst in service by mounted diode lasers with the necessary feedback control.

2.1.6.5 Material and Metallurgical Studies

In order for laser forming to be a viable method in manufacturing, the effects of the process on the materials are needed to be known. A number of material and metallurgical studies have concentrated on this area. Initial metallurgical work has been mainly carried out on steel [38, 45], both mild and stainless in a variety of thicknesses. Later work has particularly concentrated on aluminium alloys, but has included materials such as titanium alloys [71-73], aluminium-matrix composites [74], chromium [75] and other non-ferrous materials [57]. Studies into the material properties have covered mechanical properties such as fatigue properties [76] and fracture toughness [77], as well as post-forming heat treatment [78] and corrosion resistance [79].

Results reported by Thompson *et al.* [45] on laser formed mild steel show that laser forming increases the yield strength of the area local to the irradiation path, but not the bulk of the material. However a loss of ductility was also found, making laser formed parts unsuitable for areas requiring such properties or for large amount of subsequent manual shaping. Overall it was likely that laser formed parts are likely to perform at least as well as conventionally formed

equivalents. Edwardson [46] found that the effects of LF on the microstructure of mild steel are subtle when there is no obvious melting. Hardness values do increase with increasing numbers of passes and the largest increases were observed near the mid and lower sections of the plate thickness consistent with a cold working or strain hardening effect. Thin section mild steel forming was investigated by Bartowiak [56] and these findings showed an asymmetrical heat affected zone. This was explained by the geometrical effect of high angle of bend which are produced with this section material. Recrystallization was present and the microstructure was re-transformed into equiaxed grains.

Work by Shackle *et al.* [72] from UMIST concentrated on the effects of forming Ti6Al4V (Ti64) titanium alloy. It was found by optical microscopy, FEGSEM and TEM methods that after laser forming, oxygen uptake caused by processing in air, contributes to the formation of an alpha case and an increase in microhardness on the upper surface. To avoid this it was concluded that processing should be carried out in an inert atmosphere, such as argon. Work on titanium alloys by Magee [19] supported these findings

A tensile test on the LF samples was also reported, it was found that during tensile deformation the higher hardness of the HAZ acted as a local constraint on plastic deformation and failure always occurred in the parent material away from the irradiated area. The bulk tensile properties of the Ti64 sheet consequently remained relatively unaffected by the LF process. Studies in other alloys of Titanium [71, 73] also confirmed the viability of LF with these materials.

Magee [19] carried out a metallurgical study into the implications of the laser forming process on Alclad aluminium alloy 2024-T3. It was concluded that in order to apply laser forming to aerospace components it is necessary to restrict the process parameter envelope to a range which does not adversely affect the metallurgical or mechanical properties of the alloys. In the case of the aluminium alloy the as received microstructure could be maintained when an Average

Energy Density (AED) of less than 25 J/mm^2 was used for forming. At higher AED recrystallization occurred and at extremes (greater than 133 J/mm^2) a cast dendritic structure resulted from melting underneath the Alclad layer (a pure aluminium clad layer on the surface of the alloy to improve corrosion resistance). A fluctuation in the microhardness level around the as received value was found in samples processed at AED less than 25 J/mm^2. This oscillatory nature can be explained by the recrystallization and precipitation theory for this alloy.

In work by Edwardson [46] a metallurgical investigation was conducted on laser formed 1.6mm AL6061 in three different tempers, O, T4 and T6, to ascertain some of the effects of laser forming on the structure and mechanical properties of the materials. The optical microscopy of the laser formed AL6061 revealed only subtle changes to microstructure across the three tempers investigated. A possible precipitate coarsening was observed in the upper surface area after 5 passes in all of the heat treatments. These were found to revert back to the original microstructure after 30 passes. This was attributed to coating loss which limited the amount of energy coupled into the surface reduced significantly after 10 passes. Hardness tests on the laser formed AL6061 samples revealed additional effects on the metallurgy. For the O condition little effects on the hardness were observed for increasing numbers of passes. For the T4 and T6 tempers it was observed that up to 10 passes there was a decrease in the average hardness within the heated area. From 10 passes up to 30 passes there was somewhat of a recovery in the hardness values.

Work on aluminium and aluminium alloys by Merklien *et al.* [80, 81] at the University of Erlangen revealed the microsturctural development and mechanical properties in laser formed AL1050 and an AL6082 in two heat treatment conditions T41 and T61. The work was conducted on 80mm wide 1mm thick samples using a 1kW CW Nd:YAG laser and SEM and TEM methods were used for analysis. Changes in the mechanical behaviour as well as in the microstructure were observed. The soft and annealed AL1050 showed hardening

due to the LF process. This was proved by hardness tests and by SEM/TEM images showing the dislocation motion and changes in microstructure. For the two heat treatments of the AL6082 there were little or no differences in forming characteristics over a number of irradiations found between them. For the artificially aged T61 alloy, the hardness produced by ageing is lost in the HAZ and immediate area after LF and is comparable to the naturally aged T41 values. For the T41 alloy only a slight decrease in hardness is observed in the HAZ.

2.2 Fibre Metal Laminates

2.2.1 History of development

The development of Fibre Metal Laminates (FMLs) stems from work at the De Havilland aircraft factory who were the first to bond metal parts [82]. During research into producing wood laminates, which the manufacturer was famous for using, the metal plates used to apply heat and pressure became adhered to each other. De Brunije used this information at De Havilland, to start using metal bonding in aircraft construction [83]. The aircraft producer Fokker took the next step. After 1945 there was a lack of expensive milling equipment available to produce new aircraft, so Fokker took advantage of the experience of an engineer, Rob Schliekelmann. Schliekelmann had experience of working with laminate structures at De Havilland so Fokker built the new F-27 (figure 2.20) using a built up laminate structure. This had a two fold advantage, expensive milling operations were not required and the laminate structure could be tailored to provide strength applicable to the local requirements.

Figure 2.20 Fokker F-27 Friendship

Research by the Dutch National Aerospace Laboratory discovered another advantage to this process. While carrying out fatigue tests on the F-27 centre wings it was found that the laminating process helped retard fatigue crack growth. Where fatigue cracks occurred in the metal layer, the surrounding sheets provided a bridging effect, slowing the propagation of the cracks and preventing catastrophic failure.

The addition of composite materials to the laminating process occurred in the 1970's. Composite materials were being investigated around the world, but high costs of the composite materials led to a combination of metallic/composite test structures in an effort to reduce costs of research. British researchers were applying composites to rods, tube and beams in order to compare them with monolithic materials. US researchers were using composites to lighten metallic structure and therefore saving weight without having to resort to an entirely new material and the costs associated with that. It was these tests that Schliekelmann's co-workers observed at the end of the seventies and led to the addition of aramid fibres to the adhesive bonding of the metallic structures. These structures were tested and while the results were technically interesting, they were not spectacular and the addition of fibres led to inherent durability and production problems.

It was from this, and further work at Fokker, that Delft University of Technology started to optimise the material. It had become clear that fatigue in the fibre-reinforced metal laminates was a delicate process. Evidently, loads from the cracking metal layers were transmitted via the adhesive to the fibres, thus unloading the metal layers and slowing down crack growth in these layers – 'fibre bridging' [82]. Another phenomenon was observed, that of delamination of the laminate structure. Initially thought to be detrimental it was found that it protected the fibres from failing with the aluminium, slowing the crack propagation. After further research including an analytical model on fatigue crack growth a number of companies were approached with regards to commercializing the product now christened ARALL (Aramid Reinforced ALuminium Laminate). Three main companies were approached, ALCOA to provide aluminium sheeting of the desired dimension, AKZO to produce the fibres and 3M to provide adhesive and manufacture the required pre-pregs. A patent was filed in the US on 9th January 1981 with AKZO holding the rights. A number of different variants of ARALL were available with 0.3mm or 0.4mm aluminium thickness. ARALL 1 consists of high strength 7075 Aluminium and was stretched after curing to improve properties. ARALL 2 replaced the 7075 with 2024 and did not require post-curing processing. These were followed by ARALL 3 using 7475 aluminium and ARALL 4 with high temperature resins for military applications. The problem for the uptake of ARALL was cost, a number of different treatments had to be applied to the material which drove the cost up to around ten times that of aluminium per kilogram. ARALL however was tested in Fokker F-27s and F-28s belonging to the Dutch military, where a wing panel including an access hatch was replaced with an ARALL alternative. The tests highlighted the improvement in safety due to increased fatigue resistance and a 33% weight saving. Whilst ARALL failed to make a commercial breakthrough it was used for access hatches on Fokker 50s and the rear load doors on C-17 Globemaster. Other products were produced including tubes, as well as a bike and tennis racket.

In 1987 a patent was taken out on GLARE (GLAss REinforced) by AKZO. This replaced the expensive ARAMID fibres with cheaper glass fibre in an effort to lower the cost of the panels without reducing their efficiency. Also the effect of micro-buckling of fibre observed with Aramid fibres under compressive load does not occur. The glass fibres can be laid in a number of orientations offering biaxial loading [84, 85]. The use of glass fibres improves the blunt notch behaviour and shows less severe behaviour for crack-like defects [86]. As with ARALL a number of variations of glare are available and are summarised in table 2.1.

Glare grade	Sub	Metal sheet thickness (mm) & alloy	Pre-preg orientation* in each fibre layer**	Main beneficial characteristics
Glare 1	-	0.3-0.4 7475-T761	0/0	Fatigue, strength, yield stress
Glare 2	Glare 2A	0.2-0.5 2024-T3	0/0	Fatigue, strength
	Glare 2B	0.2-0.5 2024-T3	90/90	Fatigue, strength
Glare 3	-	0.2-0.5 2024-T3	0/90	Fatigue, impact
Glare 4	Glare 4A	0.2-0.5 2024-T3	0/90/0	Fatigue, strength in 0° direction
	Glare 4B	0.2-0.5 2024-T3	90/0/90	Fatigue, strength in 90° direction
Glare 5	-	0.2-0.5 2024-T3	0/90/90/0	Impact
Glare 6	Glare 6A	0.2-0.5 2024-T3	+45/-45	Shear, off-axis properties
	Glare 6B	0.2-0.5 2024-T3	-45/+45	Shear, off-axis properties

* All Aluminium rolling directions in standard laminates are in the same orientation; the rolling direction is defined as 0°, the transverse rolling direction is defined as 90°.

** The number of orientations in this column is equal to the number of pre-pregs in each layer.

Table 2.1 Standard Glare grades [6]

The next type of fibre to be introduced were carbon fibres and the FMLs panels produced were called CARE (CArbon REinforced aluminium laminate). The first laminates were based on T300 carbon fibres which produced panels with reduced notch sensitivity than the monolithic aluminium as well as reduced fatigue properties. By using stronger carbon fibres, such as TENAX IM-600 and TORAY T-800, improved tensile, compressive and fatigue properties were

attained [86]. The use of carbon fibres is problematic as they are cathodic in nature and therefore produce galvanic corrosion when in contact with the aluminium layers. A number of methods have been suggested to prevent this effect, but the problem has yet to be resolved completely, holding back full commercialization of the CARE panels [86, 87].

2.2.2 Manufacturing process

FMLs contain two main constituents, aluminium alloy and a composite pre-preg, which consists of a fibre and a matrix. In the case of the aluminium, commercial products are anodised to provide a homogenous surface and primed to give additional corrosion resistance and bond durability [88]. Whilst this provides a satisfactory aluminium/composite bond several studies have looked at characterising and improving the interfacial bonding [89-91]. Kinloch states that chemical treatments yield superior joint durability than mechanical treatments [92]. However Reyes *et al.* [93] showed that a simple abrasion and solvent wipe process promoted high interfacial fracture energies in aluminium alloy and rubber-toughened carbon fibre reinforce epoxy composite systems. Prior to lay-up the composite pre-pregs (pre impregnated mats of fibre with partially cured high viscosity matrix) are locally inspected for fibre volume fraction and thickness of the adhesive film. Once the preparation of the constituents has occurred the laminate is laid up. This is when the aluminium and pre-preg layers are stacked in the desired order prior to curing. The lay-up is then placed in an auto-clave where heat and pressure are applied at the necessary levels until the panel is cured. A batch witness panel is also processed at the same time. The batch witness panel is then mechanically tested to ensure the properties of the finished product are within tolerances. Further quality control is carried out using non-destructive testing.

2.2.3 Constituents

2.2.4.1 Aluminium

Aluminium 2024-T3 is an aluminium alloy, containing a number of alloying elements, the main elements are copper (~5%) and magnesium (~1.8%) and has been solution heat treated and age hardened to improve its mechanical properties, particularly strength and fatigue. The melt temperature falls between 843 and 933°K depending on the amount of alloying elements present. Two important properties for thermal forming are the thermal conductivity and the reflectivity of the material. The thermal conductivity of the alloy is directly proportional to the electrical resistivity and to the temperature. The electrical conductivity is a sensitive property of aluminium, being responsive to changes in composition and thermal condition. All known metallic additions to aluminium decrease its electrical conductivity. Metals in solid solution depress the conductivity to a greater extent than when out of solution. However, the aluminium 2024 shows a decrease in conductivity during the initial stages of aging, attributed to transition precipitate particle formation. Removing constituents from solid solution by aging (at elevated temperatures) or annealing increases the electrical conductivity.

As laser forming is an optical process the reflectivity is of particular importance. The reflectivity of smooth aluminium surface at wavelengths from 0.9μm to 12.0μm is more than 90%. This reduces to 70% for 0.2μm wavelength and reduces drastically below this. Sandblasted surfaces may exhibit only 15 to 25% of the reflectivity of a polished surface, reflecting between 13.5 and 22.5% of the total incident energy. A rough surface finish may lower the reflectivity to 70% [94].

2.2.3.1.1 Alloying Elements present in 2024

As stated 2024 is an alloy of aluminium and a number of other elements. They are added for the various effects they have on the mechanical properties as well as the workability of the material.

Copper is one of the most important alloying elements for aluminium, because of its appreciable solubility and strengthening effect. In AL2024 copper is a major alloying element. Copper reduces the corrosion resistance of aluminium to a greater extent than any other alloying element. The influence of copper is highly dependent upon its amount, form, and distribution throughout the microstructure.

Magnesium provides substantial strengthening with good ductility as a result of cold work. It also shows excellent corrosion resistance and weldability. If magnesium is present in solid solution during deformation, it is responsible for the work hardening produced by the cold working of aluminium. The main benefit of this addition is the increased strength possible following solution heat treatment and quenching. When magnesium is present, even in amounts as little as 0.05%, an increase in strength and ductility occurs can be gained when aged at room temperature. On artificial ageing, a further increase in strength, especially yield strength, can be obtained, but there is a substantial loss in tensile elongation.

Manganese is a transitional metal with moderate solid solubility. It is used in lesser amounts in the 2xxx alloys, only 0.3 to 0.9%. If added to the AL2024 alloy it can precipitate as a dispersion of fine intermetallic phase particles, less than 1μm in diameter, which do not dissolve during hot working and annealing. These fine, stable dispersion particles can be used to pin grain boundaries or sub-grain boundaries inhibiting the development and growth of new grains during recrystallization. They can also reduce the rate of recovery and grain growth during annealing and increase the recrystallization temperature and final grain size. An alloy of this nature retains its properties well at elevated temperatures. However, manganese present as an undissolved intermetallic compound has the effect of decreasing ductility. Another effect of manganese is to promote the formation of a fibrous structure upon hot working. Manganese is also used to correct the shape of acicular or of plate-like iron constituents and decrease their

embrittling effect. The resistance to intergranular and stress corrosion cracking are enhanced as well.

Iron is the most common impurity found in aluminium and it has a high solubility when the latter is molten. The solubility of iron in the solid state is very low (0.04%) and therefore most of the iron present in aluminium over this amount appears as an intermetallic second phase in combination with it and other elements. These relatively large particles (~10μm) add only a small increment to the strength of the alloy and better creep characteristics at elevated temperatures and decrease toughness and corrosion resistance. Iron also reduces the grain size in wrought products. Other products include silicon which contributes to the age hardening process, zinc which improves the strength of the alloy and chromium which controls grain structure. Titanium is also present in small amounts, to act as a grain refiner in casting and vanadium which raises the recrystallization temperature [95].

2.2.3.1.2 Heat Treating Process

The T3 designation indicates a heat treating process applied to increase the strength of the 2024 aluminium alloy. The treatment is a three step process involving a solution heat treatment to allow dissolution of soluble phases, quenching to develop supersaturation and then age hardening to allow precipitation of solute atoms. This last stage can occur at either room temperature (natural ageing) or elevated temperature (precipitation heat treatment).

The solution heat treating stage is necessary to take into the solid solution the maximum practical amounts of the soluble hardening elements into the alloy. The process consists of soaking the alloy at a temperature sufficiently high and for a long enough time to achieve as near a homogenous solid solution as possible. The temperature required at this stage varies, depending on the alloying elements present and in what ratio. For aluminium 2024 the solution heating

temperature is 488-499°C. This can occur in either a salt solution bath or a hot air furnace and the length of time is dependent on thickness of the sheet and ranges from 10 minutes for a <0.41mm sheet in a salt bath to 75 minutes for a 12.7mm sheet in an air furnace [95].

The next step is to quench the heated alloy. There is a maximum delay time between removing the work-piece from the heat source and full immersion in a water-bath. Following these values will ensure the complete work-piece is quenched from a temperature above 400°C ensuring the best possible improvement in material properties. In day-to-day production it is a simple matter to ensure these times are met. As a general rule of thumb, the higher the rate of quenching the greater the improvement in material properties. The highest strengths, greatest toughness and greatest resistance to corrosion are all achieved with the maximum possible quench rate, though some alloys, such as 7 series do not react in the same way. Immediately after being quenched most aluminium alloys are nearly as ductile as they are in annealed condition and it is often advantageous to form or straighten parts at this stage. The T3 temper undergoes significant mechanical property improvement due to cold work strain hardening done after quenching. The final stage is age hardening to allow precipitation to occur. With 2XXX series alloys natural age hardening at room temperature is sufficient.

2.2.3.2 Composites Layer

A composite material is a system consisting of two or more phases on a macroscopic scale, whose mechanical performance and properties are designed to be superior to those of the constituent material acting independently [96]. Composite materials can be classified into three broad areas characterised by the reinforcing phase, as illustrated in figure 2.21. For areas under light loading or secondary applications it is common to use short fibres whereas continuous fibre reinforced composites are used for primary structural application [97]. The majority of fibres used for advanced structural parts are in a continuous tow or

strand form, where untwisted fibres are used as a unit. Other types include a twisted bunch of fibres (yarn) or as a collection of continuous parallel fibres (roving). It is also possible to weave the fibres into a cloth like substance. There may be an equal number of warp and weft fibres included in the weave to give equal properties in both directions or depending on the application an unequal number to give better directional properties [98].

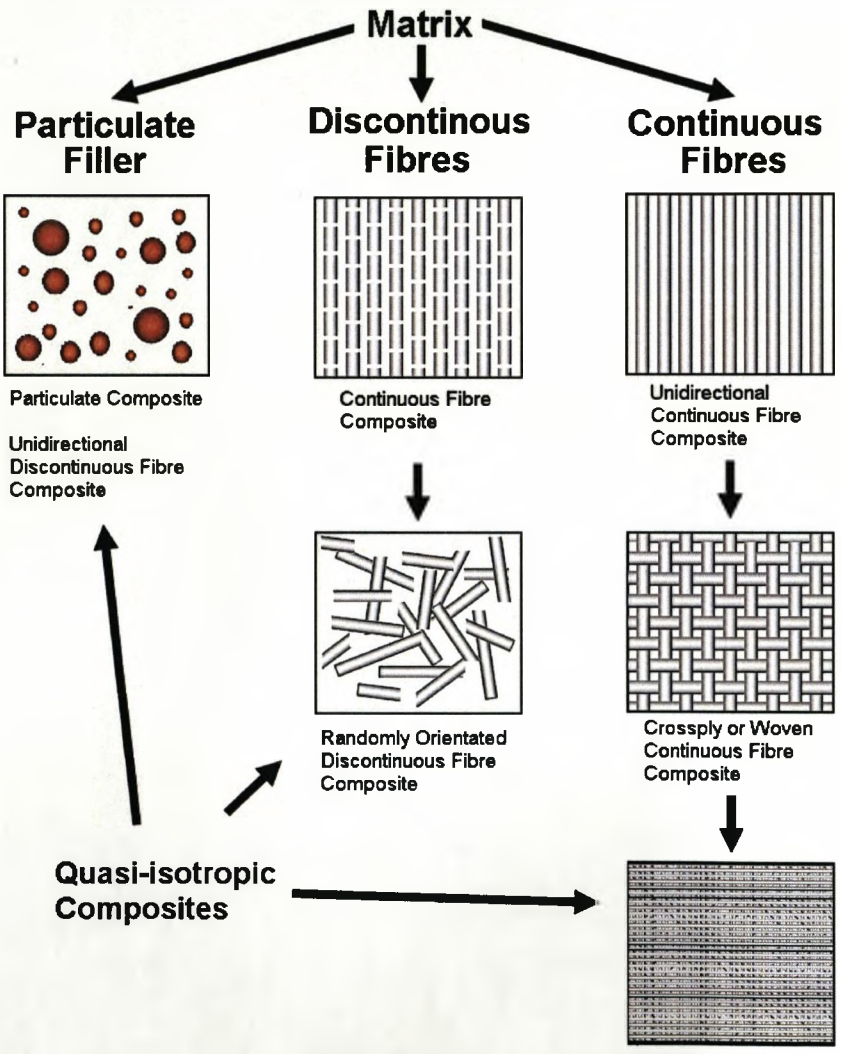

Figure 2.21 Classification of Composite Material Systems [96]

The central concept to the mechanical behaviour of composites when loaded is the load sharing between the matrix and the reinforcing phase. The stress level

may vary sharply from point to point, particularly with particulate filler or short fibres, but the proportion of the external load borne by the constituents can be gauged by volume averaging the load within them. As the external load must equal the sum of the volume averaged loads borne by the constituents the following equation is true:

$$f\overline{\sigma}_m + (1-f)\overline{\sigma}_f = \sigma_A \qquad (13)$$

Where $\overline{\sigma}_m$ is the stress on the matrix, $\overline{\sigma}_f$ is the stress on the fibres, $\overline{\sigma}_A$ is the overall stress on the component and f is the volume fraction of the fibre phase [99]. In this relationship the fibres carry most of the stress while the matrix binds the fibres and distributes the stresses to them. The transmission of such stresses is dependent on the bond between fibre and matrix. The matrix also acts as a barrier protecting the fibres from mechanical and chemical abrasion and due to its plasticity prevents the transmission of cracks from fibre to fibre [100]. The manufacture of composite materials depends on the type of materials used for the fibres and matrix and the final use of the product. Composites can be hand laid, use of a pre-preg which is fibre bundles impregnated with the matrix product prior to lay-up, bag moulding where atmospheric pressure is used to ensure complete resin impregnation, compression moulding using a hydraulic press, resin transfer moulding where resin is pumped into a mould with preinstalled fibres, pultrusion or filament winding. All methods have advantages and disadvantages in relation to the final cost and quality of the product [101].

2.2.3.2.1 Glass Fibres

Most commercial glass fibres used in reinforcement are composed mainly of Silica (SiO_2), with additions of oxides of calcium, boron, sodium, iron and aluminium (table 2.2). The variation in content and composition of the oxides present alters the characteristics of the fibres produced.

Composition (%)	E-glass	C-glass	S-glass
SiO_2	52.4	64.4	64.4
Al_2O_3+Fe_2O_3	14.4	4.1	25.0
CaO	17.2	13.4	-
MgO	4.6	3.3	10.3
Na_2O+K_2O	0.8	9.6	0.3
B_2O_3	10.6	4.7	-
BaO	-	0.9	-

Table 2.2 Glass fibre composition [99]

Three main types of fibre are commercially available in any length, up to continuous (relative to product size) and are E-glass, C-glass and S-glass. The most common grade is E-glass (E for electrical) which contains more oxides than the other two materials with a greater concentration of calcium oxide (CaO). E-glass exhibits good strength, stiffness, electrical and weathering properties (table 2.3). C-glass (C for corrosion) is particularly corrosion resistant and contains barium oxide. This increase in corrosion resistance comes at the cost of overall strength. The final grade is S-glass (S for strength) which has much higher concentrations of alumina and ferric oxide.

Properties	E-glass	C-glass	S-glass
P (Mgm^{-3})	2.6	2.49	2.48
K ($Wm^{-1}K^{-1}$)	13	13	13
A ($10^{-6}K^{-1}$)	4.9	7.2	5.6
Σ_* (GPa)	3.45	3.30	4.60
E (GPa)	76.0	69.0	85.5
T_{max} (C°)	550	600	650

Table 2.3 Glass fibre properties [99]

The production of glass fibres is done by using gravity to feed molten glass, held in a reservoir, through a series of platinum bushings. The bushings have hundreds of holes in the base and the glass fibres extruded out are mechanically

withdrawn. The fibres are then wound on a drum at the rate of several thousand metres per minute. The fibre diameter is controlled by a number of variables, the volume of molten glass in the header tank, the viscosity of the glass, the diameter of the holes in the bushings and the speed of winding. The diameter of the E-glass is usually 8 to 15μm.

To minimise the damage that occurs when the fibres rub together during processing the fibres are coated with a size to protect the outer surfaces. The size usually consists of a thin coating of an emulsified polymer. This serves several roles in that it not only protects the fibres during handling, but binds them for ease of processing, lubricates the fibres to minimise abrasion, imparts anti-static properties and improves the bond between matrix and fibre.

2.2.3.2.2 Epoxy Resin

A common matrix material is a thermo-setting polymer, epoxy resin. It is used extensively in both structural and specialty composite applications as it offers a unique combination of properties that are unavailable with other thermo-set resins. They are available in a wide range of physical forms, from low viscosity liquids to high melting temperature solids and thus can be used in wide range of applications. Epoxies offer high strength, low shrinkage, excellent adhesion to a large number of substrates, effective electrical insulation, chemical and solvent resistance with low economic cost and low toxicity. They cure without evolution of volatiles or by-products common with other systems. Epoxy resins are currently limited to a maximum service temperature of 120°C for highly loaded, long-term applications with toughened resins having a maximum temperature of about 80°C. [102]

2.2.3.2.3 Polypropylene

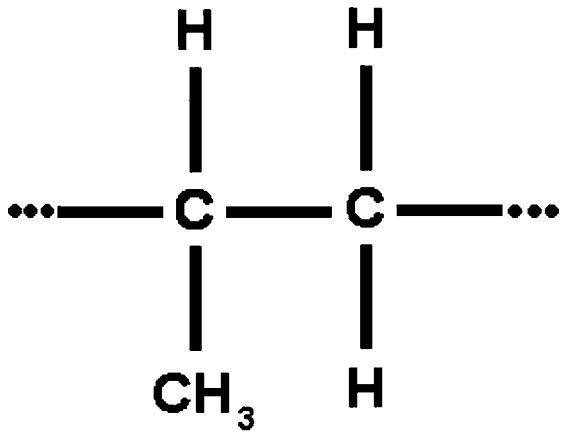

Figure 2.22 Chemical structure of polypropylene

Polypropylene (PP) is a tough lightweight thermoplastic made by the polymerisation of high-purity propylene gas in the presence of an organometallic catalyst at relatively low pressures and temperatures (figure 2.22). Due to its low density and low cost, PP is used as a matrix in numerous composite products. PP is also non-polar so absorbs little water, but with treatment can be made hydrophilic. A polyolefin of propylene, polypropylene has a T_g=-20°C and a T_m=165°C. Due to PP semi-crystalline nature, the heat distortion temperature at 0.46MPa increases significantly from 100°C to 170°C with the addition of 30% glass fibre. Also with its T_g below room temperature it exhibits good impact properties. Due to these benefits PP is widely used in glass mat thermoplastic sheet material to act as the matrix binding the fibres. The material is available in either short or long fibre forms and is made by melt impregnation and can be used in a number of manufacturing processes. [102, 103]

Polypropylene is a highly versatile polymer which can be modified and tailored for specific applications. It has good physical, mechanical, electrical, chemical and thermal properties at a competitive price and wide availability. PP products display good stability over a wide range of temperatures and can be processed

easily, simply and safely with a wide range of equipment. PP is also easily recoverable and simply requires heating to over the melt temperature, setting and then processing into pellets for reuse [103].

Polypropylene can also be used to produce self-reinforcing composite systems. Highly aligned polypropylene fibres are embedded in a polypropylene matrix in a standard weave (Curv® from Propex Fabrics). Self-reinforced polypropylene composites have a number of benefits [104];

- 50% weight saving over glass reinforced parts with the same mechanical stiffness when carefully designed
- Significant environmental advantages have been shown in independent life cycle studies
- No glass products to cause irritation and mould/tool wear
- Finished surface smooth and hard wearing without requirement for additional coatings
- Thermo-formable at low pressures and temperatures
- Significant reduction in capital costs and energy usage over alternative thermo-formable fibre-reinforced systems
- High impact strength even at low temperatures
- Inert, non-toxic and highly resistant to corrosion
- High resistance to abrasion

2.2.4 Shaping and forming

2.2.4.1 Splicing

In the initial phases of readying GLARE to market it was realized that the current maximum width of aluminium sheet available, in the necessary thickness, was only 1.65m wide while aircraft fuselage sizes of 2m and over were required. To overcome this, the use of a staggered join between the aluminium layers was used with the continuous composite fibre providing load transfer (figure 2.23).

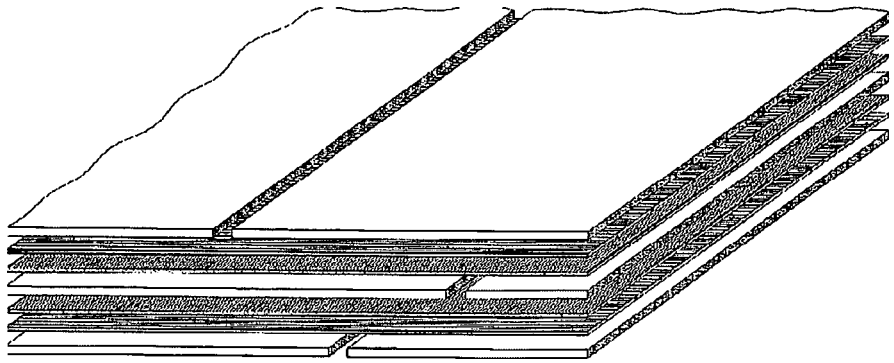

Figure 2.23 FML splice concept [105]

This procedure allows the reduction in number of joins, the reduction in joining processes as there is no drilling, riveting and sealing of joins, a reduction in weight and a reduction in maintenance and inspection costs [106]. To ensure a smooth transfer and reduce the delamination effect at splices due to load transfer a doubler (secondary GLARE layer) is applied over the join in a secondary autoclave process [105-107].

2.2.4.2 Curved Panels

A number of processes are available to produce curved panels. For single curvatures roll bending is a possibility, but fibre orientation has an effect on the final shape (figure 2.24). Springback occurs due to elastic recovery of the material and is increases as the fibres are orientated towards the circumferential direction [108]. Another possibility is the use of the pre formed panels in the initial laminate construction.

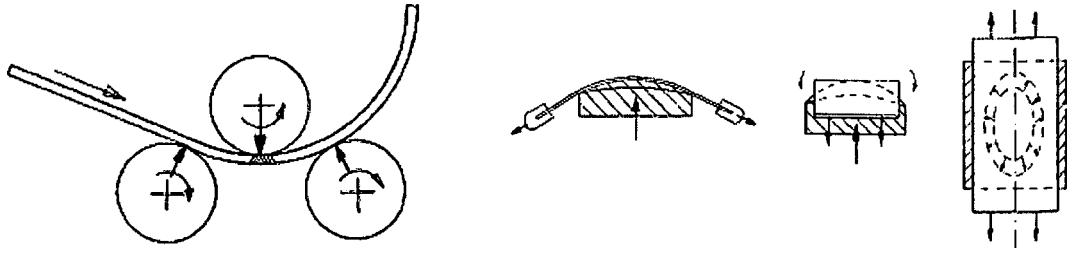

Figure 2.24 Principles of roll forming and stretch forming [108]

For double curvatures stretch forming is a possible process (figure 2.24). This is where the material to be formed is stretched in all directions and then plastically deformed. This results in negligible springback in the part. However due to the low failure strain level of the fibres, only shallow curvatures are possible. It is not possible to improve the stretch formability by heat treatments as with monolithic materials [109].

2.2.5 Mechanical properties

2.2.5.1 Tensile and Compression Strength

Wu *et al.* [110] used the rule of mixtures approach to predicting both tensile strength and tensile modulus of glass fibre/epoxy FMLs. They showed that both properties are linear functions of the metal volume fraction. These results were supported by findings of Reyes [111] on tensile tests of glass fibre reinforced polypropylene. Hagenbeek *et al.* [112] produced a model called Stress-Strain Calculation Program (SSCP), which considers the level of plasticity in the metal layers and the post stretching process. The initial results showed that the model gave an accurate prediction of the stress-strain behaviour of uni-axial FMLs.

Work on the properties of ARRALL showed that the compressive strength is lower than its tensile strength due to the poor compressive properties of the aramid fibres. The compressive strength of ARALL therefore depends on the compressive properties of the aluminium layers [84].

A study on the off-axis tensile loading of unidirectional laminates based on a glass/epoxy composite was carried out by Kawai and co-workers at the University of Tsukuba [113]. They used a classical laminated plate theory approach and showed that the fracture behaviour of hybrid laminates can be predicted accurately using the Tsai-hill fracture criteria. The study also showed that the tensile strength of the laminates in the fibre direction was significantly higher than that of the metal layer. In Work by Bucci *et al.*[114] the transverse

direction the tensile strength was up to five times stronger than the plain composite material suggesting that the metal layers control the tensile properties of FMLs in that direction. Work by Afaghi-Khatibi [115] showed that the UTS of FMLs is strongly related to the failure strain of the fibres and the yield strength of FMLs was shown to depend on the residual stresses in the metal layers and residual strain in the fibres generated during the manufacturing process. Therefore to increase the UTS of the FMLs, the use of fibres with higher strain to failure values are required [116, 117].

2.2.5.2 Residual Strength

The residual strength is defined as its remaining strength in the presence of a crack or a notch. It is important in aircraft design due to the discontinuities in the structure to provide access facilities and manufacturing features such as rivet holes [118]. Due to the importance of this property a number of studies [119-121] have been focused on the understanding the effect of notches in FMLs. Vermeenren [120] investigated the behaviour of GLARE and identified a number of failure modes. These include splitting, stable crack in the metal layers and fibre failure with or without delamination. Also noted was that the composite layers control crack extension once the fibres have failed and that the metal layers crack due to over loading from the fibre layer failure. De Vries and Vlot [119] commented that delamination is a consequence of plastic deformation in the metal layers, an effect which induces shear stress at the interface. The residual strength of an FML is related to yield stress, UTS and plastic reserve in the metal layers. Therefore a higher yield stress and UTS will result in a lower residual strength, a higher toughness or plastic reserve gives a higher residual strength [119, 122, 123]. Van Rooijen [117] showed that there was no relation between yield stress and the blunt notch strength of an FML. They also identified that there is no clear trend between strain hardening and blunt notch strength.

Afaghi-Khatibi *et al.* [121] reported that the use of untreated fibre in an FML promotes a weak fibre-matrix interface, which results in a higher residual strength

than FMLs with a strong interface as poor fibre matrix adhesion leads to extensive damage within the FML. The blunt in the notch tip reduces stress concentrations and retards crack growth in the composite layers. It has been observed that the smaller the defect size, the greater the residual strength.

A strong fibre-matrix interface can only achieve this by local mechanisms such as resin shear or fibre fracture leading to a brittle failure of the laminate giving a lower residual strength [124-126]. Hagenbeek [112] predicted blunt notch strength of GLARE using the Norris Interactive Failure criterion, which assumes a linear dependence on the volume fraction of metal and showed good agreement with the experimental data. Other models [124, 127, 128] have been used to predict blunt notch strength but the Effective Crack Growth Model (ECGM) which uses damage growth with stress relaxation and cohesive forces acting on the constituents produces the best correlation with experimental results [127].

2.2.5.3. Fatigue

Previous work on laminate structures had shown them to have superior fatigue properties over monolithic structures due to the crack arrest mechanism in the adhesive layers and the higher fracture toughness of thin sheets over thick [129]. FMLs' impressive fatigue performance has been attributed to the bridging effect of the fibre layer [130]. The intact fibre layers have the effect of reducing the stress intensity at the crack tip, constraining the crack propagation in the metal layers (figure 2.25).

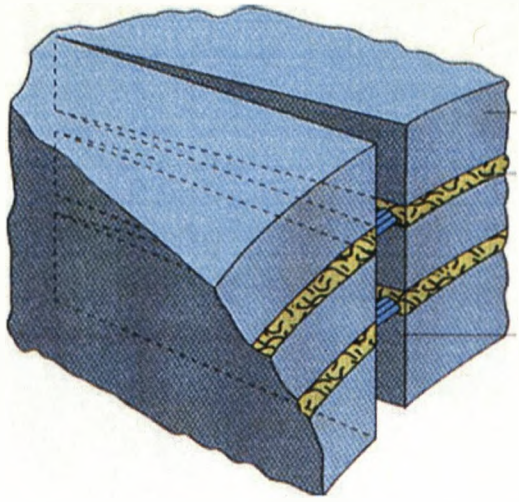

Figure 2.25 The bridging effect of the intact fibre layers during crack propagation [130]

Vlot and Alderliesten [131] identified that another crack restricting property of FMLs is delamination around the crack area due to cyclic shear stresses in the adhesive layer. The cyclic shear stress transfers the load from the metal layer to the fibres redistributing the strain generated by the crack opening. This prevents failure of the fibre layer. The magnitude of the bridging stress in the fibres is related to the crack opening displacement and the length over which the bridging fibres are elongated. They suggested that the fatigue process involves crack initiation, crack growth and failure. During the initiation phase the crack propagates quickly for 1-3mm due to stress concentrations at the notch and because the fibres require some crack length before becoming effective in reducing crack propagation. The crack then propagates at a constant rate during the next phase, staying in the initial layer for some considerable length before initiating a crack in the layer below. Eventually the third phase occurs with the failure of the specimen.

Whereas a strong fibre/matrix interface is detrimental for the residual stress properties of an FML panel, it offers superior fatigue properties [132]. A weak fibre/matrix adhesion leads to splitting at the interface which gives large areas of

delamination which reduces the effect of the fibre bridging and allows a higher crack tip opening displacement

Vogelesang and Vlot [133] looked at the research properties of two types of GLARE and monolithic aluminium under simulated fuselage landing cycles. The results showed that laminated GLARE exhibited a constant low crack growth in contrast to the high crack propagation rate in the monolithic material. The GLARE exhibited a crack growth rate of 10-100 times slower than their metallic counterparts under this type of loading (figure 2.26).

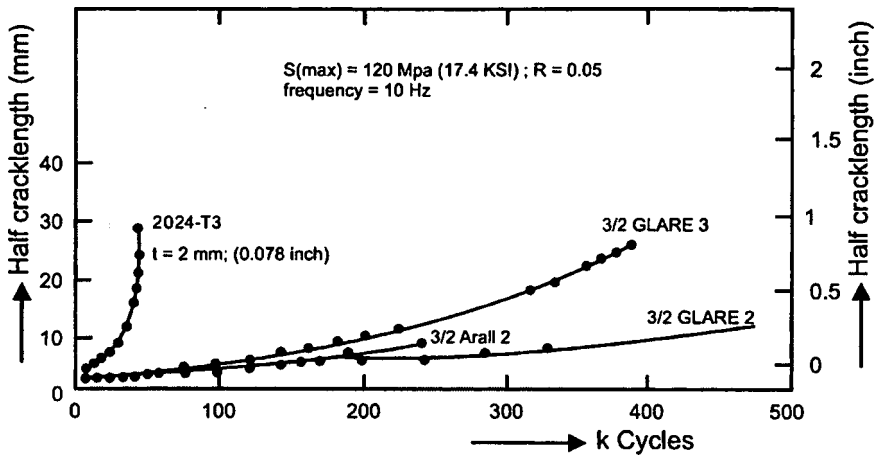

Figure 2.26 The crack growth behaviour of unidirectional GLARE 2; cross-plied GLARE 3, ARALL 2 and 2024-T3 for a fuselage loading [133]

2.2.5.4. Impact

A major advantage that monolithic aluminium alloys have over composite systems is resistance to impact loading. Low velocity impacts cause little damage to aluminium structures, with minor damage obvious as plastic deformation [134, 135]. Composites however suffer considerable effect from such low velocity impact loading, causing delamination within the composite and causing significant weakening to the stiffness of the part. The damage is also difficult to detect with no apparent surface damage [86] [136, 137].

A number of studies have been carried out on both high and low velocity impact response of FMLs based on a number of different composites. Work by Vlot [134] characterised the failures of FMLs under impact. It was found that the plastic deformations found in monolithic aluminium were of similar depth to those produce under the same conditions in FMLs. It was also observed that FMLs exhibited either fibre-critical or metal-critical failure behaviour. In fibre-critical failure the crack propagated perpendicular to the outer fibre direction with a simultaneous crack in the metal layer. In metal-critical failures the crack ran in the rolling direction of the metal. Earlier tests in ARALL by Sun *et al.* [138] agreed with these findings. A number of studies have looked at various differing types of GLARE material [139-141] and have found that it out performs aluminium and other composites in nearly every commercial lay-up in static, low and high velocity impacts.

Recent investigations have studied FMLs based on thermoplastics and show promising results with respect to impact properties. Compton *et al.* [142] showed that the specific perforation energy as 23% higher for a thermo-plastic FML over a thermoset FML. Reyes *et al.* [143] suggested a number of failure modes for thermoplastic FMLs under high impact performance. These were fibre fracture, matrix cracking, plastic deformation and folding of the aluminium layers. Cantwell *et al.* [144] tested a number of FMLs with a thermoplastic matrix and found that unidirectional GF reinforced polypropylene PP offered the highest specific perforation energy.

2.2.6 Physical Aspects

2.2.6.1 Environmental Aspects

Environmental effects on FMLs are in two areas, the effects on the components and the panel. The aluminium layers can be affected by moisture which leads to corrosion. This can be inhibited by a protective layer applied to the exterior surface, such as anodisation, cladding a layer of pure aluminium or a primer/paint

system [145, 146]. The E-glass fibres are chemically inert but can suffer from acid damage due to the presence of metal oxides which can severely decrease the strength of the fibres [147]. The epoxy resin systems used in glass fibre FMLs are most seriously affected by moisture. The rate of moisture uptake is dependent on the temperature of the polymer, the relative humidity, stress level of the part, the type of polymer and the quality of the material. The effect of moisture on the epoxy is either reversible in the case of swelling and plasticizing or irreversible in the case of hydrolysis or physical ageing. All these effects are detrimental to the physical properties of the matrix [148]. The polypropylene composite used here is generally inert with good corrosion performance against various acids and bases and has low water absorption [104].

The effect of environmental changes are well known for the components but when the systems are combined in a laminate the properties alter, mainly due to the thin cross-sections of each individual material. The laminate lay-up differs in response to corrosion in a number of ways. Electrical conductivity of the fibres can lead to galvanic corrosion, which is not present in the composite systems. Additional heat treatment of the aluminium layers during the curing cycle could affect the corrosion properties of materials, but this is probably small due to the low temperatures involved. The composite layer would act as a barrier to corrosion but corrosion could occur at the composite aluminium interface. The thin cross-section of the aluminium gives it a higher quenching rate when compared to the monolithic material that would be in its place giving better corrosion properties [6]. The effect of moisture absorption on the FML is reduced when compared with a composite structure as water ingress can only occur at the edges, and the fibres themselves act as a barrier to water absorption.

2.2.6.2 Lightening Strike

An aircraft flying through a thunderstorm will be likely to be hit by lightning as it offers the shortest path for the lightning to discharge. When traditional monolithic aluminium aircraft skin is hit burn marks and pitting will occur, with penetration of

thinner sections. When composite materials are hit by lightning severe damage occurs as the conductivity of such materials is low. Research at KEMA (a Dutch research institute) found that lightning strikes on GLARE type FMLs results in high temperatures at the surface due to the non-conducting composite layer. This causes vaporisation of the aluminium layer and carbonising of the composite layer, but structural integrity continues due to other fibre layers in the laminate [149].

2.2.6.3 Flame Resistance

To meet airworthiness requirements, an aircraft's fuselage integrity must be sustained for 90 seconds (FAR 25.803). Tests undertaken at 1100°C (temperature of kerosene flames) have shown that aluminium alloy looses integrity in approximately 60 seconds. When tested under the same conditions GLARE panels sustained over 600 seconds of heat application (figure 2.27). This superior performance is due to the high melting temperatures of glass (1500°C) which protect the layers behind it from the effect of the flames, even with the removal of the outer aluminium sheet which occurs quite rapidly. The remaining layers also prevent deterioration in the structure, avoiding collapse [82, 150].

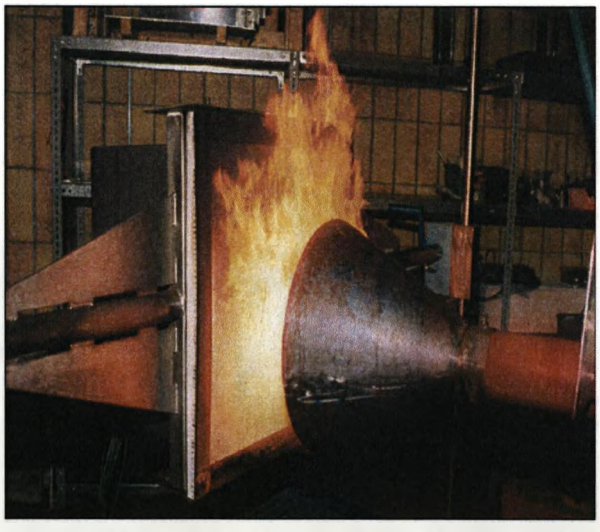

Figure 2.27 Burn through test for post crash kerosene fuelled fires [150]

2.2.6.4 Maintenance, Inspection and Repair

The maintenance procedures currently in use to inspect and repair monolithic aluminium are applicable to GLARE-type FMLs. Conventional paint stripping and corrosion removal techniques were shown to have no detrimental effect on the GLARE structures. For repair drilling, cutting and riveted patches are all acceptable techniques for the repair of GLARE structures including aluminium patches. After fatigue testing it was found that these procedures produced a moderate reduction in strength [151]. It is also possible to apply bonded patches which are more damage-tolerant and provide a smoother load introduction from skin to repair [82, 151]. Standard inspection techniques will also identify any possible defects in the GLARE panels, such as surface cracks, subsurface cracks and debonding. Ultrasonic methods can detect fatigue delamination but surface damage may affect results. The eddy current method is not capable of detection delamination but can detect cracks in secondary layers. X-ray detection gave better resolution but is difficult with parts in service [152]. Also under investigation is embedding of optical fibres to allow real-time detection of failures and assessment of remaining operational life [153-155].

2.3 Scope for further work

The benefits of FMLs, as covered in section 2.2.5, show that their material properties would attract a large number of applications, not just the aviation market [6, 105]. However one of the current issues is the method of shaping panels. The three current methods (self-forming, roll forming and stretch forming) have limitation on both size (self-forming) and geometry (stretch forming and roll forming). The laser forming process is well understood with a number of studies on a variety of materials and has been shown to be a viable method for shaping in three dimensions whilst retaining material integrity. If laser forming were proved to be a viable shaping method, and considering the restrictions of current methods (section 2.2.4) there could be an increase in both applications and overall usage.

The current objectives for this investigation stem from the preliminary work by Edwardson *et al.* [51]. While Edwardson *et al.* identified a number of important points of interest, such as the effect of fibre orientation and panel lay-up, the work lacked the level of detail required for successful shaping of FMLs. The aim of this study is to further this work and investigate a number of variables touched upon by Edwardson, as well as a number of other parameters not discussed. Requirement for this further detail is to give a fuller understanding of the process and how the addition of composite and aluminium layers to the system alter the laser forming process observed on monolithic material.

Chapter 3

Experimental Procedure

This section covers the general experimental set-up used throughout this thesis. It covers in detail the hardware, software and processes used. The laser system employed was a 35W Nd:YAG lamp pumped, continuous wave laser system with galvanometer driven mirrors to raster the beam over a circular area 180mm in diameter. A flat field optic was used to focus the beam to a spot size 0.2mm in diameter. Various experimental set ups are detailed covering the various

experiments undertaken to identify the effect of the variables involved on the process.

3.1. Hardware

3.1.1 Laser System

The system used for the majority of studies reported in this thesis was a GSi Lumonics LightWriter SPe 35w continuous wave (CW) Class 1 laser marking system, as shown in figure 3.1. It is a commercially available platform consisting of a Nd:YAG rod, Kr flash-lamp, cavity mirrors, opto-acoustic Q-switch, galvanometer driven mirrors (galvnometer-head) and a flat field optic. This is contained within an interlocked cabinet system and powered by a graphical user interface (GUI), Solo (version 1.26), which runs on a 486 based system with an OS/2 Warp operating system. The total cavity length is 660mm with a further 200mm of flight tube after the partial reflector and before the galvanometer-head. The galvanometer-head consists of two galvanometer driven mirrors which react to very small changes in the drive current passing through the coil by producing rotary deflection. The galvanometer-head rasters the beam over a final work area 180mm in diameter, at velocities up to 1000mms^{-1} with a constant 0.2mm diameter spot.

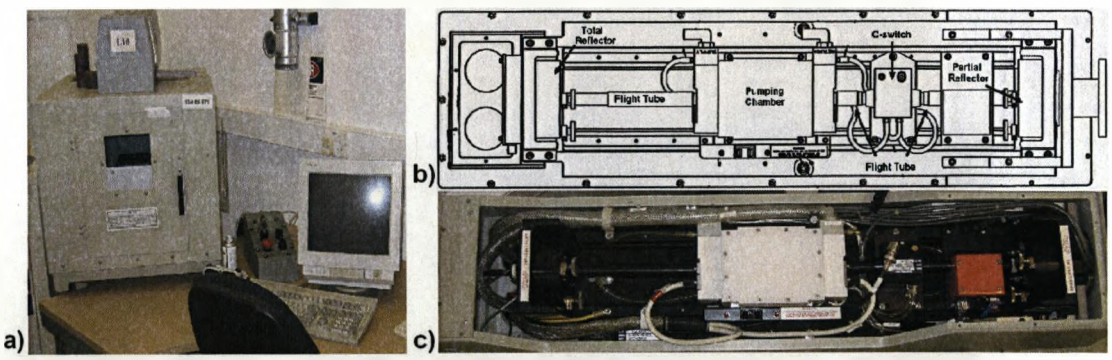

Figure 3.1 a) Image of system showing work-piece enclosure, galvanometer-head and laser head, b) schematic of laser head and c) Image of laser head internals

The work station is completely enclosed within an interlocked cabinet with an observation window (visible in figure 3.1a), allowing the equipment to be rated at Class 1. The focal point is 330mm in the vertical position but this alters as the beam is rastered in the X and Y directions due to the flat-field optic. The work-piece is held in a simple clamp arrangement which is mounted on a Z-stage, connected to a stand, incorporating a level to allow accurate placement of the stand relative to the laser (figure 3.2). Also on the stand is a laser triangulation system to allow online measurement of the bend angle (further detail on measurement in section 3.1.1.3).

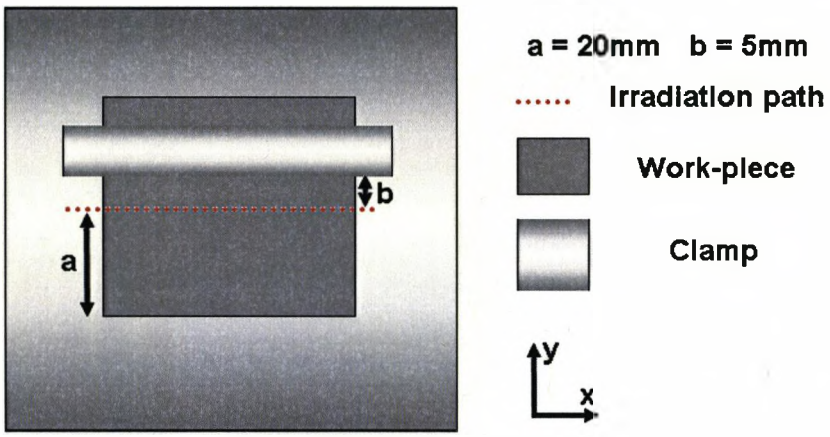

Figure 3.2 Image and schematic of clamping arrangement within work station enclosure

As previously stated the laser system is supplied with a GUI based o/s called 'Solo'. This is run on a 486 DX33 through IBM's O/S 2 WARP. All laser controls are accessed and actioned through 'Solo', however the current driving the lamps and therefore the power output of the laser is also controllable via a control panel located on the power supply unit. The initial screen shows a representation of the work area with 330mm radius which indicates the area of the flat-field objective. Above this are a number of tabs which control text input, positioning, effects etc.

As this system was designed as a marking system the default inputs are text based, however a system font allows the production of horizontal or vertical lines as either an A or B text input with the 'GSISYSTEM.fon' font. These lines can be altered using the further tab options such as positioning, effects etc. The laser parameters are set using power screen which allows the control of the power output from the laser by controlling the current fed to the lamps, which corresponds to a final output power as shown in figure 3.3. The output power was measured with a power meter where the power puck, a black metal block, was aligned centrally underneath the flat field optic, well above the focal position (to reduce the possibility of damage to the puck by a focused beam). The laser shutter was then opened and the puck irradiated. The thermal change observed in the block equated to a power reading on an analogue scale. Analogue readings were considered superior to digital as they gave an indication to the consistency of the power output, rather than a 'snap shot' of the output. An online power measurement system is included with the LightWriter (it takes a reading from a beam splitter prior to the galvanometer mirrors), but comparisons with the calibrated power puck showed that the online measurement was unreliable. Power readings were taken before and after every individual test and every time the power level was required to change to ensure accuracy.

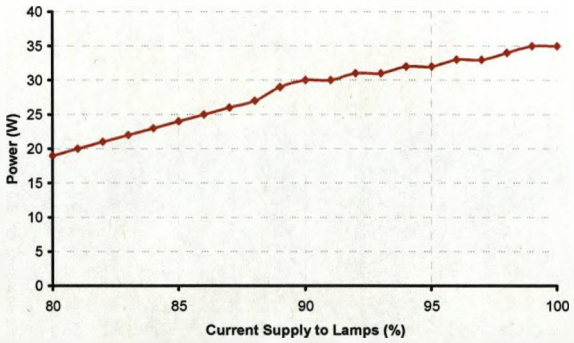

Figure 3.3 Lamp current supply against laser power output

3.1.1.2 Beam Profile

The laser had an M^2 value of approximately 14.8 (M^2 is the beam quality factor and is based on the divergence of the beam, with 1 being a perfect, none diverging beam). Which whilst relatively poor compared to most experimental apparatus (1.5-2.5), it a good representation of industrial laser systems that and commercialization of this process would occur on. Figure 3.4 shows 2D and 3D beam profiles for the system. As can be seen the system produces a good Gaussian beam profile at the focal length (ideal for marking tasks this machine was designed for) but the beam quality and shape deteriorates quickly beyond or before the focal point. Due to this and other factors it was decided to hold all experiments at the focal point to ensure beam quality and reduce the possible variable effect of the beam quality.

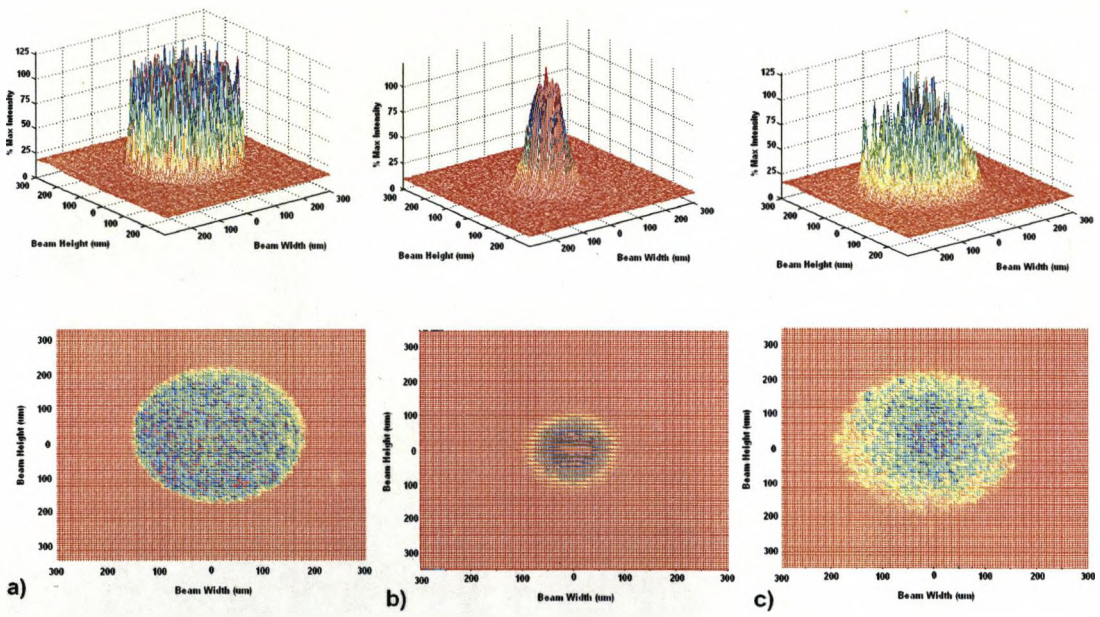

Figure 3.4 3D and 2D beam profiles showing beam width and height and intensity at a) 20mm before the focal point, b) at the focal point and c) 30mm beyond the focal point

3.1.1.3 Angle Measurement

Within the Class 1 work station there was an online measurement system, based on a laser triangulation sensor, which was used to record the change in height of the samples during 2D forming. The system was based around a MEL/20 sensor produced by Mikroelektronik GMBH which used a laser diode and off-set photosensitive diode to display changes in height as a fraction of the 10V output of the sensor system. The sensor was mounted on an armature with X and Z axis adjustment to allow for changes in work-piece dimensions to ensure the resultant sample stayed within sensor range, (figure 3.5a) which must be a minimum of 30mm away from the work-piece and no more than 50mm. The measurement point on the sample itself was required to be off-set from the form line to allow calculation of the bend angle. Throughout this investigation the sensor point was off-set 13mm from the irradiation line and 20mm from the bottom of the work-piece (figure 3.5b).

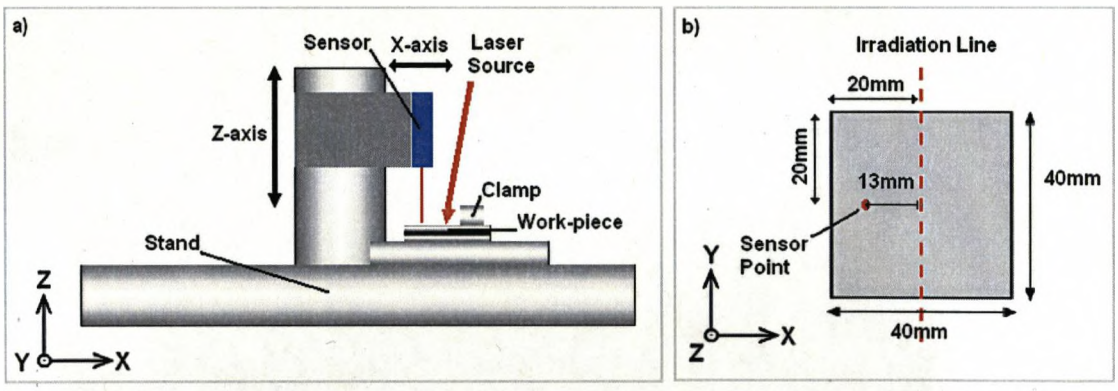

Figure 3.5 a) Sensor arrangement and b) measurement point plan

Online Measurement

For online measurement a Visual Basic program was used to record the voltage output at any given time. The system worked through a National Instruments Data card inserted into the PCI slot of a x86 system which recorded the output voltage of the sensor into a comma-separated value list, when the button was activated.

Real-time Measurement

When real-time recording of data was required an Agilent 34970A data acquisition and switch unit (figure 3.7) was used. This unit can record data at up to 250 times a second when used with either the 34902A 16 Channel Reed multiplexer or 34901 20 channel multi-function card. It can measure AC or DC voltage, current, resistance or temperature, which is selectable through the bundled software and has an on-board reference junction for the automatic calibration of thermocouples. The unit can be used standalone or can be used in conjunction with a PC via a RS232 serial cable. The data can then be exported to a .CSV file allowing manipulation in spreadsheet programs.

Figure 3.7 Agilent 34970A Data Acquisition unit.

The voltage output was then converted to a height measurement using the following equation:

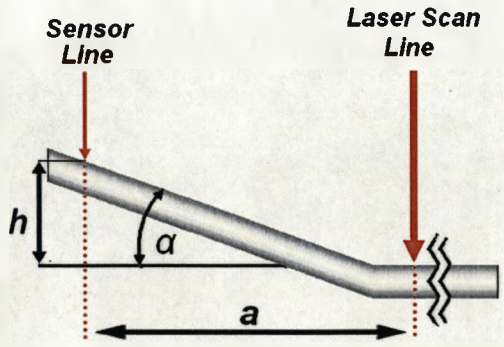

$$\tan\alpha = \frac{h_0 - h_n}{a} \qquad (15)$$

Where h_o = height h before laser forming scans, h_n = height after (n) scans and h= change in height. Throughout this thesis, unless otherwise stated a, the stand-off distance between the sensor line and the scan line was 13mm.

3.1.2 Coating

The optical nature of LF requires that a high level of absorptivity of radiation is obtained in order to ensure maximum efficiency of the process. In an un-altered state metals, and particularly aluminium, have very high levels of reflectivity in the wavelengths from visible to infrared as seen in figure 3.8. This is due to the fact that for metals, laser radiation is mainly absorbed by the free elections in an "electron gas". These free electrons are able to oscillate and reradiate without disturbance to the solid atomic structure. As the wave front arrives at the surface, the free electrons vibrate, generating an electric field 180° out of phase with the incoming beam. The sum of this field will be a beam whose angle of reflection equals the angle of incidence. This electron gas means that the irradiation is unable to penetrate metals to any significant depth, only one or two atomic diameters and metals therefore appear shiny.

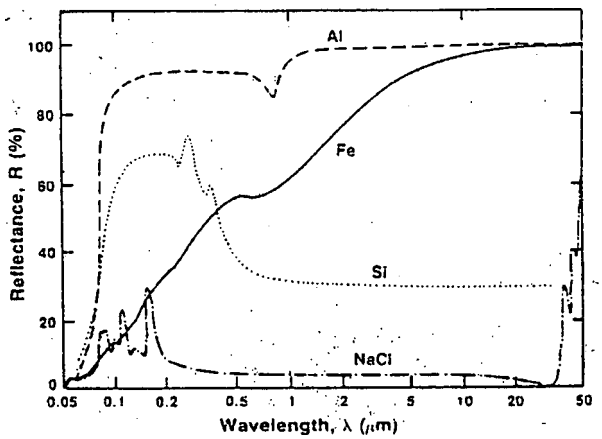

Figure 3.8 Reflectivity of various metals as a function of wavelength [13]

In order to reduce the reflectivity a number of different techniques have been used and their efficiency is summarised in Table 3.1. However most of these

result in damage to the work-piece, in the case of sand blasting and oxidation, which is unacceptable in most cases, or are difficult to apply and remove in the case of Molybdenum Sulphide and the various paints. Graphite however is easy to apply, readily available and simple to remove with acetone as well as its improved absorptive properties. The effectiveness of these coatings degrades with each pass which has an effect on the coupling efficiency of the process and therefore the forming process. A number of empirical studies were under taken looking at the effect of laser interaction with the results discussed in section 4.1.2.

Surface Type	Reflectivity (%)		
	Direct	Diffuse	Total
Sand paper roughened (1μm)	90.0	2.7	92.7
Sand blasted (19μm)	17.3	14.5	31.8
Sand blasted (50μm)	1.8	20.0	21.8
Oxidised	1.4	9.1	10.5
Graphite	19.1	3.6	22.7
Molybdenum Sulphide	5.5	4.5	10.0
Dispersion paint	0.9	0.9	1.8
Plaka paint	0.9	1.8	2.7

Table 3.1 Typical values of reflectivity of various surfaces to 10.64μm radiation at normal angle of incidence [3].

3.1.2.1 Application Method

It was necessary to investigate the effects of application strategy of the graphite to ensure repeatability of the process. The graphite used was supplied in a aerosol form using a propane/butane propellant. The 10 x 10 x 1.5mm AL2024-T3 samples were de-greased with ethanol and then either a 'thin' coating was

applied, which was until the underlying surface was not visible, a 'thick' layer, which was five application similar to the 'thin' coating or 'saturation' where a pool of graphite/propellant was allowed to form on the surface by a constant five second spray. Five samples of each method where then measured using a Wyko NT1100 vertical scanning white light interferometer (VSI) and optical microscopy with the various measurements identified by figure 3.9. The results can be seen in section 4.4.2.

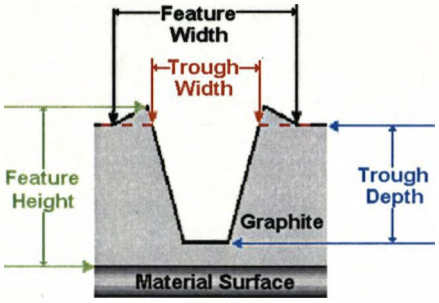

Figure 3.9 Schematic of measurements taken of various graphite features

3.1.2.2 Effect of Coating Removal on Bend Rate

For this work a number tests were carried out on 40mm x 40mm coupons of AL2024-T3 with 0.3mm thickness over 20 passes at 35W and 10mms^{-1} and with a 30s dwell between passes. Three tests were each carried out for re-applying the graphite coating, after 5, 10, 15 and 20 passes. At each re-application remaining graphite was removed using acetone and a cotton bud and then a coating was applied by spray and allowed to dry for ten minutes. The sample and clamp was remounted onto the locating bolts to ensure alignment and the next set of scans was applied. The Cumulative Bend Angle (CBA, the cumulative bend angle reached for all the previous passes) after each pass was recorded using the triangulation system and online measurement system (section 3.1.1.3). The mean results were then plotted and the results can be seen in section 4.1.2.2.

3.1.3 Dwell Time

Due to the thermal nature of the laser forming process, a build-up of heat can occur which limits the effectiveness of the TGM and can damage the underlying composite material. To prevent this from occurring a number of empirical investigations were carried out to quantify the effects and show some methods of controlling it. The first investigation was carried out with ten passes at 35W $10mms^{-1}$ on 40 x 40 x 0.3mm AL2024-T3 samples with a graphite absorption layer. The dwell time between each pass was varied from 0 to 180 seconds and the CBA was recorded using the triangulation sensor and online measurement software as described in section 3.1.1.3. The results for this are shown in section 4.1.3. To give a clearer picture of the thermal gradient produced during the process a K-type thermocouple was attached on the under-surface of the aluminium samples in line with the irradiation path. The temperature was recorded using the Agilent 34970A data acquisition unit to allow real time recording of the results.

3.1.4 Thermocouple Analysis

Because of the thermally sensitive nature of FMLs a number of investigations were carried out to show the effect of varying laser parameters, such as power and velocity, and material parameters, such as lay-up strategy and composite layer variation, have on the absorption and dissipation of the thermal input. The thermocouple relies on a voltage drop across the contact between two dissimilar metals, which is a function of temperature. Thermocouples are viewed as passive sensors as only the potential difference between the two metals is measured, no input is required. The thermocouples used in this study were welded tip 'K-type' thermocouples supplied from RS systems. The junction for these thermocouples is Nickel Chromium and Nickel Aluminium giving a linear temperature range of -270°C to 1372°C.

The first studies conducted used a single thermocouple to measure the effect of varying power and velocities have on the maximum temperature reached and on

the dissipation of that heat. The thermocouple was placed centrally underneath the irradiation line of an edge clamped 40 x 40 x 03.3mm AL2024-T3 sample. A small indentation was made into the surface at the required point to allow the rounded welded end of the thermocouple to sit in full contact with the sample. The thermocouple was attached using Loctite superglue to ensure the thermocouple stayed in contact with the surface. This was chosen over the more commonly used 'Thermopad' as the pads are quite large (approx. 12mm across) and as the CBA of the sample increased there was a tendency for the pads to lose contact with some of the sample. The thermocouples were recovered by inserting in an acetone bath until the adhesive had dissolved. Once the samples were mounted with the thermocouple they were then coated in a thin layer of graphite and processed at varying speeds and powers with 10 passes with the data being recorded in real time.

A more in depth study was carried out to ascertain the effects on thermal absorption and dissipation when varying the FML parameters. For this study three power/velocity combinations were chosen 35W 10mms^{-1}, 35W 60mms^{-1} and 22W 10mms^{-1} as these gave approximate borders to produce a bend in most lay-up parameters investigated. Again K-type thermocouples were used and the data recorded on Agilent 34970A data acquisition unit but on this occasion six thermocouples were used to give an overview of the whole sample, rather than a single data point. The thermocouples were laid out as illustrated in figure 3.10 with 102 to 106 on to top surface of the sample and 110 on the lower surface. Again the surface was indented slightly to ensure full contact of the welded tip and then the thermocouple was attached to the sample using Loctite and coated with a thin layer of graphite. Post processing, the thermocouples were recovered using acetone to breakdown the adhesive.

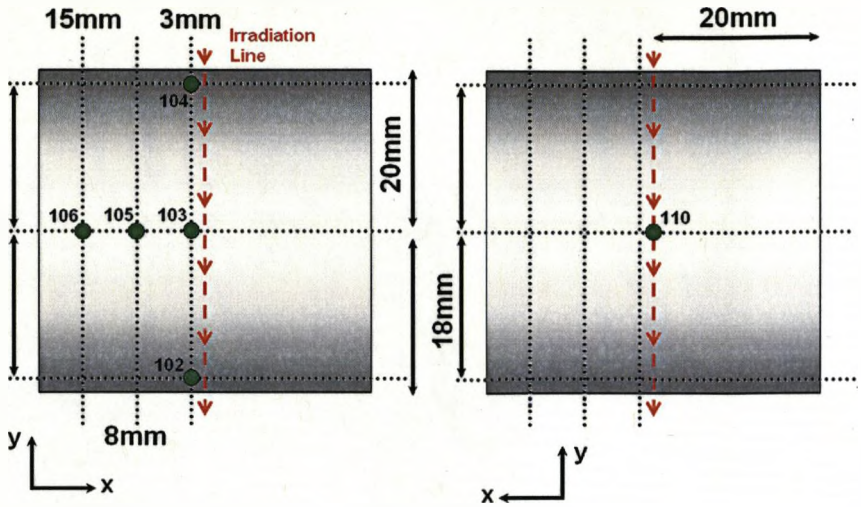

Figure 3.10 Plan of K-type thermocouple placement

3.1.5 Strain Gauge Analysis

A number of strain gauge tests were carried out using 2mm uniaxial aluminium foil strain gauges with a polymide backing. The gauges were attached using cyanoacrylate adhesive to a keyed and cleaned surface in the same position as measurement point 105, as used in the thermocouple analysis. This was done as this was the closest point to the line where the temperature range stayed within the operation range of the gauges of -30C° to 180C°. The gauges were each incorporated into a balanced and zeroed quarter Wheatstone bridge circuit (figure 3.11) the output of which was amplified by a four channel bridge amplifier and recorded using the Agilent data logger described earlier.

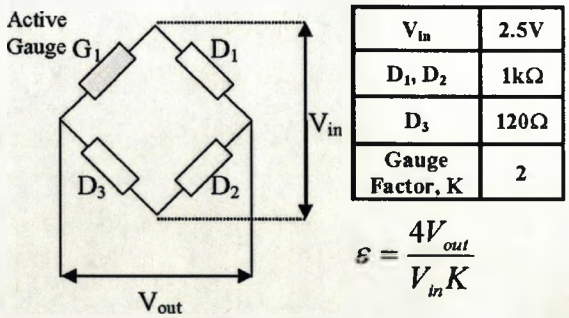

V_{in}	2.5V
D_1, D_2	1kΩ
D_3	120Ω
Gauge Factor, K	2

$$\varepsilon = \frac{4V_{out}}{V_{in}K}$$

Figure 3.11 Quarter bridge circuit

3.2 Material Manufacture

The FMLs used in this investigation are produced on site from the constituent parts, aluminium 2024-T3 and either self-reinforce polypropylene or glass fibre based composite layers. This section will concentrate on the production of these materials and the steps taken to ensure the continuity of the final material.

3.2.1 Process

FMLs are a hybrid laminate structure composing sheets of AL2024-T3 and fibre re-enforced material. In order to produce the panel necessary for experimentation the following process was used. The aircraft grade 0.3mm AL2024-T3 was supplied in 3657 x 1219mm sheets. This was then cut using an industrial guillotine into 240 x 200mm sheets with the rolling direction in the 240mm direction. These were cleaned with ethanol to remove any surface grease and print marks. The aluminium was then placed into a steel picture frame mould (figure 3.12a) and the relevant composite inserted. The mould was Teflon coated to prevent the epoxy or PP adhesive adhering to the mould. On the left side of the pre-preg, approximately 10mm from the edge, a 50 x 50mm pre-crack was created for quality control purposes (figure 3.12b). The pre-crack consisted of a layer of aluminium foil between the upper composite layer and lower face of the top aluminium layer. This sample was removed from the panel using a guillotine and was used to test the Mode 1 facture toughness of the materials. This is discussed in further detail in section 3.2.3.

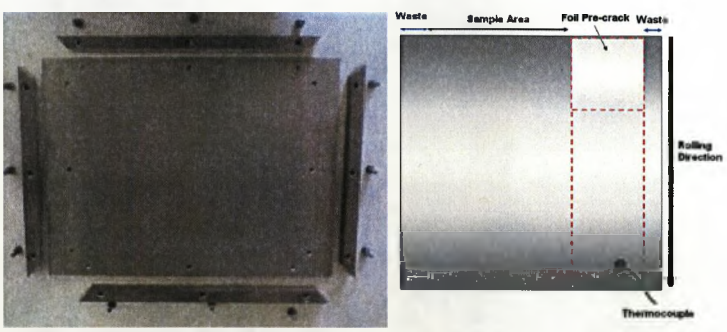

Figure 3.12 a) Picture frame type mould used for producing FMLs and b) plan view of lay-up

The production technique varies slightly for PP and GF due to manufacturing requirements:

3.2.1.1 PP FML Production

The PP composite requires additional layers of adhesive, in this case Collano Xiro 23.601, a thermoplastic adhesive based on PP, in order to bond to the aluminium. The lay-up requires alternating layers of adhesive between both the aluminium and layers of PP composite in order for the laminate to bond. Xiro 23.601 has a minimal bond line temperature of 160°C which matched well with PP composite curing temperature of 165°C. Once the desired lay-up had been place in the mould, a K-type thermocouple was placed in the bottom left corner of the mould on the surface of the aluminium. The wire is fed through the corner of the mould and the welded join of the thermocouple was approx 30mm by 30mm away from the corner of the lay-up. This thermocouple was connected to a digital thermometer and is to ensure the temperature of the curing lay-up would not exceed 180°C, which is the maximum service temperature of the PP pre-preg [156]. On top of the 'sandwich' was place a 10mm thick steel sheet to complete the mould and the aluminium spacers were used to ensure that the hot press could come in contact with the mould (see Figure 3.13). The completed mould was then placed between the plates of the hot press and the curing process started. For this particular PP composite a temperature of 160°C must be reached in order to cure the system. Due to the loss of heat at various stages this particular hot press needed to e set to 167°C in order for a temperature of 160°C to be reached in the lay-up. The system was then cured at 6 bar pressure and 160°C for 1 hour. The press was then turned off and the FML allowed to cool for 8hrs till the mould and contents reach room temperature.

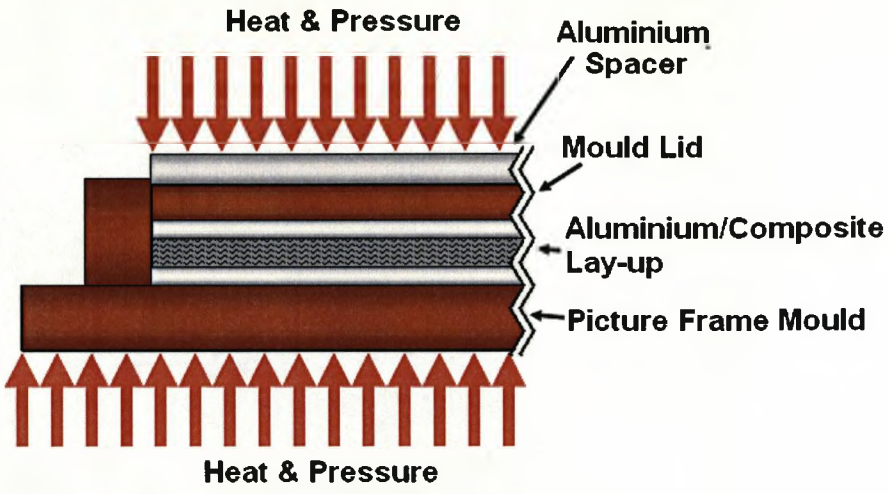

Figure 3.13 Mould Lay-up

3.2.1.2 GF FML Production

The glass fibre based systems do not require additional layers as the epoxy matrix becomes tacky at room temperature and will adhere to the aluminium layers. As with the PP composite the desired lay-up was place within the mould with a k-type thermocouple connected to a digital thermometer in the bottom left hand corner to give the temperature of the lay-up during curing. The mould lid and aluminium spacers were placed on top, then the mould and contents placed in the hot press. The hot press was set to 125°C to give a lay-up temperature exceeding 120°C and the sample were kept at this temperature and a pressure of 6 bar for 1 hour [157]. The press was then turn off and allowed to cool to room temperature for 8 hours.

Once the completed FMLs were removed from the mould they were cut again using the guillotine to separate the crack test piece of the samples. The sample area was trimmed to remove any part of the FML where the composite layer had shrunk away. This was minimal, if existent in the GF based FMLs, were as the PP composite could shrink up to 20mm from the edge (20% shrinkage in the x direction). The FML was then ready to be cut into the desired sample size, usually 40 x 40mm.

3.2.2 Hardware

The FMLs produced for this investigation were produced on a Meyer Transfer Printing and Laboratory Press, type APV 2525/16. It consisted of two electrically heated plates with a total output of 1.4kW per plate. The top plate was driven by a pneumatic ram of up to 10 bar pressure. The thermal output of the plates is controlled by Jumo iTron 16 compact microprocessor controllers. However there is an overshoot on the heating cycle which equated to about +7°C over temperature and then a -4°C under temperature due to the reaction time of the heating element. However, in this case, due to the bulk of the mould the temperature fluctuation is 1-2°C which is insignificant in this application. Figure 3.14 shows an image of the press and indicates the controls.

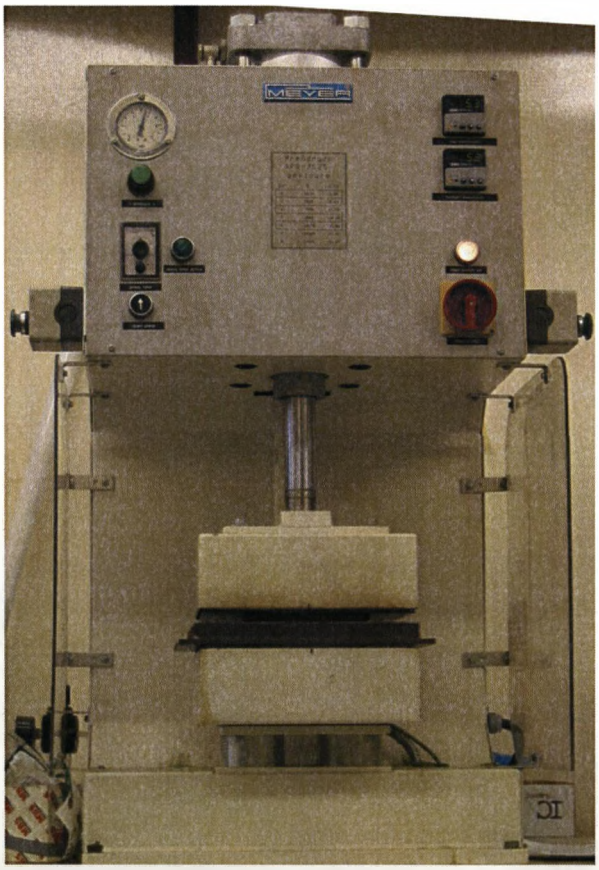

Figure 3.14 Meyer Hot Press APV 2525/16

3.2.3 Quality Control

Due to the batch production method used to produce the FML samples a method of testing the continuity of the final product was required as it is important that each lay-up produces material with similar properties, to ensure that comparisons are the result of the desired variable and not artefacts of inconsistencies in production. A number of testing methods are available. The most obvious is a simple tensile test; however the testing aims only to show continuity between the samples and information gathered from relevant literature identifies better suited tests than the tensile method. During the investigation one large area of concern is the resistance of the material to delamination; should such a failure occur it will affect the results produced by the study. Therefore after considering many of the factors it was decided that the test should be performed to ensure that the resistance to delamination, known as the inter-laminar fracture toughness, was similar for a range of samples.

In order to test the Mode 1 fracture toughness a pre-cracked sample was produced (see section 3.2.1) within every FML panel made which had more than 2 layers, as a single composite layer was unable to take the load required to fracture. Along the length of the sample, after the pre-crack, 5mm increments up to 100mm were marked to allow the recording of the force and extension for the given crack length. The samples were drilled with two holes to provide purchase for the hinges. These were then mounted in an Instron 4204 (figure 3.15) using a 5kN load cell. As load was applied across the hinges, a crack propagated at the matrix/aluminium boundary.

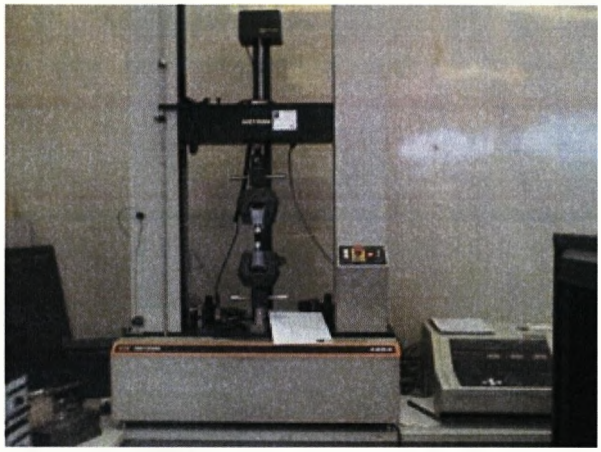

Figure 3.15 Instron 4204 tensile testing rig.

3.3 Microstructural Processing

As LF is a thermal process it was necessary to investigate any possible thermal effects on the microstructural properties of the materials. To do this a number samples were produced, mounted, polished and investigated using a number of techniques described in the following sections.

3.3.1 Specimen Selection and Mounting

The area of investigation looked at the effects of varying lay-up sequence and number of passes. The PP composite samples were produced in 1:1, 2:1, 1:2:1, 2:2 and 3:2 lay-ups at 35W 10mms^{-1} and the GF based composites were produced at the same parameters with 1:1, 1:2, 2:1, 2:2, 3:2 lay-ups with the fibre orientation in the rolling direction. 1:1 lay-up samples were also produced with the fibre orientation varying away from the rolling direction at 45° and 90°. All lay-ups were processed with 1 to 10 scans to show variation with pass strategy. The samples were made on 40 x 40mm coupons using and edge clamp. To prevent the thermal effects from previous tests a standoff between irradiation lines of 8mm was observed resulting in a maximum of 4 traverse lines per sample.

Once the samples had been irradiated the bottom 15mm in the Y direction was removed using a diamond saw to reduce heat input. The remaining part of the

sample (25mm section) was then placed in 40mm diameter sample pot (curving due to the LF process allowed this) prepared with mould release agent, with the cut edge facing down. The sample pots were then filled with Araldite 2020 which is a clear two part epoxy resin which cures at room temperature. The samples were left for 48hrs to ensure the resin had completely cured before polishing started.

Polishing was undertaken in two stages, by hand initially were each sample was polished for approximately 5 minutes per grade of paper and then on a polishing machine for approximately 1 hour. The initial hand polishing was on 80 grit paper on polishing wheels with a water feed to reduce thermal input. Around 2-3mm was removed from the sample with this coarse grit to ensure the removal of any artefacts of the cutting and mounting stage. The samples then proceeded through a number of polishing stages culminating in a 2500 grade paper. Between each polishing wheel the samples were cleaned using detergent and water and dried before being inspected under a microscope at either x5 or x10 magnification to ensure no large scratches remained. If scratches were present the sample was taken back to a courser stage and re-polished. Once polished with the 2500 grade samples they were then polished using polishing cloths and oil lubricants to 6μm and then to 1μm, again being cleaned and inspected between wheels. After this stage samples were cleaned using soap and water, dried in hot air and then any samples with oil contamination remaining were cleaned in an ultrasonic bath containing detergent overnight. The next stage in polishing was using auto polisher to polish the samples down to 0.5 microns by using colloidal silica as an abrasive. This gave the desired finish. Any etching required was done using Keller's reagent which comprises a mixture of 2 ml hydrofluoric acid (HF, 48%), 3ml of hydrochloric acid (HCL, concentrated), 5 ml of nitric acid (HNO3) and 190 ml of water. Extra safety precautions must be taken when using HF acid, this mixture must be mixed in a fume extraction chamber and in a plastic beaker, HF acid will etch glass (and destroy bone). During etching double rubber gloves, rubber apron, facial shielding and full face mask

were used. The etching time was 2 to 3 seconds. After etching the samples were washed in stream of warm water and dried in hot air.

3.3.2 Optical Microscopy

A Leitz Wetzlar Microscope was used to observe the samples using magnification up to x100. The system was connected to a Sony digital camera which was controlled through Element D.Sys software. The software allowed various measurements and was calibrated using a 200 micron wide channel in silica supplied to calibrate a Wyko VSI system.

3.3.3 Microhardness Tests

To investigate the effects of the LF process on the properties of the FMLs, a number of microhardness tests were carried out. A Vickers microhardness machine was used with a diamond indenter and a 25g load. The samples after mounting and polishing were aligned with the irradiated surface at the bottom. The variation in width due to the thickening effect necessitated a variation in the number of points and the location of these points in the sample. The initial point was placed 50μm from the lower surface with the next sample point 50μm from the first. This was continued until the sample point was within 50μm of the upper surface as a point here would be affected by a limitation of the thickness of the bulk material, giving a false reading. Five points were taken along the irradiated surface of the sample, starting with the last point of the through thickness testing and kept at the same distance from the surface.

Chapter 4.

Results and Discussion

This chapter contains the results and discussion of experimental and numerical studies into the laser forming of aluminium 2024-T3 and Fibre Metal Laminate materials (FML). Laser and material parameters are investigated and the resultant effects are analysed.

4.1 Experimental Procedure

Before a detailed study of laser forming of FMLs can take place, a number of variables not related to FMLs, which would affect the outcome of the laser processing have to be investigated and controlled. These variables relate to the laser forming process and include which of the three mechanisms (Buckling Mechanism, Temperature Gradient Mechanism or Upsetting Mechanism) is applicable, the absorptive coating to improve process efficiency, the dwell time between passes, the repeatability of the process and the quality control of the material manufacturing process. These variables need to be controlled to ensure that the effects witnessed when altering the parameters of interest is a product of said parameter, not an artefact of another variable. Rather than apply arbitrary values to these variables, where applicable, the most effective value or method can be used. This will produce the greatest cumulative bend angle (CBA), thus amplifying any effect of the parameter of interest has on the forming process. The method used in each of these areas is covered in chapter 4.

4.1.1 Forming Mechanism

As described in Chapter 2, there are three main recognized mechanisms for laser forming. Of these the Temperature Gradient Mechanism has an advantage over the Buckling Mechanism and the Upsetting (Shortening) Mechanism with thermally sensitive materials. This is for two reasons, the lower levels of thermal input introduced into the sample and the fact that the bend is always propagated towards the source. In contrast, the Buckling Mechanism gives an unpredictable bend direction and the Upsetting (Shortening) mechanism produces a change in dimension, not a through thickness strain variation resulting in a bend. Buckling Mechanism produces greater bend per pass than Temperature Gradient Mechanism. Temperature Gradient Mechanism was tested initially and gave a positive bend towards the beam when employing a spot size approximately the same diameter as the thickness of the aluminium (0.2mm spot diameter with 0.3mm aluminium thickness). With the low power system (35W max output

10mm/s), bend rate per pass of approximately 0.2° to 2°, depending on the lay-up (3:2 to 1:1), were achieved with little apparent damage to the FML. To achieve the Buckling Mechanism, a spot size of approximately 4mm was used (35W 10mm/s). Buckling Mechanism bends were consistently produced which propagated away from the source. This is a result of the strains imposed on the upper aluminium surface by the neighbouring composite layers. However, due to the levels of heat required to create a Buckling Mechanism bend, which is constant through the thickness of the work-piece, the aluminium separated from the composite. This occurred either in the form of a buckle with low passes strategies (figure 4.1a) or complete delamination of the layer at higher passes strategies (figure 4.1b). The Upsetting (Shortening) Mechanism was not investigated experimentally as it produces a shortening of the sample, not a bend. This supports the findings by Edwardson *et al.* that TGM is the only useful mechanism for forming two dimensional bends in FMLs [51]. However for three dimensional shapes the upsetting (shortening) mechanism will be required to produce non-developable shapes (shapes that cannot be flattened into a continuous flat sheet).

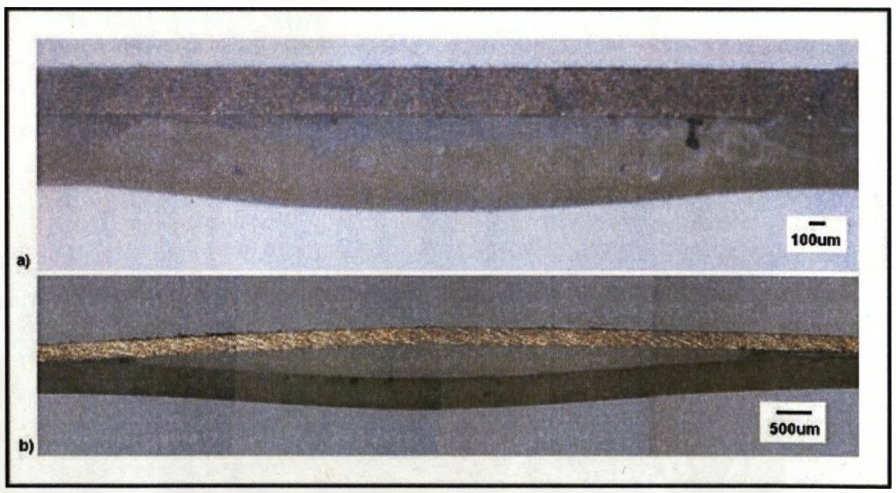

Figure 4.1 a) Delamination following Buckling Mechanism forming of FMLs after 2 passes b) after 10 passes (composite image)

4.1.2 Graphite Coating

Due to the optical nature of Laser Materials Processing (LMP), it is often necessary to reduce the reflectivity of any metallic work piece in order to improve the efficiency of the process or to protect the underlying surface from the effects of the laser interaction. In many cases, a graphite coating is applied in spray form, to achieve this. Graphite is often chosen for its poor reflective qualities, ease of application, availability and also for economic reasons.

4.1.2.1 Application of Graphite Coating

As discussed earlier, the graphite used here was in aerosol form for ease of application. However, this makes the method of application important in order to ensure a consistent layer of graphite is applied. Three possible application methods were tried: 'thin' where a light coating of the spray was applied in a single pass, 'thick' where multiple 'thin' layers were applied and each application was given time to dry between passes; and 'saturated' where the spray was held for approximately five seconds and a pool of graphite formed on the substrate. On visual inspection, the surfaces of the thin pass (figure 4.2a), thick pass (figure 4.2b) and saturated (figure 4.2c) showed some differences, with the thin layer appearing flatter than others, the thick sample showing some undulation and the saturated sample showing more pronounced peaks and troughs.

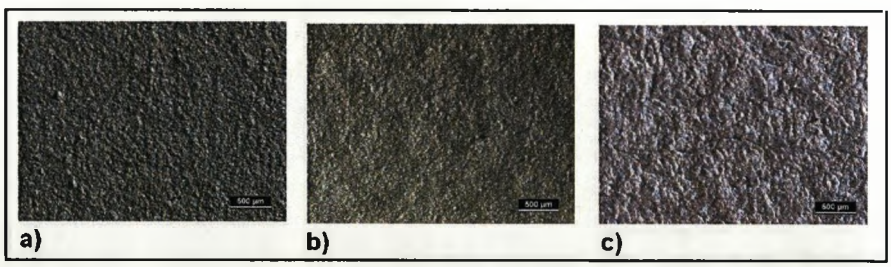

Figure 4.2: Micrographs for a) thin, b) thick and c) saturated graphite application methods taken at x5 magnification

When these samples were analysed using the vertical scanning interferometer (VSI), a surface roughness measurement was possible. A number samples were

measured in various 400 x 500µm sections across the sample surface. This was because of errors present in the data caused by the low levels of reflectivity offered by the graphite. The VSI relies on light scattered from the sample to take measurements and the parameters required to take measurements needed a high magnification. An example of measurements taken from these samples is given in figure 4.3. The results from five samples of each application method gave a similar surface roughness for the thin and thick samples, these being 2.36µm for thin and 2.86µm for the thick. In contrast the saturated samples gave a mean surface roughness of 1.5µm. This is due to a thick pool of liquid graphite formed when the saturated sample is applied. This gives a smoother surface finish than the thin and thick methods, as these were formed using light sprays where the graphite is applied in a more granular form due to the spray technique allowing some particles of graphite to dry prior to application of the surface. The build up of layer for the thick application would amplify any variation in the layer below.

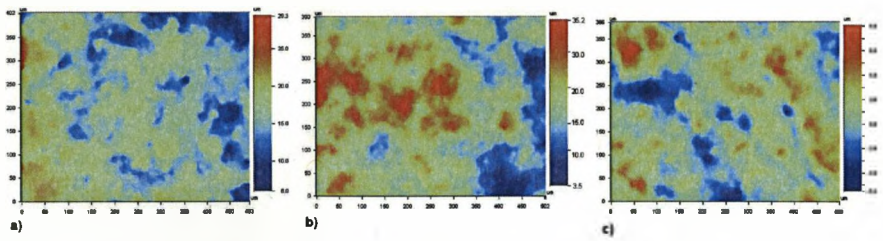

Figure 4.3: 2D VSI images of a) thin, b) thick and c) saturated application 400 x 500µm samples

The effect these application methods have on thickness was also measured using VSI. This was done by removing an area of graphite using acetone to give the original aluminium surface, thus allowing the thickness of graphite to be measured. Ten measurements for each application method were made and a mean result was calculated. The thin application method gave a thickness of 9.5µm and the saturated gave a thickness of 25µm. The thick application did not give a constant layer thickness (figure 4.4) per coating. This is due to the initial

coating having to attach to the smoother surface of the 'as received' aluminium, than the following coatings which had the rougher graphite surface to adhere to, which would reduce the volume of graphite applied.

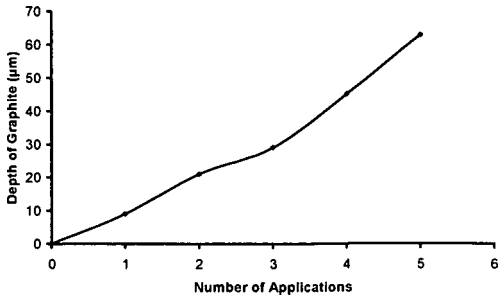

Figure 4.4 Number of coatings against thickness of graphite

4.1.2.2 Coating burn off

The initial tests on thin layer graphite are shown in figure 4.5. The results show the processing removes graphite at a constant rate until reaching a trough depth of 7.05µm after four passes. A final depth of trough of 7.36µm was reached in 9.5µm depth of graphite after ten passes of the laser. This left 15% of the total thickness of graphite remaining. The rate of increase in the depth of the trough drops from 1.74µm per pass in the first four passes to 0.05µm per pass in the last six passes. This is due to the energy of the laser melting a portion of the graphite, at the boundary between graphite which is vaporised during the passes and the bulk of the graphite which is largely unaffected by the laser. The molten layer then solidifies forming a more compact layer of graphite, when compared to the relatively loose layer achieved by the aerosol application. The more compact layer of graphite will conduct heat away more efficiently than the loose layer reducing the volume of graphite removed per pass. The aluminium work piece also in the vicinity (1.45µm deeper) of the laser/graphite interface would also increase the heat transfer rate away from the processing area, as aluminium has a thermal conductivity of 210W/mK whereas graphite is 25W/mK. This would help to arrest the removal of graphite from the base of the trough explaining why the trough did not extend down to the aluminium work piece.

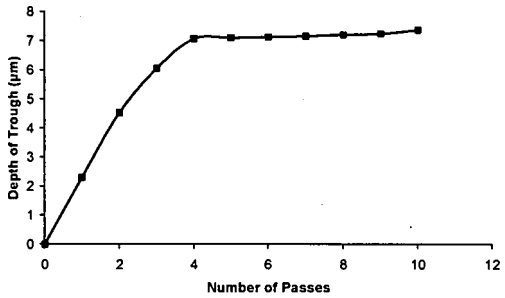

Figure 4.5 Number of laser passes verses trough depth CW processing of a thin (9.5µm) graphite layer

The effect of the laser energy on trough width (width of between two points on trough walls which are in line with the unaffected bulk of the graphite i.e. between the two piles of expelled graphite) was similar to the effect on trough depth. A high initial increase in width to 324µm after one pass occurred, the next pass only nominally affecting the width of trough, a 4µm mean increase from three tests, but then a sudden increase to 434um, then the rate of increase drops to 6µm per pass (figure 4.6). The effect is caused by the energy source moving further away from the graphite face due to burn off and trough deepening as well as the effects of solidification such as increasing reflectivity and thermal transfer.

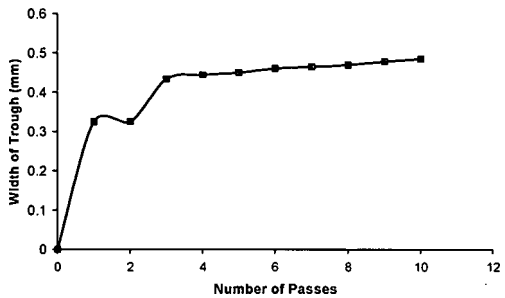

Figure 4.6 Number of laser passes verses width of trough for processing with thin (9.5µm) graphite layer

When the thick samples (63µm depth of graphite) were processed under the same conditions, similar results were observed. The process removed the graphite in the same manner as with the thin layer of graphite, with a quick initial

rate of trough deepening, which tends to reach a plateau. The final trough depth of 60µm is reached after only two passes (figure 4.7). Again the proximity of the thick aluminium layer to the graphite/aluminium interface may cause this remaining layer of graphite in the base of the trough.

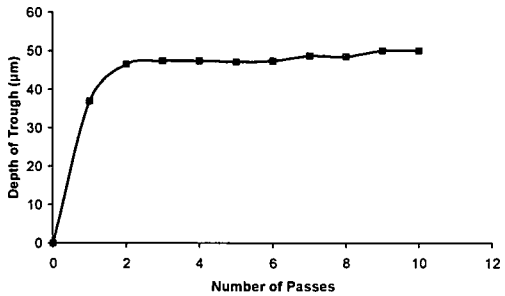

Figure 4.7 Number of laser passes verses trough depth for CW processing with thick (63µm) graphite layer

The effect of increasing passes strategy on trough width was a stepped nature, increasing then plateauing off then increasing again (figure 4.8). However, unlike with thin graphite, the width of the trough increases and levels off a total three times within the ten passes. It is again increasing on the 10^{th} pass, continuing this pattern. This could be due to removal of the loose graphite in the initial pass giving a large increase in trough width. The large trough then undergoes melting and re-solidification of the trough walls with little or no increase in trough width until a layer with a surface roughness low enough to reflect enough energy to form a 'key-hole' like effect as found in laser welding. This 'keyhole' reflects the laser energy within the trough. This leads to the removal graphite starting the process again. However further work is required to confirm this.

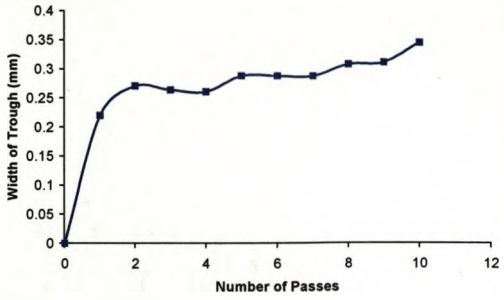

Figure 4.8 Number of passes verses width of trough for CW processing with thick (63µm) graphite layer

Figure 4.9a) shows the trough produced after a single passes with the laser beam traversing from left to right. The ejection from the trough is in a fine powdery form and is removed up to approximately 750µm away from the trough edge. After four passes (figure 4.9b) a clearly visible ridge has formed up to a height of 60µm on the lower side, 20µm on the other and both are 200µm wide. After ten passes (figure 4.9c) the lower ridge is 60µm and 190µm wide but the upper feature has been removed with the trough width increasing by 150µm and some collapse of the trough wall visible on inspection. The roughness has increased in the upper areas to 2.19µm after ten passes from 1.84µm after one pass and the lower side has increased to 2.10µm from 1.77µm. This increase in roughness suggests an increase in expelled graphite on the surface, as granules of graphite expelled during the laser passes would be ejected on to this area.

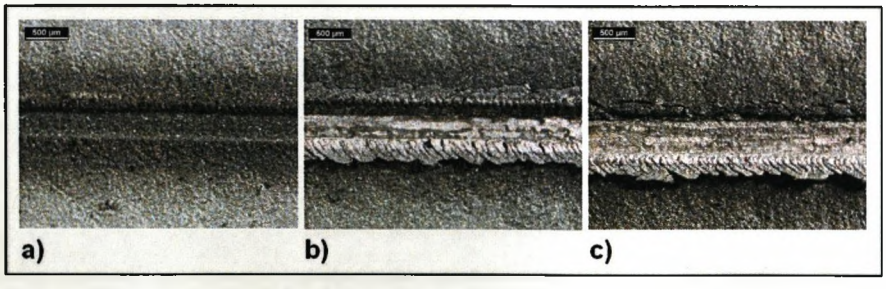

Figure 4.9 a) one pass, b) five passes and c) ten passes on thick (~50µm) graphite samples irradiated by Nd:YAG CW laser at 35W, 10mm/s and 0.2mm spot size

One possible explanation for these changes is that prior to the first pass, the graphite is in a loose and powdery form, due to the application method, and is easily ejected or vaporised by the beam. After this first pass, the graphite undergoes some melting and re-solidification, producing a more resilient layer in the bottom of the trough. This layer reduces the burn off rate and the ejected material forms a 'bow wave' in front of the beam due to the graphite being more compacted, rather than being expelled as smaller particles. This increased compaction is a result of the melting of the graphite removing the voids formed during the application. As the trough deepens a 'keyhole effect' is observed, where energy is concentrated by the walls of the trough allowing the graphite to be almost completely remove from the base and walls of the feature to widen.

The development of these features of the trough is shown in figure 4.10. The figures show a clear asymmetrical effect, with one side of the trough much higher and steeper than the other as the passes numbers increase. This asymmetrical nature may be due to the polarisation of the beam.

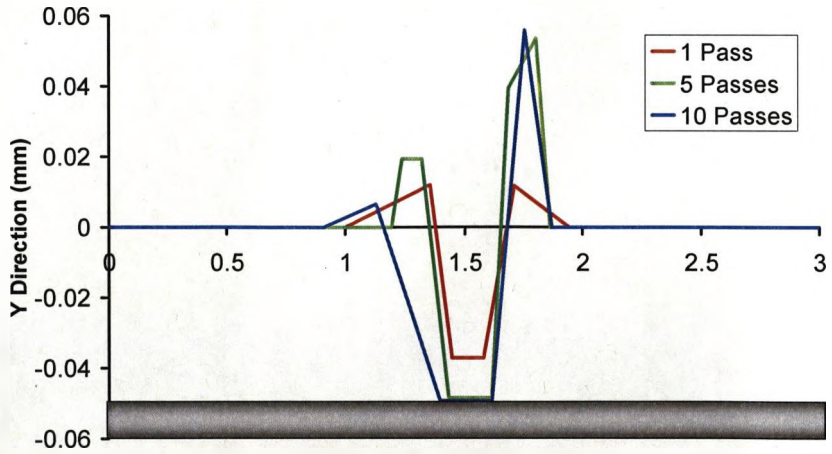

Figure 4.10 Trough features in Y direction after one, three and ten passes

The processed thin layer of graphite was imaged on an Atomic Force Microscope (AFM), where initial scans were taken in 'Contact Mode'. However this caused the graphite to be removed, giving false readings for the topography of the

sample. 'Non-Contact' mode was attempted next, but due to the large z-step heights (sometimes up to 7μm), the z feedback loop was often interrupted resulting in the tip coming out of contact with the sample. The samples were successfully profiled in 'Tapping' or 'Intermittent Contact' mode (figure 4.11). This procedure minimised direct contact with the surface, but allowed the tip to remain in feedback over the large Z step heights. These images clearly show the 'trough' produced by laser interaction with graphite.

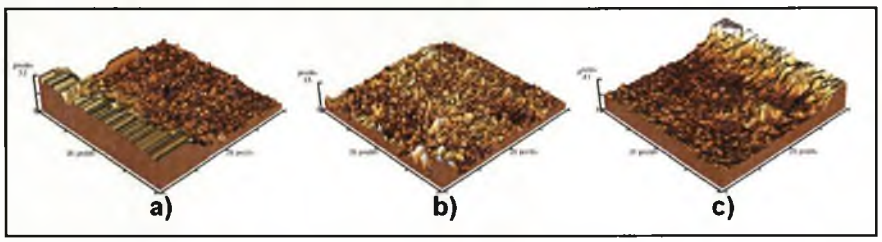

Figure 4.11: 3D 50 μm AFM scans of the laser processed graphite layer, showing the graphite structure a) left side, b) centre and c) right side after 5 laser passes at nanometre resolution

A number surface roughness tests were carried out to determine the differences between roughness of a saturated, thick and thin graphite layers. The layers were measured on the AFM in 'Tapping Mode' over 50μm^2 area. The average roughness and mean high was measured for two 50μm^2 areas on each of the graphite surfaces. The thin sample exhibited a mean surface roughness of 0.426μm, the thick a value of 0.825μm and saturated a value of 0.472μm. These values are much lower than those measured with the VSI (2.36μm, 2.86μm, and 1.50μm for the three cases respectively). These differences may be due to the size of the measurement area, as the larger VSI area takes a larger variation of surface features into account. However multiple layers of graphite cannot be achieved in a lab setting. Several days were required to produce one sample and since each sample could not be relocated without the use of a clamp. This would have required a large number of clamps and have delayed the experimentation.

4.1.2.3 Coating Reapplication

Whilst the application of multiple coats of graphite was not practical, another consideration for the graphite coating was the effect of rate of re-application. As can be seen in figure 4.12 the maximum CBA is achieved by removing and recoating the sample with graphite every five passes. This was a very labour and time intensive process with a 30 passes forming strategy taking almost 60 minutes. In addition the repeated handling and removal of the jig gave greater scope for misalignment. It was decided to re-coat the sample every ten passes since this gave a similar final bend angle to the maximum achieved and halved the processing time to 30 per sample.

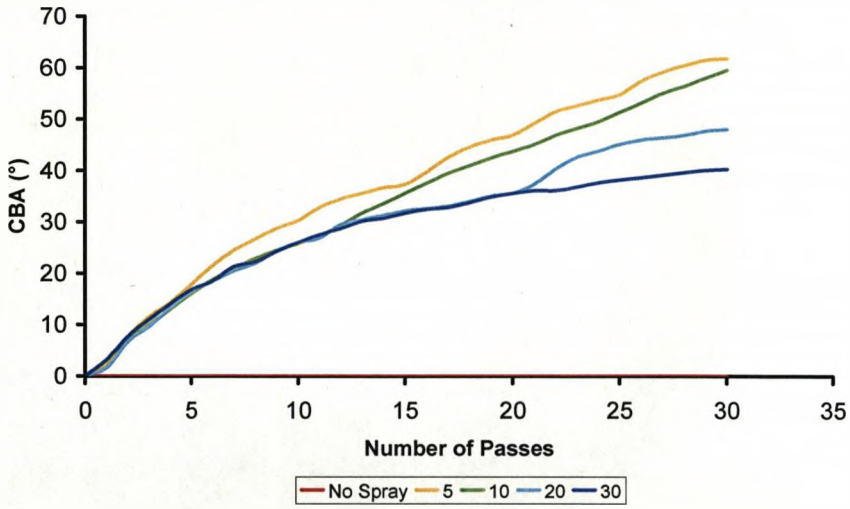

Figure 4.12 Variation on CBA of various graphite recoating strategies

4.1.3 Dwell Time

The time between passes, referred to as the dwell time, is important since it reduces the build-up of heat in the work piece. Such build up in monolithic metals reduces the temperature gradient and therefore the efficiency of the process. In FMLs, there is also the possibility of exceeding the maximum working temperature of the composite layer causing damage. The maximum operating

temperature (the glass transition temperature where cross-links are no longer locked and mechanical properties suffer significantly after this temperature) of the FM 94 resin used in commercially available FML panels is 100°C. Similarly the maximum working temperature for the CURV PP composite is 125°C. These temperatures were chosen to ensure that any thermal effects from the forming process would not be detrimental to the mechanical properties of the FML panel. The temperature the composite layer is exposed to during the laser forming cycle was investigated by applying a k-type thermocouple to the underside of a 0.3mm thick AL2024-T3 sample. A number of different methods were investigated to empirically measure the temperature at the aluminium/composite interface including mounting thermocouples within the laminate (which were damaged during the curing cycle) and removing small areas of composite to allow the placement of the thermocouple. This resulted in damage to the aluminium top layer, composite layers and poor contact between thermocouple and surface to be measured. None of the methods attempted gave consistent results so it was decided to use the single skin of aluminium. The maximum temperature reached over the ten passes was recorded. When the temperature rise is plotted against time it is evident that for short dwell time, the bulk material heats up and the temperature between passes reaches 85°C (figure 4.13). A dwell time of 30 seconds allows the bulk material to cool to around 20°C and avoiding any significant increase in the temperature of the bulk of the material. A reduction in power to 24W did not result in any significant change in the cooling rate and resulted in a drop of maximum recorded temperature of 25°C. This is a more realistic strategy, since a large period of time would pass between irradiations from a single beam traversing a long irradiation path. A dwell time of 30s with these processing parameters would allow an irradiation line of 0.3m.

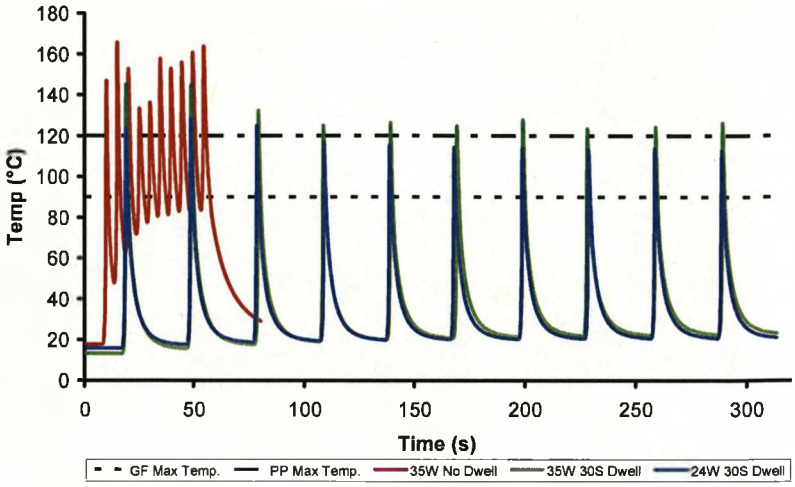

Figure 4.13 Recorded temperatures from lower surface of 0.3mm AL2024-T3 for various power levels and dwell times

4.1.4 Repeatability

In order to determine the repeatability of the laser forming process, five samples were processed at a laser power of 30W, a scan velocity of 20mm/s and a 30s dwell time. Aluminium 2024-T3 was selected in preference to an FML as the CBA was greater for aluminium, thus highlighting any error due to variation in the process. The results are shown in Figure 4.14.

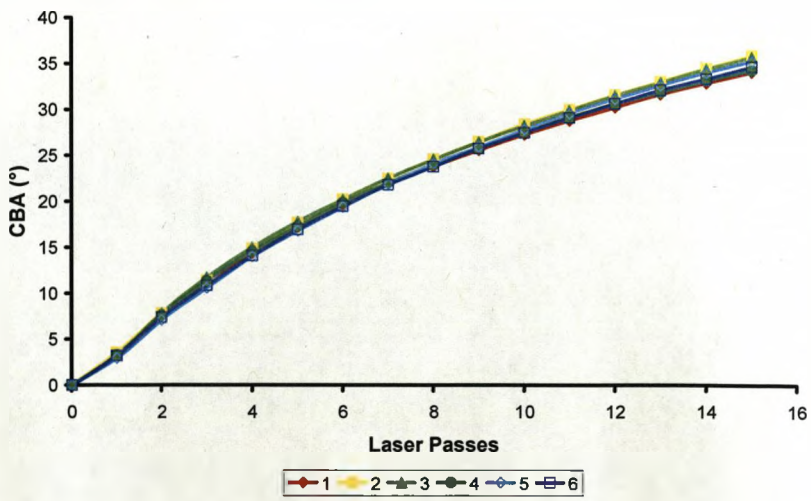

Figure 4.14. Repeatability test using plain AL2024-T3

The tests were under taken at different times of the day with the laser system having been 'warmed up' for 30 minutes prior to the first test. The mean bend angle was 34.9° +/- 5%, showing good repeatability of the process.

4.1.5 Quality Control

To investigate the consistency of the interface between the composite and metal substrate, a peel test was carried out and a number of the results are presented here, figure 4.15. The load extension graphs show good repeatability between the samples, all of which were produced over a three year period.

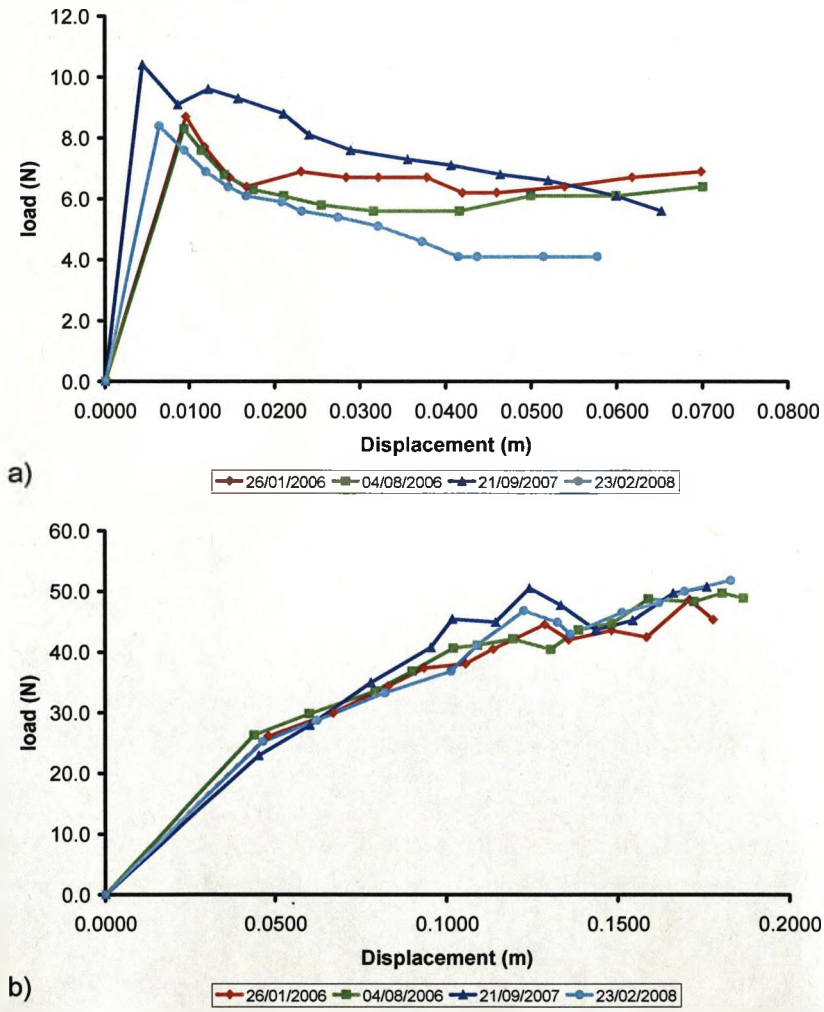

Figure 4.15 Load applied to the sample plotted against the crosshead displacement for a) GF and b) PP

4.2 Laser Parameters

The results presented in this section summarise the findings of a short study to investigate the effect of the varying a number of laser parameters on the laser forming process. These parameters have been investigated to ensure that the data collected here on thin cross-section materials (0.3mm) agrees with pervious work by Edwardson *et al.* [46] on thicker cross-section samples (>1.0mm). The work presented in this section was undertaken on a 0.3mm thick 2024-T3 aluminium alloy and two 2:1 FML lay-ups, one manufactured using E-glass fibres in an FM94 Epoxy resin and the other using a 100% polypropylene based composite. The E-glass rovings were in crowfoot and unidirectional weaves, with the unidirectional fibre orientated with the rolling direction of the aluminium and the traverse direction of the laser and the PP composite as standard plain weave. Power, traverse velocity, spot size and wavelength of the laser were all varied and the results with respect to Cumulative Bend Angle (CBA), Bend Rate Per Pass (BRPP) and Mean Bend Rate Per Pass (MBRPP). The values for MBRPP were calculated by dividing the bend angle by the number of passes required to achieve it, giving a mean value. The value for MBRPP was taken following 30 passes, whereas the BRPP was determined following each scan.

4.2.1 Power

The first part of the study investigated the effect of varying the laser power on the laser forming process. Three separate materials were investigated initially, these being aluminium 2024-T3, 2:1 GF/epoxy FML based on a crowfoot weave and 2:1 100% PP based on a plain weave FML. These materials were processed at a laser traverse velocity of 10mm/s and at two laser power levels, 24W and 35W. These results are shown in figure 4.16.

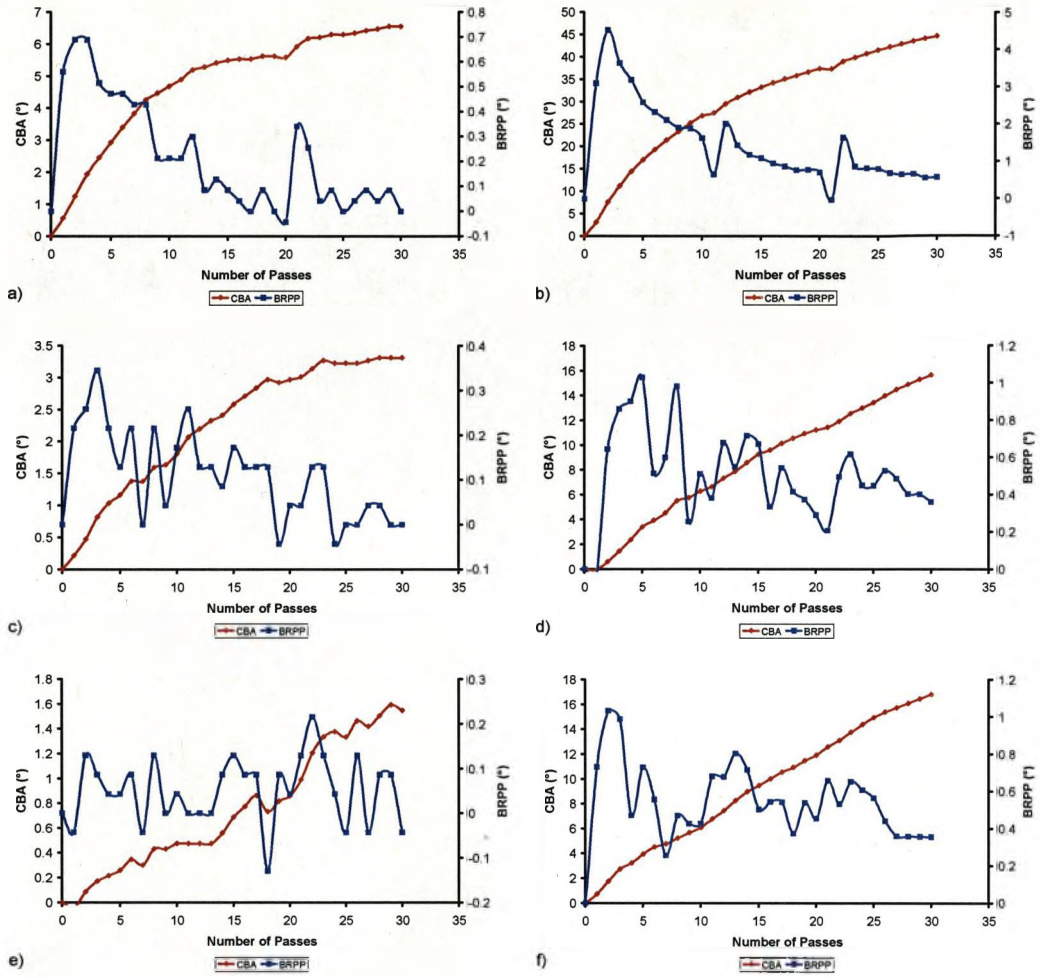

Figure 4.16 CBA and BRPP against Number of Scans processed at 10mm/s and either 24W or 35W for Aluminium, GF and PP FMLs

Comparing the data for a laser power of 24W (figure 4.16 a), c) and e)) with those for a laser power of 35W (figure 4.16 b), d) and f)) indicates that the former gives a higher CBA and therefore a higher BRPP. For a single skin of aluminium, a 750% increase in CBA is achieved for an increase in power of 150%. Similarly, increases of five fold and ten fold were recorded for GF/epoxy and PP FMLs respectively. This increase in CBA supports the TGM theory discussed in section 2.1.3. This increase in CBA is clearly linked to a rise in the temperature on the surface of the material. The greater surface temperature results in an increased temperature gradient through the thickness of the material. This leads to larger

plastic stresses being induced in the upper surface of the sample than in the lower surface, which leads in turn to a greater bend angle. Another characteristic associated with the increase in laser power is the fact that the samples processed at the higher power level exhibit a smaller variation in BRPP. To ensure that this was not an artefact of the increase in CBA, the BRPP was normalized against the highest value for BRPP measured over the 30 scans to give a normalized bend rate per pass (NBRPP) (figure 4.17). Normalizing removes the effect of angle amplitude from the charts of BRPP against Number of scans and allows fro the direct comparison of the changes in BRPP between the laser powers. It is evident from figure 4.17 that there is a correlation between the laser power level and the variation in BRPP. It evident that as the laser power increases, the variation in bend rate per pass reduces.

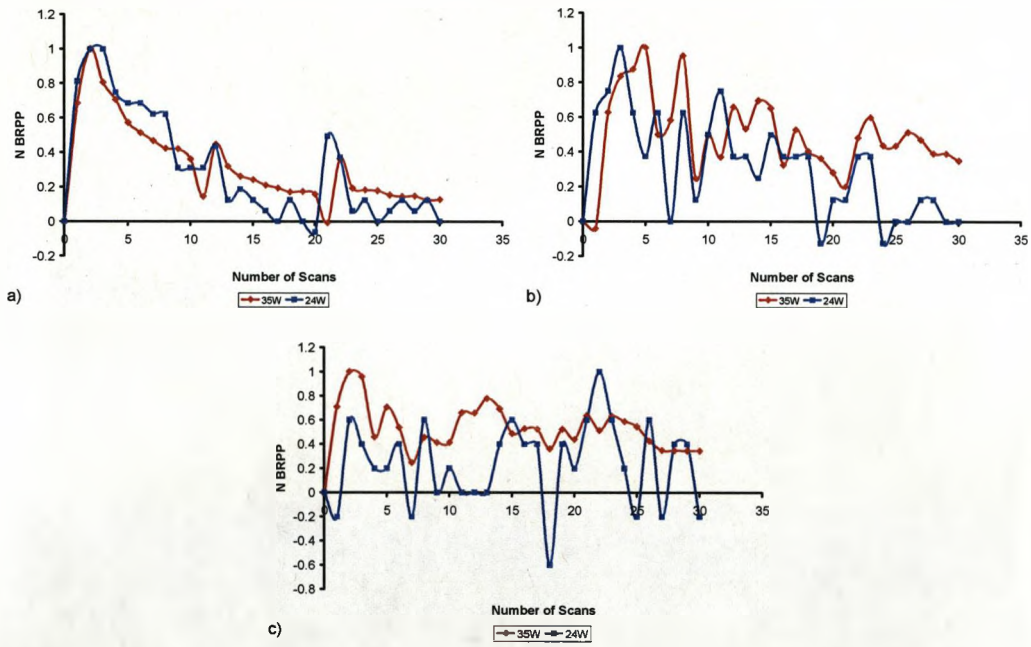

Figure 4.17 Normalized BRPP values for a) Aluminium, b) 2:1 GF FML and c) 2:1 PP FML

Figure 4.18 shows MBRPP plotted against laser power for a number of different laser traverse velocities, and shows the effect of increasing the laser power

levels. Single datum points per power/velocity setting are plotted and a polynomial fit applied.

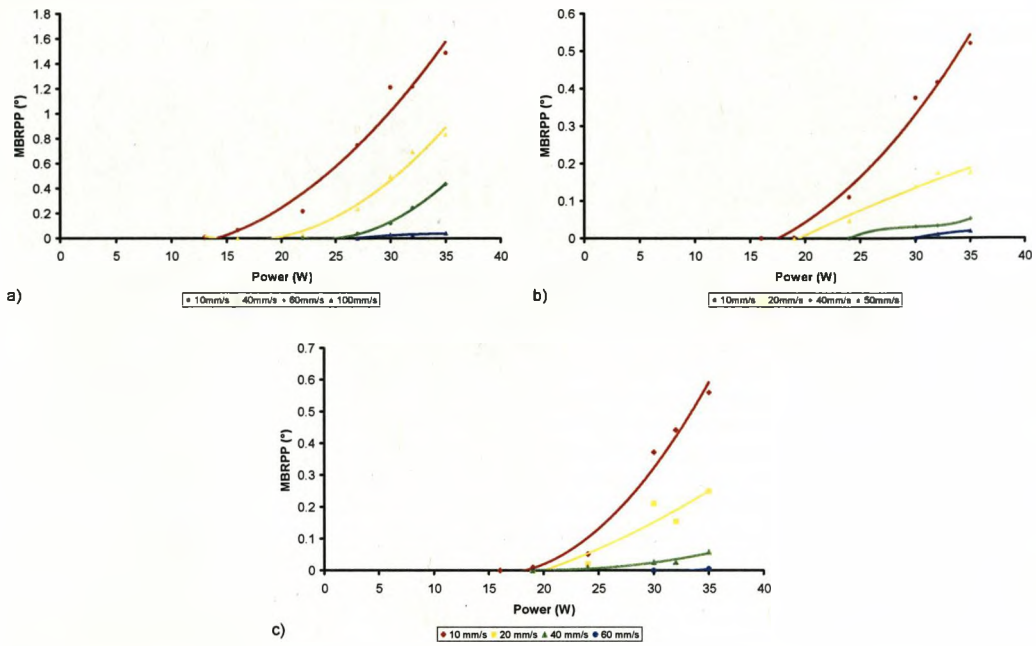

Figure 4.18 MBRPP against laser power for a) 0.3mm Aluminium 2024-T3 b) 2:1 crowfoot weave GF based FM and c) 2:1 PP based FML

These figures show that at a traverse velocity of 10mm/s an activation power of approximately 14W is required to initiate TGM forming in aluminium and approximately 19W is required for the FMLs. This difference in activation power is also apparent at 40mm/s, with approximately 20W being needed for the aluminium and 24W for the FMLs. This is due to the FMLs having a greater overall thickness, which therefore requires a greater level of plastic strain to induce bending. As the power is increased above the activation threshold, the MBRPP increases, with the rate of increase being dependent on the velocity of the scan beam. The increase in MBRPP for the single sheet of aluminium is greater than for the two types of 2:1 FML. This is to be expected as the formable thickness is lower for the FMLs than the aluminium sheet (see Section 5.3.1 for further details). These findings agree with those presented in section 2.1.6.1 following similar tests on materials with a greater thickness. Since the system used here had a maximum power of 35W, it was not possible to determine the

upper limit beyond which a further increase in power would not lead to an increase in bend angle. The failure for the increase in power to correspond to a increase in bend angle would be due to the incident energy causing a too great heat build up through the thickness of the material. This would lower the temperature gradient between the surfaces. This reduction in the temperature gradient would trigger the BM instead of the TGM. The BM is detrimental to the forming of FMLs, as discussed previously in Section 5.1.

4.2.2 Velocity

The effect of varying laser traverse velocity on the forming characteristics of the three materials is shown in figure 4.18 where the data are a laser power of 35W and a laser traverse velocity of 10mm/s or 40mm/s are presented (figure 4.19)

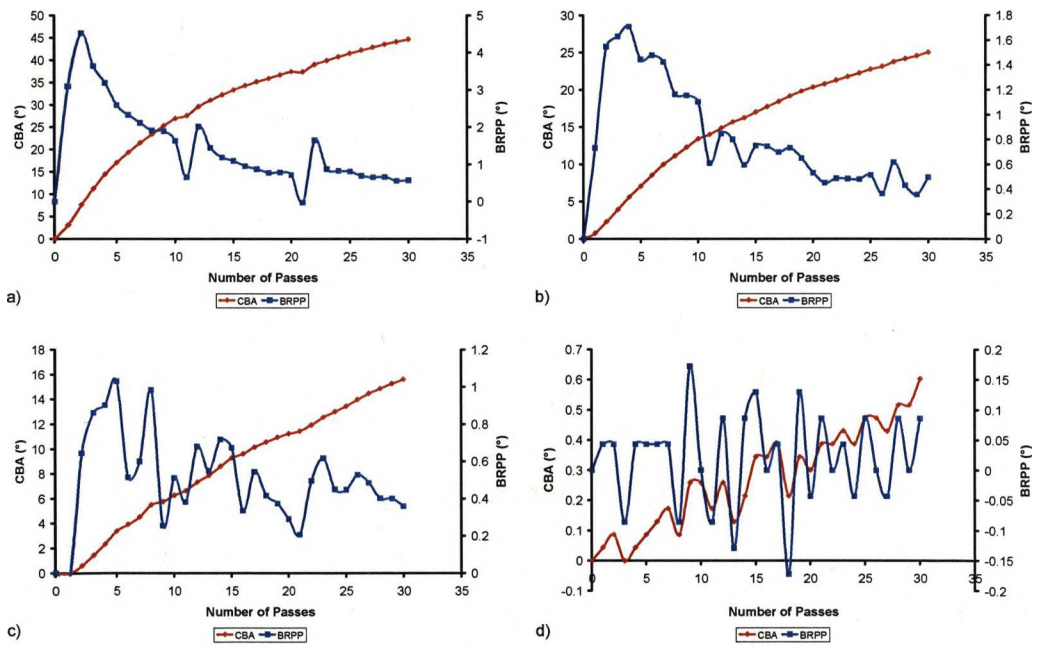

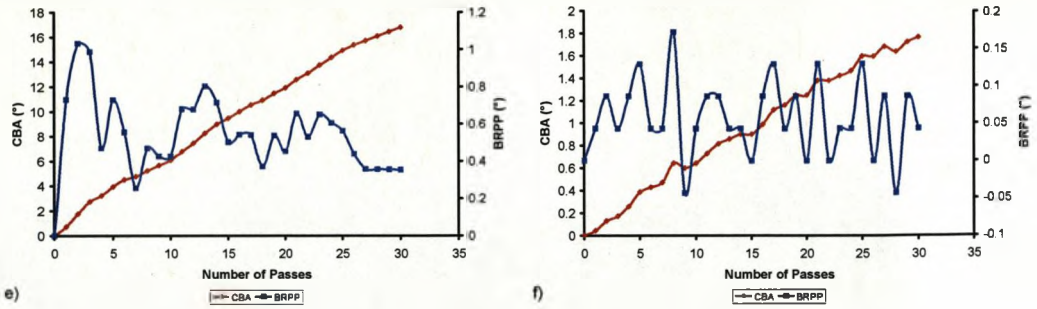

Figure 4.19 CBA and BRPP against Number of Scans processed at 35W and either 10mm/s or 40mm/s for Aluminium, GF and PP FMLs

The most striking effect of increasing velocity is the reduction in CBA and BRPP. As the processing velocity is increased from 10mm/s to 40mm/s, the maximum CBA that drops by approximately 50% for aluminium 96% and 90% for GF and PP FMLs respectively. As previously observed for a decrease in power, it appears that a lower velocity results in a more consistent BPPR, with less variation between scans. When the results are normalized with respect to the highest BRPP recorded during the 30 passes (figure 4.20), variations between individual scans appear to decrease as the velocity reduces, particularly for the GF FMLs. All three materials exhibit similar trends at the lowest velocities, with the BRPP increasing to a maximum achieved within the first five scans. The BRPP then decreases steadily, with brief increases being observed after the reapplication of graphite following 10 and 20 scans. At the higher traverse velocity the aluminium follows a similar trend to that observed at the lower velocity, whereas the FMLs exhibit random variations in BRPP, with no clear trends apparent.

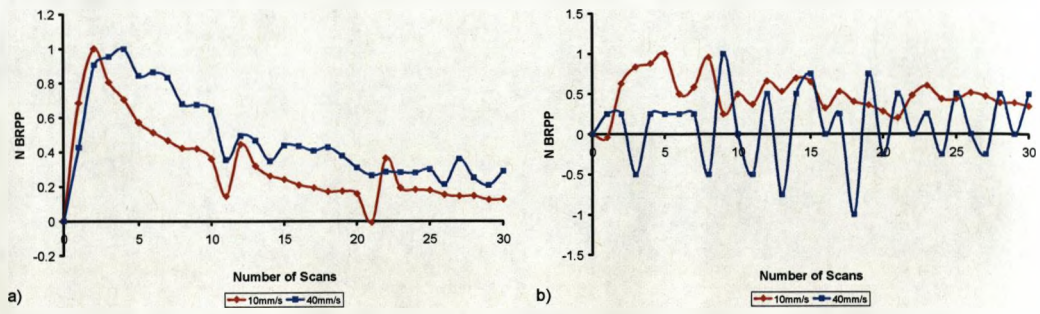

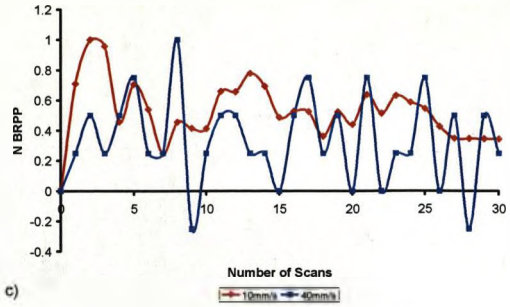

Figure 4.20 Normalized BRPP values for a) Aluminium, b) 2:1 GF FML and c) 2:1 PP FML

The effect of varying traverse velocity on MBRPP is shown in figures 4.21. The relationship between the laser traverse velocity and the mean MBRPP can be given as an inverse relationship where an increase in velocity results in a reduction of bend rate. All three materials show similar characteristics. At low velocities high BRPP is observed the BRPP subsequently reduces as the velocity increases, with the rate of reduction being dependent on the material type and the power level.

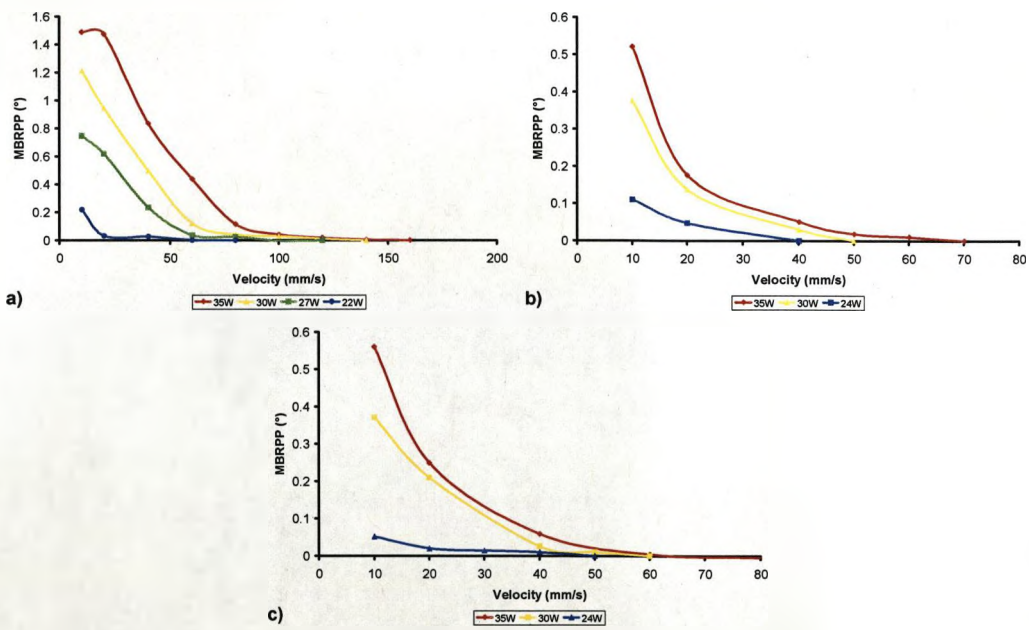

Figure 4.21 Effect on MBRPP of varying processing velocity for various powers on a) AL 2024-T3 b) 2:1 Crowfoot weave GF FML and c) 2:1 PP FML.

For the case of plain aluminium alloy (figure 4.21 a)) at the lowest traverse velocity (10mm/s) and the highest power (35W), there is no decrease in MBRPP when the velocity is doubled to 20mm/s. This is associated with a 50% reduction in the incident energy. The reason for this is that the slow traverse velocity gives a longer interaction time between the surface of the material and the laser source. The long interaction time leads to the thermal energy dispersing through the depth of the material, which in turn leads to a greater increase in temperature through the thickness of the sample. This gives a reduction in thermal gradient, since the lower and upper surfaces are at closer temperatures than at higher traverse velocities, where the thermal energy does not penetrate as deeply. The reduction in thermal gradient leads to a reduction in the efficiency of the process and results in a similar bend angle to that obtained processing at 20mm/s, i.e. at half the incident energy level. The creation of a more uniform temperature gradient through the thickness of the material leads to the propagation of the BM instead of the more desirable TGM. This effect is not observed in the GF and PP FMLs (figure 4.21 b) & c)), where an increase in velocity results in a reduction in the MBRPP.

4.2.3 Combined Effect of Laser Power and Traverse Velocity

As illustrated in the preceding sections the effects on laser forming by both laser power and traverse velocity are related. In an effort to illustrate this 'operational windows' were produced by plotting the point at which a laser power and traverse velocity form a bend of greater than 0°, 0.1°, 0.2°, 0.5° and 1.0° per pass, over a mean of 30 passes (figure 4.22). These values were extrapolated from figure 4.21 for either a given power or figure 4.18 for a given velocity. These points are then used to plot a line of best fit to give a visual approximation of the effect of varying both laser power and traverse velocity. In these graphs the area above the line of best fit or 'contour' corresponds to a bend being produced in the respective material. The various lines indicate contours where on that line it is possible to produce a BRPP of the indicated value and above the line a value of over the indicated value but below the next given contours value is produced.

Therefore the area defined by these contours corresponds to the 'formability' of the given material, giving an indication of how applicable laser forming is to that material.

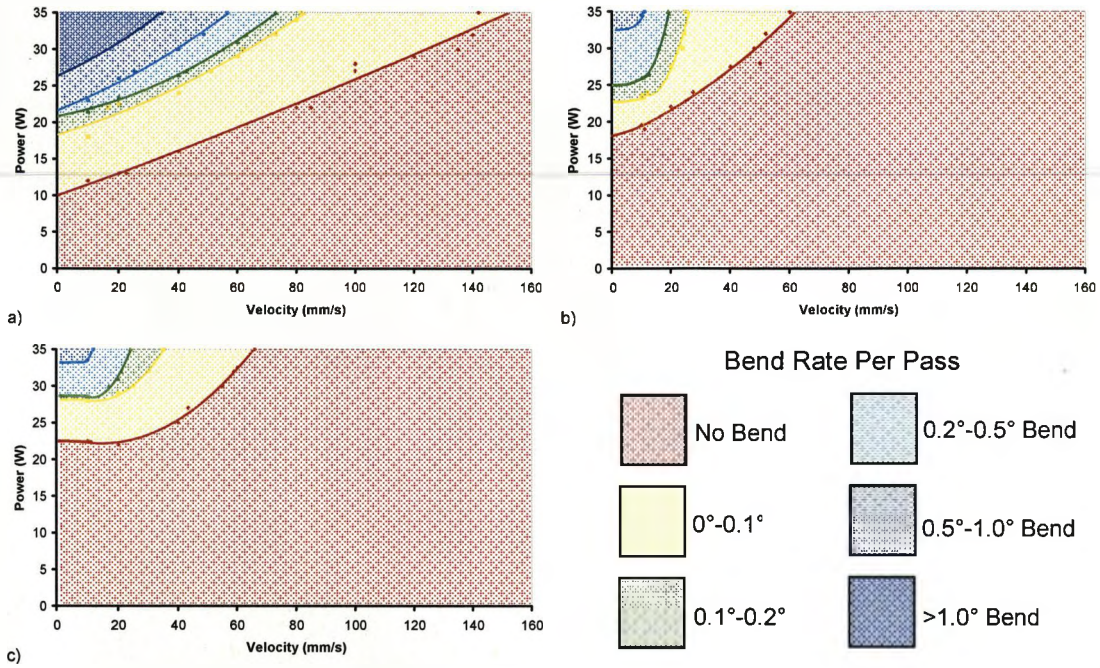

Figure 4.22 Laser power against traverse velocity for laser forming of aluminium alloy and 2:1 FMLs of GF and PP

All three materials follow similar trends, with an increase in laser power relating to an increase in BRPP (as discussed in section 5.2.1) and an increase in traverse velocity relating to a decrease in BRPP (as discussed in section 5.2.2). As would be expected from previously presented data, processing the aluminium alloy (figure 4.22 a)) gives the greatest area of possible combinations of laser power and traverse velocity that lead to the production of a bend in the material in a single pass. It also shows that the aluminium alloy also has the greatest possibility for laser forming with a number of laser power and traverse velocity settings giving a BRPP of over 1° as indicated by the dark blue area, not visible on any other chart. The GF and PP (figure 4.22 b) & c)) operational windows cover approximately the same area of the chart and react similarly to increase in velocity, in that the possible bend rate achieved drops off considerably for an

increase in velocity when compared to the plain aluminium alloy, which has lesser reaction to the increase in velocity. Were data available for higher laser powers for a given velocity, the contours would fall back towards the Y axis as the increase in power would eventually lead to melting of the aluminium, lowering the plastic strains produced by the laser forming process. Whilst these results indicate the lower boundary for laser forming of FMLs an upper boundary will be formed by effects such as microstructural changes and other detrimental thermal effects. This will give an operating window for the laser forming of these FMLs under specific circumstances.

4.2.4 Scan Strategy

The effect of scan strategy on laser forming will only briefly be discussed since Bartkowiak *et al.* [56] have covered the topic in some detail. In this study, the effect that multiple scans have on the forming process will be considered. Figure 4.23 shows an ideal TGM forming curve, where the CBA initially increases rapidly, before a number of factors, such as strain hardening, section thickening, thermal effects and geometrical effects [158], reducing the rate of bending until increases of less than 0.05° per pass are achieved after 160 passes. The effect scan strategy has on the BRPP is also illustrated by figure 4.23. The BRPP starts at a high rate initially, and then gradually drops off, but has a high amount of fluctuation between each pass.

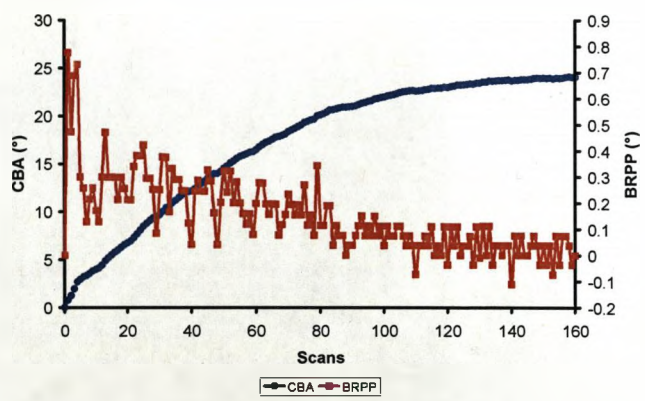

Figure 4.23 2:1 GF FML processed at 35W, 10mm/s, 30s dwell and graphite re-applied every 10 scans

4.2.5 Spot Size

Changes in the spot size affect the forming process in two ways. The main effect is to change the forming mechanism, as discussed in section 5.1.1. Increasing the spot diameter from 0.2mm to 4mm changed the mechanism from TGM to BM. This in turn changes the characteristics of the resulting bend, TGM giving a small consistent bend towards the source, whereas BM giving much higher BRPP, at the cost of material integrity. The other effect is that by increasing the spot diameter, the intensity of the beam is reduced. This reduces the surface roughening associated with melting and re-solidification of the aluminium. For the 0.2mm diameter fixed spot size of this system numerous features were present at higher power levels and lower velocities that suggested that recasting and other melting features have occurred. These effects could be removed or reduced by increasing the spot size, but as observed when profiling the system, the quality of the beam reduced significantly. Since the effects of altering spot size have been investigated previously [46], it was decided to operate the system at its fixed focal length. This ensured that the highest beam quality available with this system was used, removing the variable of beam profile from the investigation.

4.2.6 Wavelength

To investigate the effect of wavelength on the forming process, one aluminium sample was processed on the Nd:YAG laser system described in section 4 and another was processed on a Synrad sealed CO_2 unit. The CO_2 system has a maximum power output of 25W and the beam is manipulated using galvanometer driven mirrors giving a maximum raster speed of 1000mm/s. The beam is focused through a flat-field lens giving a 0.15mm diameter beam at a 180mm stand-off from the lens. The system is controlled through a Windows-based GUI system (Winmark). By varying the vertical position of the sample a spot size of 0.2mm could be achieved. The aluminium samples were then processed at 25W, with a 0.2mm spot size 10mm/s with a 30 second dwell time and the graphite coating reapplied after every ten passes (figure 4.24). The results show that the two values measured of CBA were similar (within 5%), 27° for 1.064μm the

Nd:YAG system and 26° for the 10.64μm CO_2 system. However, the way in which the CBA is reached was slightly different with the Nd:YAG system giving a more linear increase in CBA. Also the BRPP fluctuates more with the CO_2 system with a greater BRPP for the first five scans after the application of graphite and then a drop in subsequent scans. This can be explained by the metal having a higher coefficient of absorption for the shorter wavelength of the Nd:YAG system and thus less affected by the removal of graphite during processing with the Nd:YAG system than the CO_2 system. It was decided to continue the study using the Nd:YAG system instead of the CO_2 as the Nd:YAG system has a greater power output (35W compared to 25W) allowing for greater CBAs to be achieved. The potential for greater bend angle would amplify forming effects in the Fibre Metal Laminate.

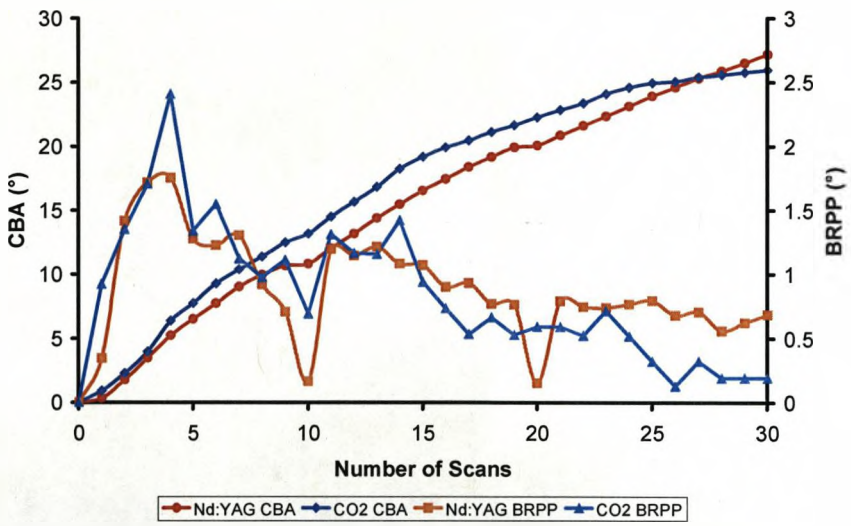

Figure 4.24 AL2024-T3 processed on Nd:YAG and CO_2 laser systems at 25W 10mm/s, 30 second dwell and graphite reapplied every ten passes.

4.2.7 Thermal Effects

Due to the sensitivity of composite materials, the epoxy resin system used here has a maximum service temperature of 100°C whilst the SRPP FML has a maximum service temperature of 120°C. A number of experiments were carried out to identify various combinations of velocity and power maximum temperature

achieved during processing. The thermocouples were attached as described in section 3.1.4 at measurement point 110 and the data recorded using the data logger. The peak temperatures from a 10 scan irradiation strategy were recorded and are shown on figure 4.25.

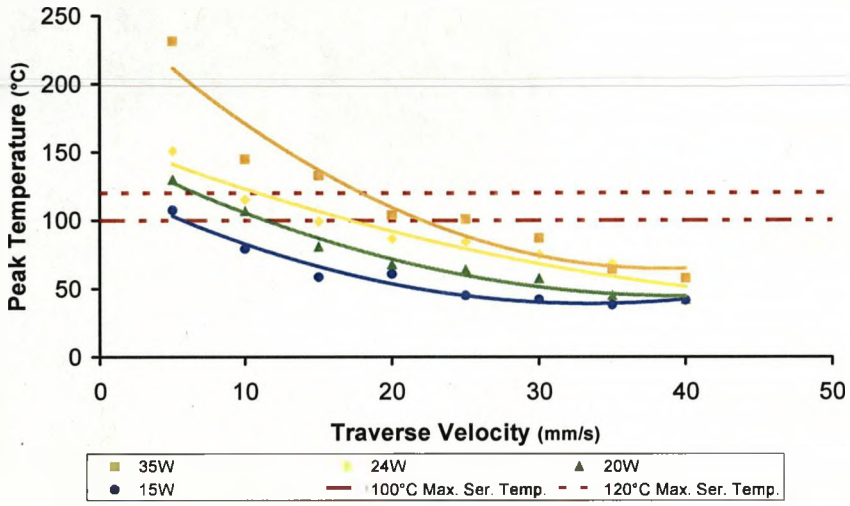

Figure 4.25 Peak recorded temperatures recorded at measurement point 110

The temperatures recorded at full power (35W) varied from 231°C at 5mm/s to 57.8°C at 40mm/s. For the GF FML the minimum processing velocity was 22mm/s and 18mm/s from the PP FML at full power. However the interaction times at these temperatures are very small. Figure 4.26 shows the data recorded at 35W laser power and 10mm/s traverse velocity. It shows the length of time in which the surface exceeds the maximum service temperature of the epoxy resin is 0.7 seconds and less than 0.1 seconds for the maximum service temperature in the case of PP FML.

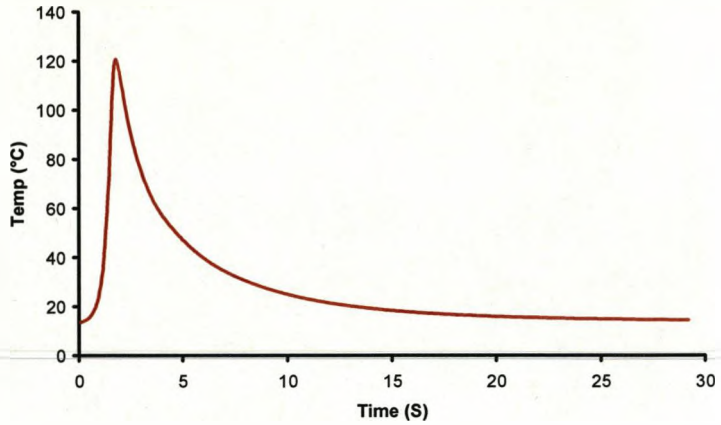

Figure 4.26 Temperature data of single scan of 35W power and 10mm/s traverse velocity

In order to ascertain weather this length of interaction is detrimental to the FML properties, further investigation is required (section 4.4)

4.3 FML Parameters

The results presented in this section summarise the findings of a study to investigate the effect that varying a number of material parameters of the Fibre Metal Laminate (FML) has on the laser forming process. The first material parameter to be considered is the effect of the stacking sequence of the FML. This involves increasing the number of composite and aluminium layers in the sample and studying the effect this has on Cumulative Bend Angle (CBA), the Bend Rate Per Pass (BRPP) and the Mean Bend Rate Per Pass (MBRPP), the effect of varying the FML lay-up on the Real Time Forming (RTF), the creation of strains in the material, and the propagation of thermal energy through the sample. The effect of altering various parameters, both material and process, has on the formability of the metal layer has been covered by others in work previously discussed (section 2.1.5). However, the effect that introducing composite layers has on formability has not been covered previously and investigations into the effect of the fibre orientation, fibre weave and increasing

the ratio of the volume fraction in the FML has on the laser forming process will also be covered.

4.3.1 Stacking Sequence

The initial parameter influencing the formability of FMLs to be discussed is the quantity and arrangement of the aluminium and composite layers. As the TGM can only occur in the aluminium layer to prevent thermal damage to the composite material, the upper aluminium layer must act as a bending arm to 'pull' the remaining layers of the FML to shape. This has implications on the laser forming process and therefore on the bend angle that is achieved. The following sections will discuss the effect that varying the number layers has on the formability of FMLs. The work presented in this section was carried out on both glass fibre (GF) and polypropylene (PP) based FMLs consisting of alternating layers of 0.3mm thick aluminium 2024-T3 alloy and composite material. The GF composite layer consisted of E-glass fibres in an FM94 epoxy resin and the PP composite was based on a self reinforced 100% polypropylene. The E-glass rovings were supplied in unidirectional pre-pregs, with the fibre orientated parallel to the rolling direction of the aluminium and parallel to the traverse direction of the laser. The PP composite was supplied as a standard plain weave. The stacking sequences used in this part of the study were 1:1, 2:1, 2:2 and 3:2 for both the GF and PP based FMLs.

4.3.1.1 Cumulative Bend Angle

There are limitations of TGM with FMLs, such as the maximum achievable bend angle, since this is limited by the bending force that can be attained in the aluminium layer. As commercially available FMLs typically have a maximum thickness of aluminium of 0.5mm [6], this limits the number of layers that can be formed by this method. In this study, with a 0.3mm aluminium layer, the maximum FML lay-up formable was a 3:2 configuration (figure 4.27).

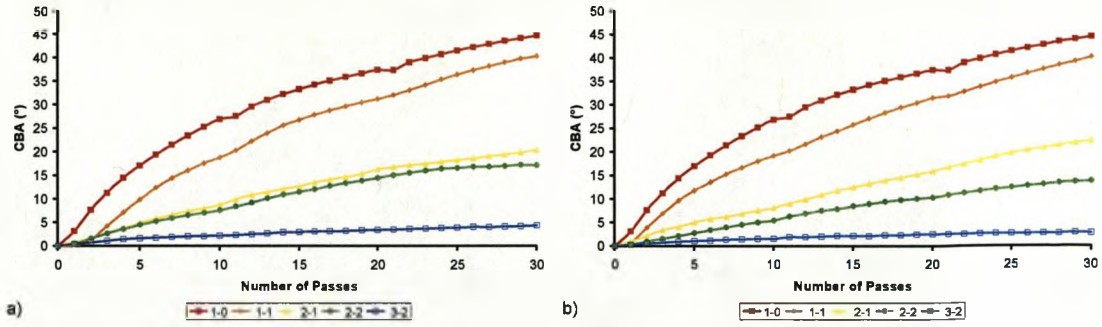

Figure 4.27 CBA against number of passes for different lay-ups of both a) GF and b) PP based FMLs processed at 35W and 10mm/s

It is clear that increasing the number of layers in the FML leads to a reduction in the CBA achieved for a given set of laser parameters. For both the GF and PP based FMLs there is a marked reduction in the CBA achieved as the number of layers increases, when processed at 35W 10mm/s (figure 4.27 a) and b)). For these parameters, the addition of an initial single composite layer results in a drop of 12% in CBA for both FML types, for the 1:1 lay-up relative to a single skin of aluminium alloy. A greater drop in CBA is observed following the addition of the next composite layer causing a drop of 15% and 36% in the case of a GF and PP layer respectively. The effect of adding a single layer of composite depends where the layer is located within the lay-up. The reduction in CBA observed between a 1:0 and a 1:1 lay-up is lower for both composite materials than the reduction observed between the 2:1 and 2:2 lay-ups. A contributing factor to this is the transfer of heat to the composite layer from the aluminium layer incident to the laser. The temperature increase leads to softening of the matrix and this is discussed in more detail in section 4.3.1.4. The addition of an extra aluminium layer causes a greater drop in the value of the CBA achieved over the 30 passes over the addition of a composite layer. When increasing to a 2:1 lay-up from a 1:1 lay-up a reduction of 50% in the case of the GF lay-up and 45% in the case of the PP based composite is observed. A drop in CBA of 70% and 75% for GF and PP based FMLs respectively occurs when going from a 2:2 to 3:2 lay-up. This

greater rate of reduction in CBA is expected as the aluminium is stronger than either cured composite, therefore requiring greater mechanical force to deform it.

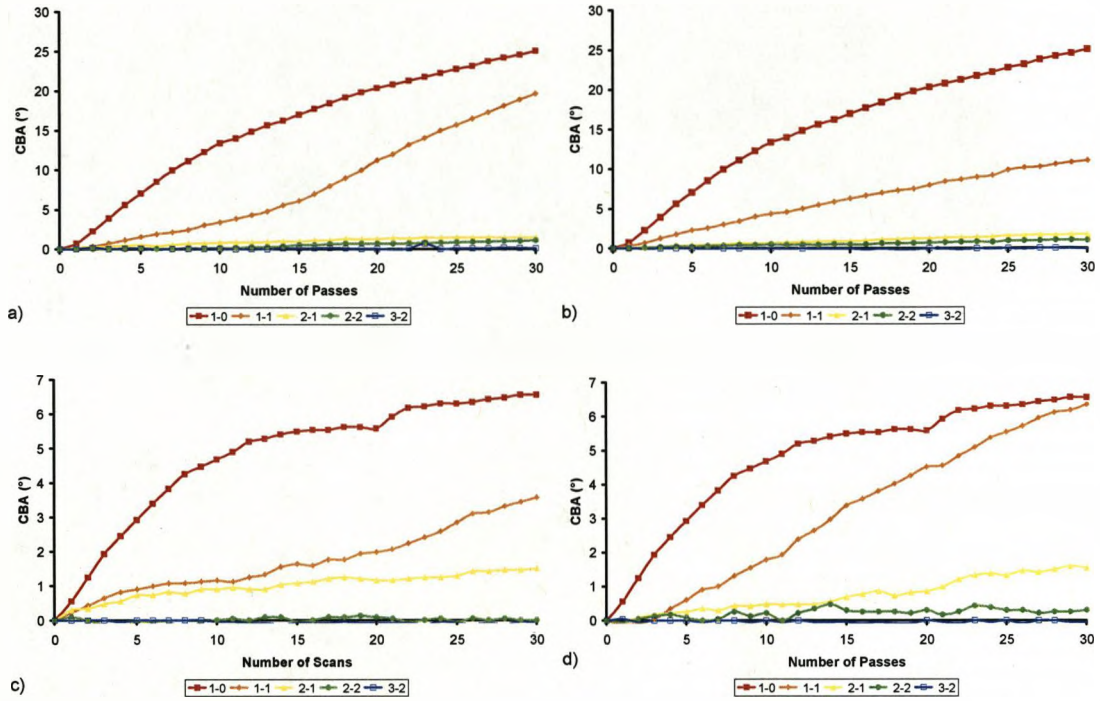

Figure 4.28 CBA against number of passes for a variety of lay-ups of both GF (a & c) and PP (b &c) based FMLs processed at 35W and 40mm/s (a & b) and 22W and 10mm/s (c & d)

Similar trends are observed at the lower energy levels (35W, 40mm/s and 22W, 10mm/s figure 4.28), as at higher energy levels, but the reduction in CBA is not as consistent for the two types of FML. This is due to other factors, such as stresses in the work-piece produced during the production of the FML panels, having a much greater influence on CBA at the lower energy levels as the plastic strains induced by the laser forming process are of a lower value.

As stated previously (Section 5.1), the method for forming FMLs is to induce the temperature gradient mechanism in the uppermost surface of the FML. This causes a bend to form in the top layer, which 'pulls' the lower layers upwards. This suggests that the effect of a reduction in CBA observed as the number of

layers in the lay-up of the FMLs increases, is due to the ratio of thickness of the formable layer to the 'un-formable' layers.

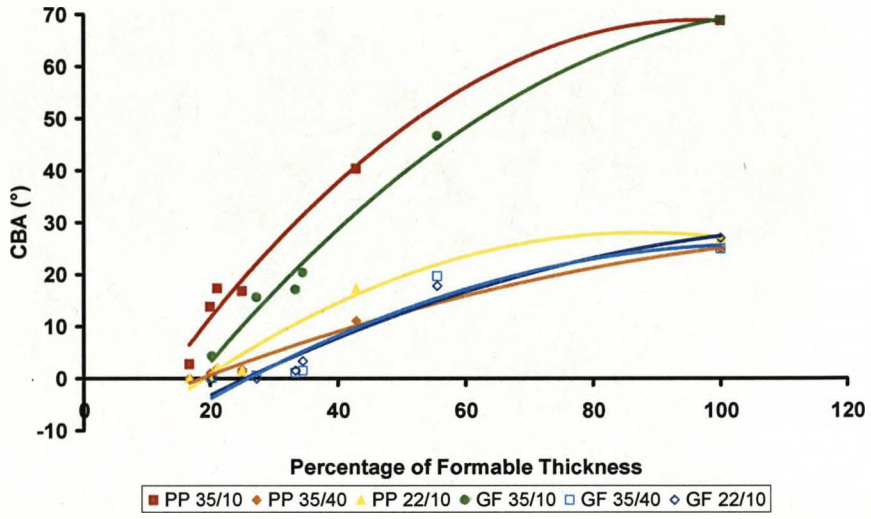

Figure 4.29 CBA against percentage of formable thickness

When the CBA is plotted against the percentage of formable thickness, the thickness of the formable layer as a percentage of the overall thickness of the FML panel (figure 4.29), a clear relationship is observed. The achievable CBA produced by a given set of laser parameters increases as the percentage of the formable thickness increases. From this chart, it appears that the rate of increase is dependent on the laser parameters, with the highest laser powers and lowest traverse velocities producing the highest rate of increase in bend angle. When the CBA values are normalized by the maximum bend angle achieved for that given set of parameters and plotted against percentage of formable thickness (figure 4.30), the variation in the rate of change of CBA with respect to the percentage of formable thickness is less obvious.

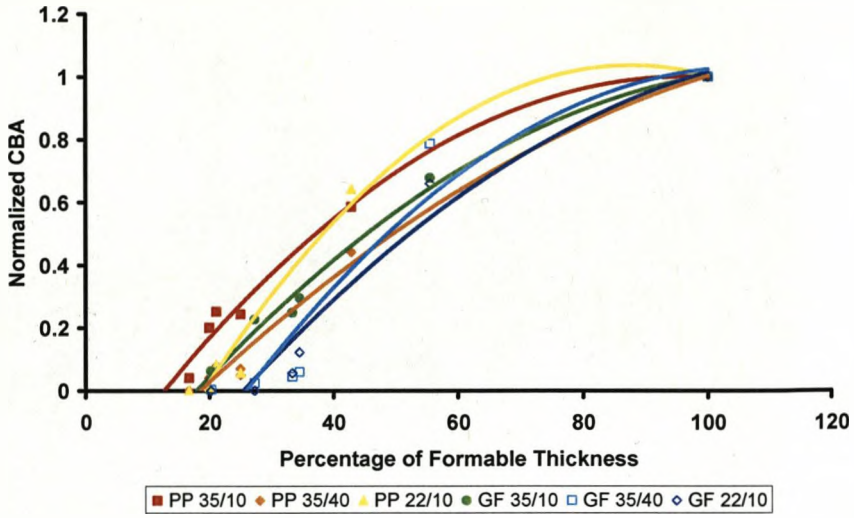

Figure 4.30 Percentage of formable thickness against normalized CBA for PP and GF FMLs

Removing the effect of the amplitude of the CBA (by normalizing) shows that whilst there is an effect on the rate of change of CBA, with respect to percentage of formable thickness, due to the laser power and traverse velocities, figure 4.30, the effect is not as consistent as observed in figure 4.29. All processing parameters show the same trends exhibiting similar rates of change in the achievable CBA as the percentage of formable thickness increases. The lowest percentage of formable thickness is 12.5% for the PP FML and 17.5% for GF FMLs of the dimensions used here, as indicated by the X axis intercept of the line of best fit. However the lowest percentage of formable thickness would alter if other parameters such as laser power and traverse velocity were changed.

4.3.1.2 Bend Rate Per Pass

The effect of increasing number of layers has on the Bend Rate Per Pass (BRPP), which is the variation in bend angle achieved per pass of the laser, is also of interest. The BRPP illustrates the how the bend varies with number of passes. A single layer of aluminium (figure 4.31 a)) displays an increasing rate of bend per pass during the first two passes, which then drops steadily until the reapplication of graphite after ten passes. This drop off is described in detail in

earlier sections (Section 5.2). In this case however, due to the highly reflective nature of the aluminium, the main drop in BRPP is attributed to the burn-off of the graphite coating. Figure 4.31 shows plots of BRPP against number of passes for 1:0, 1:1, 2:1, 2:2 and 3:2 lay-ups for process parameters of 35W and 10mm/s, 35W and 40mm/s and 22W and 10mm/s for GF (figure 4.31 a), c) & e)) and PP (figure 4.31 b), d) & f)) FMLs.

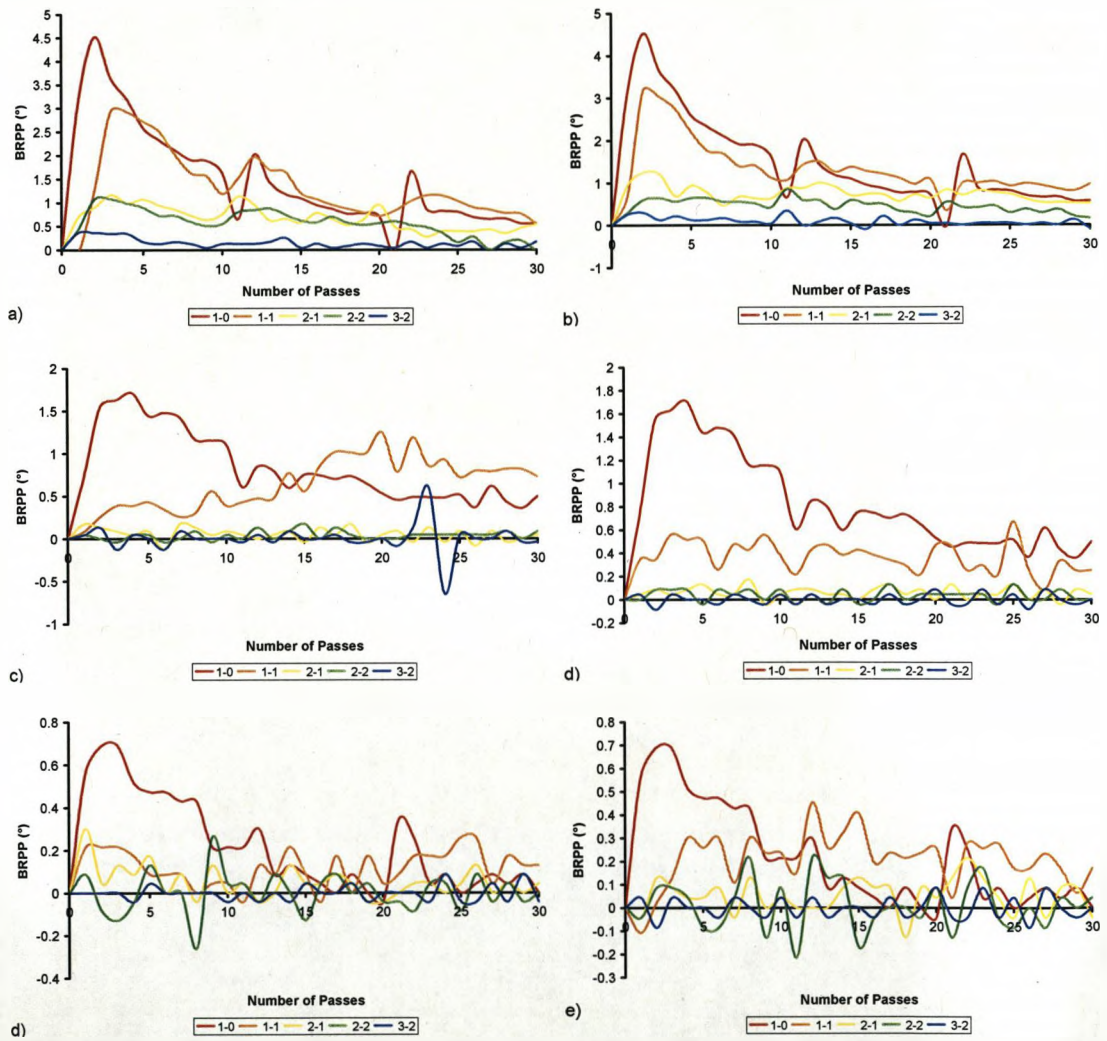

Figure 4.31 BRPP against Number of Passes for a variety of lay-ups of both GF and PP FMLs processed at 35W 10mm/s, 35W 40mm/s and 22W 10mm/s

These figures suggest that, when processing at high laser power levels and low laser traverse speeds, the effect of increasing the number of layers in the lay-up is to reduce the BRPP and reduce the level of variation between each pass. This would suggest that an increase in the number of layers in the laminate increases the linearity of the response of the work-piece to the laser forming process for both types of FML. This could be advantageous for possible automation of the process. This effect is reduced however as the level of incident energy is reduced, as shown in (figure 4.31 b),c),d) and e), where the BRPP continues to reduce as number of layers increases, but the variation between passes appears to be unaltered with an almost random distribution of data. To remove the effect of the amplitude of the BRPP, the results were normalized against the highest recorded BRPP, as outlined previously in Section 5.2. These normalized values are then plotted against the number of passes and are shown in figure 4.32 for GF and PP respectively.

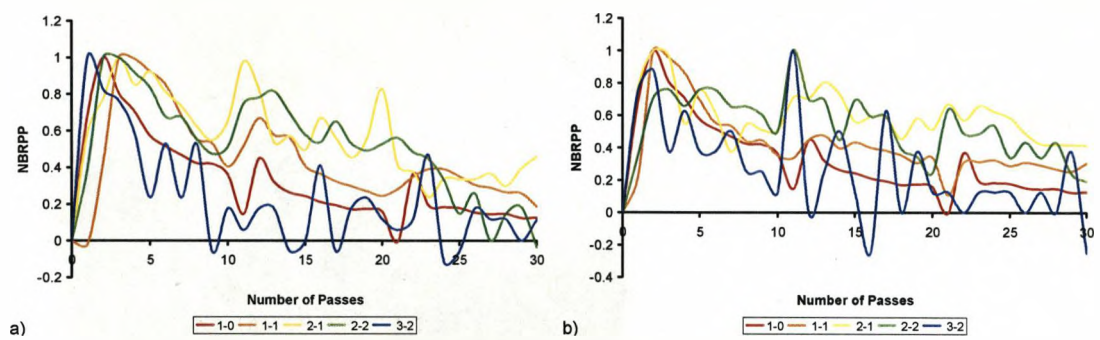

Figure 4.32 NBRPP against number of passes for a variety of lay-ups of GF FMLs and PP FMLs processed at 35W and 10mm/s

As is clearly illustrated by these charts, the variation in the BRPP increases with the increase in number of layers in the laminate. This increase in the variation in the bend rate per pass is due to the increasing force on the aluminium layer from the increased number of composite and aluminium layers. These forces are produced during the production of the FML panels, in the heating and cooling

cycles. These forces induce stresses and strains on the system, due to the differing rates of thermal expansion of the composite and aluminium layers.

4.3.1.3 Bend Propagation

The effect of increasing the number of layers in the FML not only alters the final bend angle that is achieved and the BRPP, as discussed in the previous sections, but also the way in which the bend angle propagates with respect to time. To investigate the effect that increasing the numbers of layers in the laminate has on the bend angle with respect to time, the output of the sensor used in all bend angle measurements was connected to a data logger and recorded as described in Section 3.1.1.3. Samples of both glass fibre (GF) and polypropylene (PP) based FMLs were processed at a laser power of 35W and a laser traverse speed of 10mm/s. The samples were coated with graphite and irradiated ten times using a dwell time of 30s between each pass during the test the voltage output of the sensor was recorded. The first material to be tested was the AL2024-T3 and is shown in figure 4.33.

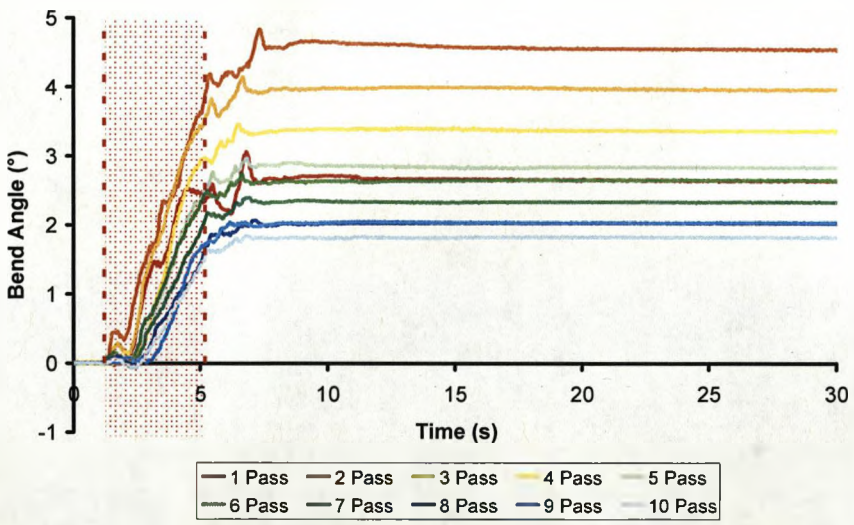

Figure 4.33 Bend angle against time for 2024-T3

The shaded area in figure 4.33 indicates the period when the laser was active on the surface of the material, this being for a time of 4 seconds in total. The final

bend angle achieved depends on which pass the data was recorded. This follows the trends discussed earlier (Section 4.2) where a high rate of forming is initially observed, which then drops off as absorptive coating burns off and other factors such as work hardening affect the bend rate. When a single pass is considered in more detail, various other features in the propagation of the bend become apparent (figure 4.34).

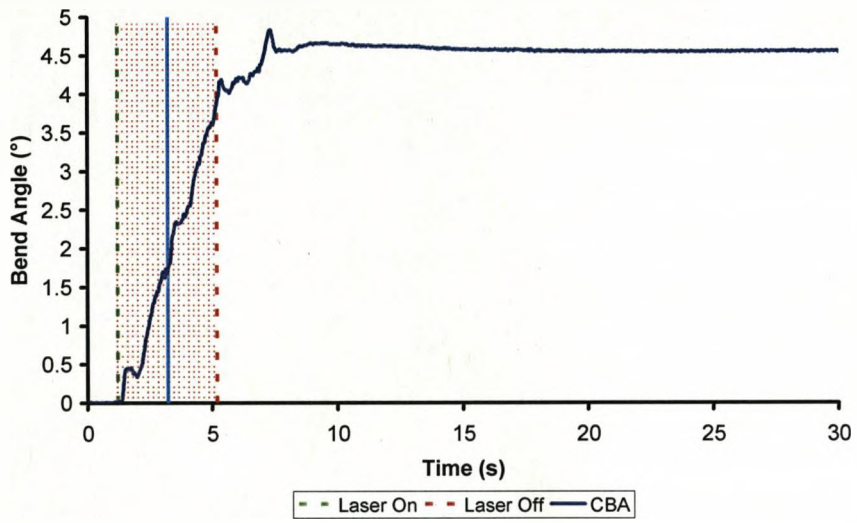

Figure 4.34 Bend angle against time for pass one

The traditional description of forming gives the production of a counter bend, away from the source, due to thermal expansion from the initial heating. On cooling, relaxation of this thermal expansion, gives positive bend towards the source from the plastic strains created during the heating phase. Figure 4.34 does not indicate the counter bend due to thermal expansion before the initial positive bend occurs. Following this positive bend, approximately 0.8 seconds after the laser is active, the bend rate drops to a negative value, reducing the bend angle already propagated, for a short period of time. After this fluctuation, the bend resumes increasing in value. This is evident in figures 4.33 and 4.34. This feature appears throughout the scan strategy, and after 10 passes reduces the bend angle to a negative value for short period of time. This reduction is due to a combination of effects. The thermal input of the laser forming process

relaxes the plastic strains induced by the laser forming process in previous passes, as well as those formed during the sheet rolling process. Another source of this variation is from the asymmetrical nature of forming a bend with a point source. The nature of the forming process with a single point causes a wave to be produced along the forming track. When the laser irradiates the surface, one end is shaped whilst the other is unaffected by the laser. This causes a wave, as one end of the work-piece will be formed, or starting to form a bend, whilst the other end will still be flat. Obviously, as these points on the surface are linked, the variation in height at a given point will be affected by these two extremes, one end of the sample being raised due to the forming process and one end remaining flat. The stresses involved in this process and the low thickness of the material lead to a wave or ripple being produced along the axis that the laser is traversed by (figure 4.35).

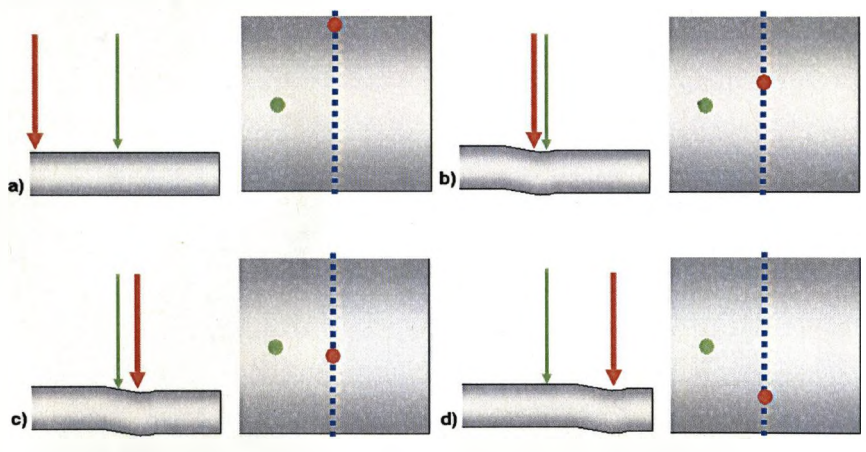

Figure 4.35 schematic of the laser forming process showing the asymmetrical nature of the formation of the bend due to the point source

This initial reduction in bend angle (due to thermal expansion) is overcome by the increased plastic strains produced as the sample starts to cool, as the laser point moves away. The second dip (indicated by the blue line in (figure 4.34) is approximately two seconds after the laser had been turned on, which is when the laser source passes the point at which the bend angle is measured. A second 'dip' in the bend angle propagation rate is observed 0.6 seconds later. This is

caused by a combination of the ratio between the area of the work-piece and its thickness and the variation in the surface of work-piece as it is heated by the laser. As the laser heats the surface the immediate area expands. However, due to the small heated area in relation with the overall sample size, the heated area is constrained by the bulk material, which is unaffected by the heating of the laser. The heated zone expands, causing the surface of the material to rise, with a zone of compression surrounding it. The transition from this zone of compression to the bulk material leads to another raised area and so on, each time lowering in amplitude until the flat surface is reached. This effect is similar to ripples on a pond when a pebble has been thrown into it. As this feature moves along the surface of the work-piece, it leads to the variations in the bend angle, this is between 2.8s and 4s in figure 4.34, as it passes the point where the height measurement was taken. If the sample was thicker, with the same planar dimensions, these features would not be observed due to the increased geometrical rigidity of the part. The thin cross-sections used here allows measurable deformation due to this heating. These effects are magnified as a result of the single point used to record the bend angle. This is because the asymmetrical effects of laser forming with a single slow moving point source adds a further 'wave' in the surface of the material. After the laser is extinguished, after five seconds in figure 4.34, fluctuations in the bend angle are recorded. These are due to the stresses present in the system changing during cooling of the work piece as the propagation of the bend continues.

1:1 FML

When a single layer of composite is added to the workpiece, the propagation of the bend angle alters, as shown in figures 4.36 and 4.37.

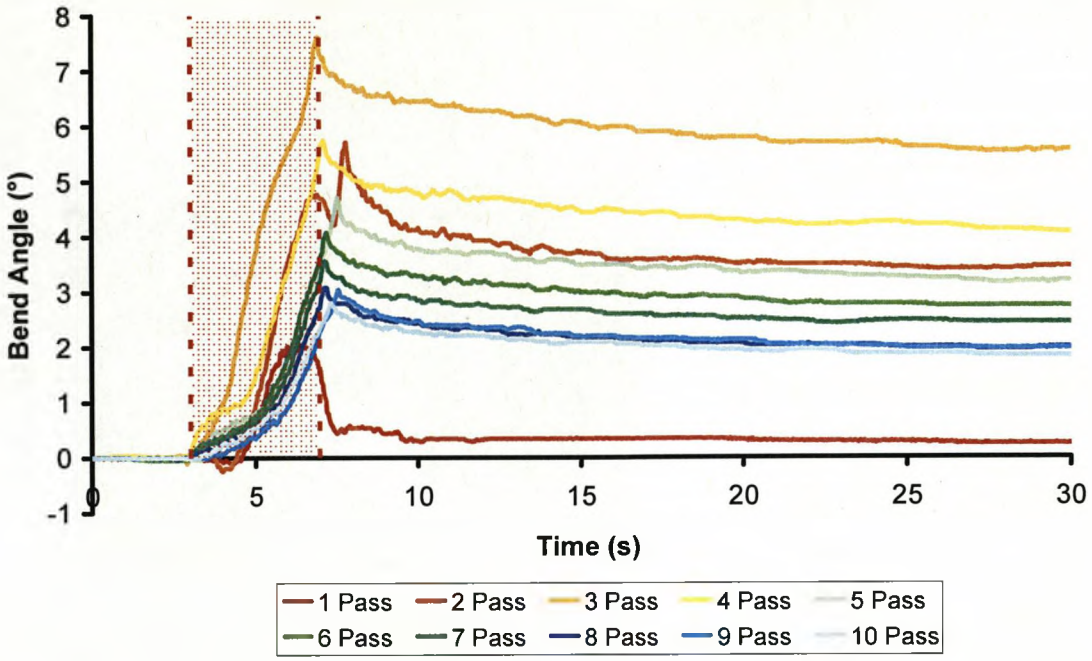

Figure 4.36 Variation of bend angle against time for a 1:1 GF FML

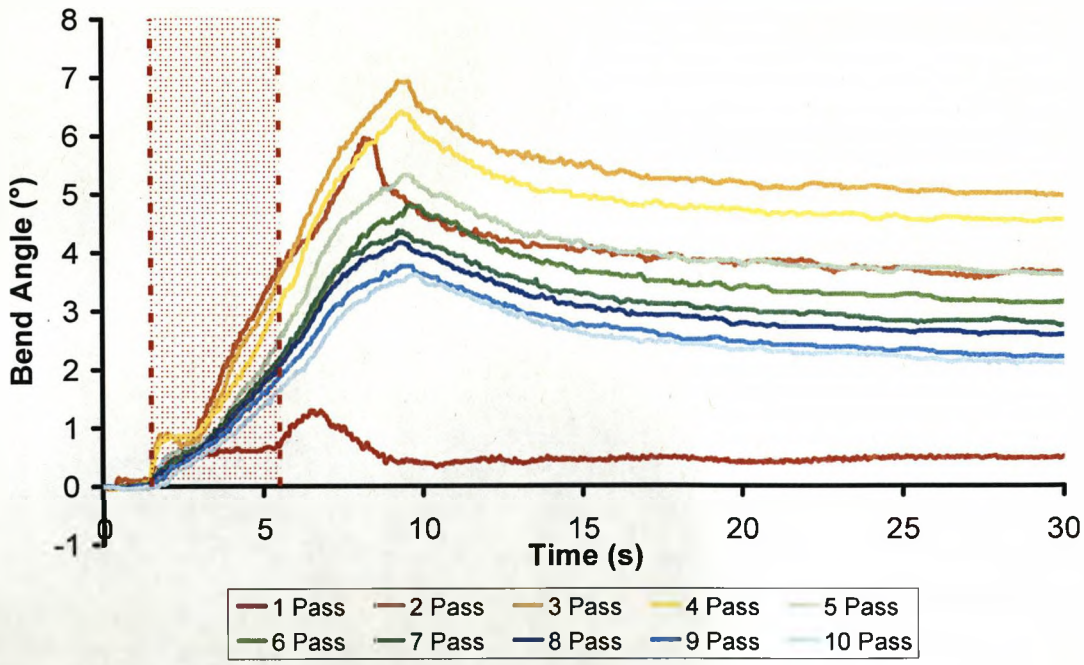

Figure 4.37 Variation of bend angle against time for a 1:1 PP FML

The variation in the propagation of the bend angle between passes follows the same trend as the monolithic material, with an increase in bend angle per pass

being achieved up to the third pass. The bend angle then gradually reduces after each pass, for reasons discussed previously. The variation in the bend angle with respect to time is obviously different for the 1:1 FMLs over the aluminium sample. The initial positive bend and dip are still present in the first three passes in both types of FML. From pass four onwards, there is no noticeable reduction in the rate of the propagation of the bend angle following the initial positive bend. The ripple effect observed during the propagation of the bend in the monolithic aluminium samples is not present as the increased thickness of the work piece constrains this effect.

In the GF FML there is a marked increase in the rate of propagation of the bend after two seconds of laser irradiation, once the laser passes the sensor, and four seconds, when the laser is turned off, in the PP composite FML. In the case of the GF, the increase in the rate of bend propagation (the gradient of the trace) increases as time elapses. For the PP the rate of bend propagation increases rapidly and then decreases with time. The increase in bend rate witnessed in the GF is thought to be due to the matrix reaching a temperature where softening occurs, therefore reducing the forces on the aluminium layer, allowing a greater bend rate to occur. This would also correspond to the reduction in bend witnessed after the laser is turned off due to the matrix cooling and hardening, reducing the bend angle. This is discussed further in section 4.3.1.4.

The increase in bend rate observed in the PP composite FML (figure 4.37) after the laser has been turned off is due to the relationship between thermal strains and plastic strains. The process of bend propagation in the work piece is due to the thermal strains induced in the system becoming smaller (due to heat dissipation) than the plastic strains induced during the laser forming process. Where these equal at all times no bend would form. The rate of heat dissipation is highest immediately after the removal of the laser source (section 4.3.1.4). The greatest effect that the plastic strain (which have reached a maximum value) on increasing the bend rate is at this point, as the thermal strains are decreasing at

their highest rate. The effect of the reduction in thermal strains lowers with time due to the dissipation of heat. The slow dissipation of this heat explains why the propagation of the bend continues after the laser is extinguished. The variation between the reaction of the PP composite FML and the GF composite FML to thermal dissipation is covered in more detail in section 4.3.1.4,

Another feature in figures 4.36 and 4.37 which differs considerably from the monolithic aluminium (figure 4.34) is the 'over bend' or springback observed. By this, the maximum bend angle achieved is not the final bend angle and the lack of springback is often stated as a benefit of laser forming in the literature [3]. Springback occurs in traditional forming due to a large amount of elastic strain energy, which is caused by the highly non-linear deformation process. This elastic energy is stored when the sample is in dynamic contact with the die, but on removal of the die this energy is released, causing the sample to deform, generally towards its original geometry. Laser forming of monolithic materials does not exhibit this feature as the whole work-piece is subjected to the forming process. In LF of FMLs, only the top layer is thermally formed. The neighbouring layers are mechanically shaped by the thermally formed layer pulling them mechanically, and as the case with any mechanical shaping, elastic recovery will occur. In these 1:1 lay-ups, the mechanically formed part contains a similar volume of composite material. The presence of the composite lowers the modulus of elasticity of the work piece as a whole, thus making it more susceptible to the spring-back phenomenon.

2:1 FML

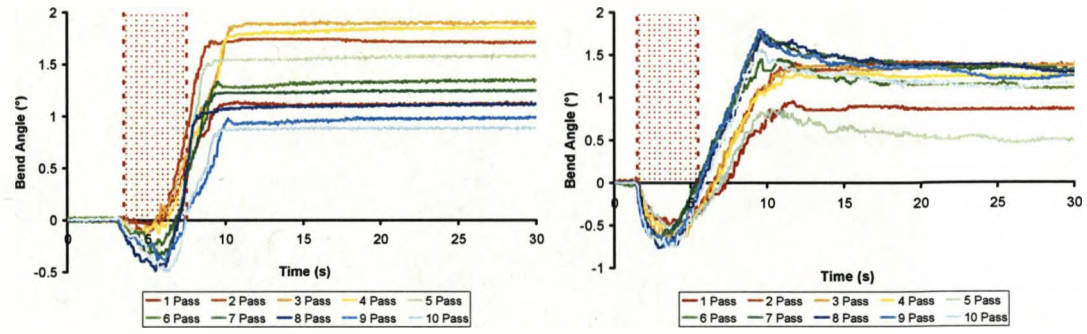

Figure 4.38 The variation of bend angle against time for 2:1 GF and PP FMLs

There is much less variation in the propagation of the bend in the 2:1 lay-ups (figure 4.38) when compared to the 1:1 lay-ups (figures 4.36 and 4.37). None of the fluctuations as the bend propagates witnessed in the 1:1 lay-ups are present. The GF composite follows a similar overall trend to the 1:1 lay-up, with the maximum bend angle being achieved after three passes, with the value reached dropping with each subsequent pass. The PP FML also achieves the highest final bend angle the third pass, once spring-back has occurred. Although the maximum bend angle is reached by pass nine, the elastic strains relax reducing the final bend angle to less than that of the third pass. The GF 2:1 lay-up does not exhibit the spring-back phenomenon to the same extent as observed in the 1:1 lay-up. In the worse case the PP FML springs back by 31% of its maximum value (pass nine). The PP FML exhibits this since the Young's modulus of the PP is lower (6 GPa) than that of the GF (47 GPa) and therefore the effective Young's modulus of the 2:1 PP FML is lower than the 2:1 GF FML. Both materials exhibit a large counter bend as described previously. The elastic counter bend effect during the initial heating stage is also amplified by the addition of further composite and aluminium layers. With a single layer of AL-2024-T3 and in the case of 1:1 FML lay-ups, no significant counter bend was detected. With the 2:1 lay-ups a maximum counter bend of 58% for the GF FML and 42% for the PP FML of the final bend angle achieved. This is due to the residual stresses present in the laminate following its manufacture, where the differing thermal expansion

coefficients of the aluminium and the composite materials cause stresses on cooling. The asymmetrical heating of the FML panel during the forming process causes the relaxation of the stresses in the irradiated surface, upsetting the balance of forces, keeping the panel at its current shape, and therefore producing a counter bend. Also the method of LF used for FMLs, where the top layer of the work-piece undergoes the forming process and 'pulls' the lower layers towards the laser source to form the bend. These induced stresses load the work-piece during the elastic phase of the LF process, causing the counter bend. The counter bend is also present for the entire time period that the laser is irradiating the surface for the 2:1 PP FML. For the 2:1 GF FML, the counter bend is present for two seconds for pass one and increasing in duration as the pass number increases, until pass nine where the counter bend is present during the entire irradiation process. This is because the stresses present in the system due to the production of the FML panel and thermal stresses induced by the heating stage of the laser forming process are greater than the sum of the plastic strains induced by the laser forming process. When the laser is turned off, cooling occurs reducing the thermally induced strains, therefore producing a positive bend.

2:2 FML

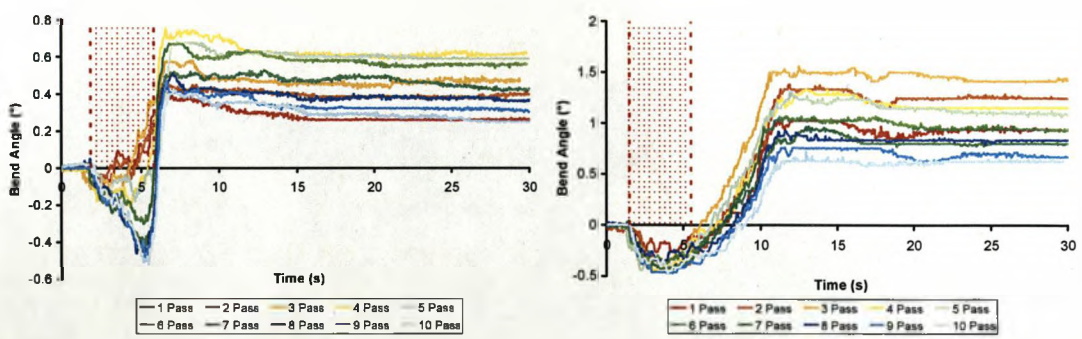

Figure 4.39 The variation of bend angle against time for 2:2 GF FML and 2:2 PP FML

The addition of a composite layer again affects the propagation of the bend as illustrated in figure 4.39. Similarly to the 2:1 GF FML, the 2:2 GF FML exhibits an increase in counter bend as the pass number increases. This is caused by a combination of the stresses and strains in the system from the panel curing cycle, the bend angle achieved from previous laser passes and the strains present in the sheet aluminium from the initial rolling and cutting. These various stresses and strains are temporally relaxed during heating the work-piece while laser forming and return during the cooling cycle. The positive bend is produced rapidly after the laser is turned off, with the maximum bend angle is achieved 1.2 seconds later. The 2:2 PP FML displays similar trends to the previous 2:1 lay-up, displaying both counter bend and a level of spring-back but the bend rate per pass differs. Here the highest value of bend angle is achieved after pass three, as with the 1:1 lay-up. The bend angle then drops off as the pass number increases. As with the 2:1 lay-up, the counter bend is present during the entire irradiation stage, with a positive bend forming as the laser is turned off. The bend then propagated for a maximum of six seconds after the removal of the laser source, as the stresses present in the system find equilibrium. The level of springback is lower than previously encountered, with pass seven suffering from a 17% reduction in the bend angle. This reduction in the level of springback is due to the increased thickness of the FML sample. The 2:2 lay-up has only 25% of its total thickness available for thermal forming, which reduces the level of elastic loading of the lower layers (as the bend angle is reduced); also the heating effects in the composite layer immediately after the top surface is not present in the bottom composite layer, removing the effect of softening of the matrix. This gives an overall smaller bend angle, so therefore a lower level of elastic strain is caused in the mechanically formed layers and therefore a lower level of springback.

3:2 FML

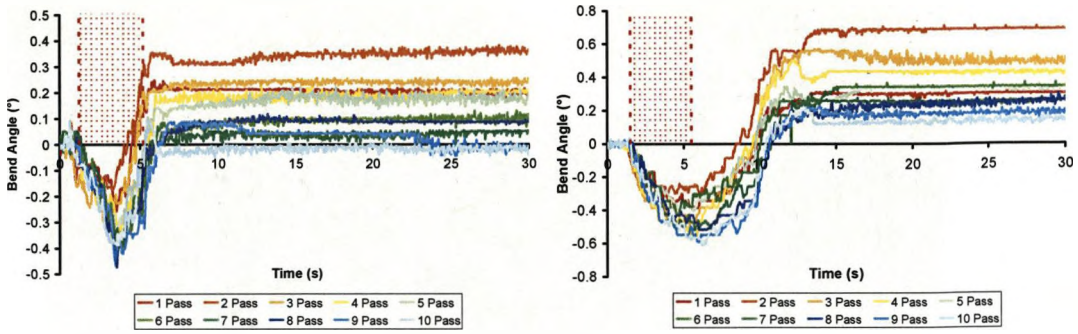

Figure 4.40 The variation of bend angle against time for 3:2 GF FML and 3:2 PP FML Lay-up

The 3:2 GF and PP FMLs exhibit similar trends to those observed earlier (figure 4.40). Increasing the number of layers increases the counter bend, as a percentage of the final bend, in both types. The springback encountered in the 2:2 lay-ups was also reduced, with individual passes showing some springback, but not all. Again the positive bend largely develops towards the end of the laser cycle and after the laser is extinguished in the case of GF FML and up to 10 seconds after the laser has finished in the case of the PP FML.

Mean Bend Angle

In order to remove the effect of varying scan strategies on the propagation of the bend angle, the mean values of the data presented previously have been calculated. This data illustrates more clearly the variation in the bend angle produced when the FML lay-up is varied. Figure 4.41 shows this data for the GF based FML.

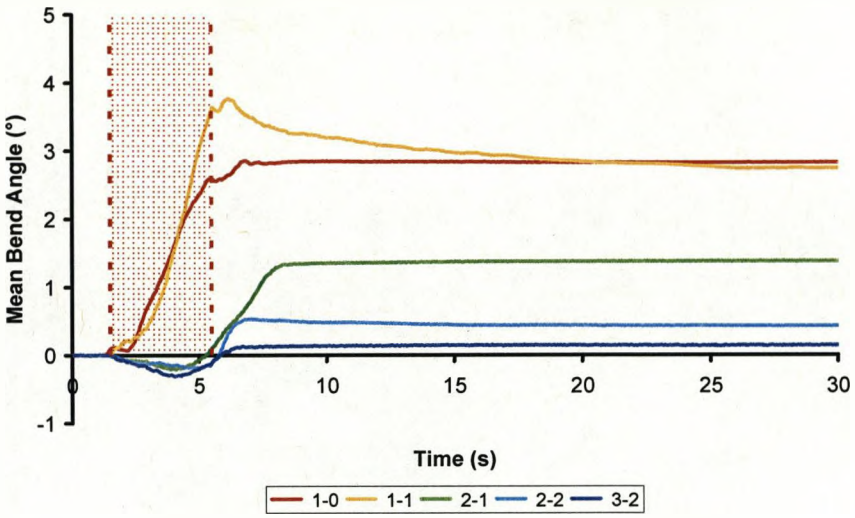

Figure 4.41 Mean bend angle against time for various GF FML lay-ups

The resulting chart shows clearly the variation of bend propagation, with respect to time, due to increasing the number of layers in the FML. The monolithic aluminium shows the initial positive bend, with there being no evidence of the counterbend mentioned in the literature [159]. This is followed by a temporary reduction in bend angle, due to the asymmetrical nature of laser forming using a point source. The propagation of the positive bend angle contains variation in the rate of propagation due to distortion in the plate from the constraining of the heated zone. Also present is a reduction and then increase in the bend angle after the laser is turned off and a slight springback (1%) which was indiscernible from noise on the individual scans. The effect of an additional layer of GF is to increase the maximum bend angle achieved, which is then reduced by 30% due to the elastic strains in the composite and cooling of the matrix, previously softened during the heating stage. The addition of another aluminium layer has a much greater effect on the bend angle achieved and the way that it propagates with time. A significant counter bend is present, this being 15% of the final bend angle. The time to propagate the bend to its maximum value is also longer, 7 seconds in the case of 2:1 lay-up, as opposed to 4.8 seconds and 5.4 seconds for 1:1 and 1:0 respectively. Due to the effect of the amplitude of the bend angle it is not immediately obvious to determine from figure 4.41 if the time delay on

reaching the maximum bend angle is due to the number and order of layers in the FML lay-up. When the data are normalized with respect to the final bend angle achieved, as shown in figure 4.42 it is apparent that as the number of layers in the FML increases, the time taken to reach the maximum bend angle also increases, suggesting that the increased level of strains present in the system are the cause for this delay.

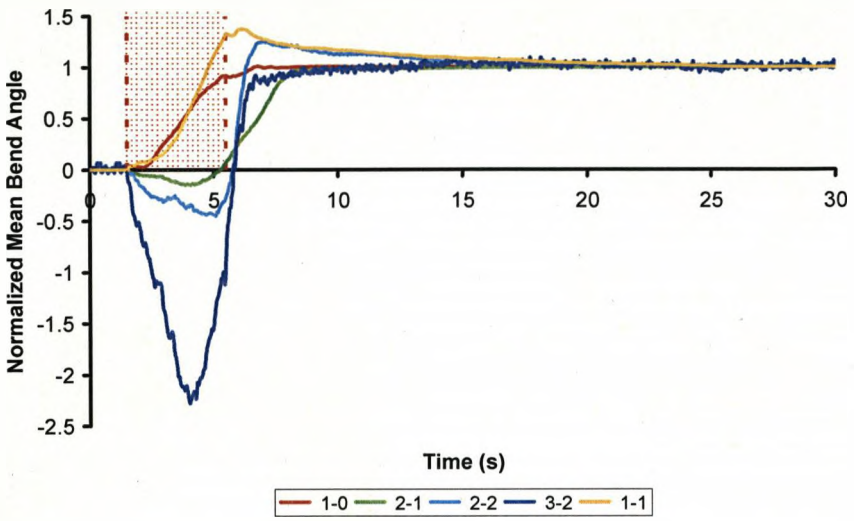

Figure 4.42 Normalized mean bend angle against time for a number of FML lay-up with glass fibre composite

Figure 4.43 shows the same trends in the variation of the bend angle propagation in the PP FMLs as those apparent in the bend rate per pass chart (figure 4.31). The 1:1 lay-up PP FML does not exhibit an apparent counter bend, but a large amount of springback, showing a 31% reduction in the maximum bend angle reached (3.99°) during the pass. The nature of the springback is also more apparent in this figure, with a reduction continuing to occur over the 20 seconds following the point at which the bend ceases to propagate. The increase in bend rate apparent in the individual passes is of a lower amplitude than in the mean results, but a small change in bend propagation rate is apparent. Again similar to the GF FML, the addition of an extra aluminium layer not only reduces the bend angle achieved per pass, but also reduces the level of spring-back encountered

and increases the amount of counter bend. The 2:2 lay-up continues this trend with a reduction in the amount of springback occurring and a measurable amount of counter bend. The additional composite layer has increased the time it takes for the system to overcome the counter bend, from 4.5 seconds in the case of 2:1 lay-up to 6 seconds in the case of 2:2 lay-up. An additional aluminium layer increases this to 8.5 seconds. The 2:2 lay-up also displays a marked increase in the bend rate, as observed in the individual passes for the 1:1 lay-up. The 3:2 lay-up exhibits a long counter bend time with little or no springback.

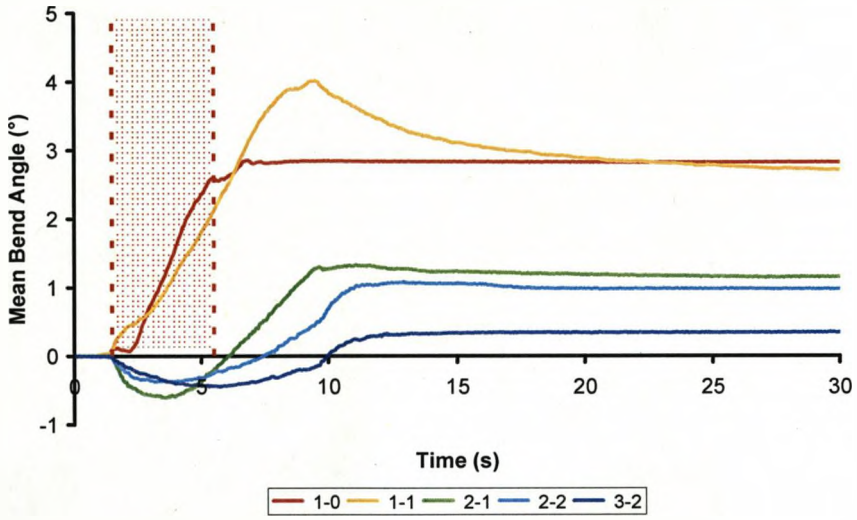

Figure 4.43 Mean bend angle against time for various PP FML lay-ups

Normalizing the results by their final bend angle (figure 4.44) shows the effect of propagation of the bend with respect to time without the effect of the amplitude of the bend produced. Also discernable on figure 4.44, as the number of layers increase, the amount of counter bend increases dramatically, with a 3:2 lay-up reaching a negative bend angle of 127% of the final positive bend achieved. This is significant as this constant bending from positive to negative to positive bend angle could lead to fatigue issues in the sample and is investigated in section 4.4. As with the GF FMLs when the layers undergoing physical deformation consist of a larger volume of composite material (1:1, 2:2 lay-ups), so the effective Young's modulus for the work-piece is lower than when there is a larger volume of

aluminium (2:1, 3:2 lay-ups). The lower Young's modulus is therefore more susceptible to spring-back.

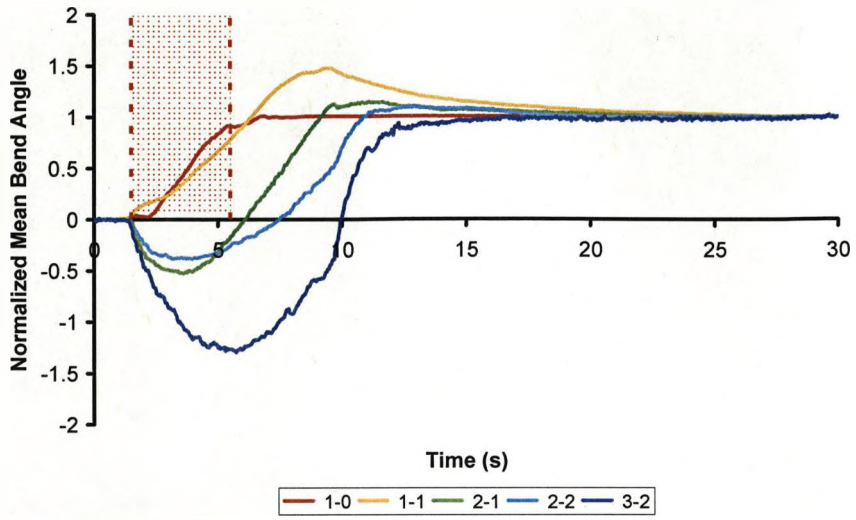

Figure 4.44 Normalized mean bend angle against time for a number of FML lay-up with PP composite

Again increasing the number of layers in the laminate results in an increase in the time for the bend to propagate, with the 3:2 lay-up taking 13.2 seconds, compared to the 4.9 seconds for the aluminium. When the bend propagation time is plotted against the percentage of formable thickness for both GF and PP FMLs (figure 4.45), there is a correlation between the two variables. The increase in time required for the bend to propagate for the PP FML gradually reduces as the percentage of formable thickness increases. The GF undergoes a much more rapid change in time to propagate, with a fast drop until over 30% of the material is formable, then the reduction in time for the bend to form is small as the percentage of formable thickness increases. This suggests that the effect of the composite material is quickly overcome in the GF FML. As the fibres in the GF FML are aligned with the bend angle, the majority of the strain is in the weak matrix. Once the number of mechanically formed layers has reduced past the point where a great enough force is applied to the matrix of the composite layer, the bend propagates at its quickest rate as the matrix is overcome by the force

applied from the laser formed aluminium layer. The PP FMLs take longer to propagate the bend as the fibres are in a standard weave pattern. This means the effect of forming the bend is also acting on the fibres, which are less likely to fail in the similar way to the epoxy resin in the matrix of the GF composite.

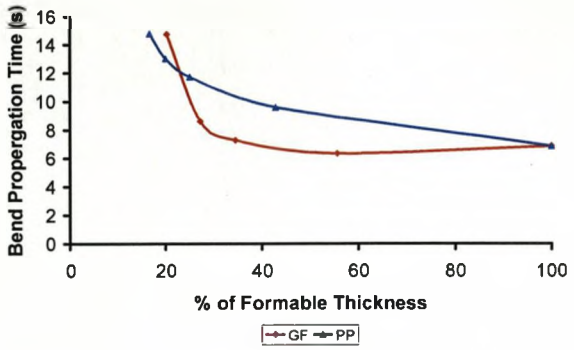

Figure 4.45 Bend propagation time against percentage of formable thickness

4.3.1.4 Thermocouple Data

Due to the thermally sensitive nature of FMLs a number of investigations were carried out to show the effect that varying laser parameters, such as power and velocity, and material parameters, such as lay-up strategy and composite layer variation, have on the absorption and dissipation of the thermal input. The results discussed here are data collected as described in Section 4.1.4. They cover the temperature propagation during the processing of 1:0, 1:1, 2:1, 2:2 and 3:2 type FML lay-ups with both GF and PP composites used previously in this section. The results are discussed in two main sections, concentrating on the GF and PP composites in turn and then a short comparison of the two composite types. The thermocouples were applied as shown in figure 3.9. The samples were processed at laser parameters of 35W 10mm/s, 35W 60mms^{-1} and 22W 10mms^{-1} for ten passes and the data recorded is presented in appendix A. In this section a number of individual scans and results taken from this data will be discussed. Figure 4.46 shows the trace of the data recorded for the six thermocouples as located on figure 3.9 with respect to time for 2:1 lay-ups of both composite systems.

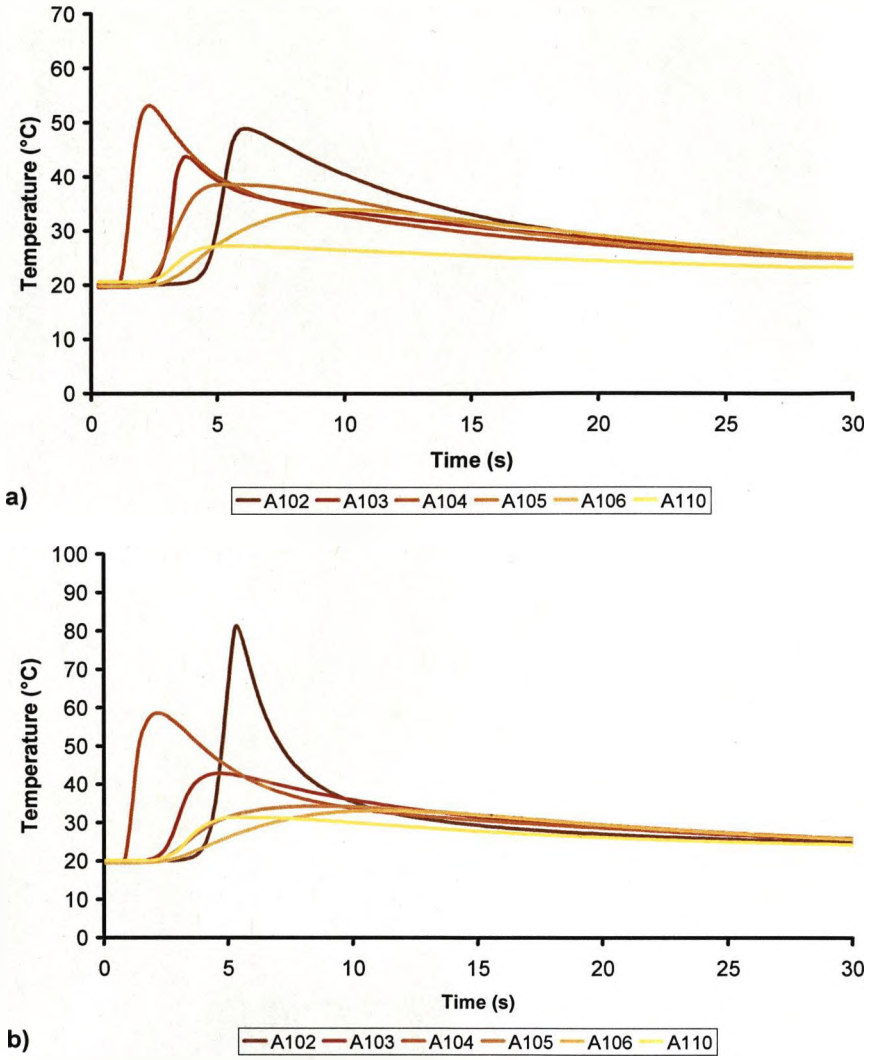

Figure 4.46 Thermocouple output on a 2:1 a) GF and b) PP FML

The results shown here are representative for the results of the whole scan strategy. The first thermocouple to register a change in temperature is at placement 104 which is the measurement point closest to the side of the work-piece. Measurement points 103 and 105 are next to register a change in temperature followed by 110, 106 and finally 102. This shows the progression of the thermal energy across the surface and through the thickness of the material. The measurement points closest to the initial point of irradiation register a temperature change first. Those measurement points that are displaced in the x

direction away from the line of irradiation also display a gradual increase in the temperatures recorded when compared to the measurement points closer to the irradiation point due to the conduction of thermal energy through the aluminium surface material. With the measurement points 102,103 and 104, which are arranged parallel to the line of irradiation, the peak temperatures recorded are higher at the start of the irradiation line (104) and the end of the irradiation line (102) than are measured in the centre of the irradiation line (103). This is due to there being a larger volume of material surrounding the centre point (103) which acts as a heat sink reducing the measured temperature at this point (figure 4.47a)).

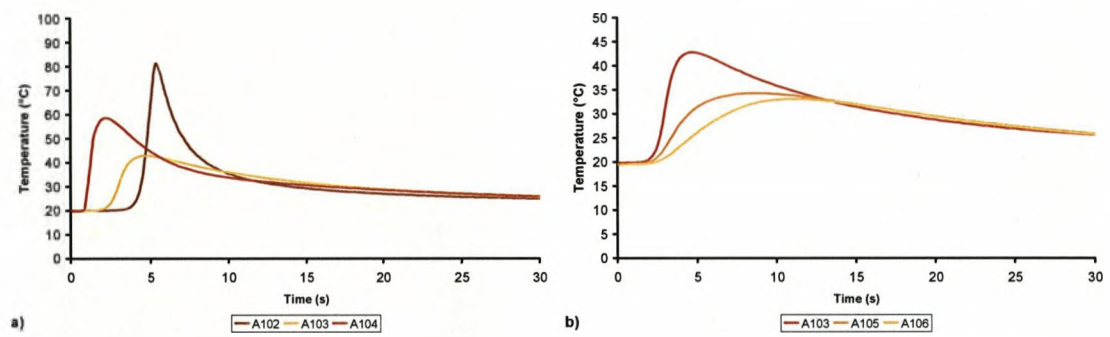

Figure 4.47 Thermocouple outputs for 2:1 PP FML a) parallel and b) perpendicular to line of irradiation

The measurement points which are arranged perpendicular to the line of irradiation (103, 105 and 106) (figure 4.47 b) register a change in temperature in order of proximity to the line of irradiation. The points furthest from the line of irradiation reach a lower maximum temperature and take the longest length of time to achieve it. This is due to thermal energy lost to the environment and to the material bulk and the distance from the source.

With a ten pass scan strategy (appendix A) the peak temperature achieved and the bulk temperature of the work-piece increases after each pass for both the GF and PP FMLs, unlike the result recorded for plain aluminium which showed no overall increase (Section 5.1.3). Figure 4.48 shows the change in bulk

temperature recorded over ten passes. The data was taken from measurement point 102 with the temperature value taken immediately prior to the laser pass. It shows an overall increase in bulk temperature, due to the insulating effect of the composite layer reducing the loss of heat to the environment, but that the change in bulk temperature is not related to the number of layers in the laminate with the 2:2 lay-up showing the least increase in bulk temperature and 3:2 showing the greatest increase in bulk temperature. This is reflected in the mean bulk temperature after ten passes being 38.34°C with a 10% variation. The polypropylene composite gave a smaller variation between lay-ups with a mean bulk temperature value of 36.16°C +/- 5%. This is due to the thicker pp composite layer (0.4mm to 0.24mm for GF) which has a greater influence on the loss of thermal energy to the environment. Once the initial PP layer is applied, the losses through the composite layer are greatly reduced allowing only conduction through the clamp and minimal losses from radiation/convection to the atmosphere.

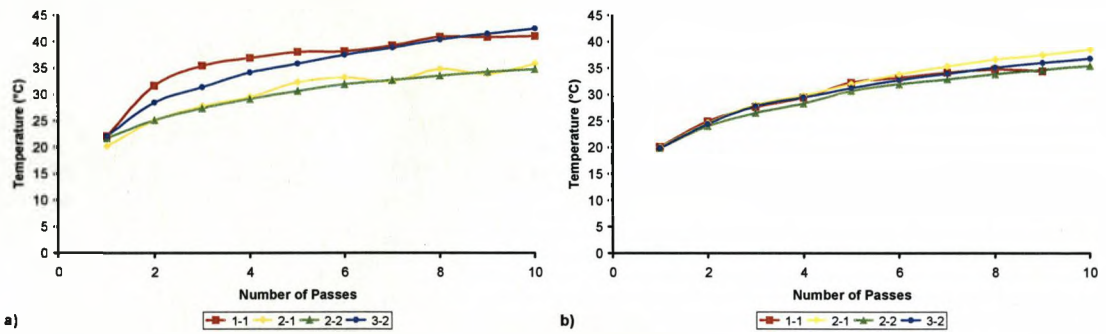

Figure 4.48 Change in bulk temperature for a) GF and b) PP FMLs

The change in peak temperature recorded also appears to be unrelated to the number of layers in the lay-up. As shown in figure 4.49 the variation in peak temperature is minimal between passes, with a slight increase as the number of passes increase. The variation due to lay-up appears to have no relationship with the number of layers present in the laminate. The variation in peak temperature can be explained by a number of reasons. The failure of the sensor to maintain complete contact with the surface during the process affects the final value

recorded, as does the sampling rate of the data logger and the reaction time of the thermocouples. Were the thermocouple to break or have incomplete contact with the aluminium surface, a lower value for the peak temperature would be recorded. If the sampling rate of the data logger was too low, the peak temperature recorded would be lower than the actual peak temperature due to the quenching by the bulk of the material. Similarly the reaction time of the thermocouple would also lead to clipping of the peak temperature recorded due to the quenching effect of the material.

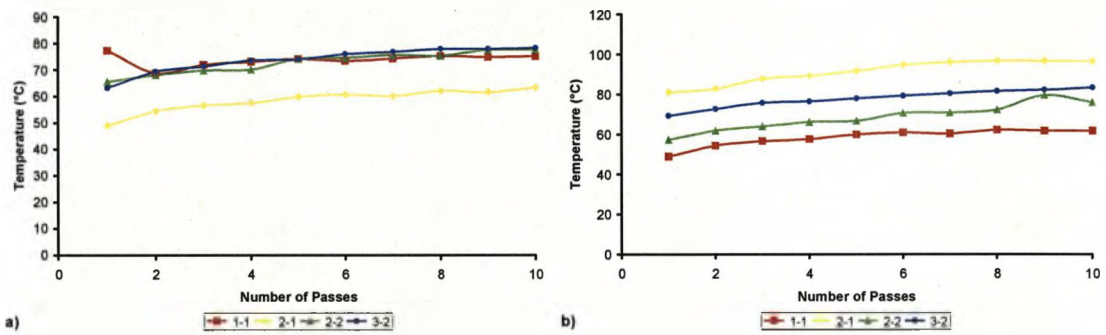

Figure 4.49 Change in peak thermocouple output for measurement point 102

A number of other variables were investigated, such as time from irradiation to peak temperature, increase in temperature during irradiation and time delay from irradiation to initial register of increase in temperature by the thermocouple. It was confirmed that there was no relationship between the number or type of layers in the laminates and the conduction of heat through the initial aluminium layer of the FML or the maximum temperature reached. This is due to the composite layer having little or no effect on the thermal conductivity of the aluminium or the input of thermal energy into the work-piece, which is controlled by the laser parameters and the efficiency of the energy coupling. The number of layers in the laminate did have an effect on the rate of thermal conduction through the thickness of the work-piece and the maximum temperature reached. Figure 4.50 shows the thermocouple output from pass five of a ten pass strategy

for point 110 and shows the variation in temperature through the thickness of the lay-up.

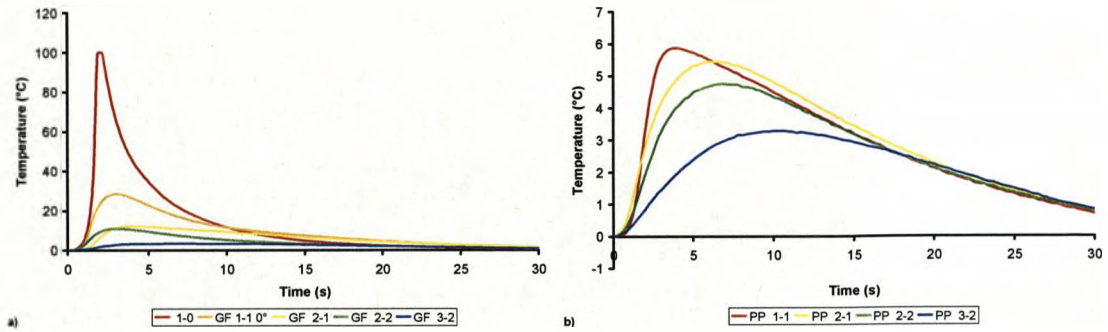

Figure 4.50. Thermocouple output of measurement point 110 for a) GF and b) PP FMLs

As illustrated by figure 4.50 the maximum temperature reached drops as the number of layers in the laminate increases due to their insulating effect. Both glass fibre and polypropylene act as an insulating layer, reducing the maximum temperature that is registered by the thermocouple. The addition of a single glass fibre/epoxy layer reduces the recorded temperature by approximately 70% from the recorded value for plain aluminium. A 2:1 laminate records a temperature drop of 88%, 2:2 laminate 90% and a 3:2 lay-up shows a drop of 97% from a single skin of aluminium. A 1:1 PP FML has a 94% drop in the temperature at measurement point 110, a 2:1 95%, 2:2 95% and a 3:2 lay-up shows a 97% drop in the recorded temperature. This agrees with the findings on the effect that lay-up has on the temperature of the bulk material. The insulating effect of the initial polypropylene layer created the greatest reduction in the conduction of heat through the thickness of the material; this also has the effect of increasing the bulk temperature of the aluminium. The increasing layers also affect the ability of the work-piece to transfer heat to the environment. Figure 4.51 shows the thermocouple output from measurement point 110 which has been normalized against the highest value recorded for that pass.

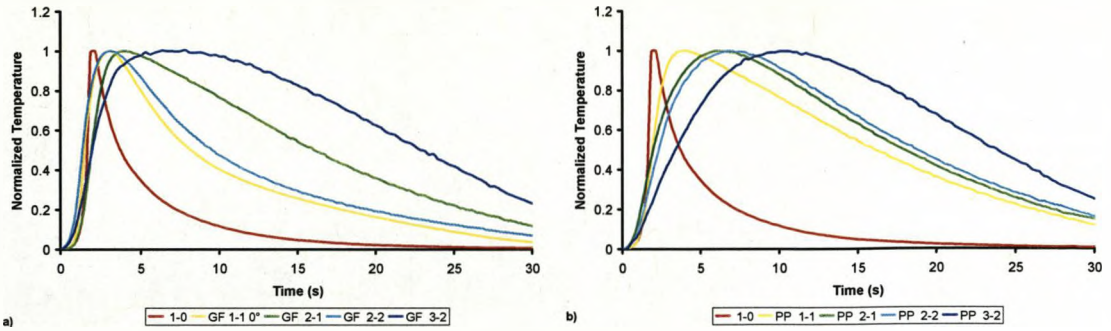

Figure 4.51 Normalized thermocouple output for various laminate lay-ups with a) GF and b) PP composite

The insulating properties of the additional laminates layers reduces the rate of heat transfer as indicated by the shallower gradients on the increasing and decreasing phase of the charts. Whereas the aluminium alloy reaches its maximum temperature within two seconds, the 3:2 GF and PP lay-ups take approximately seven seconds and ten seconds respectively. The rate of heat loss is similarly affected with no FML lay-up of either composite reaching the initial temperature before subsequent irradiation passes. This is what causes the increase in material bulk temperature discussed earlier. This heat containment is detrimental to the efficiency of the laser forming process as it reduces the thermal gradient through the thickness of the material and may have a detrimental effect on the properties of the panel.

4.3.1.5 Strain Gauge Analysis

The work discussed here is an investigation to complement the understanding of the strains present in the work-piece during the laser forming process, and how this varies as the number of layers in the laminate increases. The experiments were carried out according to the description given in Section 3.1.5 on GF and PP composite. They were processed with laser power of 35W and 10mm/s traverse velocity. The lay-ups used were 1:0, 1:1, 2:1, 2:2, 3:2 and individual passes are discussed with respect to longitudinal (LT) strain and transverse (TV) strain where longitudinal is parallel to the path of the laser scan and transverse is

at 90° to it. On the following figures a positive value of strain indicates a tensile component whilst a negative value indicates a compressive component and this was confirmed by manual manipulation of a sample. The full strain measurements recorded are presented in appendix B. The shaded area indicates the period of irradiation.

After ten passes the aluminium sample showed an overall compressive strain of 3.26 micro-strains in the transverse direction and a tensile strain of 1.7 micro-strains in the longitudinal direction. This is as observed in earlier work [46] where the upper surface is in compression in the transverse direction from the plastic strains induced during the forming process. It is these strains that cause a bend to form in the material. The tensile longitudinal strains are due to the edge effect discussed earlier (section 4.3.1.5). The addition of a composite layer reduces the overall transverse strain to 1.49 micro-strains and the longitudinal strain to 0.51 micro-strains for the PP FML after 10 passes. The GF 1:1 FML also showed a similar drop in the strains recorded with 1.5 micro-strains transverse compressive strain recorded and a 0.44 micro-strains longitudinal tensile strain observed. The addition of an aluminium layer has the effect of reversing the strain values observed for the aluminium in both materials. The FMLs are now under compressive strain longitudinally (2.89 micro-strains in the case of PP and 0.17 micro-strains in the case of GF) and tensile strain in the transverse direction (1.26 micro-strains for PP and 1.82 micro-strains for GF). The 2:2 lay-ups alters the final types of strain again, with the GF FML transverse reducing to a tensile strain of 1 micro-strains, whilst the longitudinal strain reverting to an overall compressive strain value of 0.76 micro-strains. The PP FML also alternates with a compressive transverse strain (0.67 micro-strains) and compressive longitudinal strain (0.64 micro-strains). The 3:2 lay-ups also show the same apparently random final strain value, with the PP FML exhibiting a final tensile strain of 3.5 micro-strains in the transverse direction and a compressive strain of 2 micro-strains in the longitudinal direction. The GF FML shows compressive strains in both transverse and longitudinal directions (0.33 and 0.51 micro-strains respectively). This variation in the final strain recorded over the various lay-ups is

due to a combination of factors. The 1:0 and 1:1 FMLs show the same type of strains recorded in earlier work [57] with tensile strains, due to the edge effect, detected in the longitudinal direction and compressive strains detected in the transverse direction due to the plastic strains created during the laser forming process. Once the lay-up exceeds 1:1, the final strain values change with no obvious trend connecting them. The reason for this is the increased levels of strain present in the system from the increased mechanical forming for the lower layers. Also the increasing numbers of composite materials present also causes strain to occur during the FML panel production stage. As the aluminium and composite layers have different rates of thermal expansion, strains develop in the system as the panel cools. These strains are difficult to measure or to predict the effect of laser forming these samples will have. The thicker lay-ups show less variation in the strain traces as the stresses from the production process are smaller in relation to the strains induced by the forming process and mechanical deformation. However the variation witnessed as the laser forming process occurs followed a more uniform progression. In the first four passes for the aluminium and 1:1 FMLs there is a variation in the amplitude and types of strain measured. These are caused by the effects of strains inherent in the sample from both the production of the aluminium sheet and the FML panel production. After pass seven the strain trace for all lay-ups of FML had settled down to show the reaction of the specific lay-up to the steady state forming mechanism.

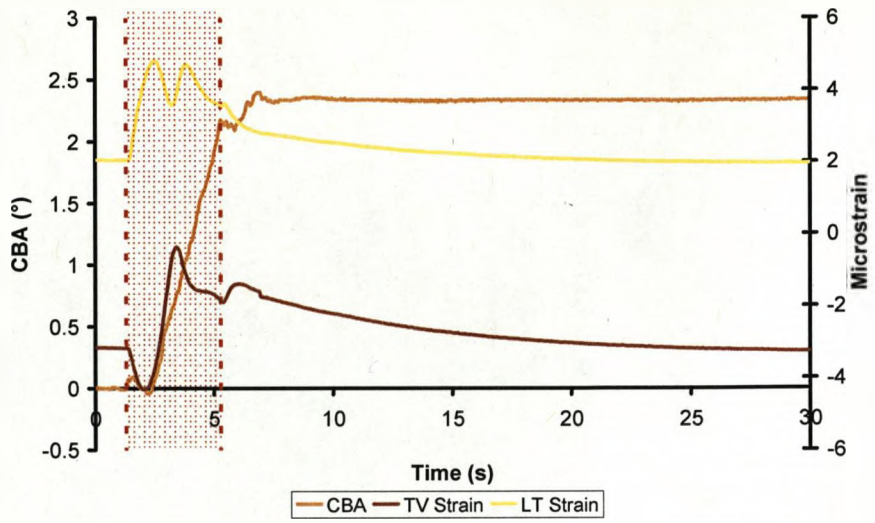

Figure 4.52 Propagation of the bend, transverse and longitudinal strains against time for aluminium

The longitudinal and transverse strains recorded when forming a single skin of aluminium are presented in figure 4.52 with the corresponding bend angle propagation against time. In the transverse direction, the initial strain recorded is compressive, due to heating by the laser source. This equates to a compressive strain at the measurement point as the expanding heated area is constrained by unaffected bulk of the material. This causes a tensile heated zone surrounded by a zone under compression. As time elapses and the laser source approaches the measurement area the compressive strain migrates to a tensile one due to a combination of the heating of the immediate area and cooling of the initial heated area which causes the propagation of the bend. As the beam passed the measurement area a compressive strain was recorded which is due to the effect of the localized heating as above. The sample ends in compression for the plastic strains produced during the laser forming process. The longitudinal strains recorded show an overall tensile strain due to the edge effect. The propagation of these strains varies with time, with an initial tensile strain being replaced with a compressive strain. As the laser source passes the point of measurement, the compressive strain changes to a tensile strain which again changes to a compressive strain as the beam moves away. The cause of this cycle is a

tension/compression wave that passes across the surface of the material as the bend propagates (figure 4.53). The point source nature of the laser forming process causes a bend to propagate at the side of the sample first irradiated whilst the opposite side is unaffected.

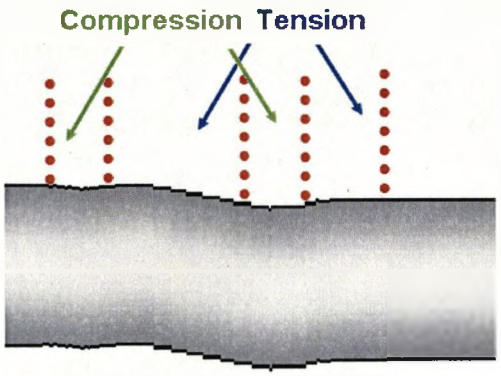

Figure 4.53 Sketch of tension/compression wave observed on sample surface due to asymmetrical formation of the bend

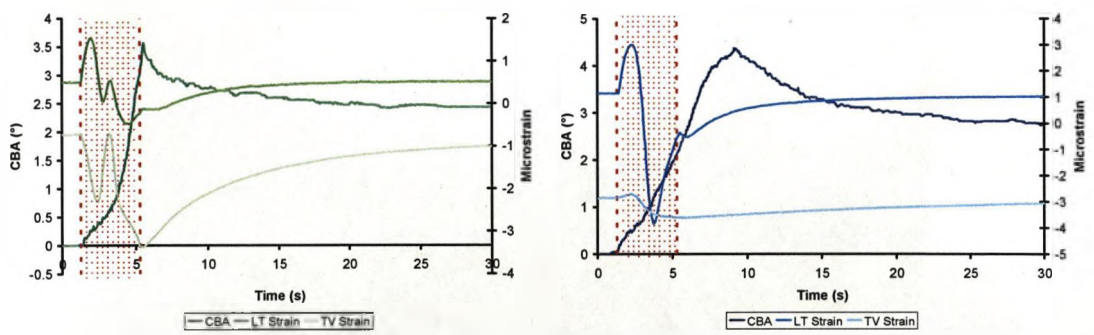

Figure 4.54 Propagation of the bend, transverse and longitudinal strains against time for 1:1 GF FML and 1:1 PP FML

The addition of a composite layer to the sample alters the magnitude of the strains measured but not the overall pattern, whilst the sample is irradiated (figure 4.54). The transverse strain recorded for both the GF and PP FMLs show an initial compression strain followed by a tensile and compression strain cycle. The amplitude of the variation observed in the PP FML is much shallower than

both the aluminium and GF samples but the same pattern of strain remains. After the laser has been turned off, a variation in the recorded strains is observed. With the aluminium sample compressive values were recorded in both longitudinal and transverse directions. With the 1:1 FML lay-ups tensile strains are recorded after the laser has been turned off. This is due to elastic loading of the composite layer during the mechanical deformation whilst the laser forming process occurred. This recovers during the cooling period causing tensile strain in the aluminium layer.

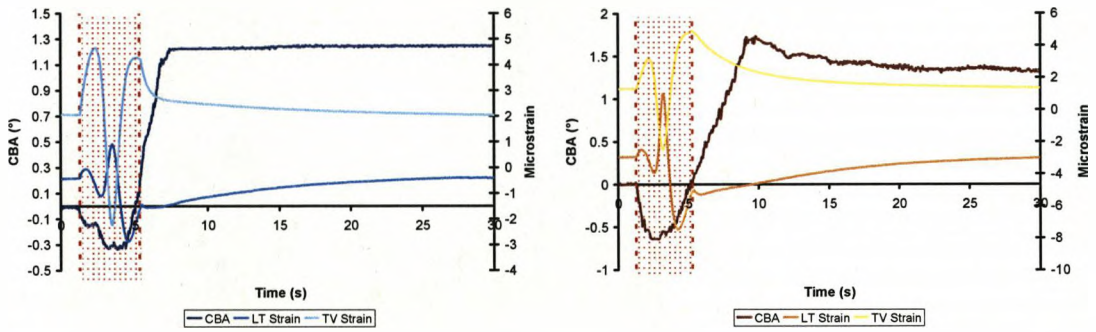

Figure 4.55 Propagation of the bend, transverse and longitudinal strains against time for 2:1 GF FML and 2:1 PP FML

The addition of an aluminium layer to the laminate structure not only alters amplitude of the strain values recorded but also the variation of the recorded strains with time (figure 4.55). The 2:1 longitudinal cycle, for both GF and PP FMLs, starts with a tensile strain, due to the loading of the sample the mechanically deformed layers, which leads to the counter bend being produced. This is then over taken by a compressive strain due to localized thermal expansion in the area of heating which is constrained by the structure. As the bend propagates and the laser source passes the area under measurement a tensile strain is measured. This is produced by a combination of the effect of thermal expansion and the propagation of the bend which occurs away from the area of measurement, but produces a tensile strain in the area of interest. The final compression-tension cycle observed is produced as the work piece cools and a positive bend propagates. The cooling cycle produces a compressive

strain in the area of measurement as the effect of thermal expansion reduces and the compressive effect of the plastic strains induced by the thermal expansion prevails. The tensile strain is caused by the propagation of the bend which loads the area of measurement causing tensile strains. As the laser is turned off, a brief recovery of the tensile strains occurs, with some compressive loading, which is then followed by an increasing level of tensile strains due the recovery of the elastic strains in the mechanically formed layers. The transverse strains recorded also follow the same pattern with both GF and PP composite, with the variation in the magnitude of the strains recorded and their rate of change the difference between the two composites. There is an initial tensile strain, due to loading as the counter bend propagated, followed by a compressive strain due to localized heating and the asymmetrical effect for laser forming. This is then followed by a tensile strain, which is caused by the propagation of the bend in the material. Once the laser is turned off a compressive strain occurs due to cooling of the work piece, both in the aluminium and composite material. Also the recovery of the elastic strains from the mechanical forming of the lower layers leads to a reduction in bend angle. This causes compressive strains in the material as the curvature from the edge effect reduces.

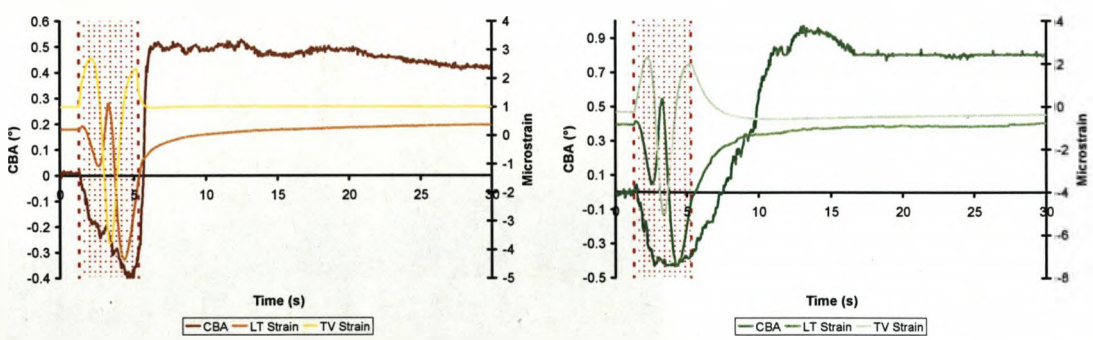

Figure 4.56 Propagation of the bend, transverse and longitudinal strains against time for 2:2 GF FML and PP FML

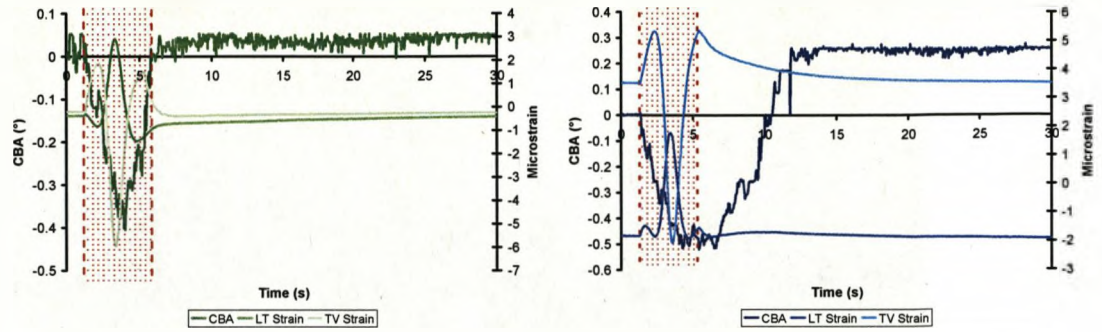

Figure 4.57 Propagation of the bend, transverse and longitudinal strains against time for 3:2 GF FML and PP FML

Increasing the number of layers in the laminate after 2:1 has little effect on the propagation of strain in the system. The strain cycle observed for both 2:2 and 3:2 lay-up of GF and 2:2 lay-up of PP have an identical pattern as discussed for the 2:1 laminates (figure 4.58 and 4.59). The only variation is a further tension/compression strain cycle in the case of 3:2 pp lay-up. Again a variation in the magnitude of the recorded strain measurements is observed. In order to compare the effect of increasing layers in the laminate the data recorded from pass seven has been normalized against the highest positive strain recorded (figures 4.58-4.61).

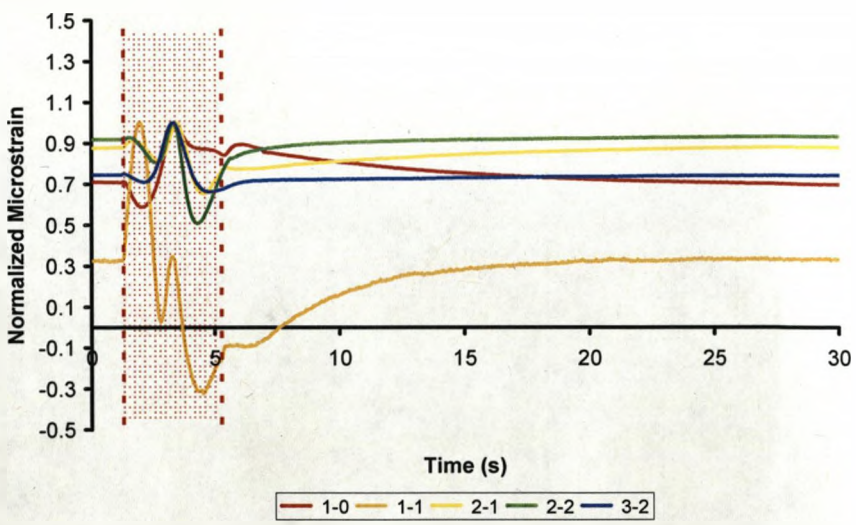

Figure 4.58 Normalized longitudinal strains against time on GF FMLs

The initial observation of the recorded longitudinal strains is the similarity of the traces for all the lay-ups except 1:1 (figure 4.58). All other lay-ups follow a compression tension compression cycle while irradiated by the laser. The amplitude of variation in the recorded strains does not follow with an increase in lay-up with 1:0 lay-up undergoing the largest tensile strain (when compared with the other strains the sample underwent) and 2:2 lay-up undergoing the largest compressive strain. The variation in recorded strain of the 1:1 sample when compared to the other samples is apparent. This is caused by the higher ratio of composite when compared to the other FML lay-ups. This affects the strain trace as the composite is more susceptible to heating cycles. This softens the matrix and causes thermal expansion. The softened matrix allows the aluminium to form a greater bend angle, which induces a tensile load in the composite. On cooling the matrix hardens and reversal of thermal expansion takes place. This induces a tensile load on the aluminium layer, as the shrinking composite pulls on the aluminium, giving the increased fluctuation in the measured strains. Also the effect of mechanical deformation on the composite layers which induces springback is greater with the higher ratio of composite to aluminium in the 1:1 lay-ups. By pass seven the overall strain is already present in the system with all lay-ups returning to the same strain value as recorded prior to the laser pass.

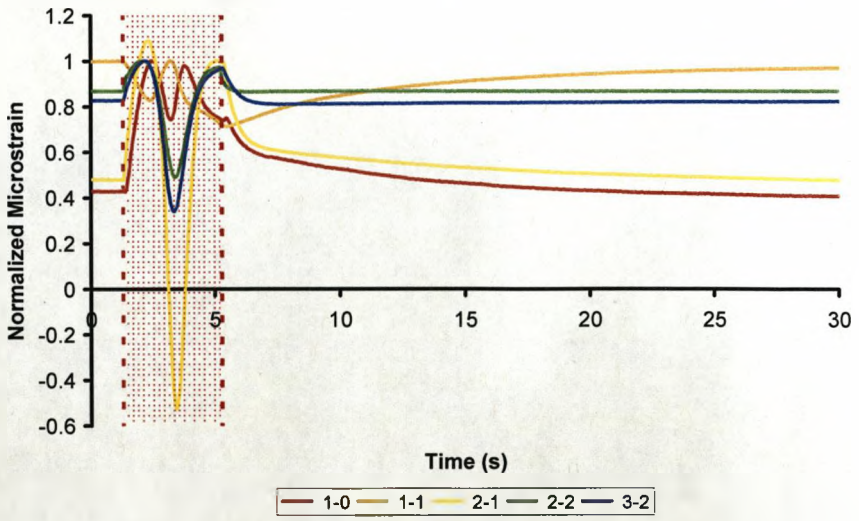

Figure 4.59 Normalized transverse strains against time on GF FMLs

As with the longitudinal strain the transverse strains recorded (figure 4.59) the strain trace recorded shows the same cycle of tension-compression-tension-compression for all lay-ups but the 1:1 lay-up. The amplitude of the strain variation does not follow the increase in lay-up and only the 1:1 shows any variation in the overall stain, with a 3% decrease in the tensile strain measured.

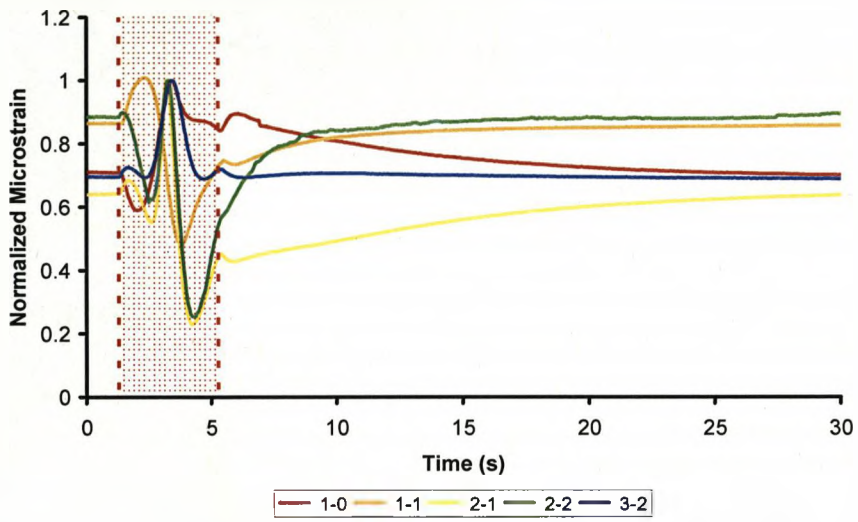

Figure 4.60 Normalized longitudinal strains against time on PP FMLs

Unlike the GF FML there is a relationship between the strain trace recorded and the number of layers in the laminate. With a PP composite all FMLs followed a tensile-compression (figure 4.60). As the number of layers increase the number of these cycles also increases, a 1:1 lay-up undergoes one and a half cycles (i.e. tension-compression-tension) 2:1, 2:2 and 3:2 lay-ups two and a half cycles. This strain cycle is completely different to the one undergone by the aluminium sample and those of the GF FML. Again however by pass seven the final strain value has been reached, with no lay-ups measured strain value significantly altering after the pass is complete.

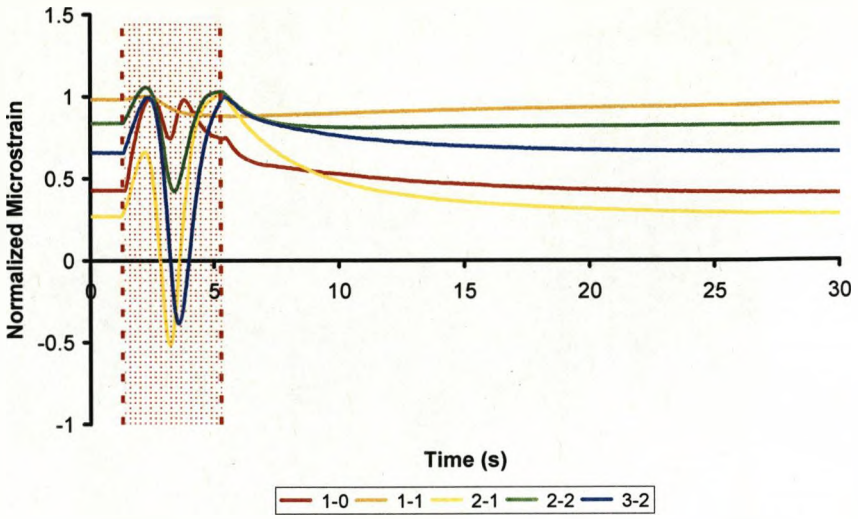

Figure 4.61 Normalized transverse strains against time on PP FMLs

The transverse strains measured form the PP FML (figure 4.61) follow a similar pattern to both the longitudinal and GF strains previously discussed. The thinner section samples, 1:0 and 1:1, follow a different strain cycle to the thicker samples. The 2:1 and thicker samples follow a tension-compression-tension cycle while the laser is on and then all undergo a reduction in the tensile strain value as the sample cools, with the final strain value unaffected by the laser pass.

The most important point of these results is the apparent effect of the composite system on the propagation of the bend and the effect on the stress/strains that the system undergoes. Whilst the laser forming process is confined to the top aluminium layer in that the strain variation in that layer produces the overall bend the results show that the forming process affects the composite layer in some way by thermal input. The conduction of heat into the composite layer caused an amount of thermal expansion as well as a softening of the matrix. The thermal expansion of the composite layer was a factor in causing the complicated stress/strain traces recorded as well as the continuing effects registered by the height sensor after the laser pass had finished. The softening of the matrix had two effects. The first in that it would allow an improvement in the total bend angle

produced as it would have been easier for the top layer of aluminium to mechanically deform the composite layer and also possibly reducing the potential for matrix cracking as at a higher temperature the material is more ductile. However on cooling the re-setting of the matrix could have attributed to the undesirable effect of spring back and would also affect the strain loading of the sample. The thermal effect on the composite also attributed to the delay in the propagation of the bend as the poor thermal properties of polymeric composites meant the cooling of the composite material to the environment was slower than that of the aluminium, increasing the time for the bends to propagate.

4.3.2 Fibre Layer Parameters

Due to the anisotropic nature of composite materials, it was necessary to investigate the effect various composite properties have on the formability of FMLs. These can be broken down into the following areas: fibre orientation, layer thickness, fibre properties and matrix properties. Of these, fibre orientation and layer thickness were the two main parameters investigated.

4.3.2.1 Fibre Orientation

A number of samples were produced to investigate the effect of fibre orientation. Each of these was a 1:1 lay-up of aluminium 2024-T3 and unidirectional E-glass epoxy pre-preg with a fibre volume of 56%. The fibres were at various orientations (0°, 15°, 30°, 45°, 60°, 75° and 90°) from the bend line. These samples were processed at a laser power of 35W and traverse velocity of 10mm/s, and the resulting bend angles were recorded using the method previously described (section 3.1.1.3).

Cumulative Bend Angle

The findings showed that as the fibre was orientated away from the bend line, the total bend angle achieved was reduced; as is illustrated in Figure 4.62. This shows a clear reduction in the CBA as the Fibre Orientation Angle (FOA) increases. These effects can be separated into two main areas, low pass scan

strategies (<5 scans) and high pass scan strategies (≥5 scans). The effect FOA has on the CBA at low scan strategies appears to be variable in nature, which suggests at small bend angles, it is other parameters such as residual stress, that have a greater effect on the bend. With high scan strategies (higher total bend angles), a more uniform effect is observed. In these cases a drop in bend rate is not observed until a fibre orientation angle greater than 15° is reached. The bend rate then drops off until an angle of 60° is reached, then the reduction plateaus off and remains roughly constant up to an angle of 90°. This variation in the CBA is due to the effect of off-axis loading of composite materials. The mechanical properties of composite materials are dependent on the orientation of load compared to the fibres due to their anisotropic nature [99].

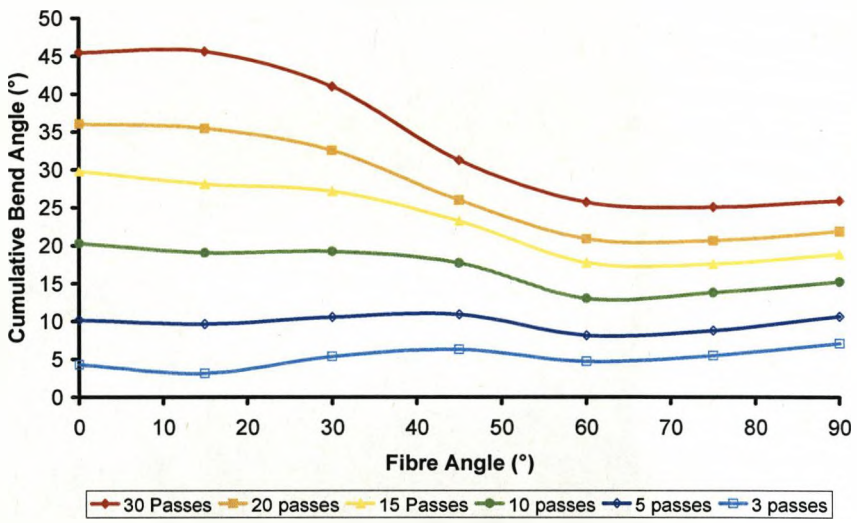

Figure 4.62 Cumulative bend angle verses fibre orientation angle verses fibre orientation angle for various FML lay-ups. Samples processed at 35w, 10mms^{-1}

If the results from figure 4.62 are normalized against the CBA for a FOA of 0° (shown in figure 4.63), the effect of fibre orientation on the CBA is seen to be more predominant. All scan strategies show this 'wave' effect in the CBA, however the effect becomes more uniform at higher pass rates (10+ passes). This is due to a combination of the increased load on the composite due to higher bend angles, a result of cumulative plastic strains in the aluminium layer, and the

reduction in the effect of residual stresses from panel production at higher scan strategies.

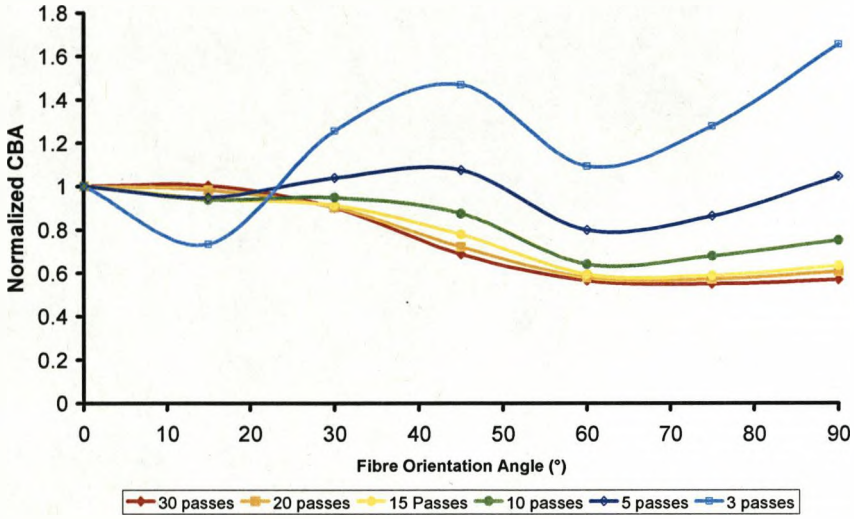

Figure 4.63 CBA of 1:1 lay-up for various fibre angles normalized against 0° result

Bend Rate per Pass

The effect that fibre orientation angle has on the BRPP is similar to the effect it has on the cumulative bend angle. As the FOA increases, the stiffness of the panel increases relative the bending angle. This reduces the BRPP that the laser forming process produces for a given set of parameters (figure 4.64). As with the effect of increasing layers in the laminate (section 4.3.1) the response per pass of the work-piece appears to show less variation as the FOA increases.

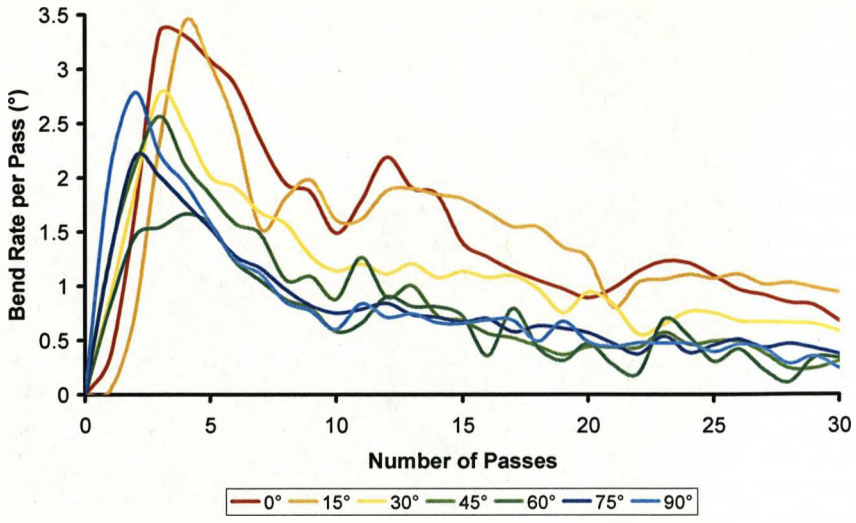

Figure 4.64 BRPP against number of passes for various fibre angles

To ensure that the reduction in variation in bend rate per pass is not an artefact of the reduction in bend angle the results were normalized (section 4.2) to remove the effect of the amplitude of the values and allow a direct comparison (figure 4.65). As illustrated the variation in the bend rate per pass does reduce as the FOA increases but not at a significant level. This reduction in variation per pass can be explained by the increased stiffness of the work-piece relative to the forming direction. As the part stiffens the effect of the plastic strains produced during the heating stage is reduced. This reduces the effect that the variations in energy coupling and incident power have on the bend produced.

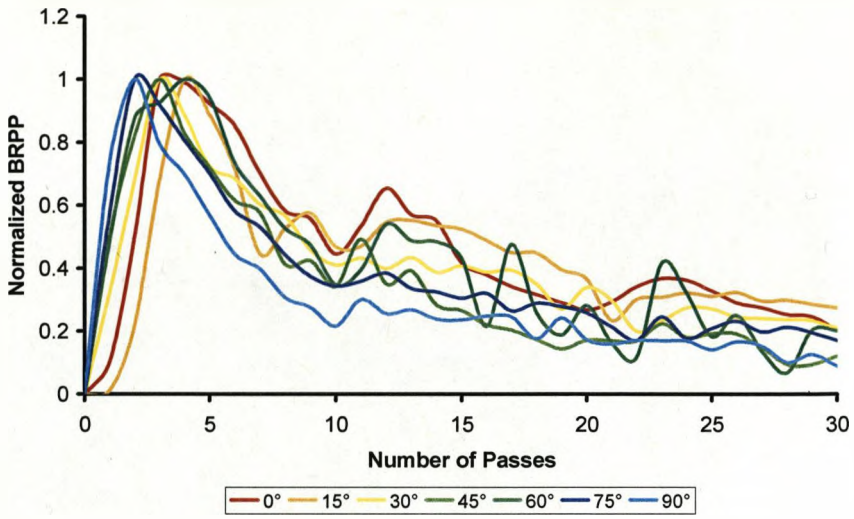

Figure 4.65 Normalized BRPP for various fibre angles

Bend Propagation

The effect that fibre orientation angle in the composite layers has on the propagation of the bend as the forming process occurs is shown in figure 4.66. The graph shows the mean values of bend rate over a ten pass scan strategy. The propagation of the bend varies in a similar way to that encountered with increasing layers in the laminate lay-up, with a reduction in bend angle as the orientation of the fibres moves away from the irradiation line.

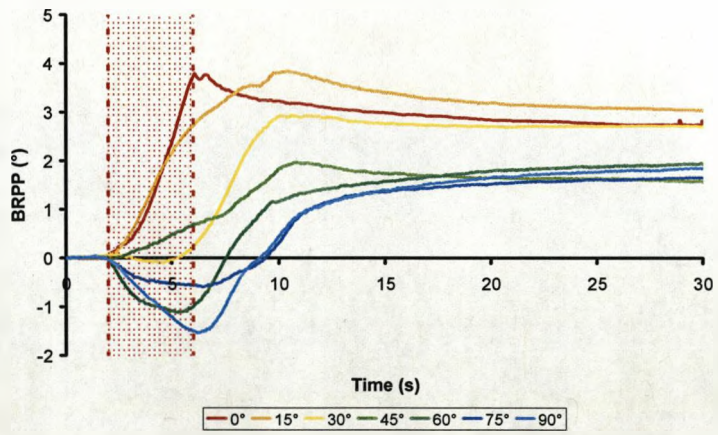

Figure 4.66 Bend angle against number of passes for various fibre angles

With the fibres orientated with the bend line (0°) the rate of bend angle propagation increases as time progresses, due to the increasing amount of plastic strains as the work-piece undergoes the forming process. The bend continues to propagate until the laser is turned off as the cooling of the work-piece occurs and the thermal expansion is converted to plastic strain. Once the laser has been turned off, recovery of the mechanically deformed composite layer occurs, causing springback of the bend reducing the angle from 3.79° to 2.74°. Having the fibres orientated 15° from the bend line produces a similar result, with an initial increase in the bend propagation rate but after three seconds of irradiation the bend propagation rate reduces due to the effect of the off axial load on the fibres. The positive bend continues to propagate for four seconds after the laser has turned off until a maximum bend angle of 3.84° is reached. The increased time for propagation of the bend is due to the loading of the fibres. With the fibres parallel to the bend line, the mechanical forming effects are mainly on the epoxy resin matrix as the fibres are aligned with the bend. Once the fibres are orientated away from the bend line they affect the propagation of the bend, not only reducing the overall bend angle, but increasing the time it takes for the maximum bend angle to be achieved as they resist the bending moment produced by the plastic strains. Recovery of elastic strains in the composite layer due to mechanical forming and the contraction of the composite layer as it cools, then causes a 20% reduction in the bend angle. When an FOA of 30° is investigated a counter bend is detected as the process starts. This is due to loading of the sample by the off-axial fibres. As fibres are orientated away from the bend line, the amount of residual stress from the differential thermal contraction rates of the constituents increases. When the aluminium in the laminates is heated during the laser forming process this relaxes the stresses present in the aluminium and allows the counter bend to form. The 30° FOA also displays a spring-back effect. The 45° FOA does not display a counter bend, but shows an almost constant propagation of the bend to a maximum value, which then springs back to a lower overall bend angle. The FOAs of 60°, 75° and 90° show a counter bend, which increases as the fibre

angle increases. Unlike all the previous fibre orientations, no over bend and spring back is encountered with the bend continuing to increase up to 20 seconds after the start of the laser pass. When these results are normalized against their respective maximum values (figure 4.67) it is apparent that the counter bend produced becomes more significant with the increasing fibre orientation. For a 90° FOA the negative counter bend produced is of the same amplitude as the positive bend achieved.

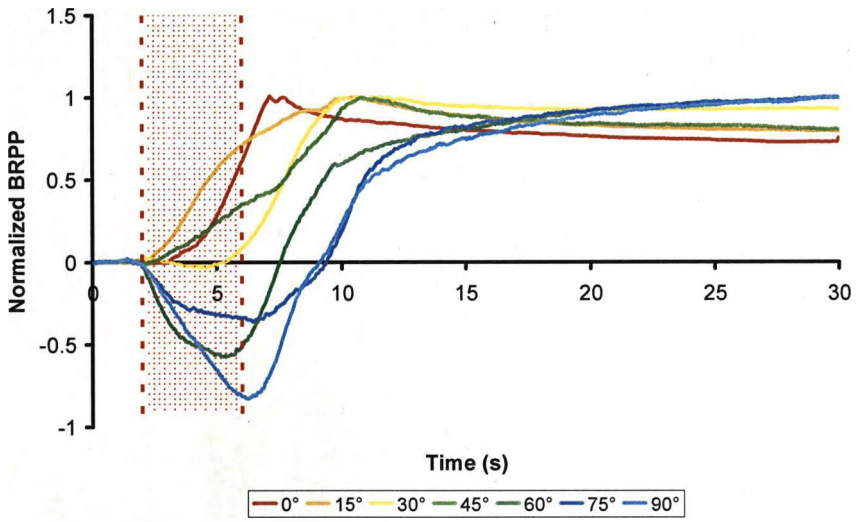

Figure 4.67 Normalized bend angle against time for various fibre angles

Thermocouple Data

Figure 4.68 shows the thermocouple data recorded when processing 1:1 0° (figure 4.68 a)) and 1:1 90° (figure 4.68 b)) GF FMLs. As discussed earlier the composite layer has little effect on the propagation though the surface of the FML (section 4.3.1.4) but does effect the propagation of heat through the thickness of the material. Therefore taking values from measurement point 110, the 0° FOA sample caused a greater increase in bulk temperature of the sample that the 90°, a 16.5°C increase compared with an 11°C increase, from 21°C. However the 90° FOA sample reached a higher peak temperature of 70°C compared to 63°C.

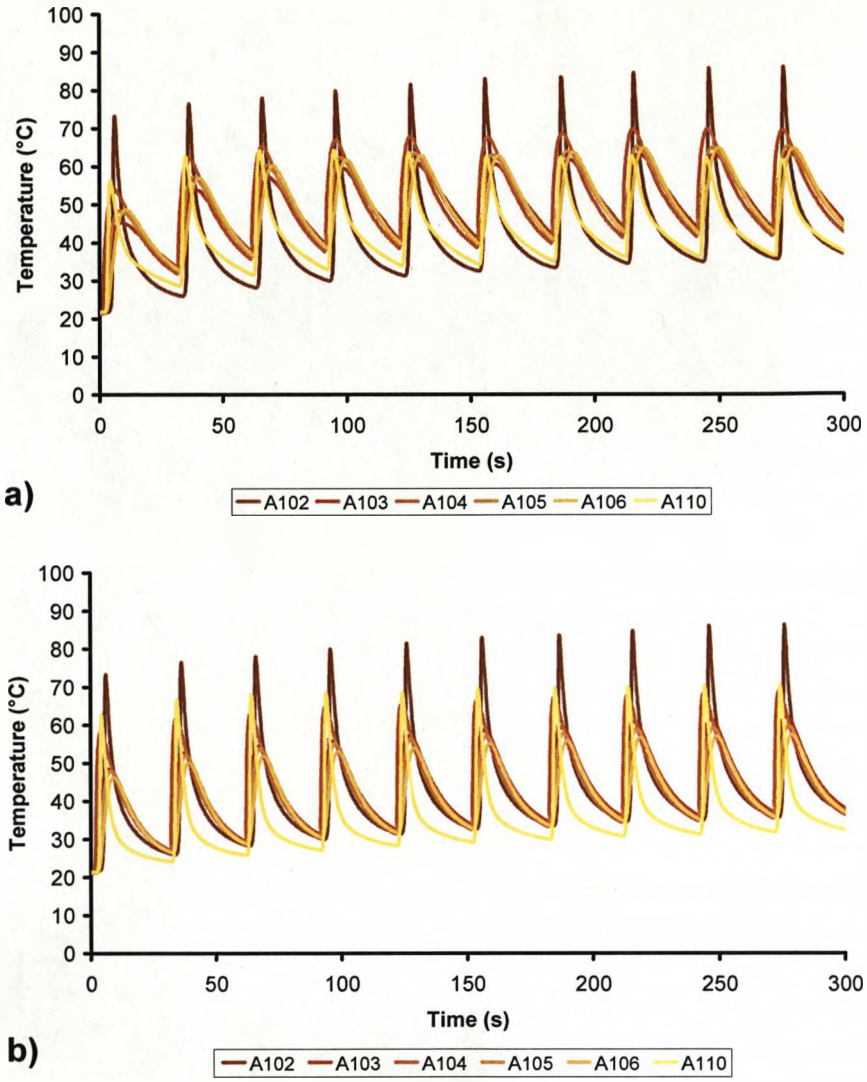

Figure 4.68 Thermocouple output from measurement point 110 for a) 1:1 0° and b) 1:1 90° GF FMLs

Figure 4.69 shows the mean change in thermocouple output (figure 4.69 a) and the normalized change in thermocouple output (figure 4.69 b) for measurement point 110. The traces show that the 0° FOA transfers the thermal input from the forming process to the environment at a lower rate than the 90° sample. As both composites are identical one would expect the propagation through the thickness to be identical.

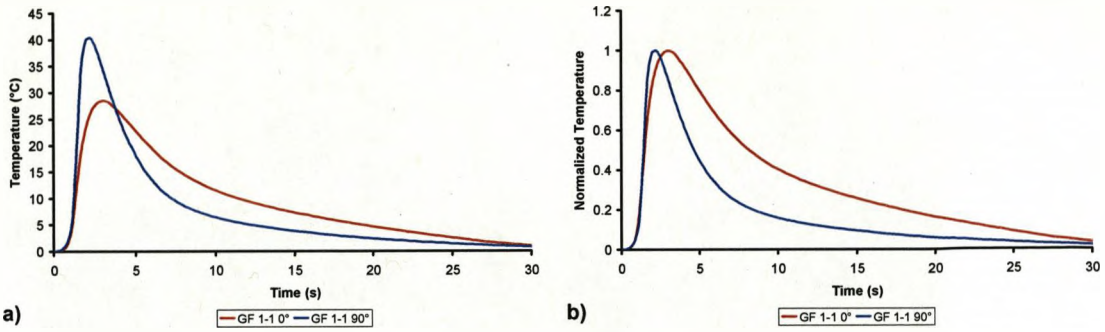

Figure 4.69 Thermocouple output for measurement point 110 a) mean temperature change and b) normalized mean temperature change

When thermocouple outputs for all three sets of processing parameters are investigated (figure 4.70) three separate samples processed on three separate occasions all show the same patterns, with the 90° FOA samples cooling quicker than the 0° FOA samples.

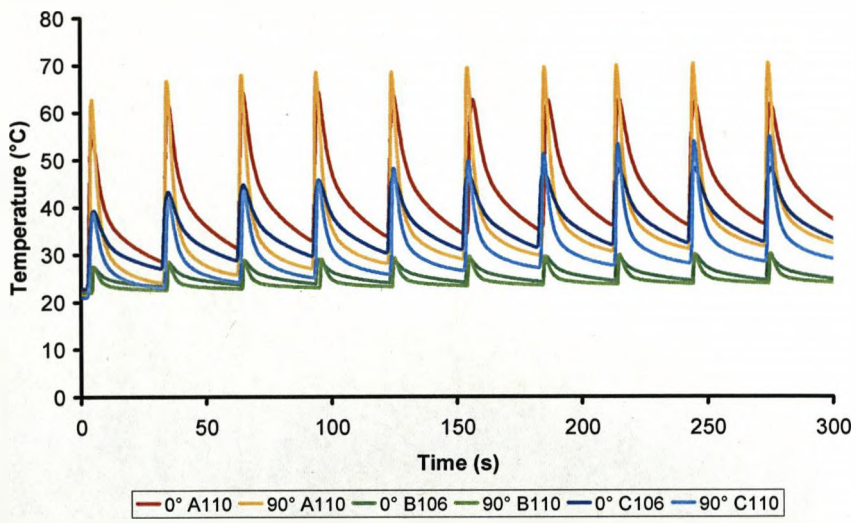

Figure 4.70 Thermocouple output for measurement point 110 for three different sets of processing parameters

This variation is due to composite orientation acting as channels. When the fibres are orientated parallel to the bend line (0° FOA) the thermal energy must be transferred through the constituents. Both constituents are poor thermal

conductors, epoxy resin has a lower value of thermal conductivity, 0.277-1.00W/m-K [160] compared to 1.38W/m-K [161] for the glass fibres (no data is available on the thermal conductivity of the specific epoxy resin system used here). This means that when heat can be conducted along just the glass fibres to the heat sink, rather than a glass/epoxy route, the reduction in temperature occurs more rapidly.

4.3.2.2 Composite layer

Cumulative Bend Angle

In commercially available FMLs, the composite layer will be a combination of unidirectional fibres with varying orientations, creating a composite layer often thicker than the aluminium. The effect this had on the laser forming process was investigated with an asymmetrical GF lay-up of one aluminium layer and two 0° glass fibre layers (1:2) and a symmetrical PP lay-up with two PP composites next to each other sandwiched between two aluminium layers (1:2:1). The effect this has on the CBA is shown in figure 4.71. Figure 4.71 a) shows 1:0, 1:2 and 2:1 lay-ups having been processed at 35W laser power and 10mm/s traverse velocity. The overall result is similar to that obtained by increasing the number of layers in the laminate, a reduction in the CBA. However, an increase in the composite thickness reduced the initial rate of bend in the first 11 passes for the 1:2 FML. After this the more characteristic LF curve is seen. A similar effect is noted in work by Dearden *et al.* [162]. Here mechanically pre-bent samples with a negative form angle were treated by LF to remove this distortion. This suggests that due to the different contraction rates of the composite and aluminium, the sample was pre-stressed even though this was not visually apparent. This therefore will affect the formability of any asymmetrical FMLs where the composite is of greater thickness ratio than the aluminium.

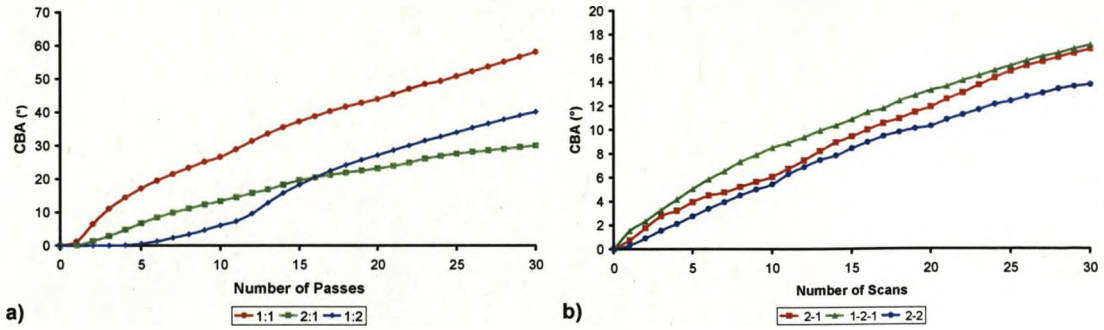

Figure 4.71 Number of scans verses cumulative bend angle for multiple composite layer FMLs and single composite layer FMLs, a) GF and b) PP

The symmetrical PP FML showed a different effect of the additional composite layer (figure 4.71 b). The constituents of this FML were the same as those used in a 2:2 FML lay-up, but present in a different order and with an additional Xiro PP adhesive layer. The 1:2:1 FML achieved a greater CBA then the 2:2 and 2:1 FMLs, 17.2° as apposed to 13.8° and 16.8° respectively. Were the bend angle achieved simply a factor of the ratio of formable thickness, the 2:1 would produce the biggest bend. The 1:2:1 FML produces a larger CBA as the aluminium layer is further away from the area of plastic strain or 'pivot' point. This increases the lever effect of the upper layer by the increase in the thickness of the sample. As the aluminium layer is the stiffest constituent in the FML this increased lever arm length produces a greater force on the aluminium layer, therefore producing a larger CBA. Also, as the PP composite is adjacent to the aluminium layer which undergoes heating during the laser process, the composite will absorb this heat, softening it and making it easier to mechanically deform.

Bend Propagation

The effect of additional layers of composite also alters the propagation of the bend in the materials. With a 1:2 lay-up (figure 4.72) the initial four passes show little increase in the bend angle, as observed with the CBA (figure 4.71). However once the residual stresses present in the system from the panel production are overcome, the bend propagates similarly to 1:1 lay-ups, with the bend propagating until the laser is turned off and then recovery of the bend due to

elastic strain during the mechanical forming. However unlike the 1:1 lay-up there is a small counter bend present at higher scan strategies, due to the loading of the work-piece by the mechanically deformed composite layers. The normalized mean bend propagation data (figure 4.72 b) further illustrate this point with an almost identical increase in the rate of bend propagation. The springback encountered with the additional composite layer is also increased due to the lower combined Young's modulus of the 1:2 laminate which makes it more susceptible to elastic recovery.

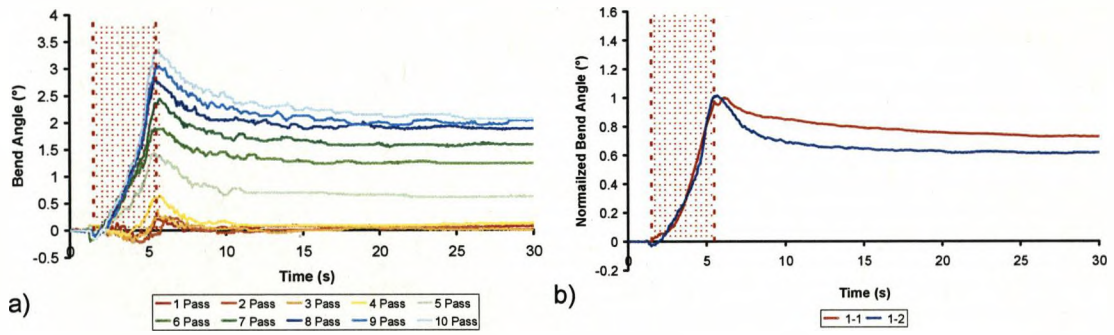

Figure 4.72 Propagation of the bend angle in time for 1:2 GF FML a) per pass and b) normalized mean

The bend propagated in the symmetrical laminate (1:2:1) with the same pattern as the 2:2 laminate, with a counter bend followed by a positive bend propagation till reaching a final bend angle after the laser was turned off (figure 4.73). The 1:2:1 FML underwent a greater amount of counter bend than the 2:2 laminate. The final bend angle was reached approximately ten seconds after the start of the irradiation process for both lay-ups.

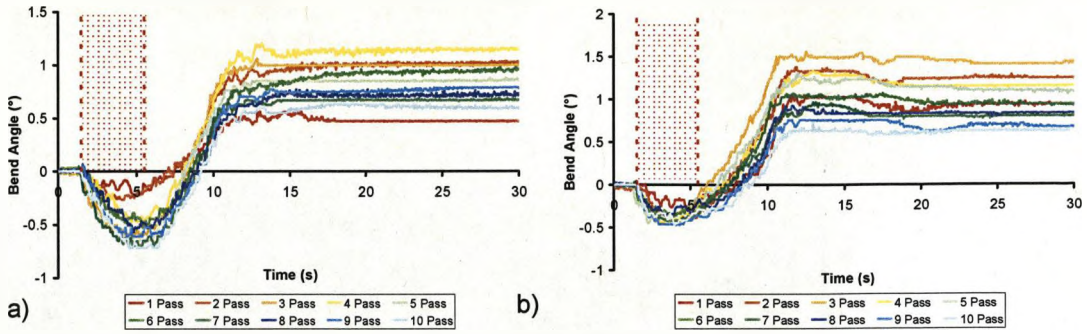

Figure 4.73 Variation in bend angle with respect to time for a) 1-2-1 PP FML and b) 2-2 PP FML

When the mean bend propagation data is normalized the increased amplitude of the counter bend encountered when forming 1:2:1 FMLs is apparent (figure 4.74). The 1:2:1 undergoing a counter bend of approximately 60% of the final bend angle, compared with 36% for 2:2 and 50% for 2:1 FMLs.

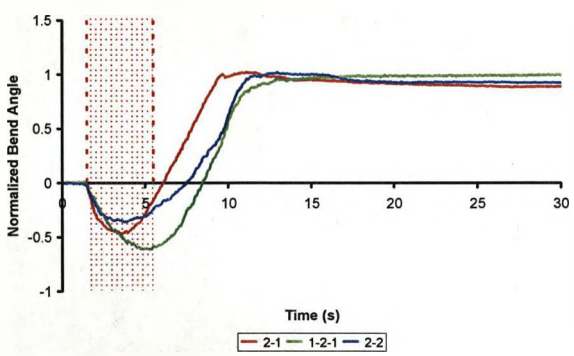

Figure 4.74 Normalized mean bend propagation for PP FMLs

Thermocouple Data

The additional composite layers affect the propagation of heat through the thickness of the material. The 1:2 GF FML exhibited a greater change in mean temperature, at measurement point 110, than 2:1 GF FML and a similar value to the 1:1 FML (figure 4.75 a). It also exhibited a variation in the rate of heat loss of the sample. When the mean temperature change for measurement point 110 was normalized (figure 4.75 b) the 1:2 laminate had the highest rate of heat loss

compared to 1:1 and 2:1 laminates. This could be due to the insulating effect of the double glass fibre layer reducing the thermal input into the composite layer. This leaves the majority of the thermal input in the aluminium layer which, with its higher thermal conductivity speeds the dissipation of heat through the aluminium clamp which is in contact with the aluminium surface layer.

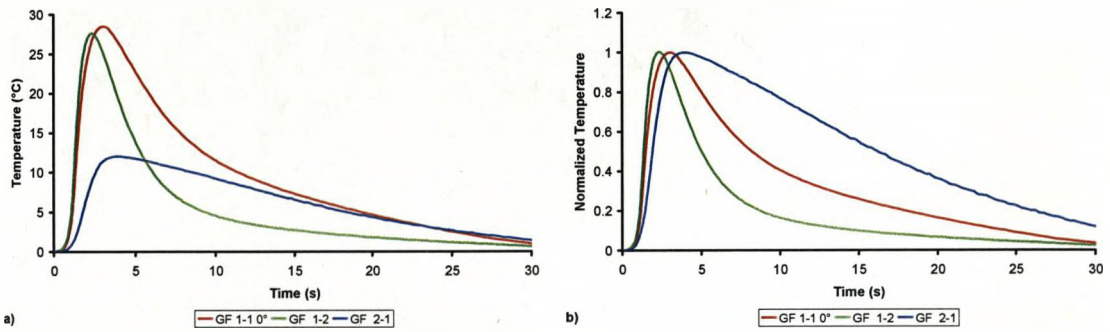

Figure 4.75 Temperature change at point 110 a) data and b) normalized

The effect on the transmission of heat through the 1:2:1 PP FML was to reduce the maximum change in temperature recorded at measurement point 110, due to the improved insulating effect of the double composite layer (figure 4.76a). The increased composite thickness also reduced the rate of thermal loss to the environment (figure 4.76 b).

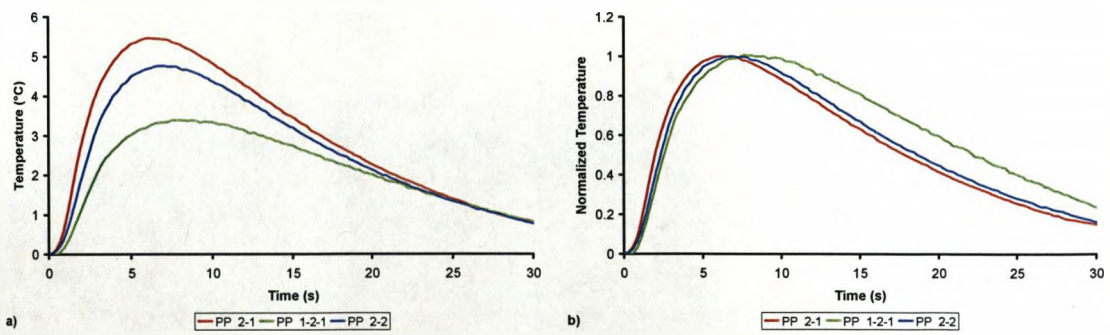

Figure 4.76 Thermocouple output for measurement point 110 for PP FMLs a) variation in temperature and b) normalized against maximum temperature

Strain Gauge Analysis

The 1:2 GF based FML underwent strain gauge analysis to complement the understanding of the variation that occurs in the laser forming process when additional layers of composite material are included in an FML laminate. The samples were processed using ten passes of 35W laser power, a traverse velocity of 10mm/s and a 30 second dwell time between scans. The longitudinal strain is measured parallel to the irradiation path and the transverse at 90° to it. The full data sets recorded for both longitudinal and transverse strains are presented in appendix B with those recorded for other lay-ups. The 1:2 lay-up is in a small amount of tensile strain in the longitudinal direction after 10 passes, which is consistent with the edge effect witnessed in other materials. In the transverse direction the 1:2 lay-up ends in compressive strain, which is the same result as found for both 1:1 and 2:1 lay-ups and is caused by the plastic strains induced during the laser forming process. Figure 4.76 shows the strain recorded in the transverse direction after seven passes for 1:1, 1:2 and 2:1 GF FML laminates.

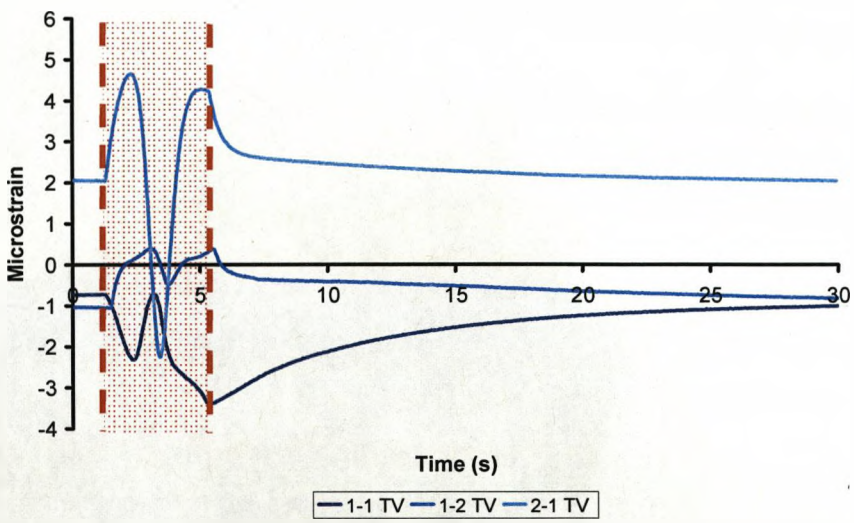

Figure 4.77 Transverse strain recorded at pass seven

The strain recorded for a 1:2 laminate follows the same cycle as recorded for a 2:1 laminate. An initial tensile strain is recorded, due to loading of the work-piece

as the counter bend propagated. The amplitude of the stain is relative to counter bend observed as the bend angle propagates. The counter bend on a 2:1 laminate is much larger and corresponds with a large recorded strain. A compressive strain due to localized heating and the asymmetrical effect for laser forming then occurs. This is then followed by a tensile strain, which is caused by the propagation of the bend in the material. Once the laser is turned off a compressive strain occurs due to cooling of the work piece, both in the aluminium and composite material and the recovery of the elastic strains from the mechanical forming or spring back.

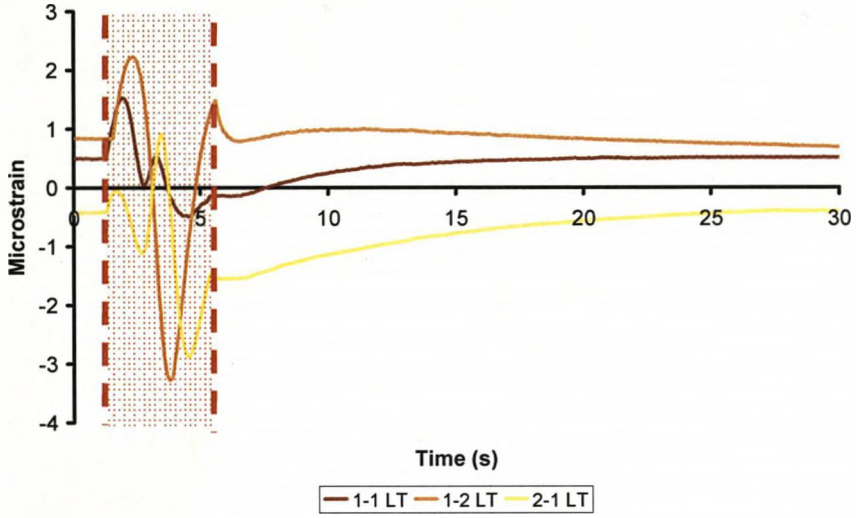

Figure 4.78 Longitudinal strain recorded at pass seven

The longitudinal strains for a 1:2 laminate also follow the trace recorded for the transverse strains (figure 4.78). A tensile/compression cycle is observed due to relaxing of stresses in the aluminium layer during the heating phase. This causes a tensile strain due to the force from the composite layer which then becomes a compressive force as the thermal expansion due to localized heating from the beam. Another tensile/compression cycle is then observed as the bend propagates and the sample cools.

4.4. Effects of Laser Processing

During processing, a number of different effects due to laser forming were observed and these can be separated in to two main areas, macro effects and micro effects. Macro effects can be observed with the naked eye while micro effects require analysis equipment, such as microscopes.

4.4.1 Macro Effects

4.4.1.1 Structural Failures

Structural failures were limited to delamination of the sandwich structure but were caused by a number of different factors. The first delaminations observed arose when processing samples at 35W laser power and 5mm/s laser traverse speed. These occurred exclusively between the surface aluminium layer and the initial composite layer. This was characterized by a visual change in the composite and on inspection a smooth break between the composite and aluminium (figure 4.79).

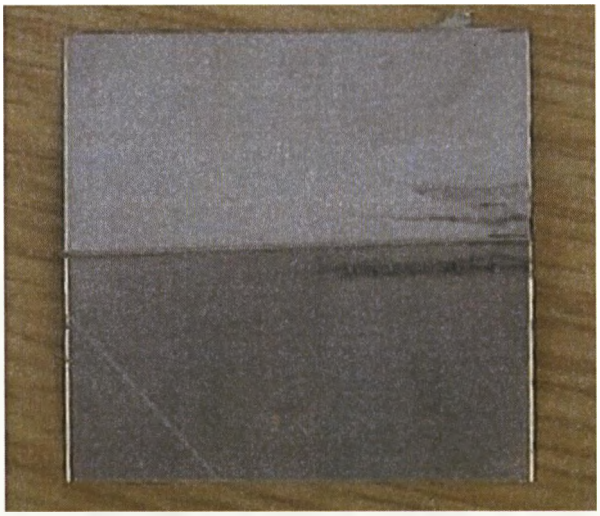

Figure 4.79 Delamination due to over heating

The cause of this type of delamination was excessive heating of the aluminium layer which softened and burned the matrix. When combined with large bend angles achieved with such a high energy input the composite would separate

from the aluminium leaving a smooth finish on the aluminium surface. These can be controlled by keeping the maximum temperature reached at the aluminium/composite interface below the maximum working temperature of the matrix. Figure 4.80 shows the operating window for 2:1 glass fibre based FML with a number on empirically derived boundaries which related to the maximum service temperature of a number of epoxy resins available from SP Composites [157] from whom the pre-pregs used in this investigation were purchased.

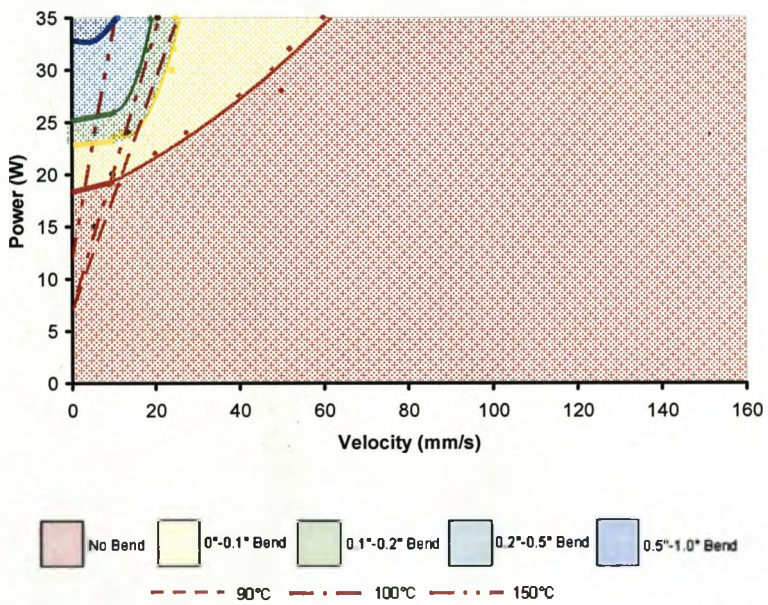

Figure 4.80 Laser power against traverse velocity for laser forming of 2:1 GF FML

The lowest service temperature for the SE84 resin system used was 90°C, indicated by the dashed line on figure 4.80. With this as a maximum boundary condition the highest achievable bend rate per pass is less than 0.1° per pass. A higher service temperature of 100°C is possible with a higher cure temperature and short cure time [157], which is indicated by the dash/dot line on figure 4.80. This 10°C increase in maximum working temperature allows a doubling of the maximum bend per pass rate, to 0.2°, before the maximum service temperature is exceeded. SP offers some resin systems that work up to 150°C (SE135) which

gives a bend rate per pass of up to 1° per pass, which meeting the thermal criteria, would allow full production of complex parts form flat FML sheet.

In order to prevent this thermal damage, a number of different forced cooling techniques were attempted. Water was used in a number of different ways, with samples sat in water baths during processing, with the work-piece surface proud of the water level and after processing by immersion in both standing and running water. The use of pressurised air to cool the sample post processing (during the dwell phase) and the use of solvents (acetone and ethanol) post processing. Various practical problems arose with all methods, such as re-aligning samples following immersion in water and the possibility of ignition of the solvents where used, prevented detailed investigation. But structural failures also occurred with delamination between the lower layers (figure 4.81). This was due to the variable rate of cooling between the layers, which led the lower layers to contracting at a greater rate than the upper layers causing delamination. These tended to be complete failures with the lower surface completely delaminating.

Figure 4.81 Delamination of lower layers of sample due to forced cooling.

A number of mechanical failures of the composite/aluminium interface were encountered at high bend angles and where characterized by a rough texture on the aluminium surface, as witnessed during peel testing. These failures occurred at CBA values of over 45° and were accompanied by thermal delamination of the composite around the irradiation line. The delamination due to thermal input reduced the adhesive area which caused the load per unit area to exceed the bond strength of the composite. These failures produced a rough surface finish on the aluminium which where also observed during the peel tests (figure 4.82).

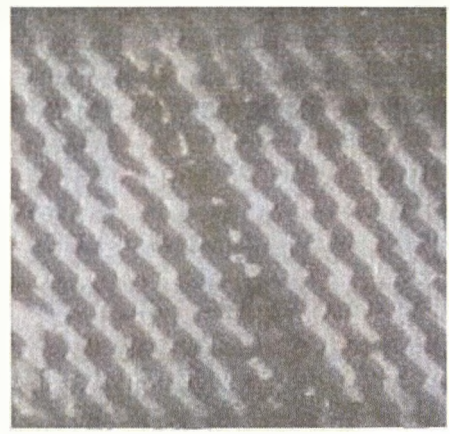

Figure 4.82 Surface finish due to mechanical failure of the composite at x2 magnification

The final form of structural failure witnessed was due to fibre orientation and occurred when the fibres were orientated further away from the line of irradiation (figure 4.83). Here delamination occurred due to a combination of factors. The excessive heat input at lower velocities caused some softening of the matrix, which when combined with the bend angle of the aluminium exceeding the minimum radius achievable by the E-glass rovings caused the laminate structure to break down. This is supported by the smooth surface finish under the delamination showing that a non-mechanical failure of the bond between aluminium and composite had occurred and some discolouration of the matrix indicating burning. As the orientation of the fibres increased away from the irradiation line the Cumulative Delamination Area (CDA) increased as the minimum curve radius for fibres aligned with the irradiation line (0°) is smaller than that of the fibre orientated perpendicular to the irradiation line.

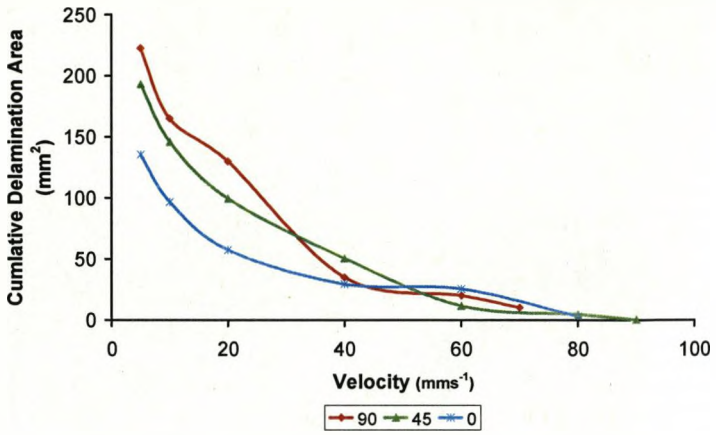

Figure 4.83 Cumulative delamination area verses velocity for various fibre orientations for the clamped and unclamped side of the sample processed at 35W

Variation in the CDA is also apparent depending on the side of the sample that is clamped. Figure 4.84 shows the variation in the mean CDA with respect to the clamped edge. The clamped edge suffers from less delamination as the presence of the clamp reduces the displacement of the composite layer during the heating phase. This reduces the separation of the composite and aluminium layers.

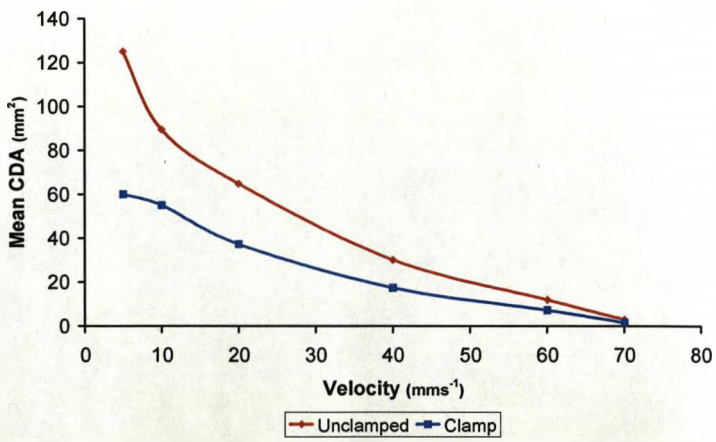

Fig. 4.84 Mean cumulative delamination area verses velocity for the clamped and unclamped side of the sample

4.4.1.2 Material Failures

The composite layer can be affected in two ways, thermally, due to laser parameters exceeding the maximum working temperature of the composite and mechanically, due to the bend angle causing failures of the fibre/resin system. Of the thermal effects, the main problem was burning of the matrix due to excessive temperatures at the composite/aluminium interface (figure 4.85). By controlling the laser processing parameters to keep the temperature at this interface below the maximum working temperature as discussed earlier it is possible to avoid this.

Figure 4.85 Detail of burning of matrix at x5 magnification

Mechanical effects to the composite were cracking in the matrix (figure 4.86) and the fibres (figure 4.87). These failures were due to the bend angle exceeding the minimum curve achievable by the composite, inducing to higher a stress levels in the composite and the matrix, leading to failures in one or both. The failures can be broadly characterized by the angle of the fibres in relation to the line of irradiation. With the fibres orientated at less than 45° from the line of irradiation, the majority of the failures were in the matrix, with fibres over 45° the majority of the failures appeared to be in the fibres. Further investigation is required to ascertain the accuracy of this and characterize the failures further. A solution to these failures would be to use a graded curve, rather than a sharp single line of laser forming to work with the minimum curve of the composites.

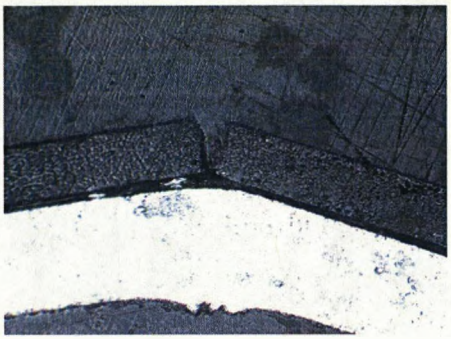

Figure 4.86 Image of matrix failure in 1:1 0° GF FML at x40 magnification

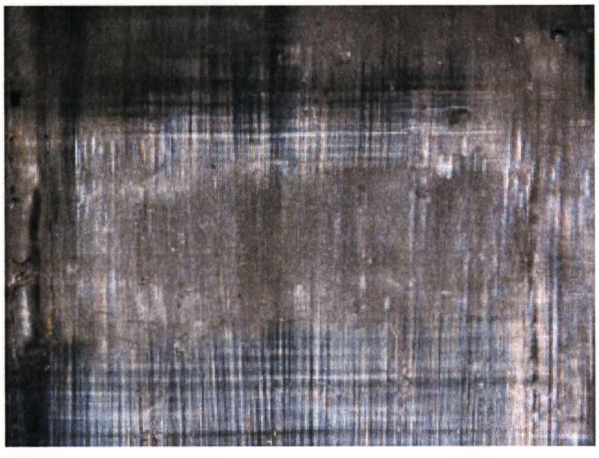

Figure 4.87 Image of failure of fibres in 1:1 90° GF FML (fibres orientated vertically in image) at x10 magnification

4.4.2 Micro Effects

4.4.2.1 Microstructural Effects

The affect of LF on aluminium has been well documented with numerous studies carried out (section 2.1.6.5). The effects identified are dependent on the temperature the area of interest is raised to. Heating to 503°K can lower the hardness locally due to recovery of the dislocations, caused by cold working, into cell substructures. Dissolution of less than 0.5% of the copper into solid solution should occur, also affecting the hardness. Further heating to 623-683°K causes re-crystallization if the exposure is for a long enough period of time, which increases the percentage of copper in solid solution to 1-2% further lowering hardness values. When the solvus temperature is exceeded (788-823°K) solution

heat treatment occurs and the elements go into solid solution. If the quench rate is sufficient then the regions stay highly saturated which facilitates re-aging at room temperature. If heating continues and the eutectic temperature is exceeded partial melting may occur and the area may undergo hot tearing. When heated above the melting temperature the material will melt and rapidly re-solidify resulting in a cast structure. A number of these processes may occur simultaneously due to the various temperature contours produced radially from the point of laser interaction. Figure 4.88 shows the as received material after polishing and etching with Keller's Regent. It features elongated grains due to cold-working after solution heat treatment. Large dark particles are possibly Cu2FeAl7 while the lighter particles possibly CuAl12.

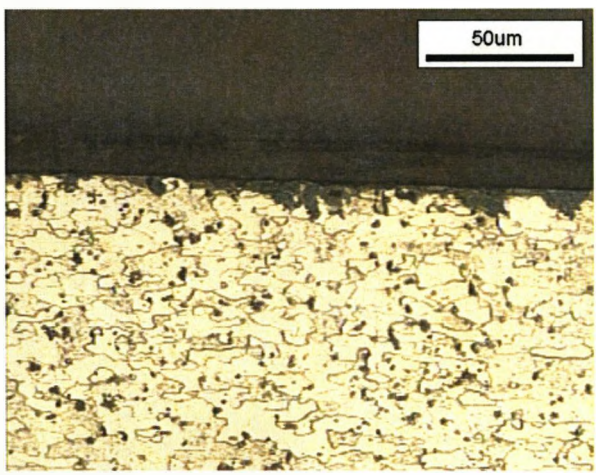

Figure 4.88 Aluminium 2024-T3 as received x50 magnification

Figure 4.89 shows an image of the material after laser processing. In the lower half of the image there is some recyrstallizing of the previous elongated grain structure. There is also present some partial melting signified by the darker banding around some of the grains. Closer to the top of the image, large recrystallized grains and dendritic structures due to melting and recasting, are present. The dendritic structures are due to growth from the base of the former grains. Figure 4.90 shows these structures and the results of partial melting in more detail.

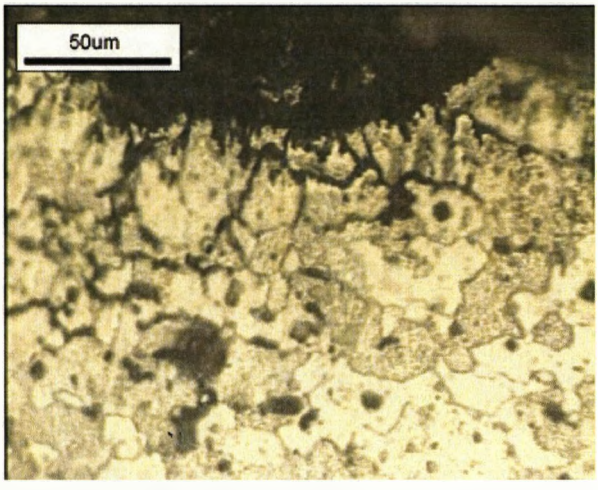

Figure 4.89 Laser processed aluminium 2024-T3 at X 50 magnification

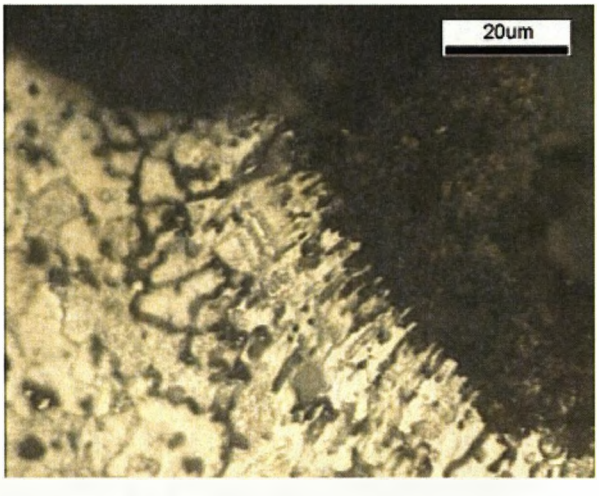

Figure 4.90 Detail of dendritic structure at x100 magnification

All these effects have been previously observed when laser forming aluminium alloys at high energy levels. The affect of the additional FML layers to these microstructural effects is limited with no disenable difference between aluminium samples and FMLs processed with the same parameters.

4.4.2.2 Micro Cracking

An unusual effect on the structure of the aluminium was detected on the 3:2 FML lay-ups when processed at 35W laser power and 10mm/s traverse velocity. On inspection of the irradiated zone for both PP and GF FMLs a number of cracks

were detected in the pass 10 sample (figure 4.91), with corresponding dislocations present in the pass 9 sample (figure 4.92). Neither feature was observed in the pass 8 sample (figure 4.93).

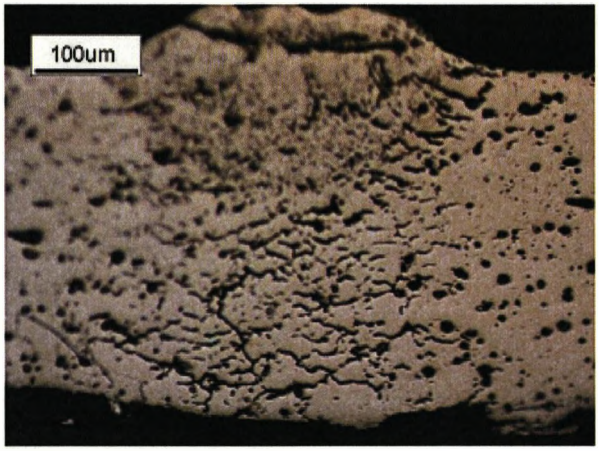

Figure 4.91 Micrograph of irradiated zone of 3:2 GF FML after ten passes

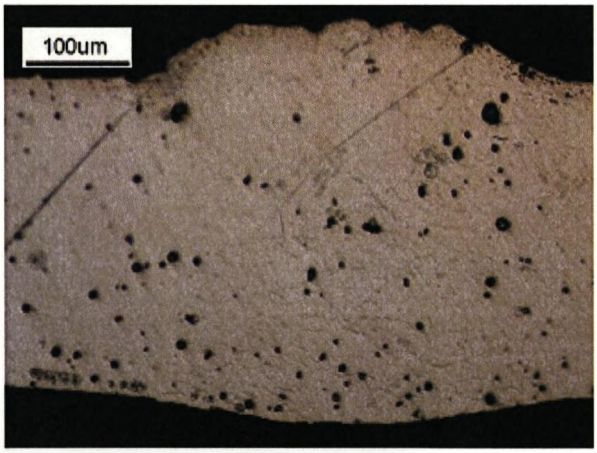

Figure 4.92 Micrograph of irradiated zone of 3:2 GF FML after nine passes

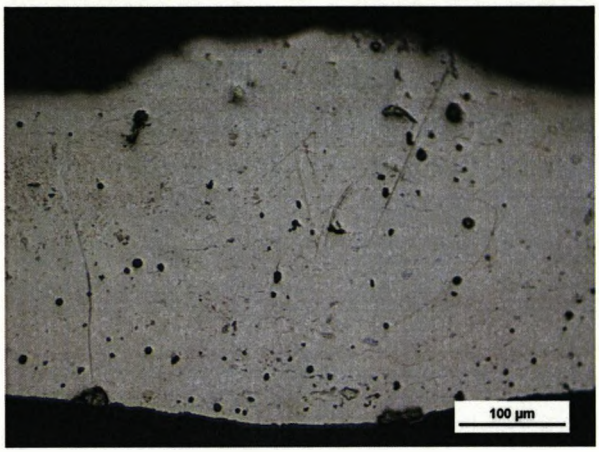

Figure 4.93 Micrograph of irradiated zone of 3:2 GF FML after eight passes

To confirm that these features were cracks and not solid solutions of alloying elements which had been removed during sample mounting and polishing as observed with other samples (figure 4.94), the samples were investigated using Vertical Scanning Interferometry (VSI). The results of this are shown in figure 4.95 and confirm the features are cracks with depths deeper than 20um (the maximum depth measured by the system). The cracks are located in an hour-glass area and traverse in all three axis of the sample and are only present in after 10 passes (figure 4.95 c)&d)). The cracks are caused by the oscillating motion that the sample undergoes during the forming process. The 3:2 lay-up undergoes considerable counter bending during processing, and is under strain from the contraction of the composite layers (during panel production) and under load form the mechanical deformation of the following layers of the FML.

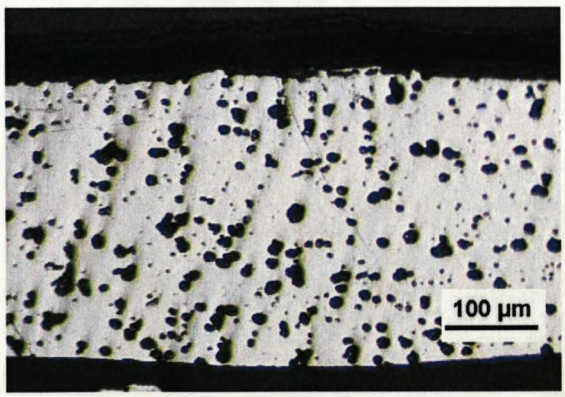

Figure 4.94 Polished sample showing removal of solid solution

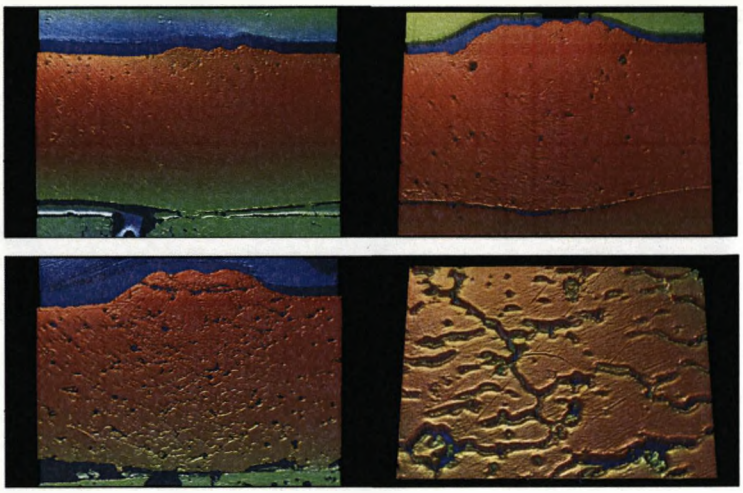

Figure 4.95 VSI images for 3:2 GF FMLs at x5 (a), x10 (b&c) and x20 magnification

4.4.2.3 Section Thickening

Another well documented effect of LF is thickening of the work-piece. This was witnessed to a greater degree in the FML sample when compared to the single thickness of aluminium and is currently under investigation. Another effect of the laser forming process on the material is the thickening of the bend. A number of studies have investigated this [158] and have reported that the thickening effect increases pass-on-pass for the first 20 passes in multiple pass laser forming strategies. The effect is due to the conservation of volume, as the lateral plastic compression in the upper surface forces the material upwards some degree in order to conserve the volume. This is present in the laser forming of FMLs with both GF and PP FMLs (figure 4.96). There is a recorded increase in the section thickening related to the number of layers that are present in the FML with the aluminium alloys showing a 25% increase in thickness after ten passes at 35W power and 10mm/s traverse velocity, whereas the FMLs of both types result in maximum increase of approximately 30% for GF and 35% for PP FMLs.

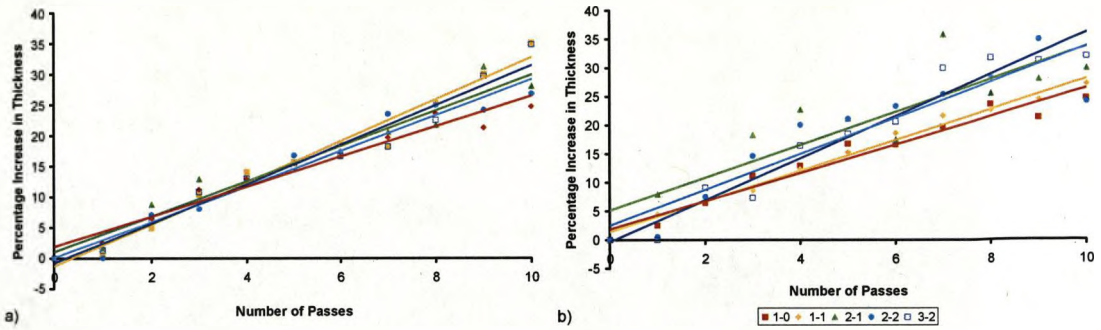

Figure 4.96 Percentage increase in section thickness for both GF and PP FMLs

Not only do the additional of layers increase the thickening of the cross-section but also the shape of the thickening. Figure 4.97 shows micrographs of AL2024-T3 and 3:2 PP FML, both processed at 35W power and ten passes at 10mm/s traverse velocity. The aluminium sample (figure 4.97 a)) shows a much smoother transmission from the unaffected bulk of the material to the laser formed area, with no noticeable change. The 3:2 PP FML (figure 4.97 b)) shows a much more noticeable localized increase in thickness in the laser formed area.

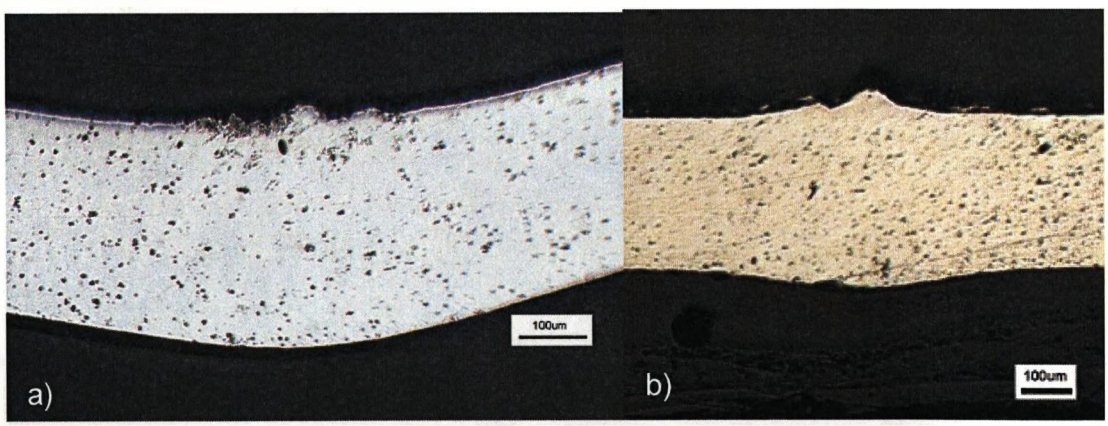

Figure 4.97 Localized Section Thickening in a) AL 2024-T3 and b) 3:2 PP FML

An initial investigation looked at the radius of the localized section thickening (figure 4.98). The increasing number of passes relates to a decreasing value for the radius of the area of section thickening for all lay-ups but no apparent relationship between the radius of the thickening an the laminate lay-up. However

the aluminium samples exhibit high bend angles which would equate to a small radius of curvature observed. The laminates exhibit much smaller cumulative bend angles, but still a similar radius of curvature for the localized thickening suggesting an effect due to the composite layers. This could be due to compressive strains the composite layer is under, post panel production, constraining the aluminium layer during the forming process, causing this affect but further work is required to confirm this.

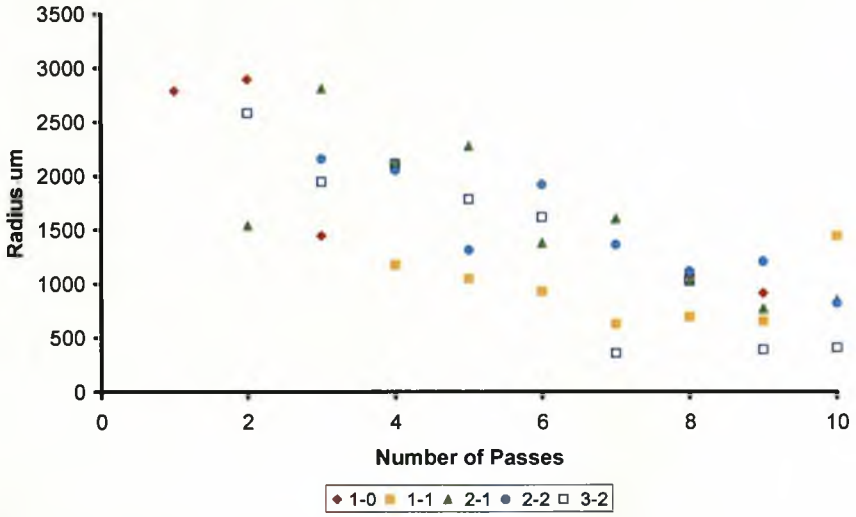

Figure 4.98 Radius of localized thickening for various GF FMLs

4.4.2.3 Micro Hardness

The effect of laser forming on the microhardness of FMLs was investigated by Vickers hardness testing of mounted samples. The tests were carried out at 50µm intervals from the lower surface of the sample at the thickest point. The last point measured was taken at least 50µm form the top surface of the sample. From this final point on the thickness measurements a number tests were taken in the y-direction of the material, from the laser formed area to the unaffected bulk. These sample locations were kept at the same distance form the upper surface (figure 4.99). The as received material gave an average Vickers hardness of 100+/-3.6 Hv

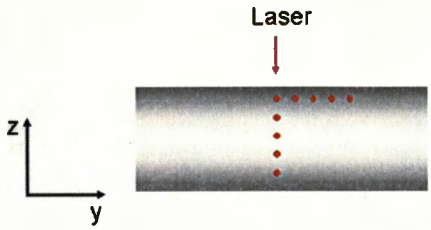

Figure 4.99 Schematic of micro-harness measurement set-up

The results across the top surface of the material show an increase in the microhardness of the material as the area of laser forming is approached (figure 4.100). This is constant with findings by Magee [19] and is due to finer gain size due to recrystallization.

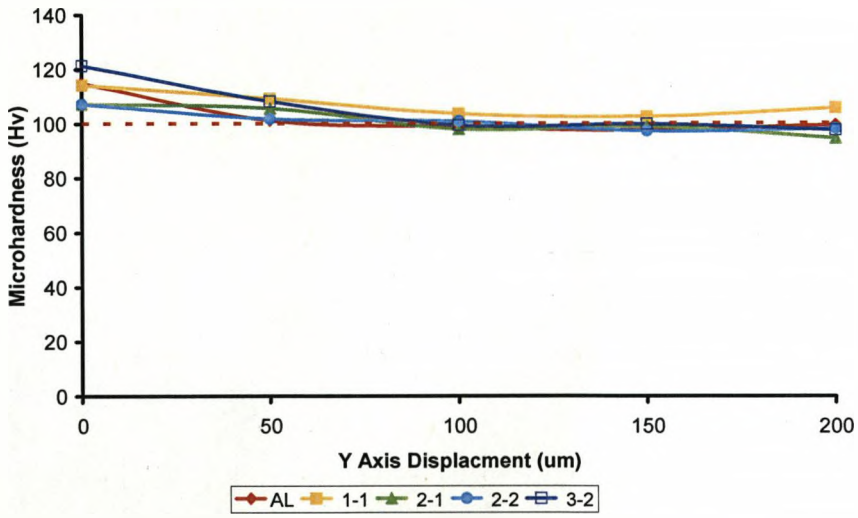

Figure 4.100 Microhardness in Y-axis

The effect of laser forming on the microhardness through the thickness of the material is show in figure 4.101. For a single skin of aluminium, an increase in the micro hardness values is detected as the testing point approach the heat affected zone from the forming process. With the FML samples a variation was found through the thickness (z-axis) with a secondary area of increased hardness in the lower half of the work-piece. This is due to the springback and counter-bend events which occur during the forming process. These add an additional cold-

working affect to the material, which causes an increase in the localized hardness values in this area.

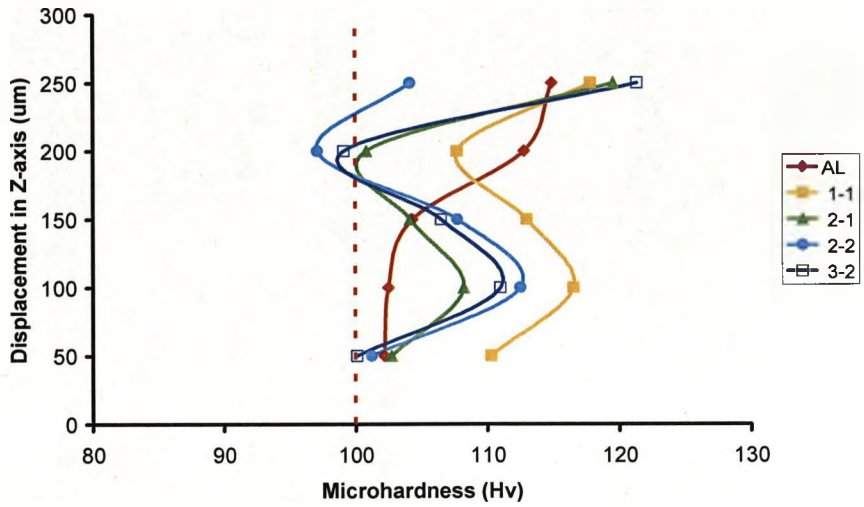

Figure 4.101 Microhardness in Z-axis

Chapter 5
Conclusions

5.1 Experimental procedure

Before an in-depth study into the effects of the Fibre Metal Laminates (FMLs) a number of other experimental variables were identified and controlled and the following conclusions can be drawn

- Of the three possible forming mechanisms, Temperature Gradient Mechanism (TGM), Buckling Mechanisms (BM) and the Upsetting Mechanism (UM), only the TGM is applicable to produce through

thickness strain variations resulting in 2D bending of FMLs. This is due to the BM causing delamination due to excessive heat input and UM producing variations in membrane strain. The UM is required for producing 3D shaping techniques.

- For thin coatings (<10μm) the majority of graphite applied to improve the coupling of the laser energy is burned off in the first four passes of processing. When thicker layers are applied (60μm), the graphite is removed by burning and particles ejecting from the trough. The majority of the thick graphite is removed in the first two passes in this case.
- Re-application of the graphite coating reduced the drop off of the bend rate observed in non-recoated samples.
- Sufficient dwell time between passes is required to allow cooling of the sample to the environment. This ensures a steep as possible thermal gradient through the material thickness is achieved and therefore the maximum bend angle.

5.2 Laser Parameters

The effects of various laser parameters had on the laser forming process were investigated and a number of conclusions can be drawn.

- As the laser power increases the maximum bend angle achieved also increases. With a constant traverse velocity the forming mechanism will change from TGM to UM to BM as the laser power is increased. At higher powers the variation in Bend Rate Per Pass (BRPP) reduces.
- As traverse velocity increases the Cumulative Bend Angle (CBA) reduces as the energy incident to the work-piece is reduced. As the traverse velocity increases the variation in BRPP increases.
- The effect of increasing number of passes is to reduce the BRPP produced.
- It was found that when processing aluminium using a graphite coating there was very little difference in the final CBA achieved when processing

with either 1.064μm (Nd:YAG) or 10.64μm (CO_2) radiation for the same energy density.

5.3 FML Parameters

The FML parameters can be split into two main subjects, the stacking sequence and the layer orientation.

5.3.1 Stacking Sequence

- Increasing number of layers in the laminate has the effect of reducing the overall CBA for a given laser power and traverse velocity. This is due to the laser forming mechanism activating a bending moments only in the top layer of the laminate, therefore as the number of layers increase the amount of force required to mechanically form the lower layers also increases. As there is a finite amount of force generated by the laser forming process for a given set of parameters, the bend angle achieved is reduced. The effect of increasing the number of layers in the laminate has on the bend rate per pass is to reduce its amplitude and increase the variation between passes.
- The propagation of the bend angle is affected by the increasing number of layers in the laminate in a number of ways. When number of layers in the composite is low (1:1 and 2:1), spring-back occurs due to the lower effective Young's modulus of the laminate.
- As the number of layers increase (2:1 or greater) a counter bend is detected at the start of the forming process. As the number of layers increases this counterbend becomes a significant percentage of the final band angle achieved. The counterbend is due to loading of the laser formed aluminium layer by the mechanically deformed layers.
- The initial composite layer is also affected by the thermal input to activate TGM in the upper aluminium layer. This has the effect of altering the length of propagation of the bend. When forming a single aluminium skin,

the bend propagated within 8 seconds from the activation of the laser. The addition of a composite layer increased the time of propagation to over 30 seconds in some cases, with the 'spring-back' still occurring as the next pass started. The majority of this spring back can be attributed to the effect of mechanical forming of the lower layers and the increased Young's' Modulus of these layers. However the longer, less significant bend reduction can be attributed to the effect of thermal contraction of the composite layer. This contraction occurs slowly due to the poor thermal properties of the composite and the increased time for cooling to the environment to occur.

- It is the first time spring-back and delay in bend propagation have been reported in the area of laser forming.
- The increasing number of layers in the laminate system has little effect on the rate of propagation of temperature through the surface of the material. However it does increase the bulk temperature of the aluminium layer due to the insulating effect of the composite layers. These layers also reduce the propagation of temperature through the thickness of the material and reduce the rate of change of the temperature, both in increasing and reducing.
- Increasing the number of layers in the laminate has a measurable effect on the strains propagated on the system with an increasing number of tension compression cycles observed. The final strain value also varies as a monolithic material that has been laser formed is in tension longitudinally, due to the edge effect and in compression transverse due to the plastic strains produced during the forming process. The FML samples registered altering final strain values after the laser forming process.
- The effect of the composite layer is not fully understood and has a significant effect on both the propagation of the bend and the strain loading of the system during forming. The residual stresses remaining

after the curing process raise the issue of repeatability of shaping FML materials using a laser source.

5.3.2 Fibre Layer Parameters

- Fibre orientation was found to reduce the CBA as the fibres were orientated away from the direction of forming. This is consistent with off-axial loading of composites. There is a corresponding reduction in BRPP but little effect on the variation per pass.
- The effect of fibre orientation on the propagation of the bend is to reduce the springback encountered with 1:1 laminates and introduce a large counterbend. This is due to the increased effect of thermal contraction which occurs during the curing cycle.
- The effect on thermal propagation is that both peak temperatures achieved and the rate of temperature reduction are reduced as the fibres are orientated away from the irradiation line.
- Additional composite layers in asymmetrical lay-ups (1:2) increase the loading on the aluminium layer reducing the CBA and BRPP, similarly to that encountered when removing distortion using laser forming. The additional composite material also increases the amount and rate of springback encountered. The increased composite layer caused a reduction in the peak temperature measured through the thickness and reduced the rate of reduction in the temperature of the material.
- Additional composite layers in symmetrical lay-ups (1:2:1) produced a greater CBA than the 2:2 lay-up due to thermal softening of the composite. Also observed was an increased amount of counter bend and the length of time it took to achieve the maximum bend angle. The thicker composite layer also reduced the maximum temperature measured and the reduced the rate of change in temperature.

5.4 Effects of Laser Processing

A number of effects were observed due to the laser processing of FML and these can be characterized into macro effects and micro effects.

5.4.1 Macro Effects

- Structural failures were observed due to excessive thermal input, differing contraction rates and mechanical failures due to excessive bend angles combined with reduced adhesive area due to thermal input.
- As fibres were oriented away from the line of irradiation an increasing area of delamination was observed around the irradiation path due to a combination of exceeding the minimum bend radius of the fibres and the loss of adhesion due to thermal heating. This was also affected by the proximity of the clamp which reduced the amount of separation between the composite layer and aluminium layer and thus reducing the delamination area.
- A number of material failures were detected including, burning of the matrix due to excessive thermal input. Cracking of the matrix occurred when the fibres were orientated towards the irradiation path, due to excessive bend angles. When the fibres were orientated away form the irradiation path cracking of the fibres occurred due to excessive bend angles.

5.4.2 Micro Effects

- Microstructural effects on the grain structure of the aluminium occurred due to intense an energy input into the surface, with no discernable difference between FMLs of various lay-ups.
- Microcracking was observed in the 3-2 lay-up after 19 and 10 passes and was attributed to fatigue cracking due to the cyclic nature of the forming process and the load which the aluminium was under due to the composite layers.

- Section thickening was also detected with a localized increase around the irradiation line due to the constraining effect of the composite layer.
- The microhardness of the samples was affected in two ways. In the heat affected zone the hardness increased due to finer grain size. Through the thickness of the sample a secondary area of increased microhardness was detected and was attributed to strain hardening due to the bend propagation cycle.

5.5 Further Work

A number of recommendations for further research have arisen from this work and these are:

- Asymmetrical FMLS – As the CBA is a resultant of the forces generated in the aluminium layer which undergoes thermal forming using a thicker aluminium layer on the surface to be laser formed would allow higher energy densities to be used and therefore increase the bend angle that could be achieved.
- Minimum Bend Radius – It has been shown that laser forming can be used to produce sharp bend lines, but graded bends would be of more use in industry and allow the production of greater bend angles while still retaining the materials integrity.
- Failure Modes – Whilst initial failure modes of laser forming of FMLs has been characterized further work, particularly on the micro-cracks detected on the 3:2 laminates is required before commercial use is possible.
- Scanning Optics/shaped beams - The point source effect of laser forming causes a large number of strains in various cycles to occur in the material. The use of fast scanning optics or large shaped beams could be a possibility to over come this.
- 3D Forming – The anisotropic nature of the FMLs would hold some interesting considerations for the 3D forming process and would require differing irradiation paths/scan strategies than those currently in use. It would also require the use of the upsetting mechanism to shorten the

aluminium surface in order to produce a 3D shape. This would require investigation of the possibilities of the upsetting mechanism on the FML panels.

- Modelling of the process – Furthering the initial work covered here by building a model which shows the effects presented will aid understanding of the process and indicate the main factors involved.
- Effect of line energy – Using line energy/interaction time to relate the effects of laser power and velocity.
- Effect of the composite layer – Further understanding of the effect of the composite layer, particularly the thermal expansion/contraction and the effect on the forming process.

References

1. Einstein, A., *On the Quantum Mechanics of Radiation.* Physikalische Zeitschrift, 1917: p. 121-128.
2. Mainman, T.H., *Stimulated Optical Radiation in Ruby.* Nature, 1960. **187**: p. 493-494.
3. Steen, W.M., *Laser Material Processing.* Third ed. 2003, London: Springer.
4. Patel, C.K.N., *Continuous wave laser action on vibrational-rotational transition of CO_2.* Physics Review A, 1964. **136**: p. 1187.
5. Geusic, J.E., Marcos, H.M., and Van Uitert, L.G., *Laser oscillations in Nd doped yttrium aluminium, yttrium gallium and gadolinium garnets.* Applied Physics Letters, 1964. **4**: p. 182.
6. Vlot, A., *Fibre Metal Laminates: An Introduction.* 1st ed. 2001, Dordrecht: Kluwer. 527.
7. Dearden, G. and Edwardson, S.P. *Laser Assisted Forming for Shipbuilding.* in *SAIL.* 2003. Williamsburg, Virginia.
8. Holt, R.E., *Flame Straightening Basics.* Welding Engineer, 1960: p. 49-53.
9. Moshaiov, A. and Vorus, W.S., *The Mechanics of the Flame Bending Process: Theory and Applications.* Journal of Ship Research, 1987. **31**(4): p. 269-281.
10. Committee on National Needs in Maritime Technology National Research Council, *Ship Building Technology and Education.* 1996: The National Academies Press. 160.
11. Araki, M., Inoue, N., Horioka, M., and Ando, M., *On Angular Distortion of Hull Steel Plates by Line Heating Methods.* Journal of the Society of Naval Architects of Japan, 1973. **133**: p. 343.
12. Holt, R.E., *Primary Concepts for Flame Bending.* Welding Journal, 1971: p. 413-423.
13. Vollertsen, F., *Forming, Sintering and Rapid Prototyping.* Handbook of the Eurolaser Academy, 1998. **2**: p. 357-453.

14. Namba, Y., *Laser Forming in Space.* Proceedings of the International Conference on Lasers 1985, ed. C.P. Wang. 1986: STS Press McLean. 403-407.
15. Vollertsen, F., *Laser Forming, Mechanisms, Models, Applications.* LFT Erlangen Monograph, 1995.
16. Vollertsen, F. and Rodle, M. *Model for the Temperature Gradient Mechanism of laser Bending.* in *LANE '94.* 1994. Meisenbach Bambërg.
17. Vollertsen, F., *An analytical model for laser bending.* Lasers in Engineering, 1994. **2**: p. 261-276.
18. Yau, C.L., Chan, K.C., and Lee, W.B. *A New Analytical Model for Laser Bending.* in *LANE '97.* 1997. Meisenbach Bamberg, Germany.
19. Magee, J., *Laser Forming of Aerospace Alloys*, in *Department of Engineering.* 1999, University of Liverpool.
20. Yongjun, S., Hong, S., Zhenqiang, Y., and Jun, H., *Temperature gradient mechanism in laser forming of thin plates.* Optics and Laser Technology, 2007. **39**: p. 858-863.
21. Vollertsen, F., Komel, I., and Kals, R., *The Laser Bending of Steel Foils for Microparts by the Buckling Mechanism.* Modelling and Simulation of Material science and Engineering, 1995. **3**: p. 107-119.
22. Kraus, J. *Basic processes in laser bending of extrusions using the Upsetting Mechanism.* in *LANE '97.* 1997. Meisenbach Bamberg, Germany
23. Suhara, T., *Study on Thermo Plastic Forming: Bending of Beam of Rectangular Cross Section.* Journal of Zosen Kyokai, 1958. **103**: p. 233-243.
24. Vollertsen, F., Geiger, M., and Li, W.M. *FDM- and FEM- simulation of laser forming: a comparative study.* in *Advanced Technology of Plasticity.* 1993.
25. Alberti, N., Fratini, L., and Micari, F. *Numerical simulation of the laser bending process by a coupled thermal mechanical analysis.* in *LANE '94.* 1994. Meisenbach Bamberg, German.

26. Alberti, N., Fratini, L., Micari, F., Cantello, M., and Savant, G. *Computer Aided Engineering of a laser assisted bending process.* in *LANE '97*. 1997. Meisenbach Bamberg, Germany.

27. Hsiao, Y.C., Shimizu, H., Firth, L., Maher, W., and Masabuchi, K. *Finite Element Modelling Of Laser Forming.* in *ICALEO '97*. 1997. San Diego.

28. Li, W. and Yao, Y.L., *Laser Forming with Constant Line Energy.* International Journal of Advanced Manufacturing Technology, 2001. **17**: p. 196-203.

29. Li, W. and Yao, Y.L. *Effects of Strain Rate in Laser Forming.* in *ICALEO'99*. 1999. San Diego CA.

30. Yu, G., Masubuchi, K., Maekawa, T., and Patrikalakis, M.N., *Thermomechanics of laser forming of metal plates.* Massachusetts Institute of Technology (MIT) Fabrication Memorandum 1999. **99-1**.

31. Cosenza, C., Fratini, L., Micari, F., Cantello, M., and Penasa, M. *Explicit Thermo- Mechanical Analysis of Laser Forming Processes.* in *LANE 2001*. 2001. Erlangen Germany.

32. Holzer, H., Arnet, M., and Geiger, M. *Physical and Numerical modelling of the Buckling Mechanism.* in *LANE '94*. 1994. Meisenbach Bamberg, Germany.

33. Zimmermann, M., Rank, M., and Schmidt, M. *Simulation and Optimization of an Actuator for Laser Micro Alignment of an Optical Fibre to a MIcrolens.* in *IWOTE 2008*. 2008. Bremen.

34. Shakeel, S., Lin, L., Sheikha, M.A., and Liu, Z., *Finite element simulation of laser tube bending: Effect of scanning schemes on bending angle, distortions and stress distribution.* Journal of Optics and Laser Technology, 2006. **39**: p. 1101-1110.

35. Prithwani, I. and Otto, A. *Simulation of Laser Beam Forming of Large Aluminium Plates.* in *IWOTE '08*. 2008. Bremen.

36. McBride, R., Bardin, F., Gross, M., Hand, D.P., Jones, J.D.C., and Moore, A.J., *Modelling and calibration of bending strains for iterative laser forming.* Journal of Physics D: Applied Physics, 2005. **38**: p. 4027-4036.

37. Namba, Y. *Laser Forming of Metals and Alloys.* in *LAMP '87.* 1987.

38. Scully, K., *Laser Line Heating.* Journal of Ship Production, 1987. **3/4**: p. 237.

39. Masabuchi, K. *Studies at M.I.T related to Applications of Laser Technologies to Metal Fabrication.* in *Laser Advanced Materials Processing (LAMP 1992).* 1992. Niigata, Japan.

40. Sprenger, A., Vollertsen, F., Steen, W.M., and Watkins, K.G., *Influence of Strain Hardening on Laser Bending.* Manufacturing Systems, 1995. **24**: p. 215-221.

41. Mucha, Z. *Efficiency of Materials Laser Forming.* in *IWOTE 2008.* 2008. Bremen.

42. Mucha, Z., Cabaj, M., Gradon, R., Pawlowski, M., and Widlaszewski, J. *Laser Forming of Plates by the use of Beam with Circular and Rectangular Cross-section.* in *LAE 2001.* 2001. Erlangnen.

43. Liqun, L., Chen, Y., and Lin, S. *The Characteristics of Laser Forming of Aluminium Sheet Under Consecutive Irradiations.* in *ICALEO 2003.* 2003. Jacksonville Florida.

44. Liqun, L., Yanbin, C., Shangyang, L., and Dayong, G. *Characterization of Laser Bending under Different Cooling Conditions.* in *ICALEO 2002.* 2002. Scottsdale Arizona.

45. Thomson, G. and Pridham, M., *Material Property Changes Associated with Laser Forming of Mild Steel Components.* Journal of Materials Processing Technology, 2001. **118**(1-3): p. 40-44.

46. Edwardson, S.P., *A Study into the 2D and 3D Laser Forming of Metallic Components*, in *Department of Engineering.* 2004, University of Liverpool: Liverpool. p. 422.

47. Abed, E., *Modelling and Experimental Investigation of 3D Laser Forming of Metallic Components*, in *Engineering.* 2007, University of Liverpool: Liverpool. p. 338.

48. Magee, J., Watkins, K.G., Steen, W.M., Calder, N., Sidhu, J., and Kirby, J. *Laser Forming of Aerospace Alloys.* in *ICALEO '97.* 1997. Meisenbach Bamberg, Germany.

49. Bao, J. and Yao, L.Y., *Analysis and Prediction of Edge Effects in Laser Bending.* Journal of Manufacturing Science and Engineering, 2000. **123**(1): p. 53-61.

50. Gopal, C.J., Nathb, A.K., and Roya, S.K., *Study of edge effect and multi-curvature in laser bending of AISI 304 stainless steel.* Journal of Materials Processing Technology, 2008. **197**: p. 434-438.

51. Edwardson, S.P., French, P., Dearden, G., Watkins, K.G., and Cantwell, W.J., *Laser Forming of Fibre Metal Laminates.* Lasers in Engineering, 2005. **15**.

52. Chan, K.C., Yau, C.L., and Lee, W.B., *Laser Bending of Thin Stainless Steel Sheets.* Journal of Laser Applications, 1999. **12**(1): p. 34-40.

53. Miyazaki, T., Saito, M., Tokunaga, T., Misu, T., and Yoshioka, S. *Forming Characteristics of Thin Metal Plate with Diode Laser Beam.* in *ICALEO 2002.* 2002. Scottsdale, Arizona.

54. Yoshioka, S., Miyazki, T., MIsu, T., Oba, T., and Saito, M., *Laser Forming of Thin Foil by Newly Developed Sample Holding Method.* Journal of Laser Applications, 2003. **15**(2).

55. G Dearden, C.T., K Bartkowiak, S P Edwardson, K G Watkins. *An Experimental study of laser micro-forming using a pulsed Nd:YAG laser and scanning optics.* in *ICALEO 2003.* 2003.

56. Bartkowiak, K., Edwardson, S.P., Borowski, J., Dearden, G., and Watkins, K.G. *Laser Forming of Thin Metal Components for 2D and 3D Applications Using a HIgh Beam Quality Low Power Nd:YAG Laser and Rapid Scanning Optics.* in *IWOTE '05.* 2005.

57. Bartkowiak, K., Borowski, J., Edwardson, S.P., Dearden, G., Carey, C., and Watkins, K.G. *Laser Forming of Thin Section Non Ferrous Metals with Nd:YAG Laser Source.* in *ICALEO 2005.* 2005.

58. Xu, X. and Chen, G., *Experimental and 3D Finite Element Studies of CW Laser Forming of Thin Stainless Steel Sheets.* Transaction of ASME, 2008. **123**: p. 66-73.

59. Gartner, E., Fruhauf, J., and Jaensch, E., *Plastic reshaping of silicon microstructure: process, characterisation and application.* Microsystem Technologies, 2001. **7**: p. 155-160.

60. Gärtner, E., Frühauf, J., Löschner, U., and Exner, H., *Laser bending of etched silicon microstructures.* Microsystem Technologies, 2001. **7**(1): p. 23-26.

61. Okamoto, Y., Miyamoto, I., Uno, Y., and Takenaka, T. *Deformation Characteristics of Plastics in YAG Laser Forming.* in *Fifth International Symposium on Laser Precision Microfabrication.* 2004.

62. Okamoto, Y., Uno, Y., Mohid, Z., and Namba, Y. *Influence of irradiation method on laser forming characteristics.* in *IWOTE '08.* 2008. Bremen.

63. Okamoto, Y., Uno, Y., Shibata, T., and Ohta, K.I. *Precision Laser Forming of Plastic with YAG laser.* in *5th International Conference on Progress of Machine Technology.* 2000.

64. Hoving, W. *Accurate Manipulation Using Laser Technology.* in *SPIE.* 1997.

65. Hoving, W. *Accurate Manipulation Using Laser Technology.* in *Laser Assisted Net-shape Engineering 2001.* 2001. Erlangen Germany.

66. Tam, A.C., Poon, C.C., and Crawford, L., *Laser Bending of Ceramics and Application to Manufacture Magnetic Head Sliders in Disk Drives.* Analytical Sciences, The Japan Society for Analytical Chemistry, 2001. **17**: p. 419-421.

67. Zhang, Z.R. and Xu, X., *Laser Bending for Adjusting Curvatures of Hard Disk Suspensions.* Journal of Microsystem Technologies, 2005. **11**(11): p. 1197-1203.

68. Muller, B. *Laser Adjustment - Models for the Design of Actuators.* in *LANE 2001.* 2001. Erlangen.

69. Widlaszewski, J. *Precise Laser Bending.* in *LANE '97.* 1997.

70. Wildaszewski, J. *Micro Adjustment by Thermal Upsetting.* in *International Workshop on Thermal Forming.* 2005.

71. Maher, W., Tong, K., Bampton, C., Bright, M., Wooten, J., and Rhodes, C. *Laser Forming of Titanium and Other Metals is Useable Within Metallurgical Constraints.* in *17th International Congress on Application of Lasers and Electro-Optics (ICALEO '98).* 1998. Orlando, FL.

72. Shackel, J., Sidhu, J., and Prangnell, P.B. *The Metallurgical Implications of Laser Forming Ti-6AL-4V Sheet.* in *ICALEO'2001.* 2001.

73. Marya, M. and Edwards, G.R., *A Study on the Laser Forming of Near-Alpha and Meta-stable Beta Titanium Alloy Sheets.* Journal of Materials Processing Technology, 2001. **108**: p. 376-383.

74. Chan, K.C., Liang J., *Thermal Expansion and Deformation Behaviour of Aluminium-Matrix Composites in Laser Forming.* Composites Science & Technology, 2001. **61**: p. 1265-1270.

75. Chan, K.C., Harada, Y., Liang, J., and Yoshida, F., *Deformation Behaviour of Chromium Sheets in Mechanical and Laser Bending.* Journal of Materials Processing Technology, 2002. **122**(272-277).

76. Zhang, J., Pirzada, D., Chu, C.C., and Cheng, G.J., *Fatigue Life Prediction After Laser Forming.* Journal of Manufacturing Science and Engineering, 2005. **127**: p. 157-164.

77. Cheng, J.G., Zhang, J., Chu, C.C., Zhe, Z., *Experimental study and computer simulation of fracture toughness of sheet metal after laser forming.* The International Journal of Advanced Manufacturing Technology, 2005. **26**: p. 1222-1230.

78. Abed, E., Edwardson, S.P., Edwards, K.R., Carey, C., Dearden, G., and Watkins, K.G. *Effect of Post Forming Heat Treatments on Laser Formed Components.* in *IWOTE '08.* 2008. Bremen Germany.

79. Liu, Z. *Phenomena and mechanisms of corrosion in laser formed metallic alloy sheets.* in *LANE 1007.* 2007. Erlangen.

80. Merklein, M. and Geiger, M. *A Comparative Study of Two Different Laser Forming Mechanisms Regarding the Mechanical Properties of Aluminium Alloys.* in *LANE '01.* 2001. Erlangen, Germany.

81. Merklein, M., Hennige, T., and Geiger, M., *Laser Forming of Aluminium and Aluminium Alloys - Microstructural Investigation.* Journal of Materials Processing Technology, 2001. **115**: p. 159-165.

82. Vermeeren, C.A.J.R., *An Historic Overview of the Development of Fibre Metal Laminates.* Applied Composite Materials, 2003. **10**: p. 189-205.

83. Vlot, A., *Glare: History of the Development of a New Aircraft Material.* 2001: Kluwer Academic Publishers.

84. Krishnakumar, S., *Fibre Metal Laminates: The synthesis of metals and composite.* Materials and Manufacturing Processes, 1994. **9**: p. 295-354.

85. Langelaan, J.W., Leo , J.J., and Kok, T., *Damage Tolerance Modelling of Fibre Metal Laminate Fuselage Structures.* American Institue of Aeronautics and Astronautics, 1997: p. 2809-2818.

86. Afaghi-Khatibi, A., Ye, L., and Mai, Y., *Hybrids and Sandwiches*, in *Comprehensive Composite Materials.* 2003. p. 249-290.

87. Vermeeren, C.A.J.R., *The application of carbon fibres in ARALL laminates.* 1991, Dept. of Aerospace Engineering, Delft University of Technology,.

88. Remmers, J.C.C. and De Borst, R., *Delamination buckling of fibre metal laminates.* Composites Science & Technology, 2001. **61**: p. 2207-2213.

89. Compston, P., Cantwell, W.J., and Jones, N., *Influence of loading rate on the interfacial fracture toughness of a polyimide-based fibre-metal laminate.* Journal of Materials Science Letters, 2002. **21**: p. 383-386.

90. Burns, M.J. and Compston, P., *Interfacial fracture toughness of polyester-based Fibre metal laminates with primary contact and secondary adhesive bonding.* Journal of Materials Science, 2004. **39**: p. 2855-2859.

91. Chinsirikul, W., Chung, T.C., and Harrison, I.R., *Adhesion Improvements in Polypropylene Aluminium Laminates.* Proceedings of the American Society for Composites, 1992: p. 42-56.

92. Kinloch, A.J., *Adhesion and Adhesives*. 1st ed. 1987, London: Chapman and Hall. 441.

93. Reyes, G. and Cantwell, W.J., *The effect of strain rate on the interfacial fracture properties of carbon fibre-metal laminates.* Journal of Material Science Letters, 1998. **17**: p. 1953-1955.

94. Hatch, J.E., *Aluminium: Properties and Physical Metallurgy*. 1984, Metals Park, Ohio: American Society for Metals.

95. ASM, *ASM Handbook Online*. 2007.

96. Daniel, I.M. and Ishai, O., *Engineering Mechanics of Composite Materials*. 1994: Oxford University.

97. Jang, B.Z., *Advanced Polymer Composites: Principles and Application*. 1994: CRC. 297.

98. Lovel, D.R., *Types of Materials in Composite Materials in Aircraft Structures*, ed. D.H. Middleton. 1990: Longman Scientific Technical.

99. Hull, D. and Clyne, T.W., *An Introduction to Composite Materials*. 2 ed. 1996, Cambridge. 325.

100. Callister, W.D., *Materials Science and Engineering: An Introduction*. 2003: Wiley & Sons.

101. Barbero, E.J., *Introduction to Composite Materials Design*. 1999: Taylor and Francis.

102. Kelly, A. and Zweben, C., *Comprehensive Composite Materials*. 2000, Amsterdam: Elsevier.

103. Karian, H.G., *Handbook of Polypropylene and Polypropylene Composites*. 2 ed. 1999, New York: Marcel Dekker Inc.

104. Propex, I. *Curv Advantage*. [Website] 2007 [cited; Available from: http://www.curvonline.com/products/index.html.

105. Vlot, A., Vogelesang, L.B., and de Veries, T.J., *Towards Application of Fibre Metal Laminates in Large Aircraft.* Aircraft Engineering Aerospace Technology, 1999. **71**(6): p. 558-570.

106. Asundi, A. and Choi, A.Y.N., *Fibre Metal Laminates: An Advanced Material for Future Aircraft.* Journal of Materials Processing Technology, 1997. **63**: p. 384-394.

107. Roebroeks, G.H.J.J. *Fibre Metal Laminates, Recent developments and Application.* in *Symp. on Fatigue of Aircraft Material.* 1992. Delft.

108. Sinke, J., *Manufacturing of GLARE Parts and Structures.* Applied Composite Materials, 2003. **10**: p. 293-305.

109. Sinke, J. and De Jong, T.W. *Formability Aspects of Fibre Metal Laminates.* in *33rd International SAMPE technical Conference.* 2001. Seattle.

110. Wu, H.F., Wu, L.L., Slagter, W.J., and Verolme, J.L., *Use of rule of mixtures and metal volume fraction for mechanical property predictions of fibre-reinforced aluminium laminates.* Journal of Material Science, 1994. **29**: p. 4583-4591.

111. Reyes, G. and Cantwell, W.J., *The mechanical properties of fibre-metal laminates based on glass fibre reinforced polypropylene.* Composites Science and Technology, 2000. **60**(7): p. 1085-1094.

112. Hagenbeek, M., van Hengal, C., Bosker, O.J., and Vermeenhan, C.A.J.R., *Static Properties of Fibre Metal Laminates* Applied Composite Materials, 2004. **10**(4-5): p. 207-222.

113. Kawai, M., Morishitia, M., Tomura, S., and Takumida, K., *Inelastic behaviour and strength of fibre-metal hybrid composite: Glare* International Journal of Mechanical Sciences, 1998. **40**(2-3): p. 183-198.

114. Bucci, R.J., Mueller, L.N., Vogelesang, L.B., and Gunnink, J.W., *ARALL Laminates.* Treatise Material Science Technology, 1989. **31**: p. 295-302.

115. Akbar, A., Lin, Y., and Yiu, W.M., *Hybrids and Sandwiches*, in *Comprehensive Composite Materials.* 2003. p. 249-290.

116. Gunnink, J.W., Verbruggen, M.L.C.E., and Vogelesang, L.B., *ARALL, a light weight structural material for impact and fatigue sensitive structures.* Vertica, 1986. **10**: p. 241-254.

117. van Rooijen, R., Sinke, J., De Veries, T.J., and van der Zwaag, S., *Property Optimisation in Fibre Metal Laminates.* Applied Composite Materials, 2004. **11**(2): p. 63-76.

118. Bosker, O.J., *Blunt Notch Strength*, in *Fibre Metal Laminates: An Introduction*, A. Vlot, Editor. 2001, Kluwer. p. 115-131.

119. De Vries, T.J. and Vlot, A., *The Influence of the Constituent Properties on the Residual Strength of Glare* Applied Composite Materials, 2004. **8**(4): p. 263-277.

120. Vermeeren, C.A.J.R. *The residual strength of fibre metal laminates: GLARE2 and GLARE3.* in *30th International SAMPE Technical Conference*. 1998. San Antonio, Texas.

121. Afaghi-Khatibi, A., Lawcock, G., Ye, L., and Mai, Y., *On the fracture mechanical behaviour of fibre reinforced metal laminates (FRMLs).* Computer Methods in Applied Mechanics and Engineering, 2000. **185**(2-4): p. 173-190.

122. De Vries, T.J. and Vlot, A. *The influence of metal properties on residual strength of GLARE.* in *30th International SAMPE Technical Conference.* 1998. San Antonio, Texas.

123. Marcheret, J. and Bucci, R.J., *A crack growth resistance curve approach to fibre/metal laminate fracture toughness evaluation.* Engineering Fracture Mechanics, 1993. **45**(6): p. 729-739.

124. Ye, L., Afaghi-Khatibi, A., Lawcock, G., and Mai, Y., *Effect of fibre/matrix adhesion on residual strength of notched composite laminates.* Composites Part A, 1998. **29A**: p. 1525-1533.

125. Afaghi-Khatibi, A., Ye, L., and Mai, Y., *An experimental study of the influence of fibre-matrix interface on fatigue tensile strength of notched composite laminates.* Composites Part B: Engineering, 2001. **32**: p. 371-377.

126. Lawcock, G., Ye, L., Mai, Y., and Sun, C.T., *Effects of fibre/matrix adhesion on carbon-fibre reinforced metal laminates-I Residual strength.* Composites Science & Technology, 1997. **57**: p. 1609-1619.

127. Afaghi-Khatibi, A., Ye, L., and Mai, Y., *Evaluations of effective crack growth and residual strength of fibre-reinforced metal laminates with sharp notch.* Composites Science & Technology, 1996. **56**: p. 1079-1088.

128. Jin, Z.H. and Batra, R.C., *Residual strength of centrally cracked metal/fibre laminates.* Materials Science and Engineering, 1996. **A216**: p. 117-124.

129. Schijve, J., Van Lipzig, H.T.M., Van Gestel, G.F.J.A., and Noeymakers, A.H.W., *Fatigue properties of adhesive-bonded laminate sheet material of aluminium alloys.* Engineering Fracture Mechanics, 1979. **12**: p. 561-579.

130. Sinke, J., *Development of Fibre Metal Laminates: Concurrent Multi-scale Modelling and Testing.* Journal of Material Science, 2006. **41**: p. 6777-6788.

131. Vlot, A. and Alderliesten, R.C., *Fatigue of Fibre Metal Laminates*, in *Encyclopaedia of Materials*. 2001, Elsevier Science.

132. Lawcock, G., Ye, L., and Mai, Y., *Fatigue crack propagation in fibre-reinforced metal laminates with treated or untreated carbon fibres.* Journal of Materials Science Letters, 1999. **18**: p. 307-308.

133. Vogelesang, L.B. and Vlot, A., *Development of fibre metal laminates for advanced aerospace structures.* Journal of Materials Processing Technology, 2000. **103**: p. 1-5.

134. Vlot, A., *Impact Loading of Fibre Metal Laminates.* Journal of Impact Engineering, 1996. **18**: p. 291-307.

135. Backman, M.V. and Goldsmith, W., *The Mechanics of Penetration of projectiles into Targets.* International Journal of Engineering Science, 1978. **16**: p. 1-99.

136. Cantwell, W.J., Curtis, P.T., and Morton, J., *Impact and subsequent fatigue damage growth in carbon fibre laminates.* International Journal of Fatigue, 1984. **6**: p. 113-118.

137. Cantwell, W.J. and Morton, J., *Detection of Impact Damage in CFRP Laminates.* Composite Structures, 1985. **3**: p. 241-257.

138. Sun, C.T. and Dicken, A., *Characterisation of impact damage in ARALL laminates.* Composite Science and Technology, 1993. **49**: p. 139-144.

139. Vlot, A. and Krull, M., *Impact damage resistance of various fibre metal laminates.* Journal of Physics IV France, 1997. **7**: p. 1045-1050.

140. Vlot, A., Kroon, E., and La Rocca, G., *Impact Response of Fibre Metal Laminates.* Key Engineering Materials, 1998. **141-143**: p. 235-276.

141. Lawcock, G., Ye, L., Mai, Y., and Sun, C.T., *Effects of fibre/matrix adhesion on carbon-fibre reinforced metal laminates-II Impact Behaviour.* Composite Science and Technology, 1997. **57**: p. 1662-1628.

142. Compston, P., Cantwell, W.J., Jones, C., and Jones, N., *Impact perforation resistance and fracture mechanisms of a thermoplastic based fibre-metal laminate.* Journal of Material Science Letters, 2001. **20**: p. 597-599.

143. Reyes, G., Compston, P., Guillen, F., Cantwell, W.J., and Jones, N. *Impact resistance of thermo-plastic based fibre metal laminates.* in *13th ICCM.* 2001. Beijing China.

144. Cantwell, W.J., Wade, G., Jones, N., Reyes, G., Radcliffe, J., and Compston, P. *The impact response of fibre metal laminates.* in *9th ICCE.* 2002. San Diego.

145. Moonen, W.A.J., *Protective coating for aircraft structures - A review.* 1983, Delft University of Technology.

146. Shreier, L.L., Jarman, R.A., and Burstien, G.T., *Corrosion, Volume 2: Corrosion Control.* Vol. 2. 1994, Oxford: Butterworth-Heinemann.

147. Hale, J.M. and Gibson, A.G., *Coupon tests of fibre reinforced plastics at elevated temperatures in offshore processing environments.* Journal of Composite Materials, 1998. **32**(6).

148. Mallick, P.K., *Fibre-reinforced composites: Materials, manufacturing and design.* 1988, New York: Marcel Dekker Inc.

149. Alderliesten, R.C., Hagenbeek, M., Homan, J.J., Hooijmeijer, P.A., De Vries, T.J., and Vermeeren, A.C.J.R., *Fatigue and Damage tolerance of GLARE.* Applied Composite Materials, 2003. **10**: p. 223-242.

150. Gunnink, J.W., Vlot, A., De Vries, T.J., and Van Der Hoeven, W., *GLARE technological advancements 1997-2000.* Applied Composite Materials, 2002. **9**: p. 201-219.

151. Woerden, H.J.M., Sinke, J., and Hooijmeijer, P.A., *Maintenance of GLARE structures and GARE as riveted or bonded repair material.* Applied Composite Materials, 2003. **10**: p. 307-329.

152. Fahr, A., Chapman, E., Lalibete, J.F., Forsyth, D.S., and Poon, C., *Non-destructive Evaluation Methods for Damage Assessment in Fibre-Metal Laminates.* Polymer Composites, 2000. **21**(4).

153. Kuang, K.S.C. and Cantwell, W.J., *Real-time damage detection in thermoplastic-based composite materials with embedded multi-mode optical fibre sensors.* Polymer Composites, 2002. **23**: p. 603-618.

154. Kuang, K.S.C., Kenny, R., Whelan, M.P., Cantwell, W.J., and Chalker, P.R., *Embedded fibre Bragg grating sensors in advanced composite materials.* Composites Science & Technology, 2002. **61**: p. 1379-1387.

155. Kuang, K.S.C., Kenny, R., Whelan, M.P., Cantwell, W.J., and Chalker, P.R., *Residual strain measurement and impact response of optical fibre Bragg grating sensors in fibre metal laminates.* Smart Materials and structures, 2001. **10**: p. 338-346.

156. Matweb. *Propex Fabrics Curv™ C100A Polypropylene/Polypropylene Thermoformable Composite* 2004 [cited 2005; Available from: http://www.matweb.com/search/datasheet.aspx?matguid=a4aa0f79b24d404da9bbabf5b4ea372a&ckck=1.

157. SP Composites, *SE 84 Data Sheet.* SE84-9-1002.

158. Edwardson, S.P., Abed, E., Bartkowaik, K., Dearden, G., and Watkins, K.G., *Geometrical influences on multipass laser forming.* Journal of Physics D: Applied Physics, 2006. **39**: p. 382-389.

159. Vollertsen, F. *Mechanisms and Models for Laser Forming.* in *Laser Assisted Net shape Engineering Conference (LANE 94).* 1994.

160. Matweb. *Epoxy Resin Material Data.* 2008 [cited; Available from: www.Matweb.com.

161. Matweb. *E-glass Fibre Material Data.* 2008 [cited; Available from: www.matweb.com.

162. Dearden, G., Edwardson, S.P., Abed, E., Bartkowaik, K., and Watkins, K.G., *Correction of Distortion and Design shape in Aluminium Structures Using Laser Forming.* 25th International Congress on Applications of Lasers & Electro-Optics (ICALEO 2006), 2006: p. 813-817.

Appendix A – Thermocouple Data

Glass Fibre Based FMLs

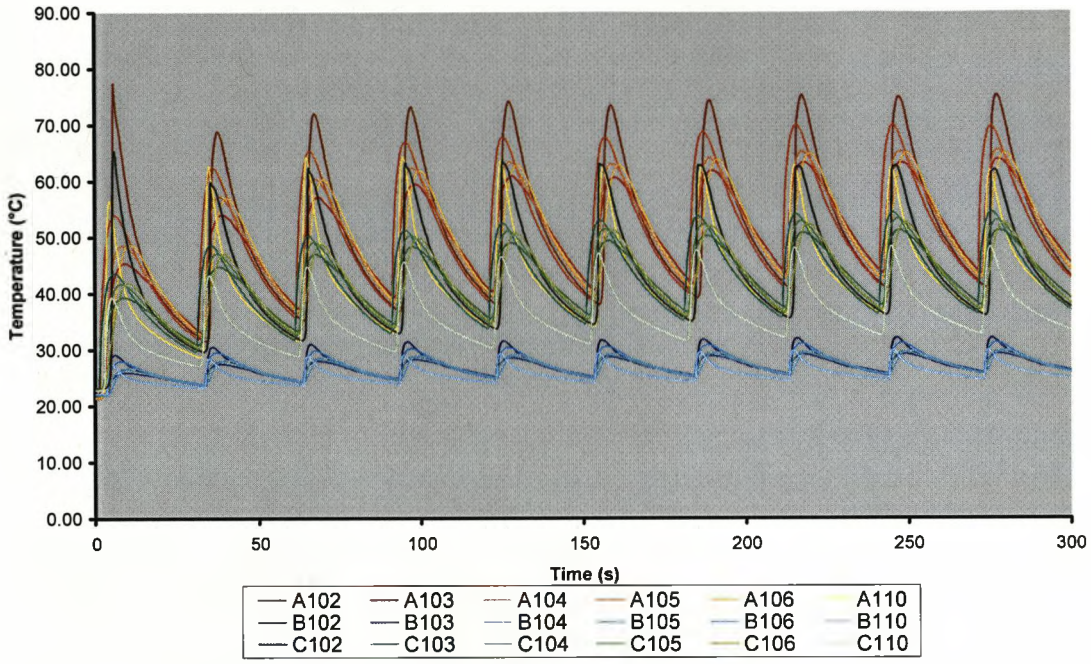

Thermocouple Output for 1:1 0° GF FML

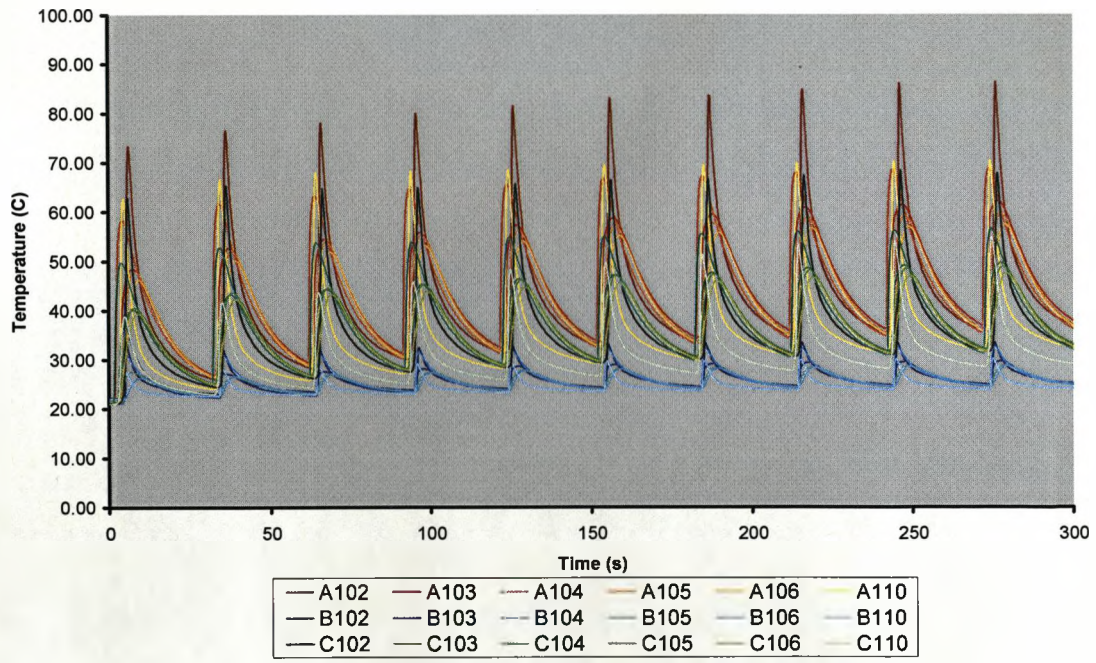

Thermocouple Output for 1:1 90° GF FML

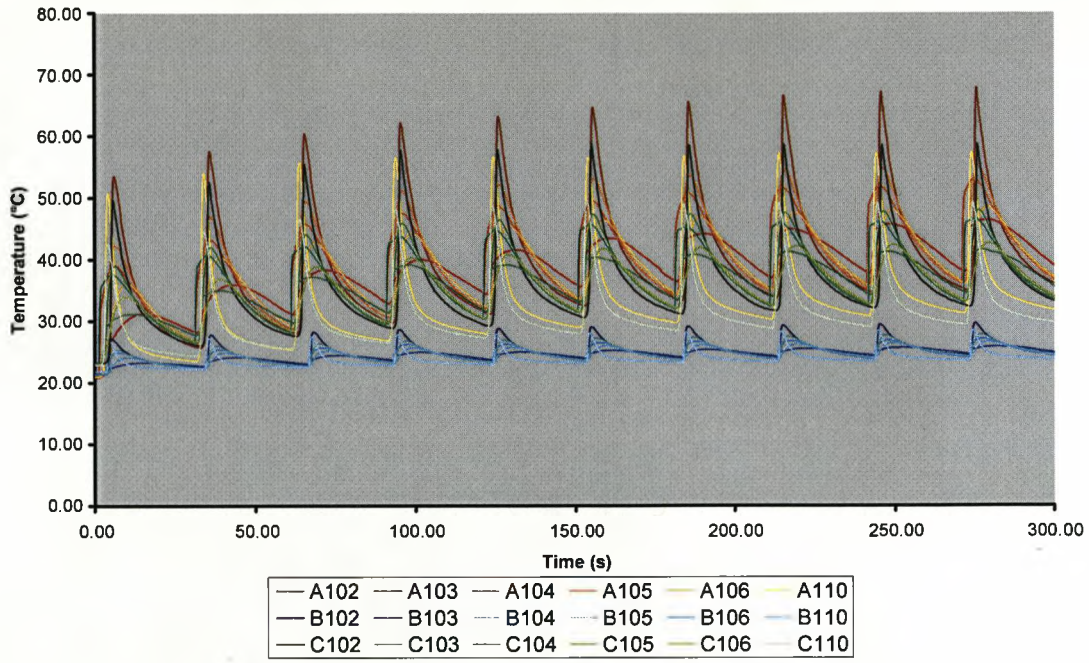

Thermocouple Output for 1:2 GF FML

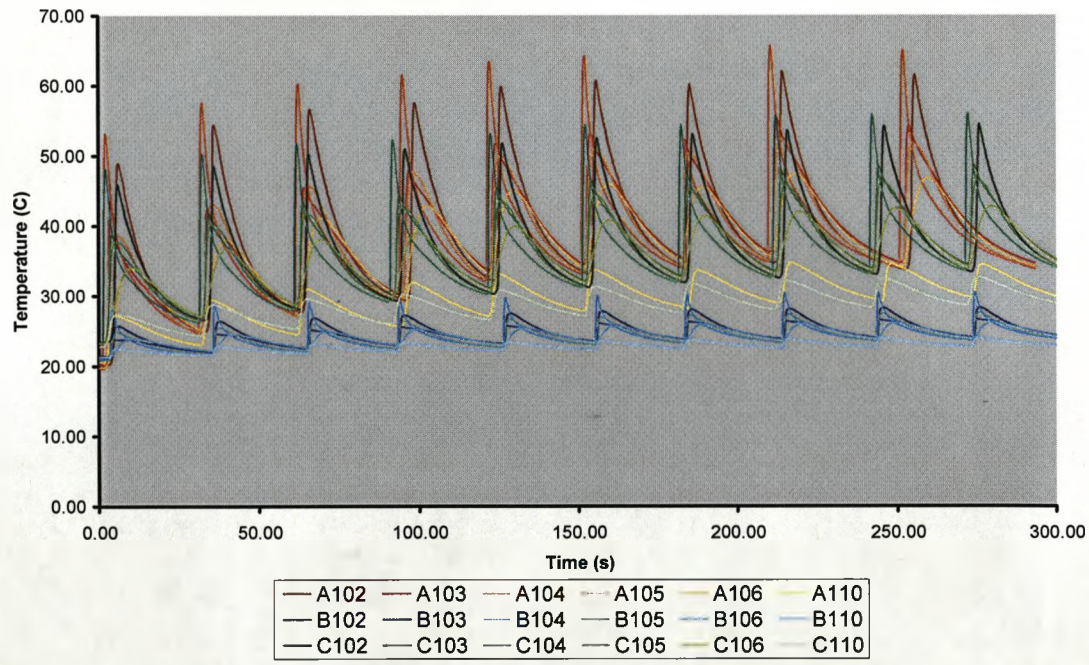

Thermocouple Output for 2:1 GF FML

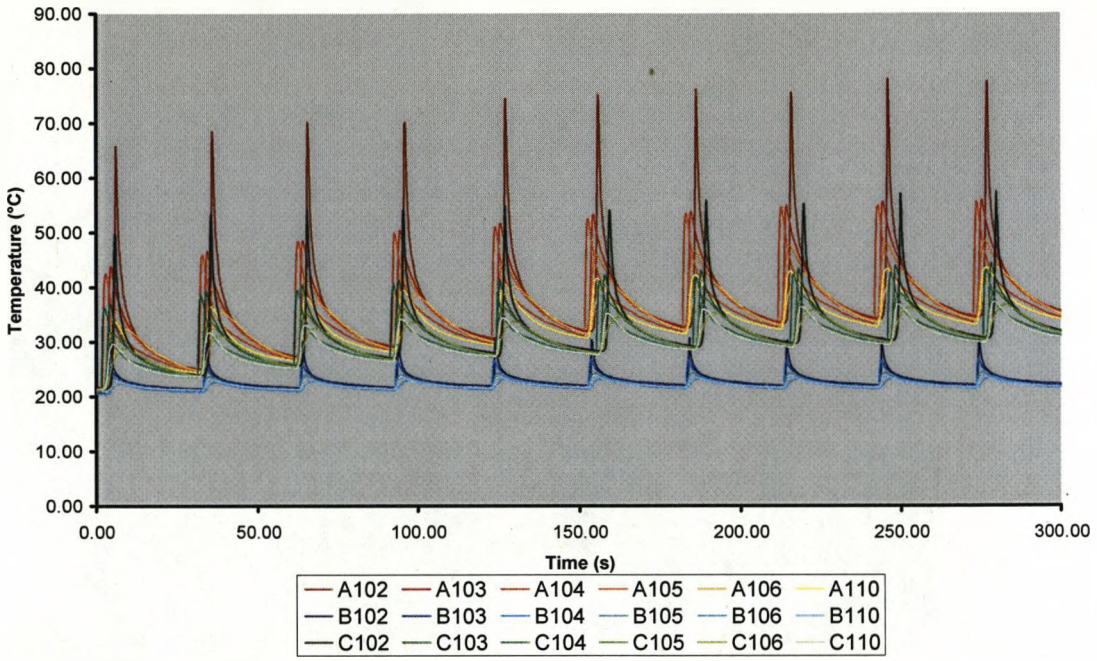

Thermocouple Output for 2:2 GF FML

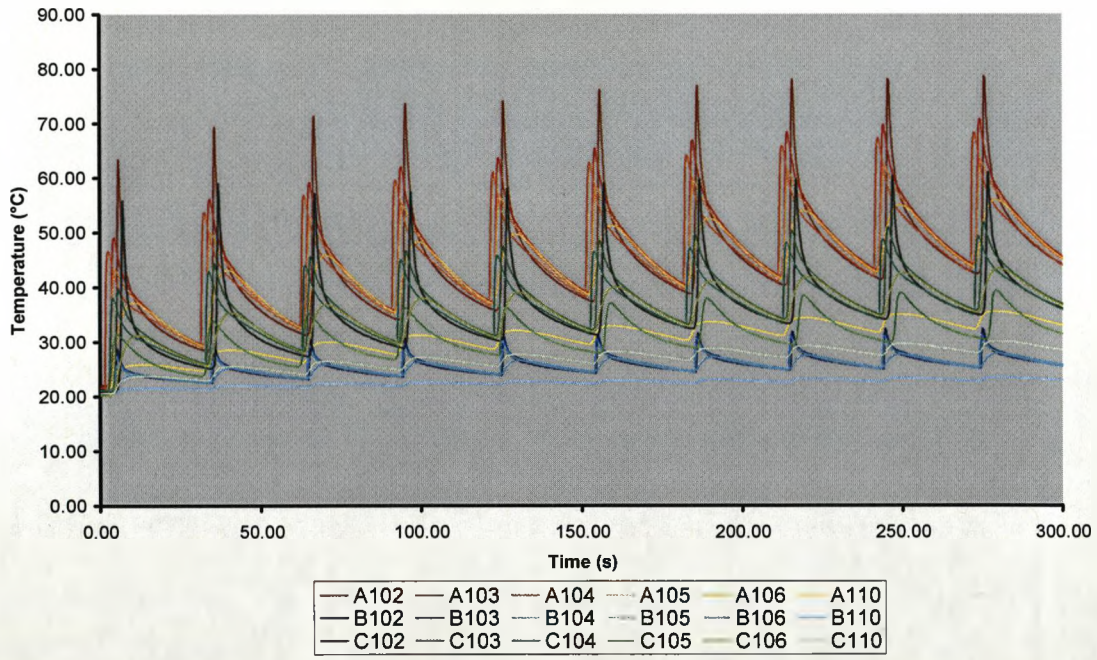

Thermocouple Output for 3:2 GF FML

Polypropylene Based FMLs

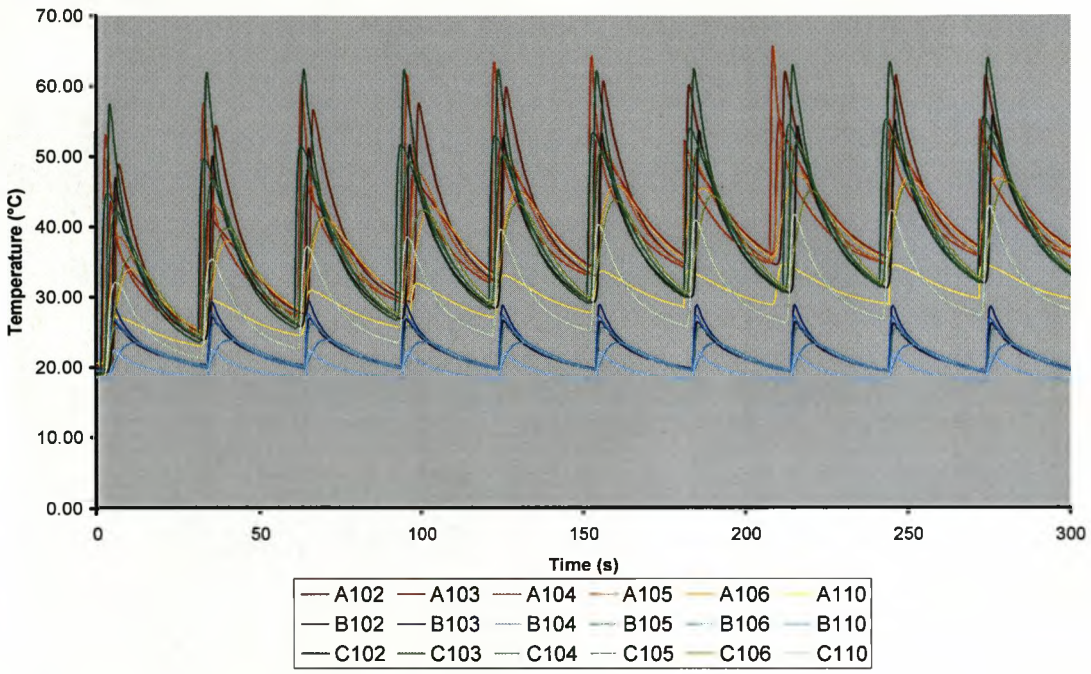

Thermocouple Output for 1:1 PP FML

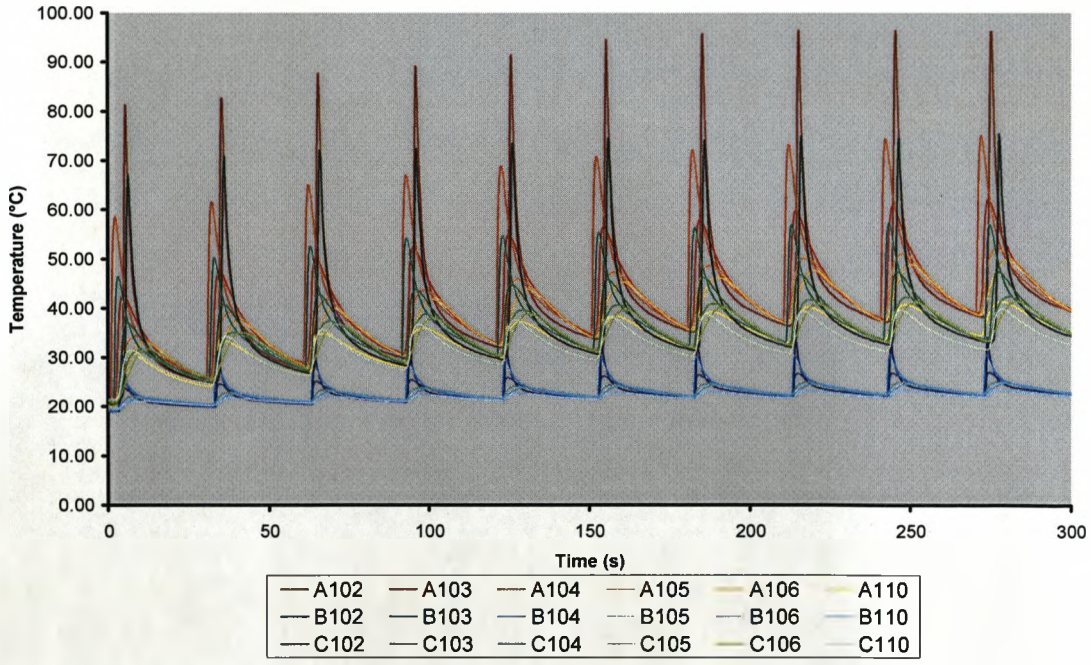

Thermocouple Output for 2:1 PP FML

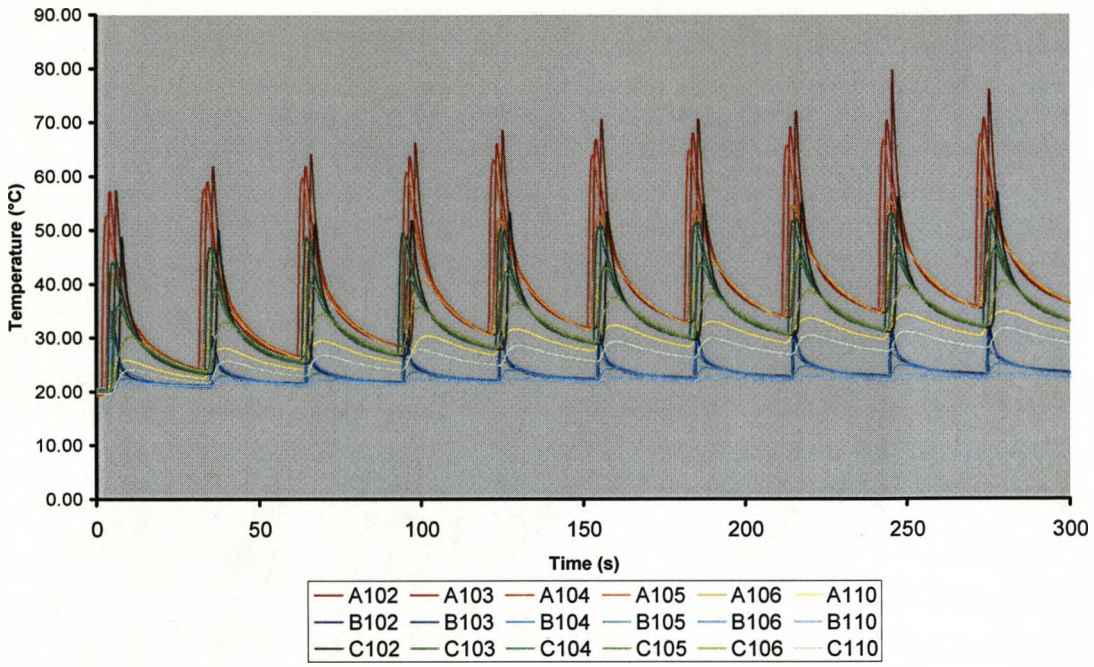

Thermocouple Output for 2:2 PP FML

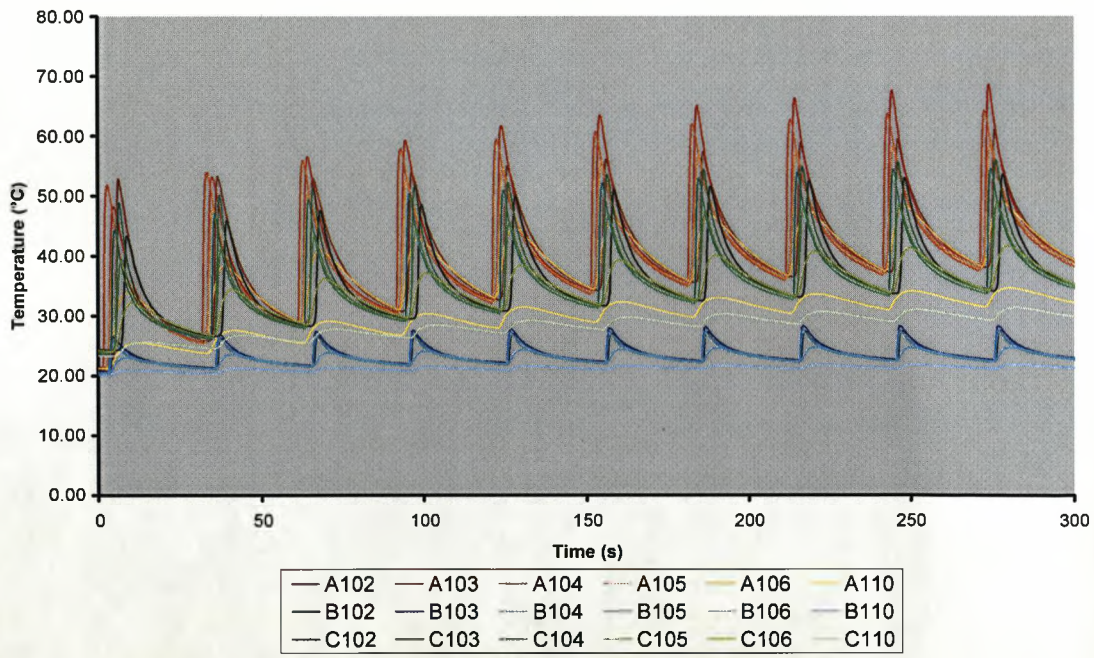

Thermocouple Output for 1:2:1 PP FML

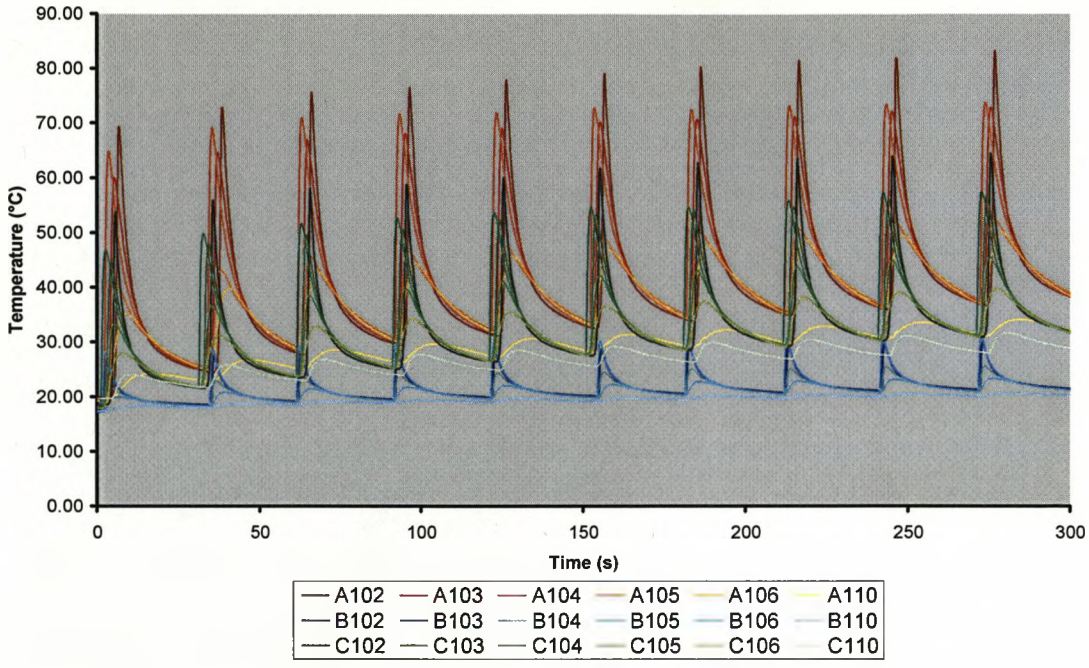

Thermocouple Output for 3:2 PP FML

Appendix B – Strain Gauge Data

Transverse Strain

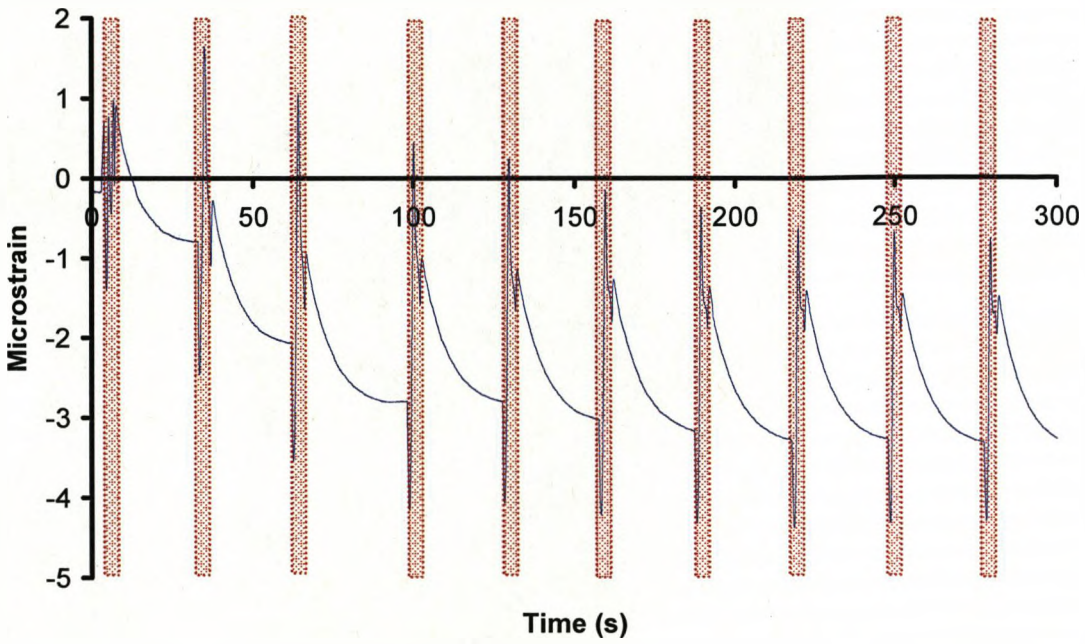

Transverse strain gauge output for aluminium

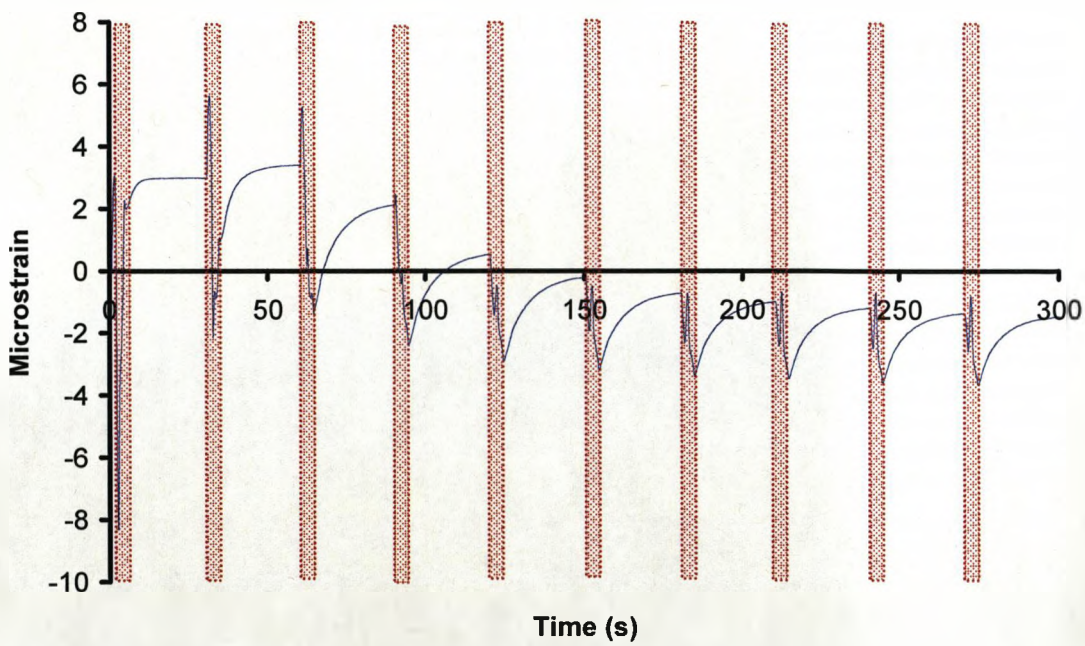

Transverse strain gauge output for 1-1 GF FML

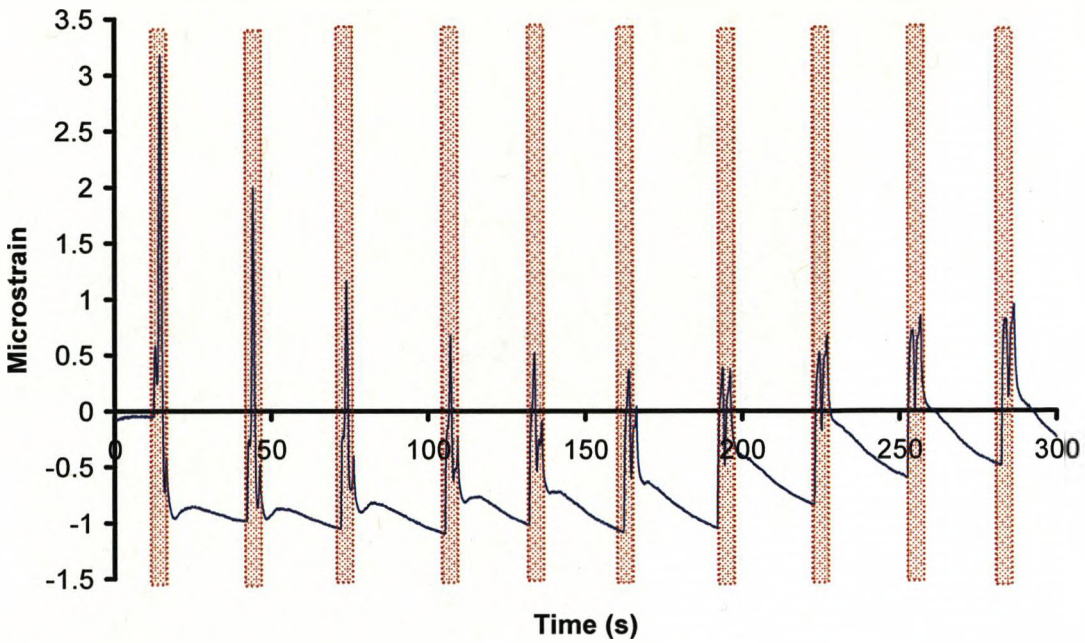

Transverse strain gauge output for 1-2 GF FML

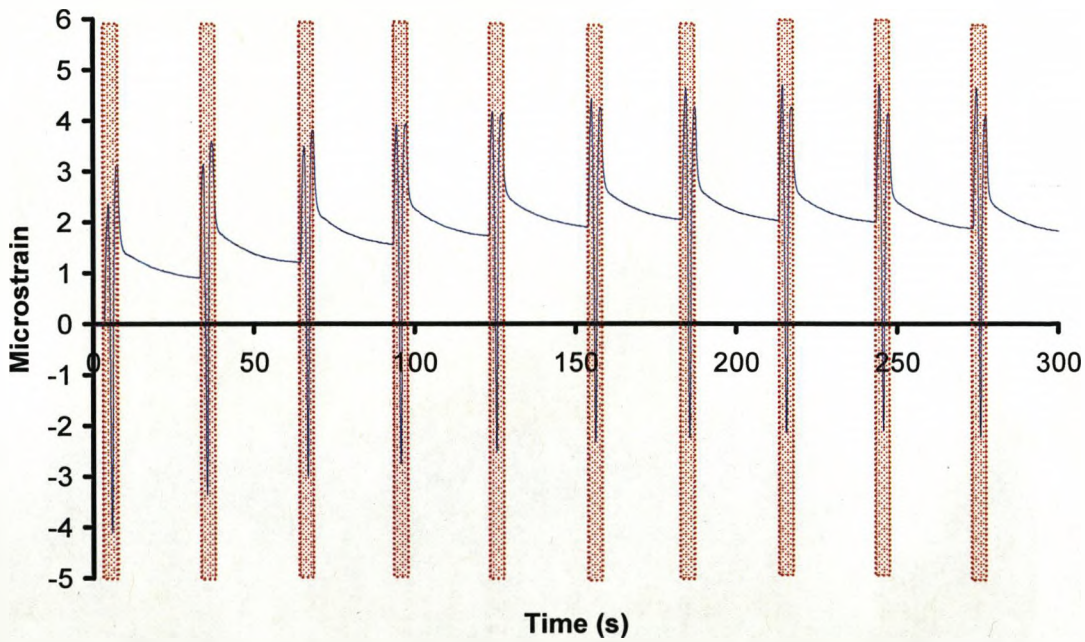

Transverse strain gauge output for 2-1 GF FML

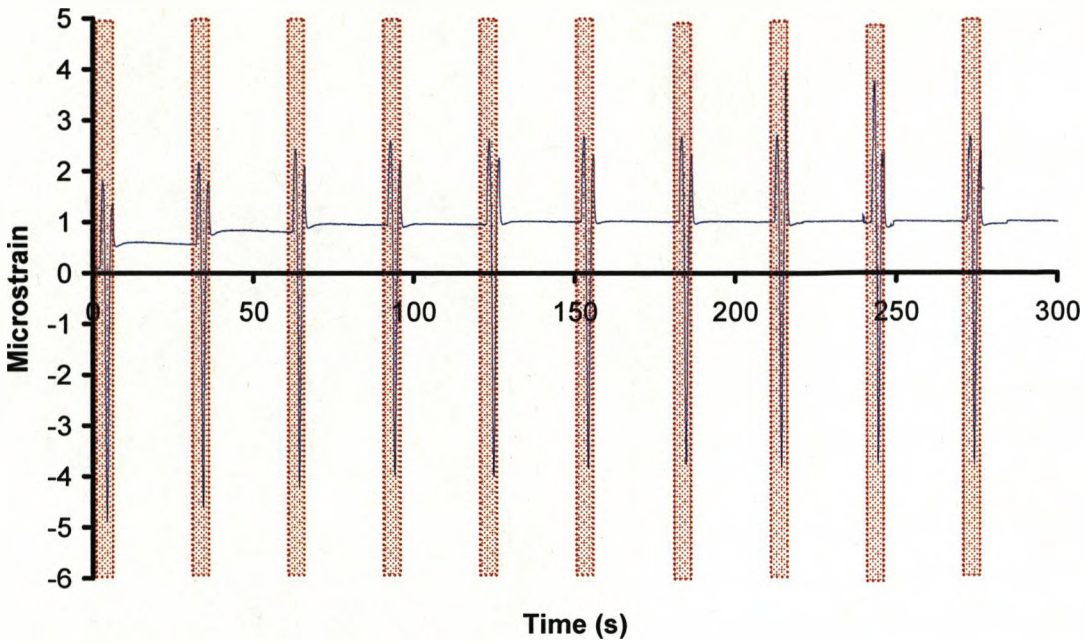

Transverse strain gauge output for 2-2 GF FML

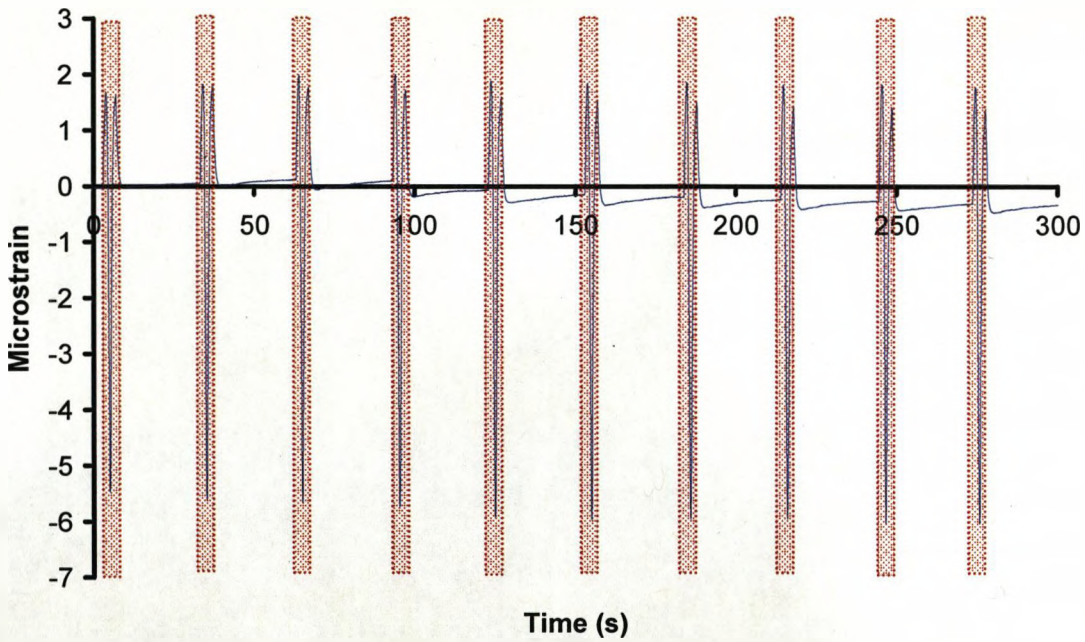

Transverse strain gauge output for 3-2 GF FML

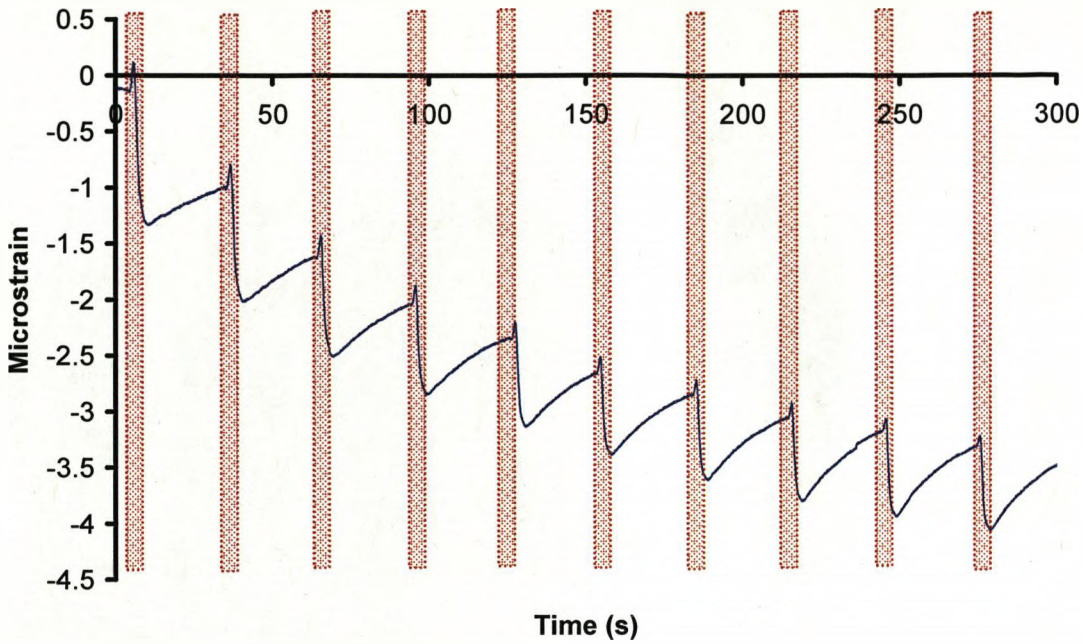

Transverse strain gauge output for 1-1 PP FML

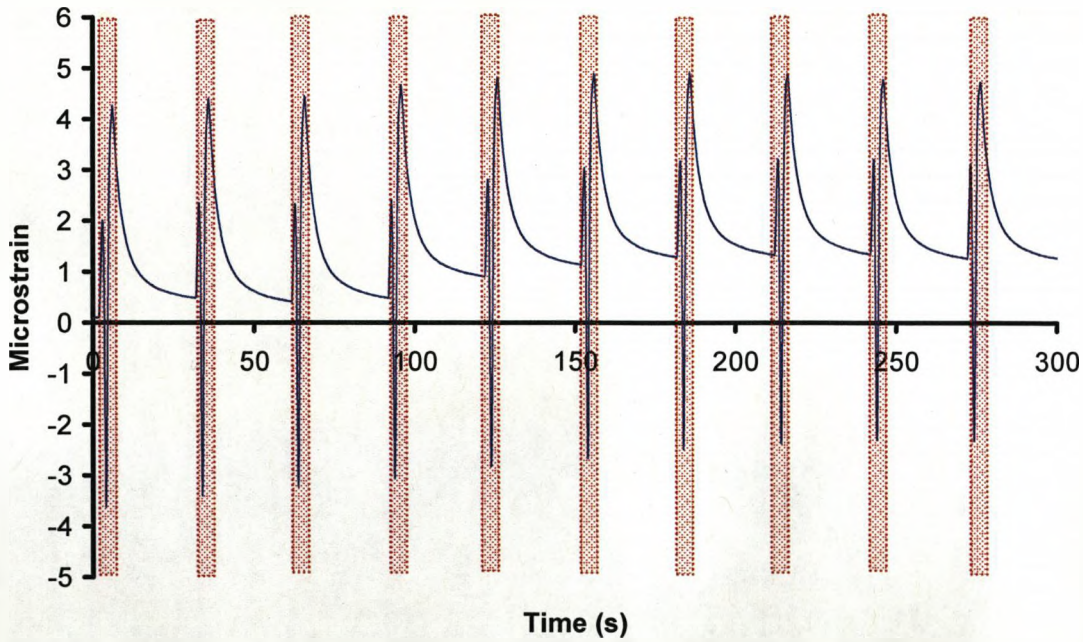

Transverse strain gauge output for 2-1 GF FML

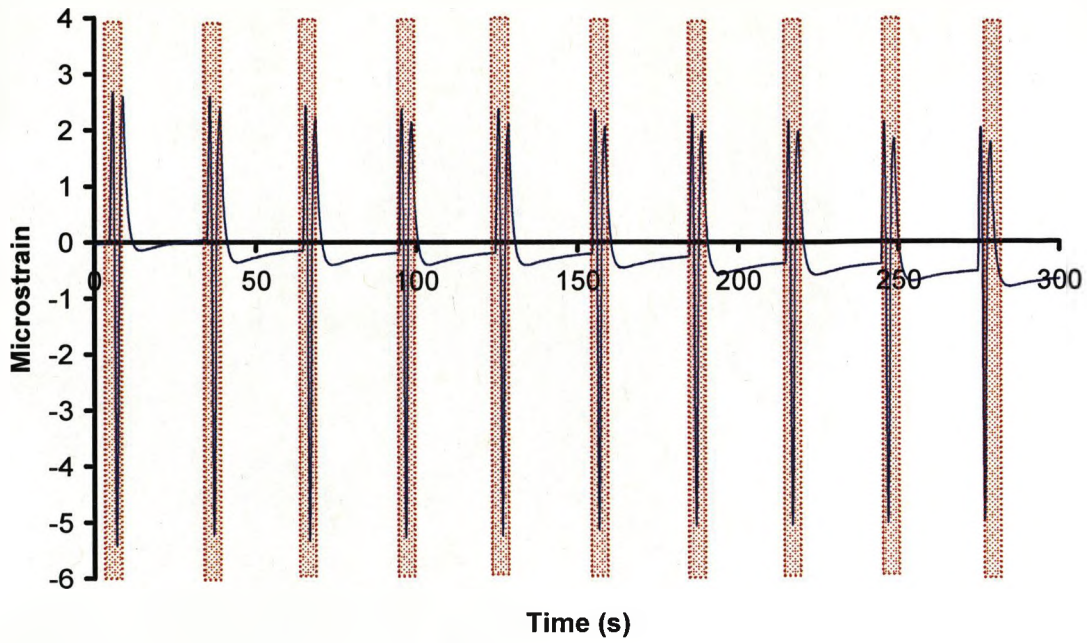

Transverse strain gauge output for 2-2 GF FML

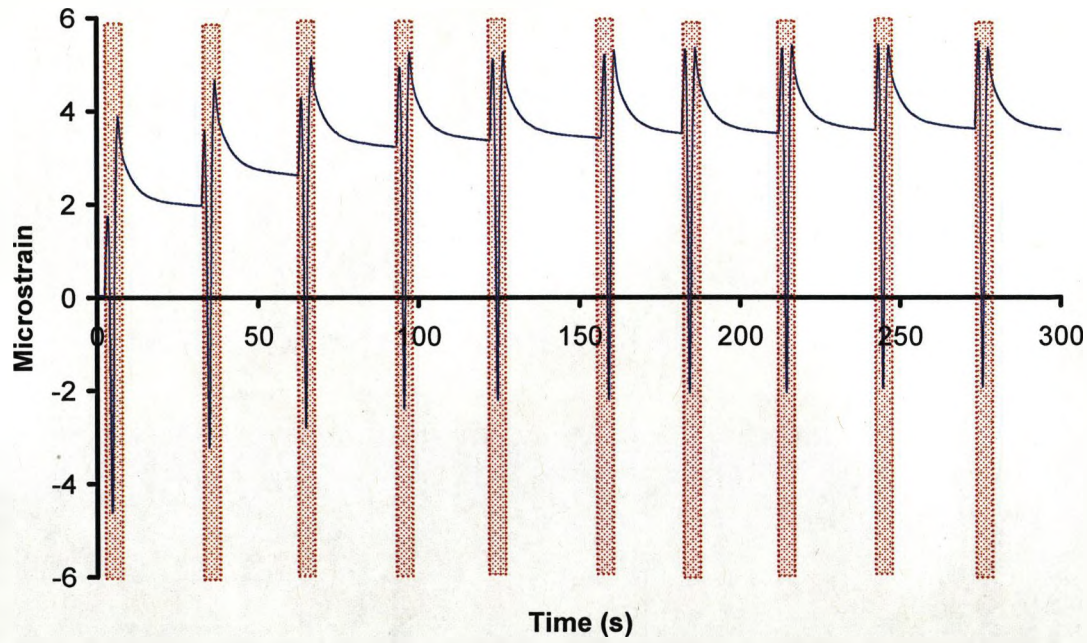

Transverse strain gauge output for 3-2 GF FML

Longitudinal Strain

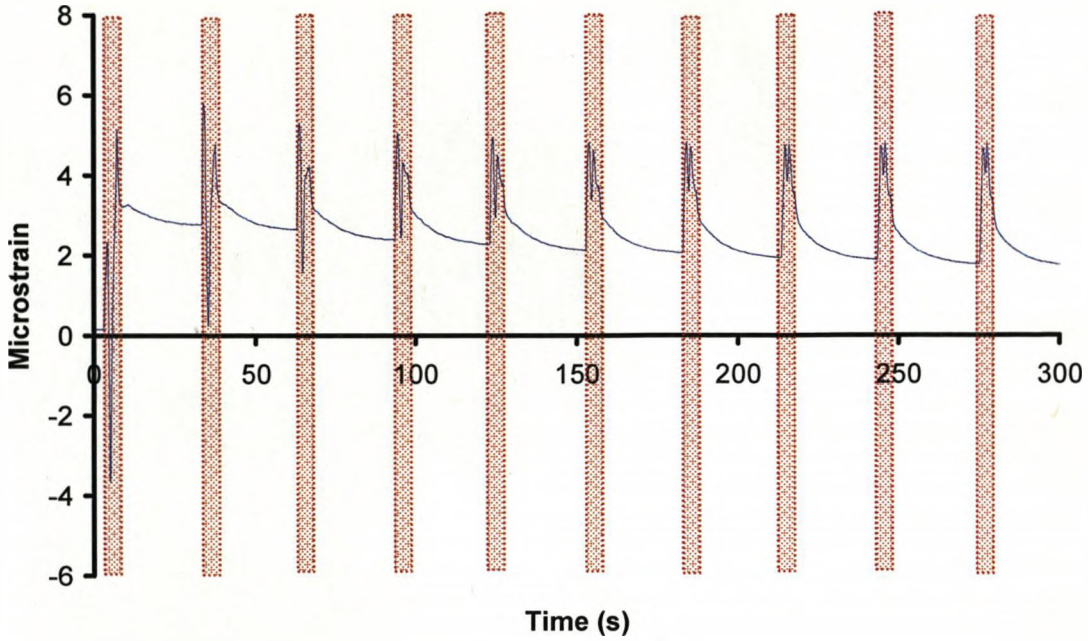

Longitudinal strain gauge output for aluminium

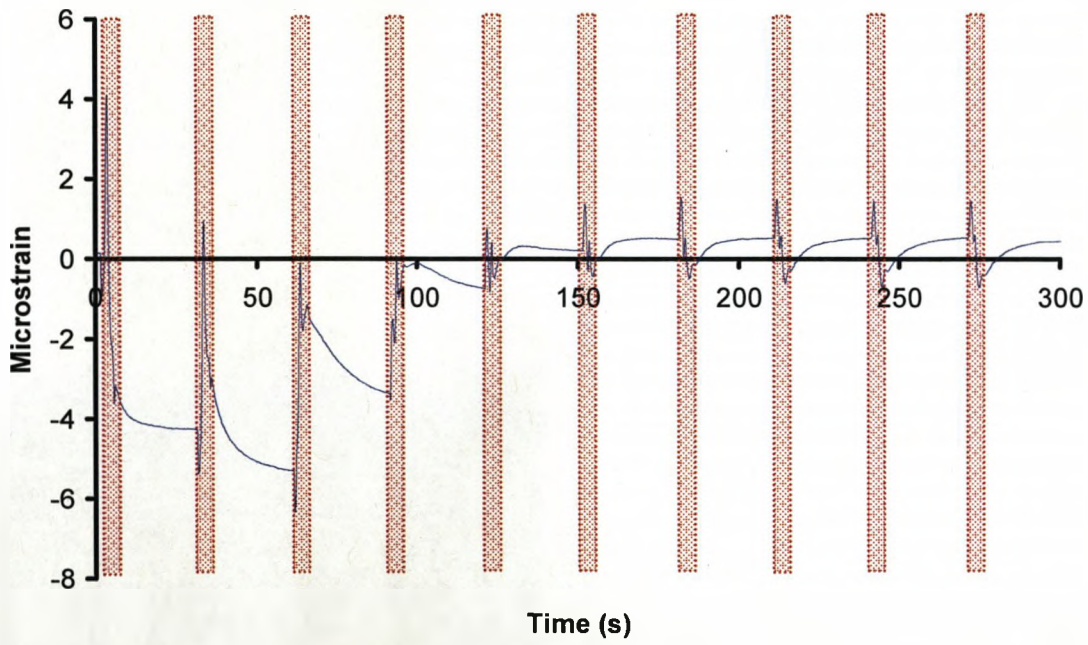

Longitudinal strain gauge output for 1-1 GF FML

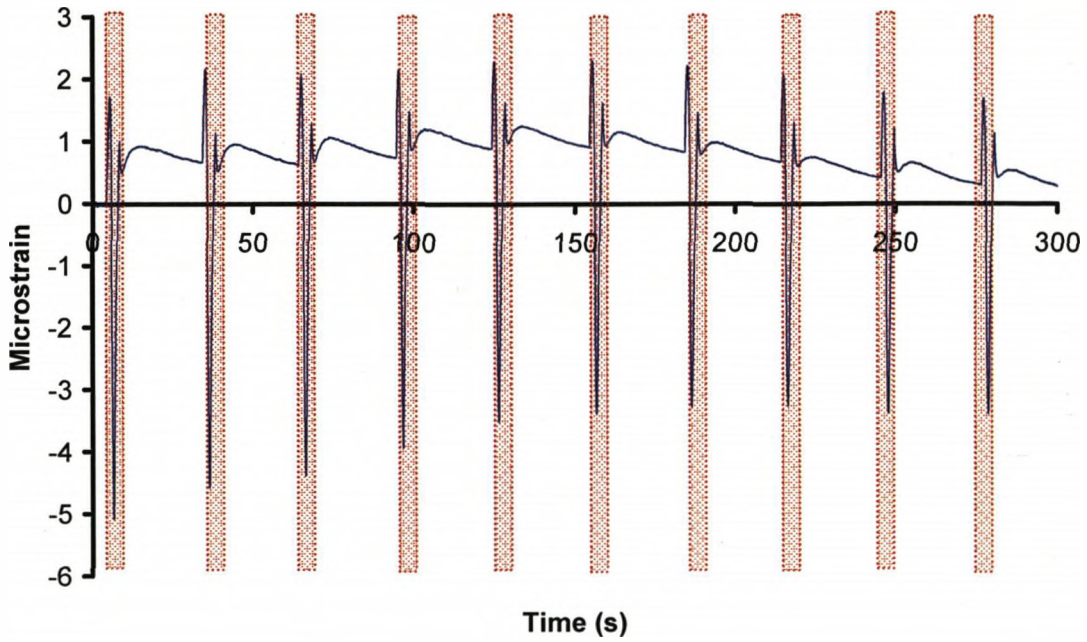

Longitudinal strain gauge output for 1-2 GF FML

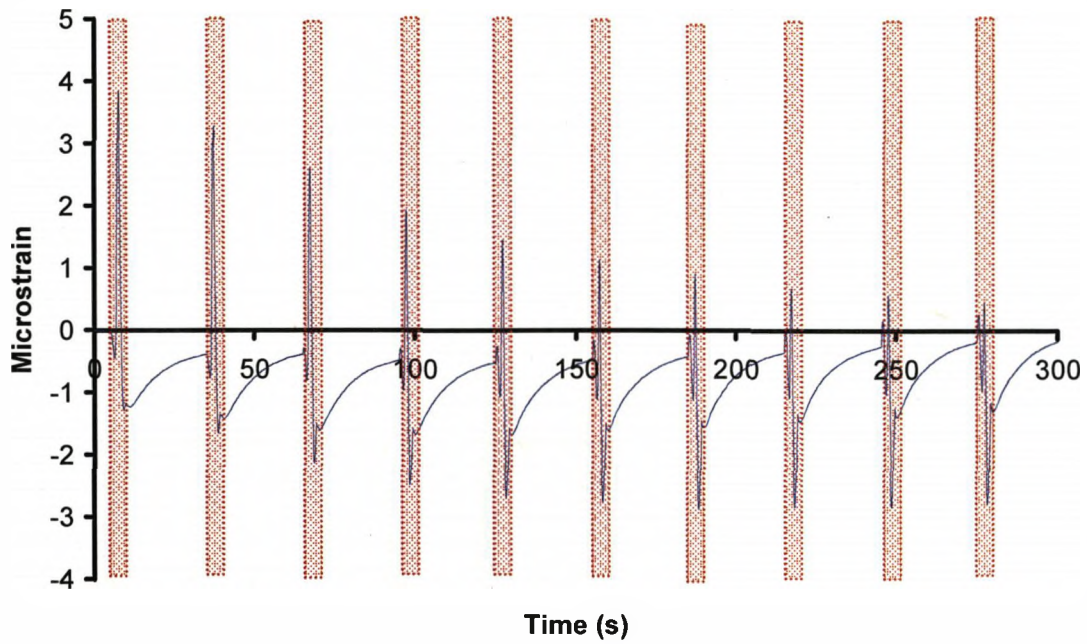

Longitudinal strain gauge output for 2-1 GF FML

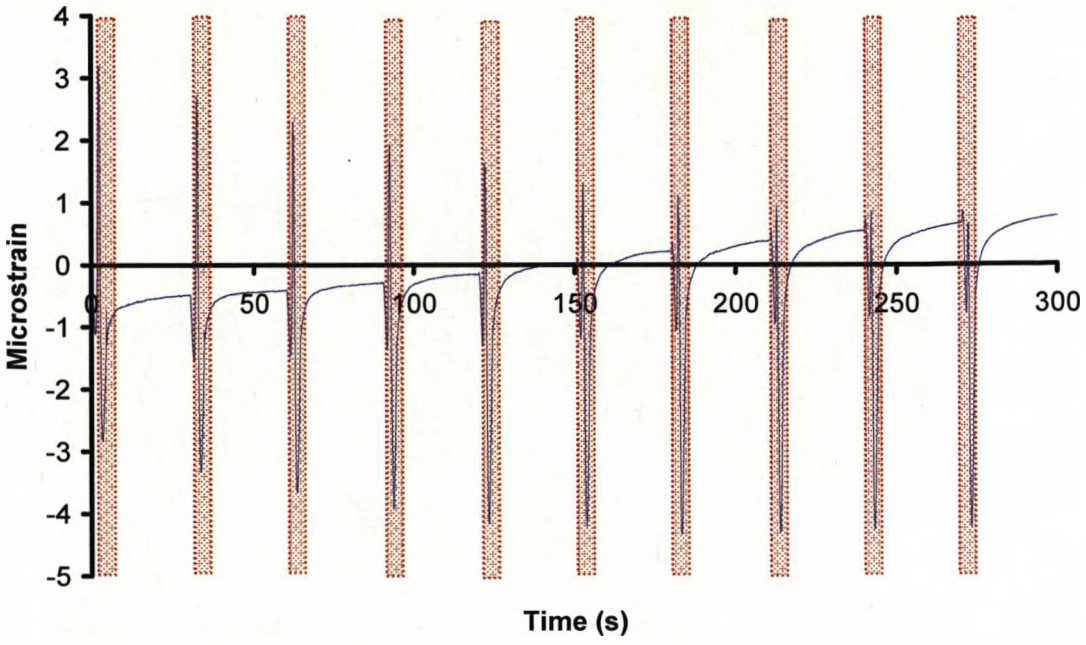

Longitudinal strain gauge output for 2-2 GF FML

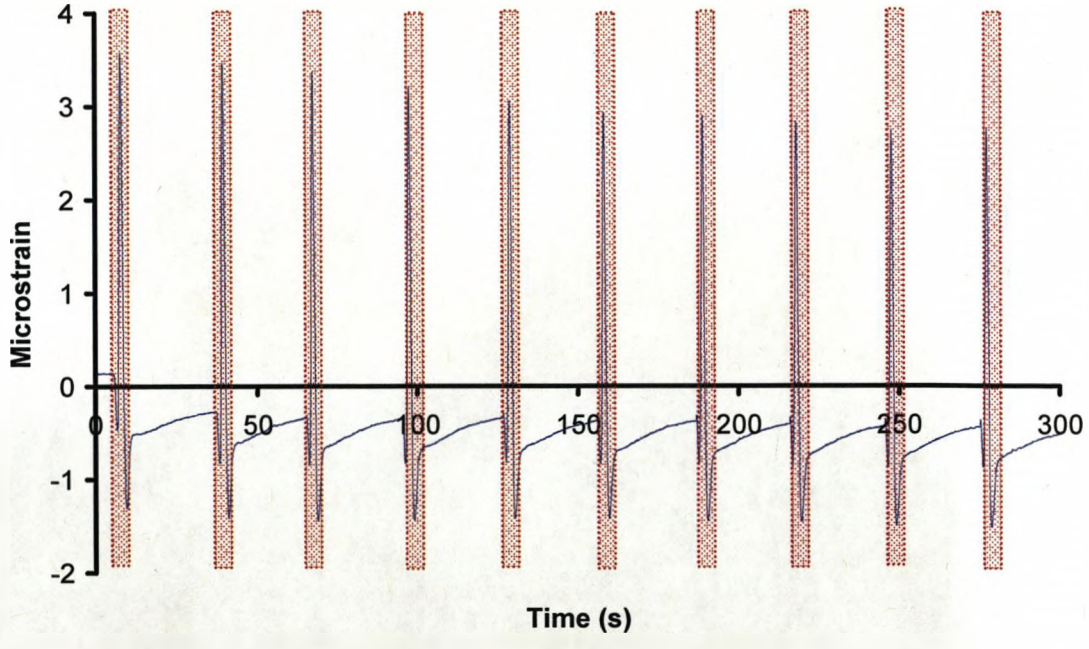

Longitudinal strain gauge output for 3-2 GF FML

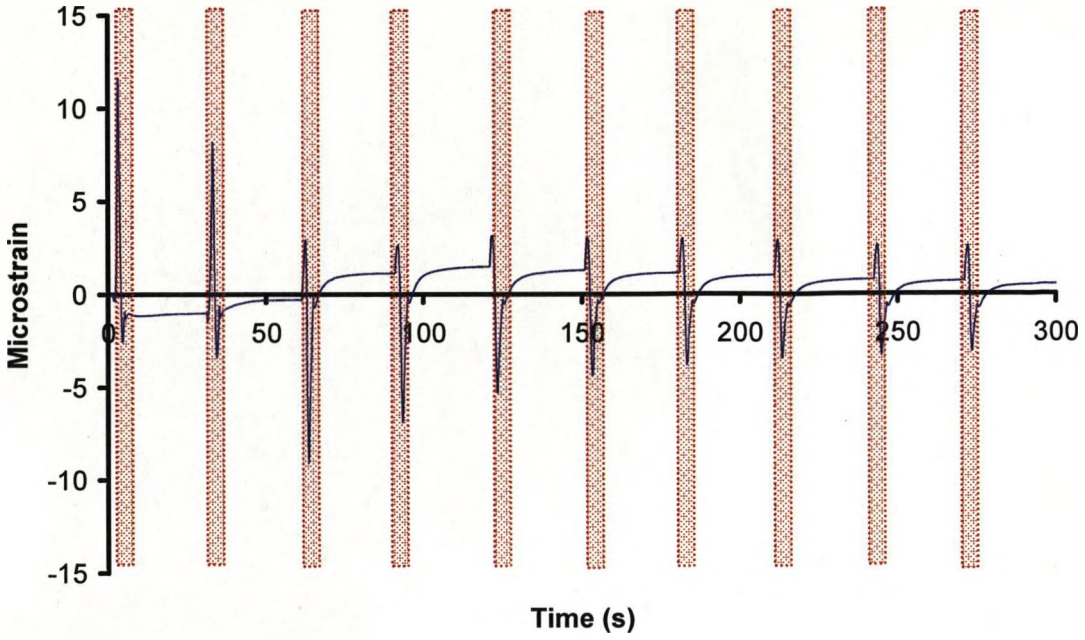

Longitudinal strain gauge output for 1-1 PP FML

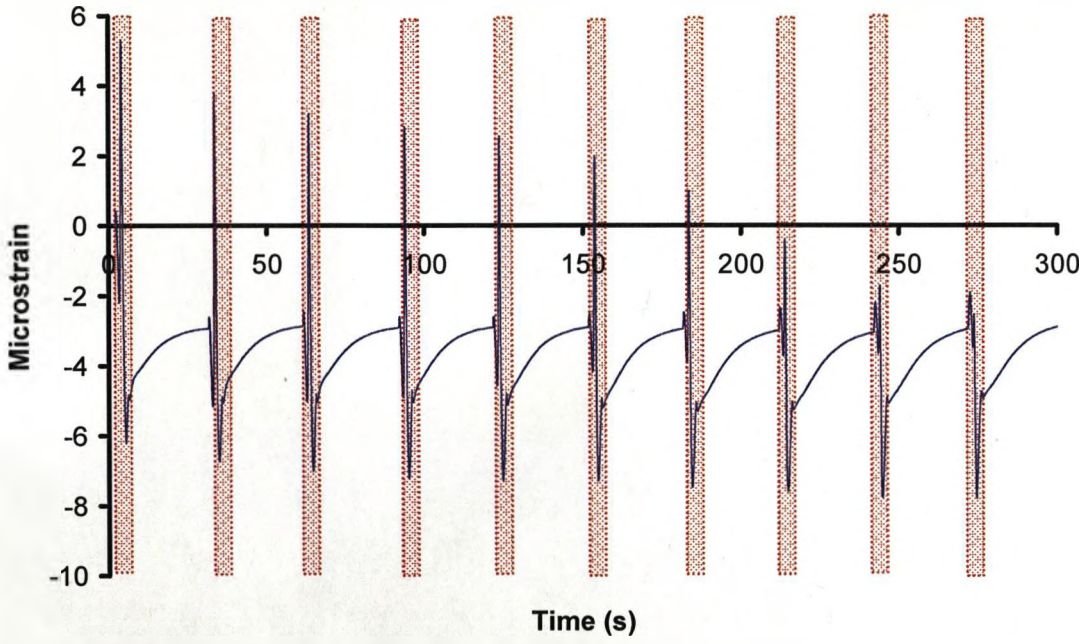

Longitudinal strain gauge output for 2-1 PP FML

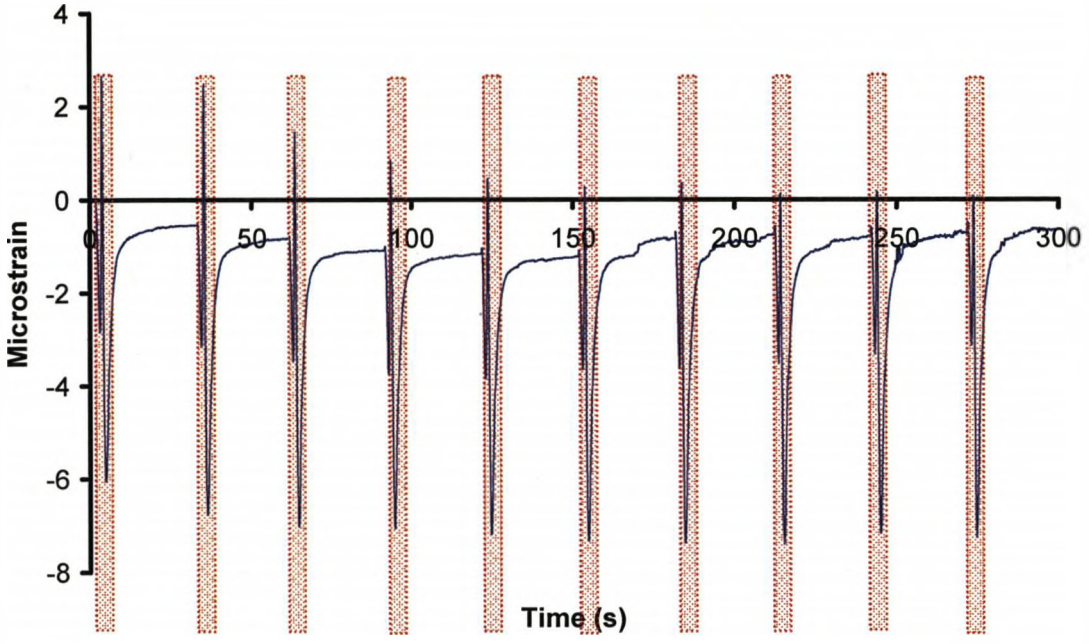

Longitudinal strain gauge output for 2-2 PP FML

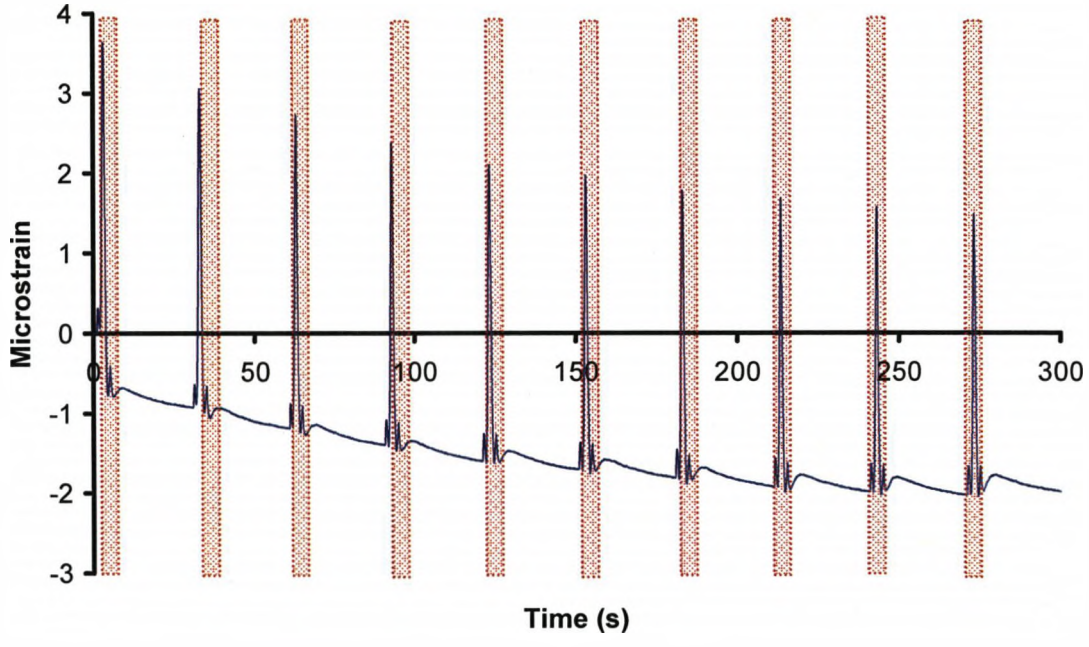

Longitudinal strain gauge output for 3-2 PP FML